Advances in Astronomy

Gamma-Ray Burst in the Swift/Fermi Era and Beyond

Lead Guest Editor: WeiKang Zheng
Guest Editors: Takanori Sakamoto, Yuji Urata, and Shashi B. Pandey

Gamma-Ray Burst in the Swift/Fermi Era and Beyond

Advances in Astronomy

Gamma-Ray Burst in the Swift/Fermi Era and Beyond

Lead Guest Editor: WeiKang Zheng
Guest Editors: Takanori Sakamoto, Yuji Urata, and Shashi B. Pandey

Editorial Board

Contents

Hindawi
Advances in Astronomy
Volume 2018, Article ID 2730676, 1 page
https://doi.org/10.1155/2018/2730676

Editorial

Gamma-Ray Burst in the Swift/Fermi Era and Beyond

WeiKang Zheng[1], **Takanori Sakamoto**[2], **Yuji Urata**[3] **and Shashi B. Pandey**[4]

[1]*Department of Astronomy, University of California, Berkeley, CA 94720-3411, USA*
[2]*Department of Physics and Mathematics, Aoyama Gakuin University, Sagamihara, Kanagawa 252-5258, Japan*
[3]*Institute of Astronomy, National Central University, Chung-Li 32054, Taiwan*
[4]*Aryabhatta Research Institute of Observational Sciences, Manora Peak, Nainital 263002, India*

Correspondence should be addressed to WeiKang Zheng; zwk@astro.berkeley.edu

Received 20 December 2016; Accepted 20 December 2016; Published 1 February 2018

The *Swift* and *Fermi* satellites have been observing gamma-ray bursts (GRBs), which are short-lived and intense flashes of gamma-rays associated with the death/explosion of massive stars and/or compact binary mergers, for nearly a decade in space since their launch in 2004 and 2008, respectively. Our understanding of GRB physics, though still far from complete, has been revolutionized thanks to their outstanding observations, as well as the ongoing ground follow-up observations. In addition to a previously published special issue, "Gamma-Ray Bursts in the Swift and Fermi Era," which discussed GRB work related to the *Swift* and *Fermi* missions, here we continue collecting reviews and research articles on GRBs and their afterglows.

In total, five reviews and one research article are published in this special issue. The review article by M. Tanaka summarizes the current understanding of kilonovae/macronovae related to the GRBs. In comparison, Z. Cano et al. present an up-to-date review of progress on the connection between supernovae and long-duration GRBs. Next, the review article by M. Dainotti et al. discusses various GRB correlations during the prompt phase and their use as redshift estimators and possibly as cosmological tools. In contrast, the review by J. J. Geng and Y. F. Huang focuses on the GRB afterglow phase, discussing the diverse features of the multiwavelength afterglows of GRBs. One other article by M. Jelinek et al. presents a decade of optical follow-up observations of GRBs by the BOOTES telescope in Spain. Lastly, P. Chandra discusses GRBs from the radio perspective, which is very important for studies of GRBs related to their calorimetry, reverse-shock emission, and circumburst environments.

Overall, this volume extends the discussions of the previously published special issue, "Gamma-Ray Bursts in the Swift and Fermi Era," and covers more topics about GRBs from gamma-ray to radio wavelengths. These are the most updated summaries of progress on GRB studies during the *Swift* and *Fermi* mission periods. We hope these two special issues provide useful information for GRB researchers, helping to lead to new results and progress even beyond the *Swift* and *Fermi* era.

Acknowledgments

We sincerely thank the authors and referees for all of their efforts.

WeiKang Zheng
Takanori Sakamoto
Yuji Urata
Shashi B. Pandey

Hindawi
Advances in Astronomy
Volume 2018, Article ID 4969503, 31 pages
https://doi.org/10.1155/2018/4969503

Review Article

Gamma-Ray Burst Prompt Correlations

M. G. Dainotti,[1,2,3] **R. Del Vecchio**,[3] **and M. Tarnopolski**[3]

[1]*Physics Department, Stanford University, Via Pueblo Mall 382, Stanford, CA, USA*
[2]*INAF, Istituto di Astrofisica Spaziale e Fisica Cosmica, Via Gobetti 101, 40129 Bologna, Italy*
[3]*Astronomical Observatory, Jagiellonian University, Orla 171, 30-244 Kraków, Poland*

Correspondence should be addressed to M. G. Dainotti; mdainott@stanford.edu

Received 25 May 2016; Accepted 27 November 2016; Published 24 January 2018

Academic Editor: Alberto J. Castro-Tirado

The mechanism responsible for the prompt emission of gamma-ray bursts (GRBs) is still a debated issue. The prompt phase-related GRB correlations can allow discriminating among the most plausible theoretical models explaining this emission. We present an overview of the observational two-parameter correlations, their physical interpretations, and their use as redshift estimators and possibly as cosmological tools. The nowadays challenge is to make GRBs, the farthest stellar-scaled objects observed (up to redshift $z = 9.4$), standard candles through well established and robust correlations. However, GRBs spanning several orders of magnitude in their energetics are far from being standard candles. We describe the advances in the prompt correlation research in the past decades, with particular focus paid to the discoveries in the last 20 years.

1. Introduction

Gamma-ray bursts (GRBs) are highly energetic events with the total isotropic energy released of the order of 10^{48}–10^{55} erg (for recent reviews, see [1–6]). GRBs were discovered by military satellites *Vela* in late 1960s and were recognized early to be of extrasolar origin [7]. A bimodal structure (reported first by Mazets et al. [8]) in the duration distribution of GRBs detected by the Burst and Transient Source Experiment (BATSE) onboard the *Compton Gamma-Ray Observatory* (CGRO) [9], based on which GRBs are nowadays commonly classified into short (with durations $T_{90} < 2$ s, SGRBs) and long (with $T_{90} > 2$ s, LGRBs), was found [10]. BATSE observations allowed also confirming the hypothesis of Klebesadel et al. [7] that GRBs are of extragalactic origin due to isotropic angular distribution in the sky combined with the fact that they exhibited an intensity distribution that deviated strongly from the $-3/2$ power law [9, 11–14]. This was later corroborated by establishing the first redshift measurement, taken for GRB970508, which with $0.835 < z \lesssim 2.3$ was placed at a cosmological distance of at least 2.9 Gpc [15]. Despite initial isotropy, SGRBs were shown to be distributed anisotropically on the sky, while LGRBs are distributed isotropically [16–23]. Cosmological consequences of the anisotropic celestial distribution of SGRBs were discussed lately by Mészáros et al. [24] and Mészáros and Rees [6]. Finally, the progenitors of LGRBs are associated with supernovae (SNe) [25–29] related to collapse of massive stars. Progenitors of SGRBs are thought to be neutron star–black hole (NS–BH) or NS–NS mergers [12, 30–32], and no connection between SGRBs and SNe has been proven [33].

While the recent first direct detection of gravitational waves (GW), termed GW150914, by the Laser Interferometer Gravitational Wave Observatory (LIGO) [34], interpreted as a merger of two stellar-mass BHs with masses $36^{+5}_{-4}\ M_\odot$ and $29^{+4}_{-4}\ M_\odot$, is by itself a discovery of prime importance, it becomes especially interesting in light of the finding of Connaughton et al. [35] who reported a weak transient source lasting 1 s and detected by *Fermi*/GBM [36] only 0.4 s after the GW150914, termed GW150914-GBM. Its false alarm probability is estimated to be 0.0022. The fluence in the energy band 1 keV–10 MeV is computed to be $1.8^{+1.5}_{-1.0} \times 10^{49}$ erg s^{-1}. While these GW and GRB events are consistent in direction, its connection is tentative due to relatively large uncertainties in their localization. This association is unexpected as SGRBs have been thought to originate from NS–NS or NS–BH mergers. Moreover, neither *INTEGRAL* [37] nor *Swift* [38] detected any signals that could be ascribed

to a GRB. Even if it turns out that it is only a chance coincidence [39], it has already triggered scenarios explaining how a BH–BH merger can become a GRB; for example, the nascent BH could generate a GRB via accretion of a mass $\simeq 10^{-5}\ M_{\odot}$ [40], indicating its location in a dense medium (see also [41]), or two high-mass, low-metallicity stars could undergo an SN explosion, and the matter ejected from the last exploding star can form—after some time—an accretion disk producing an SGRB [42]. Also the possible detection of an afterglow that can be visible many months after the event [43] could shed light on the nature of the GW and SGRB association.

From a phenomenological point of view, a GRB is composed of the prompt emission, which consists of high-energy photons such as γ-rays and hard X-rays, and the afterglow emission, that is, a long lasting multiwavelength emission (X-ray, optical, and sometimes also radio), which follows the prompt phase. The first afterglow observation (for GRB970228) was due to the *BeppoSAX* satellite [44, 45]. Another class, besides SGRBs and LGRBs, that is, intermediate in duration, was proposed to be present in univariate duration distributions [46–51], as well as in higher dimensional parameter spaces [51–56]. On the other hand, this elusive intermediate class might be a statistical feature that can be explained by modeling the duration distribution with skewed distributions, instead of the commonly applied standard Gaussians [57–61]. Additionally, GRB classification was shown to be detector-dependent [1, 62, 63]. Moreover, a subclass classification of LGRBs was proposed [64], and Norris and Bonnell [65] discovered the existence of an intermediate class or SGRBs with extended emission, that show mixed properties between SGRBs and LGRBs. GRBs with very long durations (ultralong GRBs, with $T_{90} > 1000$ s) are statistically different than regular (i.e., with $T_{90} < 500$ s) LGRBs [66] and hence might form a different class (see also [67–70]). Another relevant classification appears related to the spectral features distinguishing normal GRBs from X-ray flashes (XRFs). The XRFs [71, 72] are extragalactic transient X-ray sources with spatial distribution and spectral and temporal characteristics similar to LGRBs. The remarkable property that distinguishes XRFs from GRBs is that their νF_{ν} prompt emission spectrum peaks at energies which are observed to be typically an order of magnitude lower than the observed peak energies of GRBs. XRFs are empirically defined by a greater fluence (time-integrated flux) in the X-ray band (2–30 keV) than in the γ-ray band (30–400 keV). This classification is also relevant for the investigation of GRB correlations since some of them become stronger or weaker by introducing different GRB categories. Grupe et al. [73], using 754 *Swift* GRBs, performed an exhaustive analysis of several correlations as well as the GRB redshift distribution, discovering that the bright bursts are more common in the high-z (i.e., $z \gtrsim 3$) than in the local universe.

This classification has further enhanced the knowledge of the progenitor system from which GRBs originate. It was soon after their discovery that LGRBs were thought to originate from distant star-forming galaxies. Since then, LGRBs have been firmly associated with powerful core-collapse SNe and the association seems solid. Nevertheless, there have been puzzling cases of LGRBs that were not associated with bright SNe [74, 75]. This implies that it is possible to observe GRBs without an associated bright SNe or there are other progenitors for LGRBs than core-collapse of massive stars. Another relevant uncertainty concerning the progenitor systems for LGRBs is the role of metallicity Z. In the collapsar model [27], LGRBs are only formed by massive stars with $Z/Z_{\odot}$ below $\simeq$ 0.1–0.3. However, several GRBs have been located in very metal-rich systems [76] and it is an important goal to understand whether there are other ways to form LGRBs than through the collapsar scenario [77]. One of the models used to explain the GRB phenomenon is the "fireball" model [78–80] in which a compact central engine (either the collapsed core of a massive star or the merger product of an NS–NS binary) launches a highly relativistic, jetted electron-positron-baryon plasma. Interactions of blobs within the jet are believed to produce the prompt emission. Instead, the interaction of the jet with the ambient material causes the afterglow phase. However, problems in explaining the light curves within this model have been shown by Willingale et al. [81]. Specifically, for ≃50% of GRBs, the observed afterglows are in agreement with the model, but for the rest the temporal and spectral indices do not conform and suggest a continued late energy injection. Melandri et al. [82] performed a multiwavelength analysis and found that the forward shock (FS) model does not explain almost 50% of the examined GRBs, even after taking into account energy injection. Rykoff et al. [83] showed that the fireball model does not model correctly early afterglows. Reference [84] analysed the prompt and afterglow light curves and pointed out that some GRBs required energy injection to explain the outflows. The crisis of the standard fireball models appeared when *Swift* [85] observations revealed a more complex behaviour of the light curves than observed in the past [86–88] and pointed out that GRBs often follow "canonical" light curves [89]. Therefore, the discovery of correlations among relevant physical parameters in the prompt phase is very important in this context in order to use them as possible model discriminators. In fact, many theoretical models have been presented in the literature in order to explain the wide variety of observations, but each model has some advantages as well as drawbacks, and the use of the phenomenological correlations can boost the understanding of the mechanism responsible for the prompt emission. Moreover, given the much larger (compared to SNe) redshift range over which GRBs can be observed, it is tempting to include them as cosmological probes, extending the redshift range by almost an order of magnitude further than the available SNe Ia. GRBs are observed up to redshift $z = 9.4$ [90], much more distant than SNe Ia, observed up to $z = 2.26$ [91], and therefore they can help to understand the nature of dark energy and determine the evolution of its equation of state at very high z. However, contrary to SNe Ia, which originate from white dwarves reaching the Chandrasekhar limit and always releasing the same amount of energy, GRBs cannot yet be considered standard candles with their (isotropic-equivalent) energies spanning 8 orders of magnitude (see also [92] and references therein). Therefore, finding universal relations among observable properties can help to standardize their

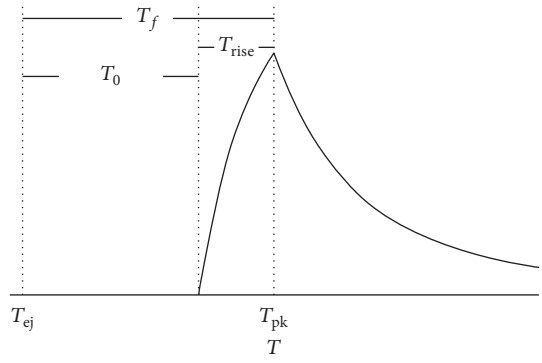

FIGURE 1: A sketch of the pulse displaying $T_{\rm ej}$ and $T_{\rm peak}$ (denoted by $T_{\rm pk}$ here) and the quantities T_f and $T_0 = T_f - T_{\rm rise}$. (Figure after Willingale et al. [108]; see Figure 1 therein.)

energetics and/or luminosities. They can serve as a tracer of the history of the cosmic star formation rate [93–97] and provide invaluable information on the physics in the intergalactic medium [98–100]. This is the reason why the study of GRB correlations is so relevant for understanding the GRB emission mechanism, for finding a good distance indicator, and for exploring the high-redshift universe [101].

This paper is organized in the following manner. In Section 2, we explain the nomenclature and definitions adopted in this work, and in Section 3 we analyse the correlations between various prompt parameters. We summarize in Section 4.

2. Notations and Nomenclature

For clarity we report a summary of the nomenclature adopted in the review. L, F, E, S, and T indicate the luminosity, the energy flux, the energy, the fluence, and the timescale, respectively, which can be measured in several wavelengths. More specifically,

(i) T_{90} is the time interval in which 90% of the GRB's fluence is accumulated, starting from the time at which 5% of the total fluence was detected [10];

(ii) T_{50} is defined, similar to T_{90}, as the time interval from 25% to 75% of the total detected fluence;

(iii) T_{45} is the time spanned by the brightest 45% of the total counts detected above background [102];

(iv) $T_{\rm peak}$ is the time at which the pulse (i.e., a sharp rise and a slower, smooth decay [103–106]) in the prompt light curve peaks (see Figure 1);

(v) $T_{\rm break}$ is the time of a power law break in the afterglow light curve [107, 108], that is, the time when the afterglow brightness has a power law decline that suddenly steepens due to the slowing down of the jet until the relativistic beaming angle roughly equals the jet-opening angle $\theta_{\rm jet}$ [109];

(vi) $\tau_{\rm lag}$ and $\tau_{\rm RT}$ are the difference of arrival times to the observer of the high-energy photons and low energy photons defined between 25–50 keV and 100–300 keV energy band and the shortest time over which the light curve increases by 50% of the peak flux of the pulse;

(vii) T_p is the end time prompt phase at which the exponential decay switches to a power law, which is usually followed by a shallow decay called the plateau phase, and T_a is the time at the end of this plateau phase [81];

(viii) T_f is the pulse width since the burst trigger at the time $T_{\rm ej}$ of the ejecta;

(ix) $E_{\rm peak}$, $E_{\rm iso}$, E_γ, and $E_{\rm prompt}$ are the peak energy, that is, the energy at the peak of the νF_ν spectrum [110], the total isotropic energy emitted during the whole burst (e.g., [111]), the total energy corrected for the beaming factor [the latter two are connected via $E_\gamma = (1 - \cos\theta_{\rm jet})E_{\rm iso}$], and the isotropic energy emitted in the prompt phase, respectively;

(x) $F_{\rm peak}$, $F_{\rm tot}$ are the peak and the total fluxes, respectively [112];

(xi) L_a, $L_{X,p}$, and L_f are the luminosities respective to T_a, T_p (specified in the X-ray band), and T_f;

(xii) L is the observed luminosity, and specifically $L_{\rm peak}$ and $L_{\rm iso}$ are the peak luminosity (i.e., the luminosity at the pulse peak, [113]) and the total isotropic luminosity, both in a given energy band. More precisely, $L_{\rm peak}$ is defined as follows:

$$L_{\rm peak} = 4\pi D_L\left(z, \Omega_M, \Omega_\Lambda\right)^2 F_{\rm peak}, \quad (1)$$

with $D_L(z, \Omega_M, \Omega_\Lambda)$ the luminosity distance given by

$$D_L\left(z, \Omega_M, \Omega_\Lambda\right) = \frac{c\,(1+z)}{H_0}\int_0^z \frac{dz'}{\sqrt{\Omega_M\left(1+z'\right)^3 + \Omega_\Lambda}}, \quad (2)$$

where Ω_M and Ω_Λ are the matter and dark energy density parameters, H_0 is the present-day Hubble constant, and z is the redshift. Similarly, $L_{\rm iso}$ is given by

$$L_{\rm iso} = 4\pi D_L\left(z, \Omega_M, \Omega_\Lambda\right)^2 F_{\rm tot}; \quad (3)$$

(xiii) S_γ, $S_{\rm obs}$, $S_{\rm tot}$ indicate the prompt fluence in the whole gamma band (i.e., from a few hundred keV to a few MeV), the observed fluence in the range 50–300 keV, and the total fluence in the 20 keV–1.5 MeV energy band;

(xiv) V is the variability of the GRB's light curve. It is computed by taking the difference between the observed light curve and its smoothed version, squaring this difference, summing these squared differences over time intervals, and appropriately normalizing the resulting sum [102]. Different smoothing filters may be applied (see also [114] for a different approach). V_f denotes the variability for a certain fraction of the smoothing timescale in the light curve.

Most of the quantities described above are given in the observer frame, except for $E_{\rm iso}$, $E_{\rm prompt}$, $L_{\rm peak}$, and $L_{\rm iso}$, which are already defined in the rest frame. With the upper index "$*$" we explicitly denote the observables in the GRB rest frame. The rest frame times are the observed times divided by the cosmic time expansion; for example the rest frame time in the prompt phase is denoted by $T_p^* = T_p/(1+z)$. The energetics are transformed differently, for example, $E_{\rm peak}^* = E_{\rm peak}(1+z)$.

The Band function [115] is a commonly applied phenomenological spectral profile, such that

$$N_E(E) = A_{\rm norm} \times \begin{cases} \left(\dfrac{E}{100\,\text{keV}}\right)^{\alpha} \exp\left(-\dfrac{E}{E_0}\right), & E \le (\alpha-\beta)E_0, \\ \left[\dfrac{(\alpha-\beta)E_0}{100\,\text{keV}}\right]^{\alpha-\beta} \left(\dfrac{E}{100\,\text{keV}}\right)^{\beta} \exp(\alpha-\beta), & E \ge (\alpha-\beta)E_0, \end{cases} \tag{4}$$

where $A_{\rm norm}$ is the normalization. Here, α and β are the low- and high-energy indices of the Band function, respectively. $N_E(E)$ is in units of photons cm^{-2} s^{-1} keV^{-1}. For the cases $\beta < -2$ and $\alpha > -2$, $E_{\rm peak}$ can be derived as $E_{\rm peak} = (2+\alpha)E_0$, which corresponds to the energy at the maximum flux in the νF_ν spectra [115, 116].

The Pearson correlation coefficient [117, 118] is denoted by r, the Spearman correlation coefficient [119] is denoted by ρ, and the p value (a probability that a correlation is drawn by chance) is denoted by P.

Finally, we mostly deal with correlations of the form $y = ax + b$. However, when the intercept b is neglected in the text, but its value is nonnegligible (or not known due to lacking in the original paper), we use the notation $y \sim ax$ to emphasize the slope.

3. The Prompt Correlations

Several physical relations between relevant quantities in GRBs were found since the 1990s. In each paragraph below, we follow the discovery of the correlation with the definition of the quantities, the discussions presented in literature, and their physical interpretation.

3.1. The L_{peak}-τ_{lag} Correlation

3.1.1. Literature Overview. Liang and Kargatis [120], using 34 bright GRBs detected by BATSE, found that $E_{\rm peak}$ depends linearly on the previous flux emitted by the pulse, that is, that the rate of change of $E_{\rm peak}$ is proportional to the instantaneous luminosity. Quantitatively

$$\frac{L_{\rm peak}}{N} = -\frac{{\rm d}E_{\rm peak}}{{\rm d}t}, \tag{5}$$

where N is a normalization constant expressing the luminosity for each pulse within a burst, and $L_{\rm peak}$ was calculated from the observed flux via (1).

The $L_{\rm peak}$-$\tau_{\rm lag}$ correlation was introduced for the first time by Norris et al. [113] who examined a sample of 174 GRBs detected by BATSE, among which 6 GRBs had an established redshift and those were used to find an anticorrelation between $L_{\rm peak}$ and $\tau_{\rm lag}$ in the form of the following (see Figure 2(a)):

$$\log L_{\rm peak} = 55.11 - 1.14 \log \tau_{\rm lag}^*, \tag{6}$$

with $L_{\rm peak}$, in units of 10^{53} erg s^{-1}, computed in the 50–300 keV range, and $\tau_{\rm lag}^*$ is measured in seconds. A remarkably consistent relation was found by Schaefer et al. [121], who used a sample of 112 BATSE GRBs and reported that

$$\log L_{\rm peak} = 52.46 - (1.14 \pm 0.20) \log \tau_{\rm lag}, \tag{7}$$

being in perfect agreement with the result of Norris et al. [113]. Here, $L_{\rm peak}$ is in units of 10^{51} erg s^{-1} and $\tau_{\rm lag}$ in seconds. This relation has been confirmed by several studies (e.g., [122–124]).

Schaefer [125] showed that the $L_{\rm peak}$-$\tau_{\rm lag}$ relation is a consequence of the Liang and Kargatis [120] empirical relation from (5), and he derived this dependence to be of the form $\log L_{\rm peak} \sim -\log \tau_{\rm lag}$. This correlation was useful in the investigation of Kocevski and Liang [126], who used a sample of 19 BATSE GRBs and the $L_{\rm peak}$-$\tau_{\rm lag}$ relation from [121] to infer their pseudoredshifts. Their approach was to vary the guessed z until it allowed matching the luminosity distance D_L measured with the GRB's energy flux and D_L that can be calculated from the guessed redshift within a flat ΛCDM model, until the agreement among the two converged to within 10^{-3}. Next, the rate of $E_{\rm peak}$ decay, as in [120], was measured. Finally, Kocevski and Liang [126] showed that the $L_{\rm peak}$ is directly related to the GRB's spectral evolution. However, Hakkila et al. [127] found a different slope, -0.62 ± 0.04 and argued that the $L_{\rm peak}$-$\tau_{\rm lag}$ relation is a pulse rather than a burst property; that is, each pulse is characterized by its own $\tau_{\rm lag}$, distinct for various pulses within a GRB.

Tsutsui et al. [128], using pseudoredshifts estimated via the Yonetoku relation (see Section 3.6.2) for 565 BATSE GRBs, found that the $L_{\rm peak}$-$\tau_{\rm lag}$ relation has a ρ of only 0.38 (see Figure 2(b)). However, assuming that the luminosity is a function of both the redshift and the lag, a new redshift-dependent $L_{\rm peak}$-$\tau_{\rm lag}$ relation was found as

$$\log L_{\rm peak} = 50.88 + 2.53 \log(1+z) - 0.282 \log \tau_{\rm lag}, \tag{8}$$

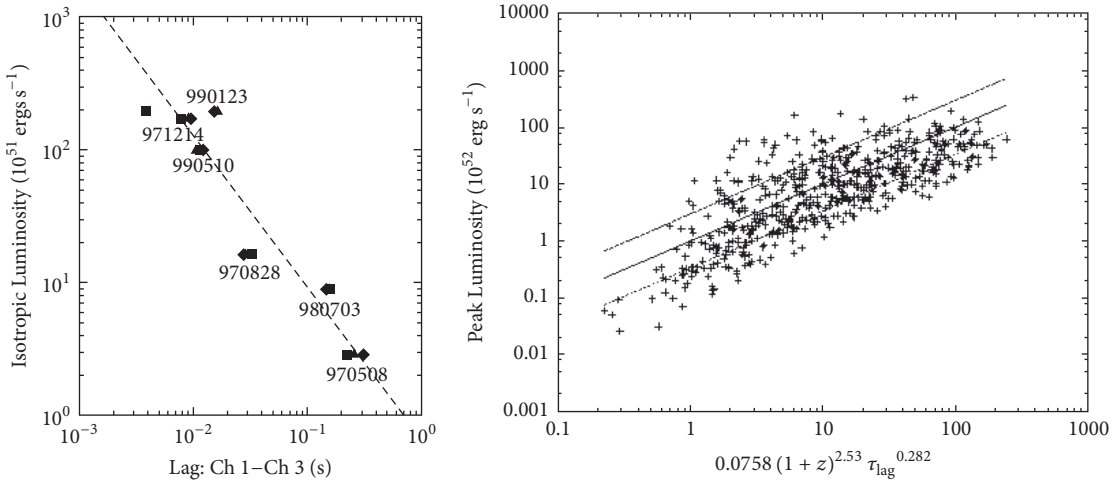

FIGURE 2: (a) L_{peak} versus τ^*_{lag} distribution for six GRBs with measured redshifts. The dashed line represents the power law fit to the lag times for ranges consisting of count rates larger than 0.1 × peak intensity (squares), yielding $\log L_{peak} \sim -1.14 \log(\tau^*_{lag}/0.01\ \text{s})$. The lag time is computed using channel 1 (25–50 keV) and channel 3 (100–300 keV) of the BATSE instrument. (Figure after Norris et al. [113]; see Figure 6 therein. @ AAS. Reproduced with permission.) (b) The L_{peak}-τ_{lag} distribution in the $\log L_{peak}$ versus $\sim 2.53 \log(1+z) - 0.282 \log \tau_{lag}$ plane. The correlation coefficient is $\rho = 0.77$, $P = 7.9 \times 10^{-75}$. The solid line represents the best-fit line and two dashed lines delineate 1σ deviation. (Figure after Tsutsui et al. [128]; see Figure 4 therein. Copyright @ 2008 AIP Publishing.)

with L_{peak} in units of 10^{50} erg s^{-1}, τ_{lag} in seconds, $\rho = 0.77$ and $P = 7.9 \times 10^{-75}$. Although the spectral lag is computed from two channels of BATSE, this new L_{peak}-τ_{lag} relation suggests that a future lag-luminosity relation defined within the *Swift* data should also depend on the redshift.

Afterwards, Sultana et al. [129] presented a relation between the z- and k-corrected τ_{lag} for the *Swift* energy bands 50–100 keV and 100–200 keV, and L_{peak}, for a subset of 12 *Swift* long GRBs. The z-correction takes into account the time dilatation effect by multiplying the observed lag by $(1+z)^{-1}$ to translate it into the rest frame. The k-correction takes into account a similar effect caused by energy bands being different in the observer and rest frames via multiplication by $(1+z)^{0.33}$ [130]. The net corrected τ^*_{lag} is thence $(1+z)^{-0.67}\tau_{lag}$. In addition, Sultana et al. [129] demonstrated that this correlation in the prompt phase can be extrapolated into the L_a-T^*_a relation [131–134]. Sultana et al. [129] found the following (Note that Sultana et al. [129] used L_{iso} to denote the peak isotropic luminosity.):

$$\log L_{peak} = (54.87 \pm 0.29) - (1.19 \pm 0.17) \log\left[(1+z)^{-0.67}\tau_{lag}\right], \quad (9)$$

$$\log L_a = (51.57 \pm 0.10) - (1.10 \pm 0.03) \log T^*_a,$$

with τ_{lag} in ms, T^*_a in seconds, and L in erg s^{-1}. The correlation coefficient is significant for these two relations ($\rho = -0.65$ for the L_{peak}-τ_{lag} and $\rho = -0.88$ for the L_a-T^*_a relations) and has surprisingly similar best-fit power law indices (-1.19 ± 0.17 and -1.10 ± 0.03, resp.). Although τ_{lag} and T^*_a represent different GRB time variables, it appears distinctly that the L_{peak}-τ_{lag} relation extrapolates into L_a-T^*_a for timescales $\tau_{lag} \simeq T^*_a$. A discussion and comparison of this extrapolation with the L_f-T_f relation are extensively presented in [135].

Ukwatta et al. [136] confirmed that there is a correlation between L^*_{peak} and the z- and k-corrected τ_{lag} among 31 GRBs observed by *Swift*, with $r = -0.68$, $P = 7 \times 10^{-2}$ and the slope equal to -1.4 ± 0.3, hence confirming the L_{peak}-τ_{lag} relation, although with a large scatter. This was followed by another confirmation of this correlation [137] with the use of 43 *Swift* GRBs with known redshift, which yielded $r = -0.82$, $P = 5.5 \times 10^{-5}$, and a slope of -1.2 ± 0.2, being consistent with the previous results.

Finally, Margutti et al. [138] established that the X-ray flares obey the same L_{peak}-τ^*_{lag} relation (in the rest frame energy band 0.3–10 keV) as GRBs and proposed that their underlying mechanism is similar.

3.1.2. Physical Interpretation of the L_{peak}-τ_{lag} Relation. The physical assumption on which the work by Norris et al. [113] was based is that the initial mechanism for the energy formation affects the development of the pulse much more than dissipation. From the study of several pulses in bright, long BATSE GRBs, it was claimed that, for pulses with precisely defined shape, the rise-to-decay ratio is ≤1. In addition, when the ratio diminishes, pulses show a tendency to be broader and weaker.

Salmonson [122] proposed that the L_{peak}-τ_{lag} relation arises from an entirely kinematic effect. In this scenario, an emitting region with constant (among the bursts) luminosity is the source of the GRB's radiation. He also claimed that variations in the line-of-sight velocity should affect the observed luminosity proportionally to the Lorentz factor of the jet's expansion, $\Gamma = [1-(v/c)^2]^{-1/2}$ (where v is the relative velocity

between the inertial reference frames and c is the speed of light), while the apparent $\tau_{\rm lag}$ is proportional to $1/\Gamma$. The variations in the velocity among the lines of sight is a result of the jet's expansion velocity combined with the cosmological expansion. The differences of luminosity and lag between different bursts are due to the different velocities of the individual emitting regions. In this case, the luminosity is expected to be proportional to $1/\tau_{\rm lag}$, which is consistent with the observed relation. This explanation, however, requires the comoving luminosity to be nearly constant among the bursts, which is a very strong condition to be fulfilled. Moreover, this scenario has several other problems (as pointed out by Schaefer [125]):

(1) It requires the Lorentz factor and luminosity to have the same range of variation. However, the observed $L_{\rm peak}$ span more than three orders of magnitude (e.g., [121]), while the Lorentz factors span less than one order of magnitude (i.e., a factor of 5) [139].

(2) It follows that the observed luminosity should be linearly dependent on the jet's Lorentz factor, yet this claim is not justified. In fact, a number of corrections are to be taken into account, leading to a significantly nonlinear dependence. The forward motion of the jet introduces by itself an additional quadratic dependence [140].

Ioka and Nakamura [141] proposed another interpretation for the $L_{\rm peak}$-$\tau_{\rm lag}$ correlation. From their analysis, a model in which the peak luminosity depends on the viewing angle is elaborated: the viewing angle is the off-axis angular position from which the observer examines the emission. Indeed, it is found that a high-luminosity peak in GRBs with brief spectral lag is due to an emitted jet with a smaller viewing angle than a fainter peak with extended lag. It is also claimed that the viewing angle can have implications on other correlations, such as the luminosity-variability relation presented in Section 3.2. As an additional result from this study, it was pointed out that XRFs can be seen as GRBs detected from large angles with high spectral lag and small variability.

On the other hand, regarding the jet angle distributions, Liang et al. [142] found an anticorrelation between the jet-opening angle and the isotropic kinetic energy among 179 X-ray GRB light curves and the afterglow data of 57 GRBs. Assuming that the GRB rate follows the star formation rate, and, after a careful consideration of selection effects, Lü et al. [143] found in a sample of 77 GRBs an anticorrelation between the jet-opening angle $\theta_{\rm jet}$ and the redshift in the following form:

$$\log\theta_{\rm jet} = (-0.90 \pm 0.09) - (0.94 \pm 0.19)\log(1+z), \quad (10)$$

with $\rho = 0.55$ and $P < 10^{-4}$. Using a mock sample and bootstrap technique, they showed that the observed $\theta_{\rm jet}$-z relation is most likely due to instrumental selection effects. Moreover, they argued that while other types of relation, for example, $\tau_{\rm lag}$-z [144] or the redshift dependence of the shallow decay in X-ray afterglows by Stratta et al. [145], might have connections with the jet geometry, they are also likely to stem from observational biases or sample selection effects. Also, Ryan et al. [146] investigated the jet-opening angle properties using a sample of 226 *Swift*/XRT GRBs with known redshift. They found that most of the observed afterglows were observed off-axis; hence the expected behaviour of the afterglow light curves can be significantly affected by the viewing angle.

Zhang et al. [33] argued, on the basis of the kinematic model, that the origin of the $L_{\rm peak}$-$\tau_{\rm lag}$ relation is due to a more intrinsic $L_{\rm peak}$-V relation (see Section 3.2). They also gave an interpretation of the latter relation within the internal shock model (see Section 3.2.2). Recently, Uhm and Zhang [147] constructed a model based on the synchrotron radiation mechanism that explains the physical origin of the spectral lags and is consistent with observations.

Another explanation for the origin of the $L_{\rm peak}$-$\tau_{\rm lag}$ relation, given by Sultana et al. [129], involves only kinematic effects. In this case, $L_{\rm peak}$ and $\tau_{\rm lag}$ depend on the quantity:

$$D = \frac{1}{\Gamma\left(1-\beta_0\cos\theta\right)(1+z)}, \quad (11)$$

depicting the Doppler factor of a jet at a viewing angle θ and with velocity $\beta_0 \equiv v/c$ at redshift z. In this study there is no reference to the masses and forces involved and, as a consequence of the Doppler effect, the factor D associates the GRB rest frame timescale τ with the observed time t in the following way:

$$t = \frac{\tau}{D}. \quad (12)$$

Therefore, considering a decay timescale $\Delta\tau$ in the GRB rest frame, (12) in the observer frame will give $\Delta t = \Delta\tau/D$. Furthermore, taking into account a spectrum given by $\Phi(E) \propto E^{-\alpha}$, the peak luminosity (as already pointed out by Salmonson [122]) can be computed as

$$L_{\rm peak} \propto D^{\alpha}, \quad (13)$$

with $\alpha \approx 1$. In such a way, (12) and (13) allow retrieving the observed $L_{\rm peak}$-$\tau_{\rm lag}$ relation. Finally, the analogous correlation coefficients and best-fit slopes of the $L_{\rm peak}$-$\tau_{\rm lag}$ and L_a-T_a^* correlations obtained by Sultana et al. [129] seem to hint toward a similar origin for these two relations.

3.2. The L_{peak}-V Correlation. The first correlation between $L_{\rm peak}$ and V was discovered by Fenimore and Ramirez-Ruiz [148] and was given as

$$\log L_{\rm peak} = 56.49 + 3.35\log V, \quad (14)$$

with $L_{\rm peak}$ measured in erg s^{-1}. Here, the luminosity is per steradian in a specified (rest frame) energy bandpass (50–300 keV), averaged over 256 ms. First, seven BATSE GRBs with a measured redshift were used to calibrate the $L_{\rm peak}$-V relation. Next, the obtained relationship was applied to 220 bright BATSE GRBs in order to obtain the luminosities and distances and to infer that the GRB formation rate scales as $(1+z)^{3.3\pm0.3}$. Finally, the authors emphasized the need of confirmation of the proposed $L_{\rm peak}$-V relation.

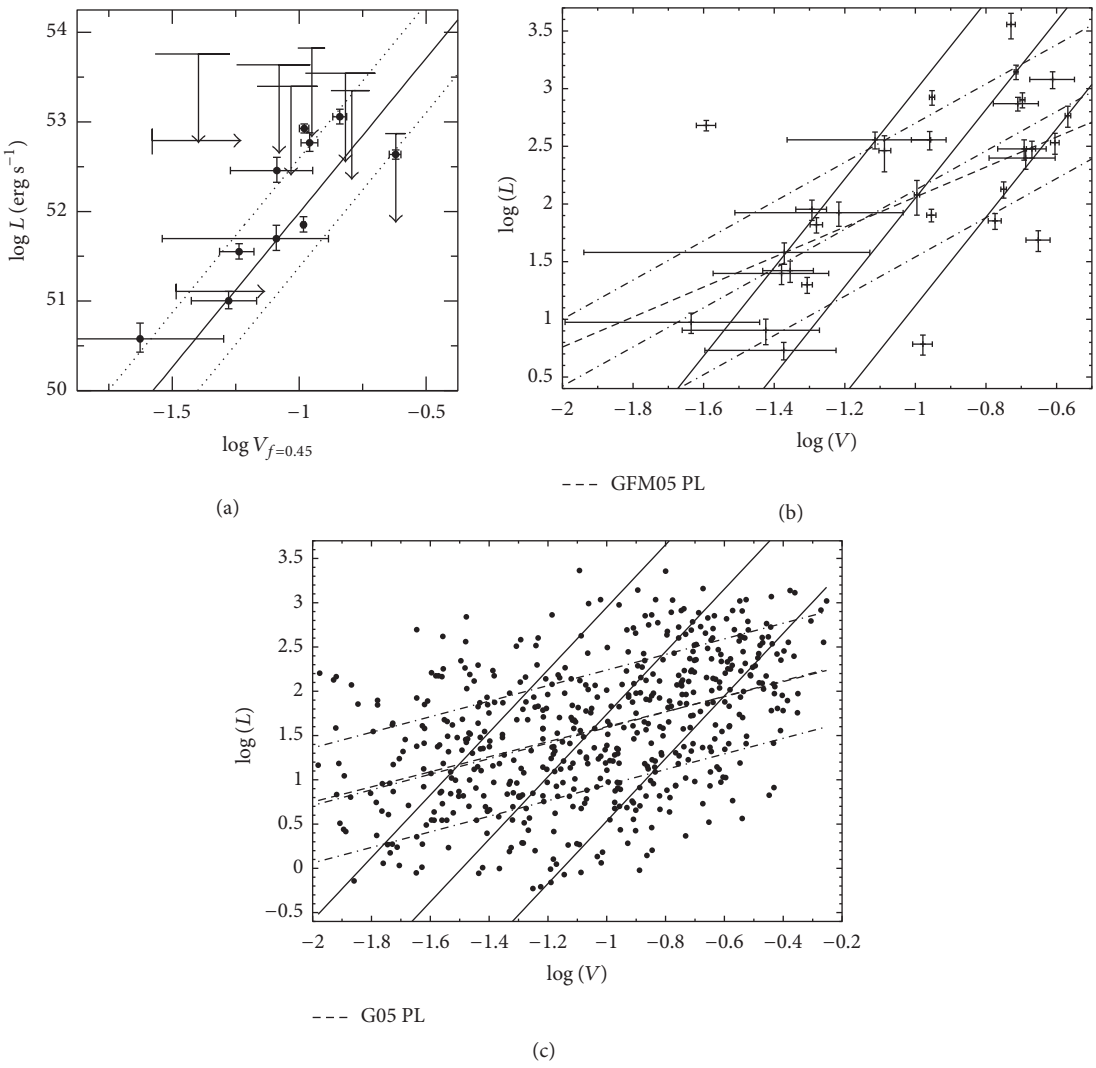

FIGURE 3: (a) The variabilities $V_{f=0.45}$ and peak luminosities $L_{\rm peak}$ of the data set, excluding GRB980425. In this case, $V_{f=0.45}$ indicates the variabilities for the 45% smoothing timescale of the light curve. The solid and dotted lines are the best-fit line and 1σ deviation, respectively, in $\log L_{\rm peak}$- $\log V_{f=0.45}$ plane. (Figure after Reichart et al. [102]; see Figure 9 therein. @ AAS. Reproduced with permission.) (b) The $\log L_{\rm peak}$- $\log V$ plane for the sample of 32 GRBs with measured redshift. The best-fit lines and 1σ deviations are also displayed: solid lines are computed with the Reichart et al. [102] method, dashed-dotted lines with the D'Agostini [153] method, and the dashed lines are recovered by Guidorzi et al. [149]. (Figure after Guidorzi et al. [151]; see Figure 1 therein.) (c) $\log L_{\rm peak}$- $\log V$ relation for the set of 551 BATSE GRBs. The best-fit lines and 1σ regions are also shown, the solid lines are fitted with the Reichart et al. [102] method, the dashed-dotted lines with the D'Agostini [153] method, and the dashed lines are recovered by Guidorzi et al. [149]. (Figure after Guidorzi et al. [151]; see Figure 2 therein.)

3.2.1. Literature Overview. Reichart et al. [102] used a total of 20 GRBs observed by *CGRO*/BATSE (13 bursts), the *KONUS*/Wind (5 bursts), the *Ulysses*/GRB (1 burst), and the *NEAR*/XGRS (1 burst), finding

$$\log L_{\rm peak} \sim \left(3.3^{+1.1}_{-0.9}\right) \log V, \tag{15}$$

with $\rho = 0.8$ and $P = 1.4 \times 10^{-4}$ (see Figure 3(a)); $L_{\rm peak}$ was computed in the 50–300 keV observer-frame energy band, which corresponds roughly to the range 100–1000 keV in the rest frame for $z \simeq$ 1-2, typical for GRBs in the sample examined. The distribution of the sample's bursts in the $\log L_{\rm peak}$- $\log V_f$ plane appears to be well modeled by the following parameterization:

$$\log V_f\,(L) = \log \overline{V}_f + b + m\left(\log L_{\rm peak} - \log \overline{L}_{\rm peak}\right), \tag{16}$$

where $b = 0.013^{+0.075}_{-0.092}$ is the intercept of the line, $m = 0.302^{+0.112}_{-0.075}$ is its slope, and $\overline{V}_f$ and $\overline{L}_{\rm peak}$ are the median values of V_f and $L_{\rm peak}$ for the bursts in the sample for which spectroscopic redshifts, peak fluxes, and 64 ms or better resolution light curves are available.

Later, Guidorzi et al. [149] updated the sample to 32 GRBs detected by different satellites, that is, *BeppoSAX*, *CGRO*/BATSE, *HETE-2*, and *KONUS* (see Figure 3(b)). The

existence of a correlation was confirmed, but they found a dramatically different relationship with respect to the original one:

$$\log L_{\rm peak} = 3.36^{+0.89}_{-0.43} + 1.30^{+0.84}_{-0.44} \log V, \quad (17)$$

with $\rho = 0.625$ and $P = 10^{-4}$, and $L_{\rm peak}$ in units of 10^{50} erg s^{-1}.

However, Reichart and Nysewander [150] using the same sample claimed that this result was the outcome of an improper statistical methodology and confirmed the previous work of Reichart et al. [102]. Indeed, they showed that the difference among their results and the ones from Guidorzi et al. [149] was due to the fact that the variance of the sample in the fit in [149] was not taken into account. They used an updated data set, finding that the fit was well described by the slope $m = 3.4^{+0.9}_{-0.6}$, with a sample variance $\sigma_V = 0.2 \pm 0.04$.

Subsequently, Guidorzi et al. [151], using a sample of 551 BATSE GRBs with pseudoredshifts derived using the $L_{\rm peak}$-$\tau_{\rm lag}$ relation [152], tested the $L_{\rm peak}$-V correlation (see Figure 3(c)). They also calculated the slope of the correlation of the samples using the methods implemented by Reichart et al. [102] and D'Agostini [153]. The former method provided a value of the slope in the $L_{\rm peak}$-V correlation consistent with respect to the previous works:

$$\log L_{\rm peak} \sim 3.5^{+0.6}_{-0.4} \log V. \quad (18)$$

Instead, the slope for this sample using the latter method is much lower than the value in [102]:

$$\log L_{\rm peak} \sim 0.88^{+0.12}_{-0.13} \log V. \quad (19)$$

The latter slope m is consistent with the results obtained by Guidorzi et al. [149], but inconsistent with the results derived by Reichart and Nysewander [150].

Afterwards, Rizzuto et al. [154] tested this correlation with a sample of 36 LGRBs detected by *Swift* in the 15–350 keV energy range and known redshifts. The sample consisted of bright GRBs with $L_{\rm peak} > 5 \times 10^{50}$ erg s^{-1} within 100–1000 keV energy range. In their study, they adopted two definitions of variability, presented by Reichart et al. [102], called $V_{\rm R}$, and by Li and Paczyński [114], hereafter $V_{\rm LP}$. $V_{\rm R}$ and $V_{\rm LP}$ differ from each other with a different smoothing filter which, in the second case, selects only high-frequency variability. Finally, Rizzuto et al. [154] confirmed the correlation and its intrinsic dispersion around the best-fitting power law given by

$$\log L_{\rm peak} \sim (2.3 \pm 0.17) \log V_{\rm LP}, \quad (20)$$

with $\rho = 0.758$ and $P = 0.011$, and

$$\log L_{\rm peak} \sim (1.7 \pm 0.4) \log V_{\rm R}, \quad (21)$$

with $\sigma_{\log L} = 0.58^{+0.15}_{-0.12}$, $\rho = 0.115$, and $P = 0.506$. Six low-luminosity GRBs (i.e., GRB050223, GRB050416A, GRB050803, GRB051016B, GRB060614, and GRB060729), out of a total of 36 in the sample, are outliers of the correlation, showing values of $V_{\rm R}$ higher than expected. Thus, the correlation is not valid for low-luminosity GRBs.

As is visible from this discussion, the scatter in this relation is not negligible, thus making it less reliable than the previously discussed ones. However, investigating the physical explanation of this correlation is worth being depicted for further developments.

3.2.2. Physical Interpretation of the L_{peak}-V Relation. We here briefly describe the internal and external shock model [80, 155], in which the GRB is caused by emission from a relativistic, expanding baryonic shell with a Lorentz bulk factor Γ. Let there be a spherical section with an opening angle $\theta_{\rm jet}$. In general, $\theta_{\rm jet}$ can be greater than Γ^{-1}, but the observer can detect radiation coming only from the angular region with size $\simeq \Gamma^{-1}$. An external shock is formed when the expanding shell collides with the external medium. In general, there might be more than one shell, and the internal shock takes place when a faster shell reaches a slower one. In both cases one distinguishes an FS, when the shock propagates into the external shell or the external medium, and a reverse shock (RS), when it propagates into the inner shell.

Fenimore and Ramirez-Ruiz [148] pointed out that the underlying cause of the $L_{\rm peak}$-V relation is unclear. In the context of the internal shock model, larger initial Γ factors tend to produce more efficient collisions. After changing some quantities such as the Γ factors, the ambient density, and/or the initial mass of the shells, the observed variability values are not recovered. Therefore, the central engine seems to play a relevant role in the explanation for the observed $L_{\rm peak}$-V correlation. In fact, this correlation was also explored within the context of a model in which the GRB variability is due to a change in the jet-opening angles and narrower jets have faster outflows [156]. As a result, this model predicts bright luminosities, small pulse lags, and large variability as well as an early jet break time for on-axis observed bursts. On the other hand, dimmer luminosities, longer pulse lags, flatter bursts, and later jet break times will cause larger viewing angles.

Guidorzi et al. [151] gave an interpretation for the smaller value of the correlation in the context of the jet-emission scenario where a stronger dependence of Γ of the expanding shells on the jet-opening angle is expected. However, Schaefer [157] attributed the origin of the $L_{\rm peak}$-V relation to be based on relativistically shocked jets. Indeed, V and $L_{\rm peak}$ are both functions of Γ, where $L_{\rm peak}$ is proportional to a high power of Γ, as was already demonstrated in the context of the $L_{\rm peak}$-$\tau_{\rm lag}$ relation (see Section 3.1.2), and hence fast rise times and short pulse durations imply high variability.

3.3. The L_{iso}-τ_{RT} Correlation and Its Physical Interpretation. Schaefer [158] predicted that $\tau_{\rm RT}$ should be connected with $L_{\rm iso}$ in a following manner:

$$L_{\rm iso} \propto \tau_{\rm RT}^{-N/2}, \quad (22)$$

with the exponent $N \simeq 3$ (see also Schaefer [157, 158]). Therefore, fast rises indicate high luminosities and slow rises low luminosities. $\tau_{\rm RT}$ can be directly connected to the physics of the shocked jet. Indeed, for a sudden collision of a material within a jet (with the shock creating an individual pulse

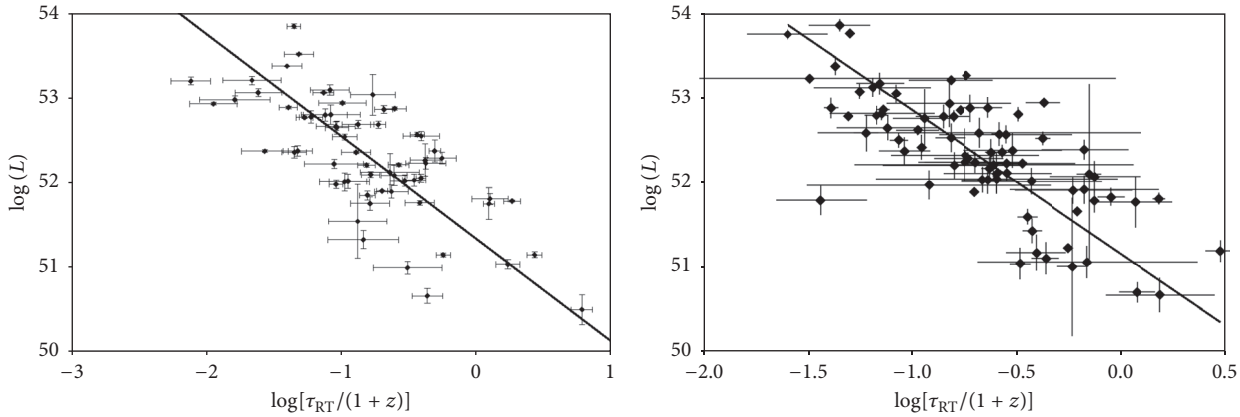

FIGURE 4: (a) The $\log L_{\rm iso}$- $\log \tau^*_{\rm RT}$ relation with the best-fit line displayed. The errors are given by the 1σ confidence interval. (Figure after Schaefer [157]; see Figure 5 therein. @ AAS. Reproduced with permission.) (b) The $\log L_{\rm iso}$- $\log \tau^*_{\rm RT}$ correlation with the best fit line. (Figure after Xiao and Schaefer [159]; see Figure 3 therein. @ AAS. Reproduced with permission.)

in the GRB light curve), $\tau_{\rm RT}$ will be determined as the maximum delay between the arrival time of photons from the center of the visible region versus their arrival time from its edge.

The angular opening of the emitted jet, usually associated with Γ, could cause this delay leading to a relation $\tau_{\rm RT} \propto \Gamma^{-2}$. The radius at which the material is shocked affects the proportionality constant, and the minimum radius under which the material cannot radiate efficiently anymore should be the same for each GRB [139]. In addition, a large scatter is expected depending on the distance from which the collisions are observed.

With both $\tau_{\rm RT}$ and $L_{\rm iso}$ being functions of Γ, Schaefer [157] confirmed that $\log L_{\rm iso}$ should be $\sim -N/2 \log \tau_{\rm RT}$. From 69 GRBs detected by BATSE and *Swift*, the following relation was obtained:

$$\log L_{\rm iso} = 53.54 - 1.21 \log \tau^*_{\rm RT}, \tag{23}$$

with $L_{\rm iso}$ in erg s^{-1} and $\tau^*_{\rm RT}$ measured in seconds. The 1σ uncertainties in the intercept and slope are $\sigma_a = 0.06$ and $\sigma_b = 0.06$ (see Figure 4(a)). The uncertainty in the log of the burst luminosity is

$$\sigma^2_{\log L_{\rm iso}} = \sigma^2_a + \left[\sigma_b \log \frac{\tau^*_{\rm RT}}{0.1\ {\rm s}}\right]^2 + \left(\frac{0.43 b \sigma_{\rm RT}}{\tau_{\rm RT}}\right)^2 + \sigma^2_{\rm RT,sys}, \tag{24}$$

where Schaefer [157] takes into account the extra scatter, $\sigma_{\rm sys}$. When $\sigma_{\rm RT,sys} = 0.47$, χ^2 of the best-fit line is unity.

Xiao and Schaefer [159] explained in detail the procedure of how they calculated $\tau_{\rm RT}$ using 107 GRBs with known spectroscopic redshift observed by BATSE, *HETE*, *KONUS*, and *Swift* (see Figure 4(b)), taking into account also the Poissonian noise. Their analysis yielded

$$\log L_{\rm iso} = 53.84 - 1.70 \log \tau^*_{\rm RT}, \tag{25}$$

with the same units as in (23). As a consequence, the flattening of the light curve before computing the rise time is an important step. The problem is that the flattening should be done carefully, in fact if the light curve is flattened too much, a rise time comparable with the smoothing-time bin is obtained, while if it is flattened not enough, the Poissonian noise dominates the apparent fastest rise time, giving a too small rise time. Therefore, for some of the dimmest bursts, the Poissonian-noise dominant region and the smoothing-effect dominant region can coincide, thus not yielding $\tau_{\rm RT}$ values for the weakest bursts. Finally, the physical interpretation of this correlation is given by Schaefer [157]. It is shown that the fastest rise in a light curve is related to the Lorentz factor Γ simply due to the geometrical rise time for a region subtending an angle of $1/\Gamma$, assuming that the minimum radius for which the optical depth of the jet material is of order of unity remains constant. The luminosity of the burst is also a power law of Γ, which scales as Γ^N for $3 < N < 5$. Therefore, the $\tau_{\rm RT}$-Γ and the $L_{\rm iso}$-Γ relations together yield the observed $L_{\rm iso}$-$\tau_{\rm RT}$ relation.

3.4. The Γ_0-E_{prompt} and Γ_0-L_{iso} Correlations and Their Physical Interpretation. Freedman and Waxman [160] in their analysis of the GRB emission, considering a relativistic velocity for the fireball, showed that the radiation detected by an observer is within an opening angle $\simeq 1/\Gamma(t)$. Hence, the total fireball energy E should be interpreted as the energy that the fireball would have carried if this is assumed spherically symmetric. In particular, it was claimed that the afterglow flux measurements in X-rays gave a strong evaluation for the fireball energy per unit solid angle represented by $\epsilon_e = \xi_e E/4\pi$, within the observable opening angle $1/\Gamma(t)$, where ξ_e is the electron energy fraction. It was found that

$$\Gamma(t) = 10.6 \left(\frac{1+z}{2}\right)^{3/8} \left(\frac{E_{\rm prompt}}{n_0}\right)^{1/8} t^{-3/8}, \tag{26}$$

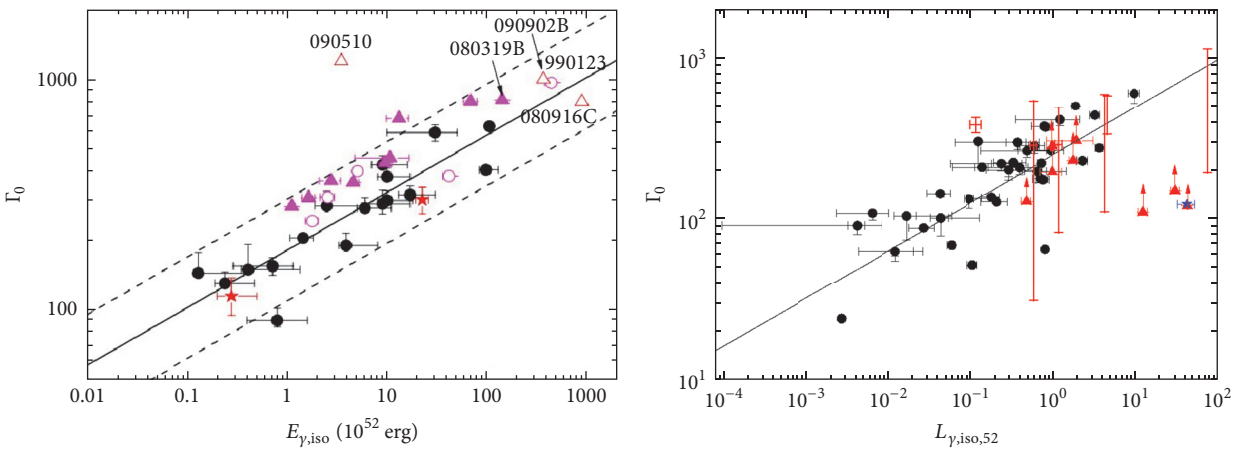

FIGURE 5: (a) $\log\Gamma_0$-$\log E_{\mathrm{prompt}}$ relation with the addition of GRBs with an onset trend in the X-ray band (GRBs 070208 and 080319C; red stars), Γ_0 computed by RS peaks or probable afterglow peaks (pink open circles), lower values of Γ_0 obtained from single power law decay light curves (pink solid triangles), and strong lower values of Γ_0 for *Fermi*/LAT GRBs 080916C, 090902B, and 090510 (red open triangles) calculated from opacity limits with *Fermi*/LAT observations. The solid line indicates the best fit of the Γ_0-E_{prompt} relation, $\log\Gamma_0 = 2.26 + 0.25\log E_{\mathrm{prompt}}$. The two dashed lines represent the 2σ deviation, where the standard deviation of the ratio $\Gamma_0/E^{0.25}_{\mathrm{prompt}}$ for the data sample is $\sigma = 0.11$. (Figure after Liang et al. [164]; see Figure 8 therein. @ AAS. Reproduced with permission.) (b) $\log\Gamma_0$ versus $\log L_{\mathrm{iso}}$ distribution. The best-fit line is given by $\log\Gamma_0 \simeq 2.40 + 0.30\log L_{\mathrm{iso}}$ with $r = 0.79$. The triangles represent the bursts with only lower values and the star indicates the only short burst in the sample, GRB090510. (Figure after Lü et al. [143]; see Figure 2 therein. @ AAS. Reproduced with permission.)

where E_{prompt} is in units of 10^{53} erg, n_0 is the uniform ambient density of the expanding fireball in units of cm^{-3}, and t is the time of the fireball expansion in days. Finally, it was pointed out that ξ_e from the afterglow observations should be close to equipartition, namely, $\xi_e \simeq 1/3$. For example, for GRB970508, it was found that $\xi_e \simeq 0.2$ [161–163]. A similar conclusion, that is, that it is also close to equipartition, could be drawn for GRB971214; however Wijers and Galama [162] proposed another interpretation for this GRB's data, demanding $\xi_e \simeq 1$.

Liang et al. [164] selected from the *Swift* catalogue 20 optical and 12 X-ray GRBs showing the onset of the afterglow shaped by the deceleration of the fireball due to the circumburst medium. The optically selected GRBs were used to fit a linear relation in the $\log\Gamma_0$-$\log E_{\mathrm{prompt}}$ plane, where Γ_0 is the initial Lorentz factor of the fireball and E_{prompt} is in units of 10^{52} erg (see Figure 5(a)). The best-fit line of the Γ_0-E_{prompt} relation is given by

$$\log\Gamma_0 = (2.26 \pm 0.03) + (0.25 \pm 0.03)\log E_{\mathrm{prompt}}, \quad (27)$$

with $\rho = 0.89$, $P < 10^{-4}$, and $\sigma = 0.11$ which can be measured with the deviation of the ratio $\Gamma_0/E^{0.25}_{\mathrm{prompt}}$. It was found that most of the GRBs with a lower limit of Γ_0 are enclosed within the 2σ region represented by the dashed lines in Figure 5(a), and it was pointed out that GRBs with a tentative Γ_0 derived from RS peaks or the afterglow peaks, as well as those which lower limits of Γ_0 were derived from light curves with a single power law, are systematically above the best-fit line. The lower values of Γ_0, obtained from a set of optical afterglow light curves with a decaying trend since the start of the detection, were compatible with this correlation.

Later, this correlation was verified by Ghirlanda et al. [165] and Lü et al. [143]. Ghirlanda et al. [165], studying the spectral evolution of 13 SGRBs detected by *Fermi*/GBM, investigated spectra resolved in the 8 keV–35 MeV energy range, and confirmed the results of Liang et al. [164].

Lü et al. [143] enlarged this sample reaching a total of 51 GRBs with spectroscopically confirmed redshifts and engaged three methods to constrain Γ_0: (1) the afterglow onset method [166] which considers T_{peak} of the early afterglow light curve as the deceleration time of the external FS; (2) the pair opacity constraint method [167] which requires that the observed high-energy γ-rays (i.e., those in the GeV range) are optically thin to electron-positron pair production, thus leading to a lower limit on Γ_0 of the emitting region; (3) the early external forward emission method [168] where an upper limit of Γ_0 can be derived from the quiescent periods between the prompt emission pulses, in which the signal of external shock has to go down the instrument thresholds. Considering some aspects of the external shock emission, the Γ_0-E_{prompt} correlation was statistically reanalysed using 38 GRBs with Γ_0 calculated using method (1) (as the other two provide only a range of the Lorentz factors, not a definite value), finding

$$\log\Gamma_0 = (1.96 \pm 0.002) + (0.29 \pm 0.002)\log E_{\mathrm{prompt}}, \quad (28)$$

with $r = 0.67$, and E_{prompt} in units of 10^{52} erg. In addition, applying the beaming correction, a relation between Γ_0 and L_{iso}, using the same sample (see Figure 5(b)), was found to be

$$\log\Gamma_0 = (2.40 \pm 0.002) + (0.30 \pm 0.002)\log L_{\mathrm{iso}}, \quad (29)$$

with $r = 0.79$ and L_{iso} in units of 10^{52} erg s^{-1}.

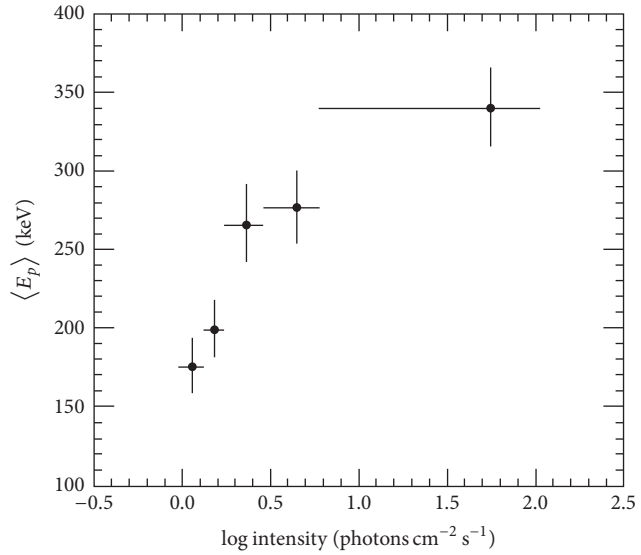

FIGURE 6: The average νF_ν peak energies as a function of intensity for five groups of GRB spectra. The vertical bars represent 1σ estimated error in the mean, where the peak energy distributions were assumed to be approximately Gaussian in logarithm of energy. The horizontal bars mark the bin widths. (Figure after Mallozzi et al. [110]; see Figure 2 therein. @ AAS. Reproduced with permission.)

Regarding the physical interpretation, Liang et al. [164] claimed that this correlation clearly shows the association of E_{prompt} with Γ_0 angular structure, and this result yielded another evidence for the fireball deceleration model. Instead, Lü et al. [143] found that this relation is well explained by a neutrino-annihilation-powered jet during the emission, indicating a high accretion rate and not very fast BH spin. Besides, evidence for a jet dominated by a magnetic field have already been presented [169–171]. From the studies of the BH central engine models it was also indicated that magnetic fields are a fundamental feature [172]. Nevertheless, the baryon loading mechanism in a strongly magnetized jet is more complex, and it has still to be fully investigated.

3.5. Correlations between the Energetics and the Peak Energy

3.5.1. The $\langle E_{peak} \rangle$-F_{peak} and the E_{peak}-S_{tot} Correlations. Mallozzi et al. [110] analysed 399 GRBs observed by BATSE and discovered a correlation between the logarithmic average peak energies $\langle E_{\text{peak}} \rangle$ and F_{peak}. Choosing as a selection criterion for the bursts $F_{\text{peak}} \geq 1$ ph cm^{-2} s^{-1}, they derived F_{peak} from the count rate data in 256 ms time bins in the energy band 50–300 keV and used the E_{peak} distribution derived from the Comptonized photon model (the differential photon number flux per unit energy):

$$\frac{dN}{dE} = A e^{-E(2+\beta_S)/E_{\text{peak}}} \left(\frac{E}{E_{\text{piv}}} \right)^{\beta_S}, \tag{30}$$

with A the normalization, β_S the spectral index, and $E_{\text{piv}} = 100$ keV. Then, they grouped the sample into 5 different width F_{peak} bins of about 80 events each (see Figure 6). The bursts were ranked such that group 1 had the lowest peak flux values and group 5 had the highest values. They found a correlation with $\rho = 0.90$ and $P = 0.04$. Lower intensity GRBs exhibited a lower $\langle E_{\text{peak}} \rangle$.

Later, Lloyd et al. [173] examined the E_{peak}-S_{tot} correlation with 1000 simulated bursts in the same energy range as Mallozzi et al. [110] and found a strong correlation between E_{peak} and S_{tot} (see Figure 7(a)). The relation between the two variables was as follows:

$$\log E_{\text{peak}} \sim 0.29 \log S_{\text{tot}}, \tag{31}$$

with the Kendall correlation coefficient [174] $\tau = 0.80$ and $P = 10^{-13}$. In addition, they compared it to the E_{peak}-F_{peak} relation (see Figure 7(b)). This relation was for the whole spectral sample and consistent with earlier results [110, 175]. However, they selected a subsample composed of only the most luminous GRBs, because spectral parameters obtained from bursts near the detector threshold are not robust. Therefore, to better understand the selection effects relevant to E_{peak} and burst strength, they considered the following selection criteria: $F_{\text{peak}} \geq 3$ ph cm^{-2} s^{-1}, $S_{\text{obs}} \geq 10^{-6}$ erg cm^{-2}, and $S_{\text{tot}} \geq 5 \times 10^{-6}$ erg cm^{-2}. Due to the sensitivity over a certain energy band of all the detectors, especially BATSE, and to some restrictions to the trigger, the selection effects are inevitable. However, the subsample of the most luminous GRBs presents a weak E_{peak}-F_{peak} correlation. Instead, a tight E_{peak}-S_{tot} correlation was found for the whole sample as well as the subsample of the brightest GRBs. Lloyd et al. [173] paid more attention to the E_{peak}-S_{tot} correlation for the brightest GRBs because it is easier to deal with the truncation effects in this case, and the cosmological interpretation is simpler.

This correlation has been the basis for the investigation of the Amati relation (see Section 3.5.2) and the Ghirlanda relation (see Section 3.5.3). Lloyd et al. [173] concluded that "the observed correlation can be explained by cosmological expansion alone if the total radiated energy (in the γ-ray range) is constant." In fact, their finding does not depend on the GRB rate density or on the distribution of other parameters. However, the data from GRBs with known redshift are incompatible with a narrow distribution of radiated energy or luminosity.

Following a different approach, Goldstein et al. [176] pointed out that the ratio $E_{\text{peak}}/S_{\text{tot}}$ can serve as an indicator of the ratio of the energy at which most of the γ-rays are radiated to the total energy and claimed that the E_{peak}-S_{tot} relation is a significant tool for classifying LGRBs and SGRBs. The fluence indicates the duration of the burst without providing a biased value of T_{90} and $E_{\text{peak}}/S_{\text{tot}}$ displays, as a spectral hardness ratio, an increased hardness for SGRBs in respect to LGRBs, in agreement with [10]. This correlation is quite interesting, since the energy ratio, being dependent only on the square of the luminosity distance, gets rid of the cosmological dependence for the considered quantities. Therefore, it was evaluated that the energy ratio could be used as a GRB classifier.

Later, Lu et al. [177], with the results of time-resolved spectral analysis, computed the E_{peak}-S_{tot} relation for 51 LGRBs and 11 bright SGRBs observed with *Fermi*/GBM. For

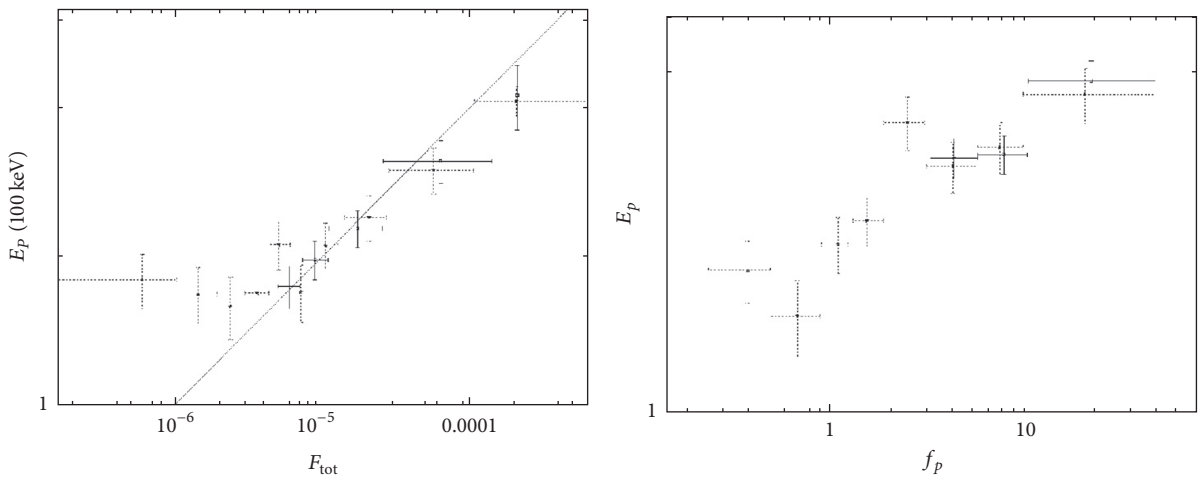

FIGURE 7: $E_{\rm peak}$ versus (a) $S_{\rm tot}$ and (b) $F_{\rm peak}$ distributions for the complete (dashed elements) and sub (solid elements) spectral sample. The flux suggests a tight correlation at low values, but not for the most luminous GRBs. The solid line represents a least squares fit compatible with the correlation computed by statistical methods. (Figures after Lloyd et al. [173]; see Figure 3 therein. @ AAS. Reproduced with permission.)

each GRB, they fitted a simple power law function. They measured its scatter with the distance of the data points from the best-fit line. The measured scatter of the $E_{\rm peak}$-$S_{\rm tot}$ relation is 0.17 ± 0.08. This result was reported for the first time by Golenetskii et al. [178] and later confirmed by Borgonovo and Ryde [179]; Ghirlanda et al. [180]; Guiriec et al. [181]; Ghirlanda et al. [165].

3.5.2. The E_{peak}-E_{iso} Correlation. Evidence for a correlation between $E_{\rm peak}$ and $S_{\rm tot}$ was first found by Lloyd and Petrosian [182] and Lloyd et al. [183] based on 46 BATSE events, but this relation was in the observer frame due to the paucity of the data with precise redshift measurement, as was shown in previous paragraphs. Evidence for a stronger correlation between $E_{\rm peak}$ and $E_{\rm iso}$, also called the Amati relation, was reported by Amati et al. [111] based on a limited sample of 12 GRBs with known redshifts (9 with firm redshift and 3 with plausible values) detected by *BeppoSAX*. They found that

$$\log E_{\rm peak} \sim (0.52 \pm 0.06) \log E_{\rm iso}, \tag{32}$$

with $r = 0.949$, $P = 0.005$, and $E_{\rm iso}$ calculated as

$$E_{\rm iso} = 4\pi D_L \left(z, \Omega_M, \Omega_\Lambda\right)^2 S_{\rm tot} \left(1+z\right)^{-2}. \tag{33}$$

Regarding the methodology considered, instead of fitting the observed spectra, as done, for example, by Bloom et al. [184], the GRB spectra were blue-shifted to the rest frames to obtain their intrinsic form. Then, the total emitted energy is calculated by integrating the Band et al. [115] spectral model in 1–10^4 keV energy band and scaling for the luminosity distance. This was computed employing a flat Friedmann-Lemaitre-Robertson-Walker cosmological model with $H_0 = 65\,{\rm km\,s^{-1}\,Mpc^{-1}}$, $\Omega_M = 0.3$, $\Omega_\Lambda = 0.7$ and taking into account both the cosmological time dilation and spectral redshift.

Amati et al. [185] enlarged the set of Amati et al. [111] by including 20 GRBs from *BeppoSAX* with known redshift for which new spectral data (*BeppoSAX* events) or published best-fitting spectral parameters (BATSE and *HETE-2* events) were accessible. The relation was found to be

$$\log E_{\rm peak} = (2.07 \pm 0.03) + (0.35 \pm 0.06) \log E_{\rm iso}, \tag{34}$$

with $r = 0.92$, $P = 1.1 \times 10^{-8}$, $E_{\rm peak}$ in keV and $E_{\rm iso}$ in units of 10^{52} erg. Therefore, its statistical significance increased, providing a correlation coefficient comparable to that obtained by Amati et al. [111], but based on a larger set.

Based on *HETE-2* measurements, Lamb et al. [186] and Sakamoto et al. [187] verified the previous results and considered also XRFs, finding out that the Amati relation remains valid over three orders of magnitude in $E_{\rm peak}$ and five orders of magnitude in $E_{\rm iso}$. The increasing amount of GRBs with measured redshift allowed verifying this relation and strengthen its validity, as found by Ghirlanda et al. [188] with 29 events ($r = 0.803$ and $P = 7.6 \times 10^{-7}$; see Figure 9(a)).

Ghirlanda et al. [189] verified the $E_{\rm peak}$-$E_{\rm iso}$ correlation among LGRBs considering a set of 442 BATSE GRBs with measured $E_{\rm peak}$ and with pseudoredshifts computed via the $L_{\rm peak}$-$\tau_{\rm lag}$ correlation. It was shown that the scatter of the sample around the best-fitting line is comparable with that of another set composed of 27 GRBs with measured spectroscopic redshifts. This is because the weights of the outliers were marginal. It was noted that the relation for the 442 BATSE GRBs has a slope slightly smaller (0.47) than the one obtained for the 27 GRBs with measured spectroscopic redshifts (0.56).

Afterwards, Amati [190] (see Figures 8(a) and 8(c)) updated the study of the $E_{\rm peak}$-$E_{\rm iso}$ correlation considering a sample of 41 LGRBs/XRFs with firm values of z and $E_{\rm peak}$, 12 GRBs with uncertain z and/or $E_{\rm peak}$, 2 SGRBs with certain values of z and $E_{\rm peak}$, and the subenergetic events

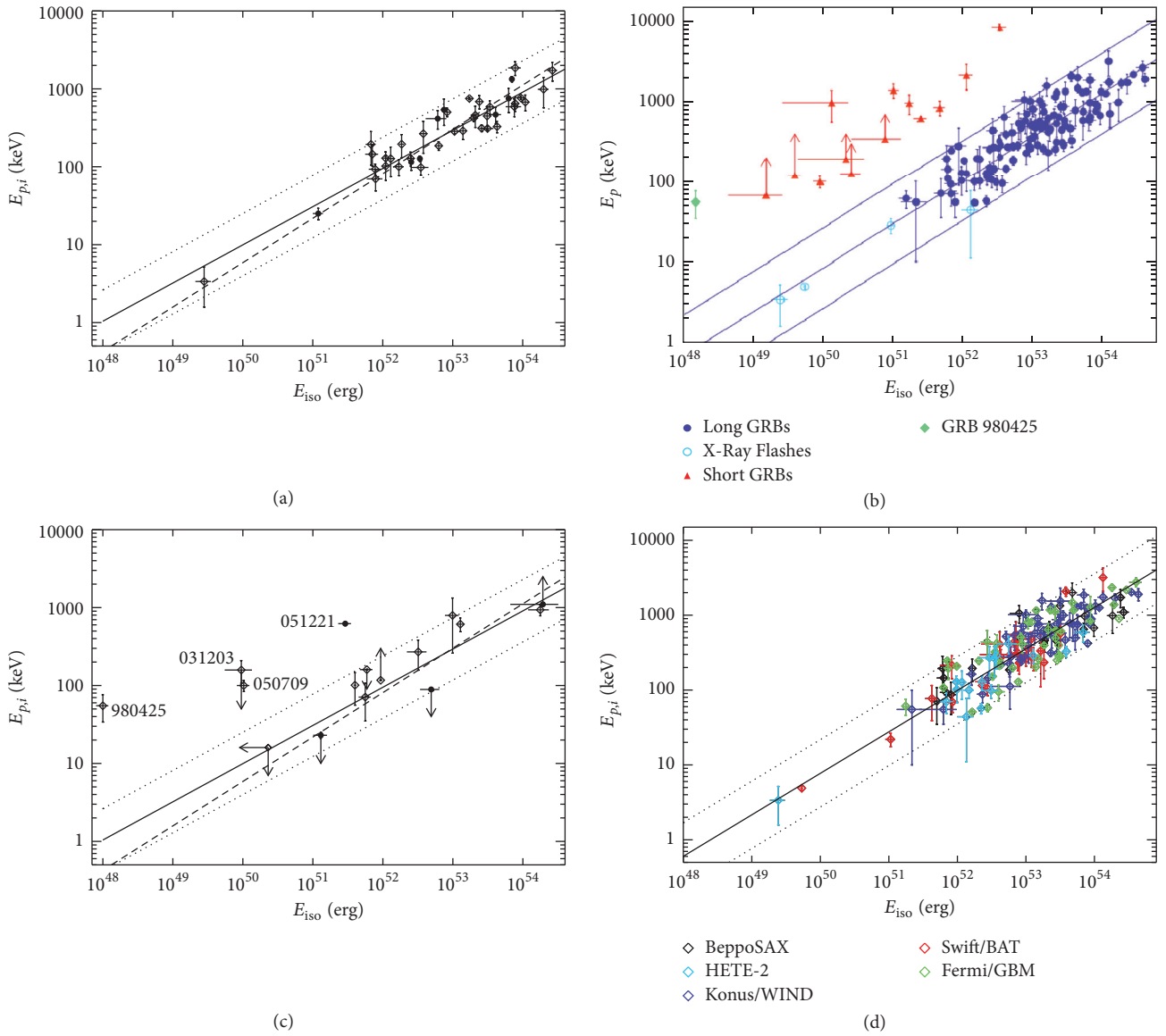

FIGURE 8: (a) E_{peak}-E_{iso} distribution for 41 GRBs/XRFs with measured redshifts and E_{peak} values. Filled circles indicate Swift GRBs. The solid line represents the best-fit line $\log E_{peak} = 1.98 + 0.49 \log E_{iso}$; the dotted lines show the region within a vertical logarithmic deviation of 0.4. The dashed line represents the best-fit line $\log E_{peak} = 1.89 + 0.57 \log E_{iso}$ computed without taking into account the sample variance. (Figure after Amati [190]; see Figure 2 therein.) (b) The distribution of the sample in the E_{peak}-E_{iso} plane. The lines indicate the best-fit line and the $\pm 2\sigma$ confidence region for LGRBs and XRFs. (Figure after Amati [193]; see Figure 4 therein. Copyright @ 2012 World Scientific Publishing Company.) (c) E_{peak}-E_{iso} distribution of 12 GRBs with uncertain values of z and/or E_{peak}, for the subenergetic event GRB980425 and for the two SGRBs 050709 and 051221. Filled circles represent *Swift* GRBs. The solid line is the best-fit line $\log E_{peak} = 1.98 + 0.49 \log E_{iso}$; the dotted lines mark the region within a vertical deviation in logarithmic scale of 0.4. The dashed line is the best-fit line $\log E_{peak} = 1.89 + 0.57 \log E_{iso}$ computed without taking into account the sample variance. (Figure after Amati [190]; see Figure 3 therein.) (d) The E_{peak}-E_{iso} distribution for the LGRBs. The black line represents the best-fit line and, for each point, the color indicates the instrument which performed the spectral measurement. (Figure after Amati and Valle [197]; see Figure 4 therein. Copyright @ 2013 World Scientific Publishing Company.)

GRB980425/SN1998bw and GRB031203/SN2003lw. The different sets are displayed in Figure 8(b). Taking into account also the sample variance, it was found that

$$\log E_{peak} = 1.98^{+0.05}_{-0.04} + \left(0.49^{+0.06}_{-0.05}\right) \log E_{iso}, \qquad (35)$$

with $\rho = 0.89$, $P = 7 \times 10^{-15}$, and units being the same as in (34). Moreover, subenergetic GRBs (980425 and possibly 031203) and SGRBs were incompatible with the E_{peak}-E_{iso} relation, suggesting that it can be an important tool for distinguishing different classes of GRBs. Indeed, the increasing number of GRBs with measured z and E_{peak} can provide the most reliable evidence for the existence of two or more subclasses of outliers for the E_{peak}-E_{iso} relation. Moreover, the relation is valid also for the particular subenergetic event

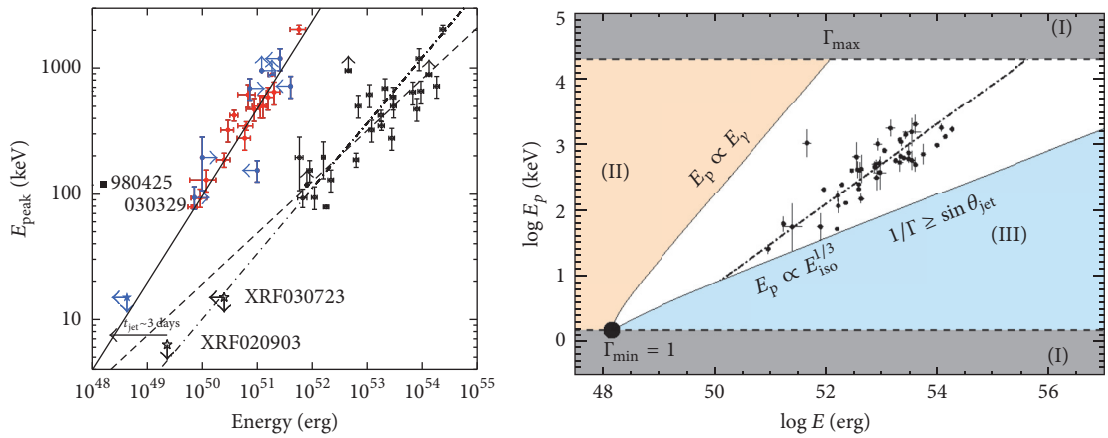

FIGURE 9: (a) E^*_{peak}-E_γ relation for GRBs with known redshift. The filled circles represent E_γ for the events where a jet break was detected. Grey symbols indicate lower/upper limits. The solid line represents the best fit, that is, $\log E_{peak} \sim 53.68 + 0.7 \log E_\gamma$. Open circles denote E_{iso} for the GRBs. The dashed line represents the best fit to these points and the dash-dotted line is the relation shown by Amati et al. [111]. (Figure after Ghirlanda et al. [188]; see Figure 1 therein. @ AAS. Reproduced with permission.) (b) Rest frame plane of GRB energy. The large black dot indicates that all simulated GRBs were assigned $E^*_{peak} = 1.5$ keV and $E^*_\gamma = 1.5 \times 10^{48}$ erg. Since $\Gamma > 1$ but less than 8000, regions (I) are forbidden. Since for all the simulated GRBs $\theta_{jet} \leq 90^\circ$, they cannot stay in region (II). When Γ is small, the beaming cone turns out to be larger than the jet. Therefore, the isotropic-equivalent energy is given by $\log E_{iso} = \log E_\gamma + \log(1 + \beta_0) + 2 \log \Gamma$, lower than the energy computed by $\log E_{iso} = \log E_\gamma - \log(1 - \cos\theta_{jet})$. This brings in a constraint, $\log E_{peak} \sim 1/3 \times \log E_{iso}$, and GRBs cannot lie to the right of this constraint. Hence, region (III) is not allowed. The black dots indicate the actual GRBs of the *Swift* sample. The fit to the Swift sample is displayed as the dot-dashed line. (Figure after Ghirlanda et al. [209]; see Figure 1 therein.)

GRB060218. Finally, the normalization considered by Amati [190] is consistent with those obtained by other instruments.

Ghirlanda et al. [191] confirmed the E_{peak}-E_{iso} correlation for softer events (XRFs). The sample consisted of 76 GRBs observed by several satellites, mainly *HETE-2*, *KONUS*/Wind, *Swift*, and *Fermi*/GBM. The most important outcome is a tight correlation with no new outliers (with respect to the classical GRB980425 and GRB031203) in the E_{peak}-E_{iso} plane. The obtained relation was

$$\log E_{peak} \sim (0.54 \pm 0.01) \log E_{iso}. \quad (36)$$

Amati et al. [192] studied 95 *Fermi* GRBs with measured z and obtained an updated E_{peak}-E_{iso} relation, which read

$$\log E_{peak} \sim 0.57 \log E_{iso}, \quad (37)$$

with $\rho = 0.88$ and $P < 10^{-3}$. In particular, they investigated two GRBs (080916C and 090323) with very energetic prompt emission and found that they follow the E_{peak}-E_{iso} relation well. On the other hand, an SGRB, 090510, also a very luminous and energetic event, was found not to obey the relation. Hence, Amati et al. [192] proposed that the correlation might serve as a discriminating factor among high-energetic GRBs. In addition, they claimed that the physics of the radiation process for really luminous and energetic GRBs is identical to that for average-luminous and soft-dim long events (XRFs), because all these groups follow the Amati relation.

Later, Amati [193] provided an update of the analysis by Amati et al. [194] with a larger sample of 120 GRBs (see Figure 8(b)) finding it to be consistent with the following relation:

$$\log E_{peak} = 2 + 0.5 \log E_{iso}. \quad (38)$$

with units the same as in (34) and (35). Afterwards, Qin and Chen [195] analysed a sample of 153 GRBs with measured z, E_{peak}, E_{iso}, and T_{90}, observed by various instruments up to 2012 May. The distribution of the logarithmic deviation of E_{peak} from the Amati relation displayed a clear bimodality which was well represented by a mixture of two Gaussian distributions. Moreover, it was suggested to use the logarithmic deviation of the E_{peak} value for distinguishing GRBs in the E_{peak} versus E_{iso} plane. This procedure separated GRBs into two classes: the Amati type bursts, which follow the Amati relation, and the non-Amati type bursts, which do not follow it. For the Amati type bursts it was found that

$$\log E_{peak} = (2.06 \pm 0.16) + (0.51 \pm 0.12) \log E_{iso}, \quad (39)$$

with $r = 0.83$ and $P < 10^{-36}$, while, for non-Amati bursts,

$$\log E_{peak} = (3.16 \pm 0.65) + (0.39 \pm 0.33) \log E_{iso}, \quad (40)$$

with $r = 0.91$ and $P < 10^{-7}$. In both relations E_{peak} is in keV, and E_{iso} is in units of 10^{52} erg.

In addition, it was pointed out that almost all Amati type bursts are LGRBs at higher energies, as opposed to non-Amati type bursts which are mostly SGRBs. An improvement to this classification procedure is that the two types of GRBs are clearly separated; hence different GRBs can be easily classified.

Heussaff et al. [196], applying particular selection criteria for the duration and the spectral indices, obtained a set of *Fermi* GRBs and analysed their locations in the $E_{\rm peak}$-$E_{\rm iso}$ plane. The sample, composed of 43 GRBs with known redshifts, yielded the following relation:

$$\log E_{\rm peak} = 2.07 + 0.49 \log E_{\rm iso}, \tag{41}$$

with $\rho = 0.70$, $P = 1.7 \times 10^{-7}$, and the same units as in previous relations of this type.

Amati and Della Valle [197] pointed out that an enlarged sample of 156 LGRBs with known z and $E_{\rm peak}$ also follows the Amati relation with a slope $\simeq 0.5$ (see Figure 8(d)). Additionally, Basak and Rao [198] showed that a time-resolved Amati relation also holds within each single GRB with normalization and slope consistent with those obtained with time-averaged spectra and energetics/luminosity and is even better than the time-integrated relation [199]. Time-resolved $E_{\rm peak}$ and $E_{\rm iso}$ are obtained at different times during the prompt phase (see also [177, 180, 200] and Section 3.6).

3.5.3. The E_{peak}-E_γ Correlation. The $E_{\rm peak}$-E_γ relation (also called the Ghirlanda relation) was first discovered by Ghirlanda et al. [188], who used 40 GRBs with z and $E_{\rm peak}$ known at their time of writing. Considering the time $T_{\rm break}$, its value can be used to deduce E_γ from $E_{\rm iso}$. Indeed, even if only a little less than half of the bursts have observed jet breaks (47%), from [107] we know that

$$\theta_{\rm jet} = 0.161 \left(\frac{T_{\rm break}}{1+z}\right)^{3/8} \left(n \eta_\gamma E_{\rm iso}\right)^{1/8}, \tag{42}$$

where $T_{\rm break}$ is measured in days, n is the density of the circumburst medium in particles per cm^3, η_γ is the radiative efficiency, and $E_{\rm iso}$ is in units of 10^{52} erg. Here, $\theta_{\rm jet}$ is in degrees and it is the angular radius (the half opening angle) subtended by the jet. For GRBs with no measured n, the median value $n = 3\ {\rm cm}^{-3}$ of the distribution of the computed densities, extending between 1 and 10 cm^{-3}, was considered [139, 201–203].

Later, Liang and Zhang [204] using a sample of 15 GRBs with measured z, $E_{\rm peak}$ and $T_{\rm break}$, considered a purely phenomenological $T^*_{\rm break}$ of the optical afterglow light curves, thus avoiding the assumption of any theoretical model, contrary to what was done by Ghirlanda et al. [188]. The functional form of this correlation is given by:

$$\log E_\gamma = (0.85 \pm 0.21) + (1.94 \pm 0.17) \log E^*_{\rm peak} - (1.24 \pm 0.23) \log T^*_{\rm break}, \tag{43}$$

where E_γ is in units of 10^{52} erg, $E^*_{\rm peak}$ in units of 100 keV, $T^*_{\rm break}$ is measured in days, and $\rho = 0.96$ and $P < 10^{-4}$.

Nava et al. [205] found that the Ghirlanda relation, assuming a wind-like circumburst medium, is as strong as the one considering a homogeneous medium. They analysed the discrepancy between the correlations in the observed and in the comoving frame (with Lorentz factor identical to the fireball's one). Since both $E_{\rm peak}$ and E_γ transform in the same way, the wind-like Ghirlanda relation remains linear also in the comoving frame, no matter what the Lorentz factor's distribution is. The wind-like relation corresponds to bursts with the same number of photons emitted. Instead, for the homogeneous density medium scenario, it is common to consider a tight relation between the Lorentz factor and the total energy, thus limiting the emission models of the prompt radiation. Using 18 GRBs with firm z, $E_{\rm peak}$, and $T_{\rm break}$, Nava et al. [205] found for the homogeneous density case

$$\log \frac{E^*_{\rm peak}}{100\ {\rm keV}} = 0.45^{+0.02}_{-0.03} + (0.69 \pm 0.04) \log \frac{E_\gamma}{2.72 \times 10^{52}\ {\rm erg}}, \tag{44}$$

with $\rho = 0.93$ and $P = 2.3 \times 10^{-8}$. Instead, for the wind case

$$\log \frac{E^*_{\rm peak}}{100\ {\rm keV}} = 0.48^{+0.02}_{-0.03} + (1.03 \pm 0.06) \log \frac{E_\gamma}{2.2 \times 10^{50}\ {\rm erg}}, \tag{45}$$

with $\rho = 0.92$ and $P = 6.9 \times 10^{-8}$.

Ghirlanda et al. [206] tested the $E_{\rm peak}$-E_γ correlation using 33 GRBs (16 new bursts detected by *Swift* with firm z and $E_{\rm peak}$ up to December 2006, and 17 pre-*Swift* GRBs). They claimed that, for computing $T_{\rm break}$, the following is required:

(1) The detection of the jet break should be in the optical.

(2) The optical light curve should continue up to a time longer than the $T_{\rm break}$.

(3) The host galaxy flux and the flux from a probable SN should be removed.

(4) The break should not depend on the frequency in the optical, and a coincident break in the X-ray light curve is not necessary, because the flux in X-rays could be controlled by another feature.

(5) The considered $T_{\rm break}$ should be different from the one at the end of the plateau emission (the time T_a in [81]); otherwise the feature affecting the X-ray flux is also influencing the optical one.

Therefore, considering all these restrictions, the sample was reduced to 16 GRBs, all compatible with the following $E_{\rm peak}$-E_γ relation:

$$\log \frac{E_{\rm peak}}{100\ {\rm keV}} = (0.48 \pm 0.02) + (0.70 \pm 0.04) \log \frac{E_\gamma}{4.4 \times 10^{50}\ {\rm erg}}. \tag{46}$$

No outliers were detected. Therefore, the reduced scatter of the $E_{\rm peak}$-E_γ relation corroborates the use of GRBs as standardizable candles.

3.5.4. Physical Interpretation of the Energetics versus Peak Energy Relations. Lloyd et al. [173] investigated the physical explanation of the $E_{\rm peak}$-$S_{\rm tot}$ correlation assuming the emission process to be a synchrotron radiation from internal and external shocks. Indeed, they claimed that this correlation is easily obtained considering a thin synchrotron radiation by a power law distribution of electrons with Γ larger than some minimum threshold value, Γ_m. Moreover, the internal shock model illustrates the tight $E_{\rm peak}$-$S_{\rm tot}$ relation and the emitted energy better than the external shock model.

Lloyd-Ronning and Petrosian [207] pointed out that the GRB particle acceleration is not a well analysed issue. Generally, the main hypothesis is that the emitted particles are accelerated via recurrent scatterings through the (internal) shocks. They found that the recurrent crossings of the shock come from a power law distribution of the particles with a precise index, providing a large energy synchrotron photon index. Moreover, the connection between $E_{\rm peak}$ and the photon flux can be justified by the variation of the magnetic field or electron energy in the emission events. Finally, they claimed that, in the majority of GRBs, the acceleration of particles is not an isotropic mechanism but occurs along the magnetic field lines.

Amati et al. [111] confirmed the findings of Lloyd et al. [183] that the $\log E_{\rm peak}$~$0.5 \log E_{\rm iso}$ relation is obtained assuming an optically thin synchrotron shock model. This model considers electrons following the $N(\Gamma) = N_0 \Gamma^{-p}$ distribution for $\Gamma > \Gamma_m$ with Γ_m, GRB duration, and N_0 constant in each GRB. However, the above assumptions are not fully justifiable. In fact the duration is different in each GRB and $E_{\rm iso}$ might be smaller in the case of beamed emission.

Amati [190] pointed out the impact that the correlation has on the modeling of the prompt emission and on the possible unification of the two classes of GRBs and XRFs. In addition, this correlation is often applied for checking GRB synthesis models (e.g., [208, 209]).

In every model, $E_{\rm peak}$ and $E_{\rm iso}$ depend on Γ, and the $E_{\rm peak}$-$E_{\rm iso}$ relation can help to relate the parameters of the synchrotron shock model and inverse-Compton model [203, 208]. Specifically, Zhang and Mészáros [208] and Rees and Mészáros [210] found that, for an electron distribution given by a power law and produced by an internal shock in a fireball with velocity Γ, the peak energy is given as

$$\log E^{*}_{\rm peak} \sim -2 \log \Gamma + 0.5 \log L - \log t_{\nu}, \quad (47)$$

where L is the total fireball luminosity and t_{ν} is the variability timescale. However, to recover the $E_{\rm peak}$-$E_{\rm iso}$ relation from this relation, Γ and t_{ν} should be similar for each GRB, a condition that cannot be easily supported. A further issue arises when one considers that $L \propto \Gamma^{N}$, with N between 2 and 3 in different models [203, 208, 211]. An explanation could be that direct or Comptonized thermal radiation from the fireball photosphere [208, 210–219] can affect significantly the GRB prompt emission. This can be a good interpretation of the really energetic spectra presented for many events [220–222] and the flat shape in GRB average spectra. In such cases, $E_{\rm peak}$ depends on the peak temperature $T_{bb,\rm peak}$ of photons distributed as by a blackbody, and therefore it is associated with the luminosity or emitted energy. For Comptonized radiation from the photosphere the relations are

$$\log E_{\rm peak} \sim \log \Gamma + \log T_{bb,\rm peak} \sim 2 \log \Gamma - 0.25 \log L \quad (48)$$

or

$$\begin{aligned} \log E_{\rm peak} &\sim \log \Gamma + \log T_{bb,\rm peak} \\ &\sim -0.5 \log r_0 + 0.25 \log L, \end{aligned} \quad (49)$$

where r_0 is a particular distance between the central engine and the energy radiating area, such that the Lorentz factor evolves as $\Gamma \simeq r/r_0$ up to some saturation radius r_s [210]. As suggested by Rees and Mészáros [210], in this scenario the $E_{\rm peak}$-$E_{\rm iso}$ relation could be recovered for particular physical cases just underneath the photosphere, though it would rely on an undefined number of unknown parameters.

Also for high-energetic GRBs (i.e., $E_{\rm iso} \approx 10^{55}$ erg) the nonthermal synchrotron emission model can explain the $E_{\rm peak}$-$E_{\rm iso}$ correlation. This can be possible by considering either the minimum Lorentz factor and the normalization of the power law distribution of the emitting electrons constant in each GRB or constraints on the slope of the relation between Γ and the luminosity [183, 208].

Panaitescu [223] used 76 GRBs with measured redshifts to analyse the case in which the $E_{\rm peak}$-$E_{\rm iso}$ relation for LGRBs is due to the external shock generated by a relativistic outflow interacting with the ambient medium. He considered the effect of each parameter defining the $E_{\rm peak}$-$E_{\rm iso}$ relation on the radial distribution of the external medium density and pointed out that the $\log E_{\rm peak} \sim 0.5 \log E_{\rm iso}$ relation is recovered if the external medium is radially stratified. For some combinations of radiative (synchrotron or inverse-Compton) and dissipation (such as RS or FS) mechanisms, it is concluded that the external medium requires a particle density distributed distinctly from R^{-2}, with R being the distance at which the GRB radiation is generated. This tendency should be commonly associated with uniform mass-loss rate and final velocity.

Mochkovitch and Nava [224] checked whether the $E_{\rm peak}$-$E_{\rm iso}$ relation can be recovered in a case when the prompt emission is due to internal shocks, or alternatively if the correlation can give some limits for the internal shock scenario defined through the impact of only two shells. Simulated GRB samples were obtained considering different model parameter distributions, such as the emitted power in the relativistic emission and Γ. Simulated $E_{\rm peak}$-$E_{\rm iso}$ distributions were plotted for each case and analysed together with the observed relation (based on 58 GRBs). The sample contained only luminous *Swift* GRBs with $F_{\rm peak} > 2.6$ ph cm^{-2} s^{-1} in the 15–150 keV energy band. In conclusion, a correspondence between the model and data was found, but exclusively if the following restrictions for the dynamics of the emission and for the dispersion of the energy are assumed:

(1) The majority of the dispersed energy should be radiated in few electrons.

(2) The spread between the highest and the lowest Lorentz factor should be small.

(3) If the mean Lorentz factor grows as $\overline{\Gamma} \propto \dot{E}^{1/2}$ (where $\dot{E}$ is the rate of injected energy, or mean emitted power, in the relativistic outflow), the $E_{\rm peak}$-$E_{\rm iso}$ relation is not retrieved and $E_{\rm peak}$ is diminishing with larger $E_{\rm iso}$. However, the $E_{\rm peak}$-$E_{\rm iso}$ relation can be regained if $\overline{\Gamma} \propto \dot{E}^{1/2}$ is a lower constraint for a particular $\dot{E}$.

(4) When the timescale or the width of the variability of the Lorentz factor is associated with $\overline{\Gamma}$, $E_{\rm peak}$-$E_{\rm iso}$ relation is recovered.

For the Ghirlanda relation [188], with the assumption that the line of sight is within the jet angle, the $E_{\rm peak}$-E_γ relation indicates its invariance when moving from the rest frame to the comoving frame. As a result, the number of radiated photons in each GRBs is comparable and should be about 10^{57}. The last characteristic could be important for understanding the dynamics of GRBs and the radiative mechanisms (see also Figure 9(b)).

Collazzi et al. [225] found that the mean $E^*_{\rm peak}$ is near to 511 keV, the electron rest-mass energy $m_e c^2$. Therefore, it is claimed that the tight shape of the $E_{\rm peak}$ distribution does not stem only from selection effects. No studied mechanism can drive this effect; however, with the $E^*_{\rm peak}$ compatible with the effective temperature of the γ-ray radiating area, the almost constant temperature needs some mechanism similar to a thermostat, keeping the temperature at a steady value. It was suggested that such a mechanism could be an electron-positron annihilation.

Ghirlanda et al. [209], using a simulated sample, analysed if different intrinsic distributions of Γ and $\theta_{\rm jet}$ can replicate a grid of observational constraints. With the assumption that, in the comoving frame each GRB has similar $E_{\rm peak}$ and E_γ, it was found that the distributions of Γ and $\theta_{\rm jet}$ cannot be power laws. Instead, the highest concordance between simulation and data is given by log-normal distributions and a connection between their maxima, like $\theta^{2.5}_{\rm jet,max}\Gamma_{\rm max} =$ const. In this work $\theta_{\rm jet}$ and Γ are important quantities for the calculation of the GRB energetics. Indeed, from a sample of ≈30 GRBs with known $\theta_{\rm jet}$ or Γ it was found that the E_γ distribution is centered at 10^{50}–10^{51} erg and it is tightly related to $E_{\rm peak}$. It was obtained that

$$\log E_{\rm peak} \sim \log \frac{E_\gamma}{5 - 2\beta_0}. \quad (50)$$

Present values of Γ and $\theta_{\rm jet}$ rely on incomplete data sets and their distributions could be affected by biases. Nevertheless, Ghirlanda et al. [209] claimed that greater values of Γ are related to smaller $\theta_{\rm jet}$ values; that is, the faster a GRB, the narrower its jet.

Furthermore, GRBs fulfilling the condition $\sin\theta_{\rm jet} < 1/\Gamma$ might not display any jet break in the afterglow light curve, and Ghirlanda et al. [209] predicted that this group should comprise ≈6% of the on-axis GRBs. Finally, their work is crucial as it allowed finding that the local rate of GRBs is ≈0.3% of the local SNe Ib/c rate and ≈4.3% of the local hypernovae(i.e., SNe Ib/c with wide-lines) rate.

3.6. Correlations between the Luminosity and the Peak Energy

3.6.1. The L_{iso}-E_{peak} Correlation. The $L_{\rm iso}$-$E_{\rm peak}$ relation was discovered by Schaefer [203] who used 84 GRBs with known $E_{\rm peak}$ from the BATSE catalogue [121] and 20 GRBs with luminosities based on optically measured redshift [111, 226]. It was found that (see Figure 10) for the 20 GRBs

$$\log E_{\rm peak} \sim (0.38 \pm 0.11) \log L_{\rm iso}, \quad (51)$$

with $r = 0.90$ and $P = 3 \times 10^{-8}$, and among the 84 GRBs the relation was

$$\log E_{\rm peak} \sim (0.36 \pm 0.03) \log L_{\rm iso}. \quad (52)$$

The underlying idea is that $L_{\rm iso}$ varies as a power of Γ, as we have already discussed in Section 3.1.2, and $E_{\rm peak}$ also varies as some other power of Γ, so that $E_{\rm peak}$ and $L_{\rm iso}$ will be correlated to each other through their dependence on Γ. For the general case where the luminosity varies as Γ^N and $E_{\rm peak}$ varies as Γ^M, and therefore $\log E_{\rm peak}$ will vary as $(M+1)/N \times \log L_{\rm iso}$.

Frontera et al. [200], using a sample of 9 GRBs detected simultaneously with the Wide Field Camera (WFC) on board the *BeppoSAX* satellite and by the BATSE instrument, reported the results of a systematic study of the broad-band (2–2000 keV) time-resolved prompt emission spectra. However, only 4 of those GRBs (970111, 980329, 990123, 990510) were bright enough to allow a fine time-resolved spectral analysis, resulting in a total of 40 spectra. Finally, the study of the time-resolved dependence (see also the end of Section 3.5.2) of $E_{\rm peak}$ on the corresponding $L_{\rm iso}$ was possible for two bursts with known redshift (i.e., 990123 and 990510) and found using the least squares method (see Figure 11):

$$\log E^*_{\rm peak} \sim (0.66 \pm 0.03) \log L_{\rm iso}, \quad (53)$$

with $\rho = 0.94$ and $P = 1.57 \times 10^{-13}$.

Afterwards, Nava et al. [227], using a sample of 46 *Swift* GRBs with measured z and $E_{\rm peak}$, found a strong $L_{\rm iso}$-$E_{\rm peak}$ correlation, with a functional form of

$$\log E^*_{\rm peak} = -(25.33 \pm 3.26) + (0.53 \pm 0.06) \log L_{\rm iso}, \quad (54)$$

with $\rho = 0.65$ and $P = 10^{-6}$; $E_{\rm peak}$ is in keV and $L_{\rm iso}$ is in units of 10^{51} erg s^{-1}. Furthermore, using 12 GRBs with only an upper limit on z (3 events) or no redshift at all (3 events), or with a lower limit on $E_{\rm peak}$ (3 events) or no estimate at all (3 events), they found that these bursts also obey the obtained $L_{\rm iso}$-$E_{\rm peak}$ relation.

3.6.2. The L_{peak}-E_{peak} Correlation. It was also found that the Amati relation holds even if $E_{\rm iso}$ is substituted with $L_{\rm iso}$ and $L_{\rm peak}$, which is not surprising given that these "energy indicators" are strongly correlated. To this end, the Yonetoku correlation ([116], see Figure 12(a)) relates $E_{\rm peak}$ with $L_{\rm peak}$. The relation was obtained employing 11 GRBs with known redshifts detected by BATSE, together with *BeppoSAX* GRBs from [111]. This relation uses $L_{\rm peak}$ of the burst instead of $L_{\rm iso}$,

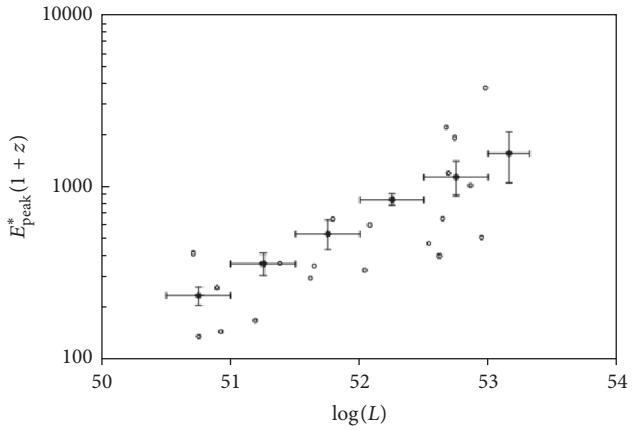

FIGURE 10: Direct fit of $\log L_{\rm iso}$ - $\log E_{\rm peak}$ data. This is shown here for two independent data sets for which the luminosities are derived by two independent methods. The first data set consists of 20 bursts with spectroscopically measured redshifts (the open circles). The second one is for 84 bursts (whose binned values are shown as filled diamonds, and the horizontal bars are the bin widths) whose luminosity (and then redshift) were determined with the spectral lag and variability light curve parameters. Both data sets show a highly significant and similar power law relations. (Figure after Schaefer [203]; see Figure 3 therein. @ AAS. Reproduced with permission.)

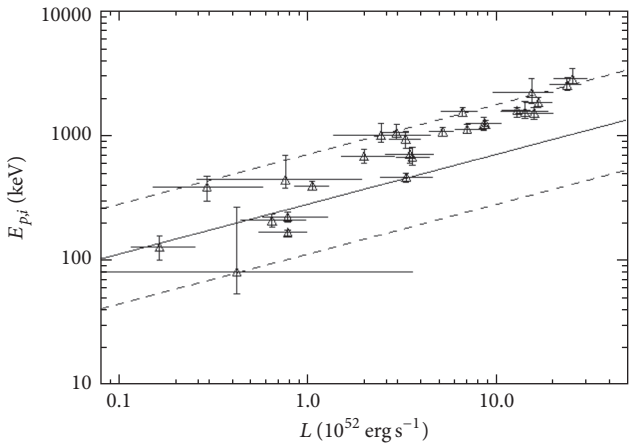

FIGURE 11: $E^*_{\rm peak}$ versus $L_{\rm iso}$, obtained from data for GRBs 990123 and 990510. The solid line is the best-fit power law. (Figure after Frontera et al. [200]; see Figure 6 therein. @ AAS. Reproduced with permission.)

and it is tighter than previous prompt correlations. The best-fit line is given by

$$\log L_{\rm peak} \sim (2.0 \pm 0.2) \log E^*_{\rm peak}, \tag{55}$$

with $r = 0.958$, $P = 5.31 \times 10^{-9}$, and the uncertainties are 1σ error. This relation agrees well with the standard synchrotron model [183, 208]. Finally, it has been used to estimate pseudoredshifts of 689 BATSE LGRBs with unknown distances and to derive their formation rate as a function of z.

Ghirlanda et al. [228] selected 36 bright SGRBs detected by BATSE, with an $F_{\rm peak}$ on the 64 ms timescale in the 50–300 keV energy range exceeding $10\,{\rm ph\,cm^{-2}\,s^{-1}}$. In 7 cases, the signal-to-noise-ratio was too low to reliably constrain the spectral best-fit parameters. One case yielded missing data. Hence, the sample consisted of 28 events. Due to unknown redshifts, $E^*_{\rm peak}$, $E_{\rm iso}$, and $L_{\rm peak}$ were expressed as functions of the redshift in the range $z \in [0.001, 10]$. It was found that SGRBs are unlikely to obey the Amati relation, $E_{\rm iso}$-$E^*_{\rm peak}$, but the results were consistent with the $L_{\rm peak}$-$E^*_{\rm peak}$ relation of Yonetoku et al. [116]. Hence, assuming that this relation indeed holds for SGRBs, their pseudoredshifts were estimated and found to have a similar distribution as LGRBs, with a slightly smaller average redshift.

Afterwards, Yonetoku et al. [229] investigated the prompt emission of 101 GRBs with measured redshifts and a reported $F_{\rm peak}$ detected until the end of 2009. The sample comes from events detected in a number of independent missions: the satellites used for this purpose are *KONUS*, *Swift*, *HXD-WAM*, and *RHESSI*. Using this data set, the $E_{\rm peak}$-$L_{\rm peak}$ correlation was revised, and its functional form could be written as

$$\log L_{\rm peak} = (52.43 \pm 0.037) + (1.60 \pm 0.082) \log E^*_{\rm peak}, \tag{56}$$

with $r = 0.889$ for 99 degrees of freedom and an associated $P = 2.18 \times 10^{-35}$; $L_{\rm peak}$ is expressed in ${\rm erg\,s^{-1}}$ and $E^*_{\rm peak}$ in units of 355 keV. To provide reference to previous works, the 1–10^4 keV energy band in the GRB rest frame was used to calculate the bolometric energy and $L_{\rm peak}$. Finally, it was demonstrated that this relation is intrinsic to GRBs and affected by the truncation effects imposed by the detector threshold.

Lu and Liang [230], using time-resolved spectral data for a sample of 30 pulses in 27 bright GRBs detected by BATSE, investigated the $L_{\rm peak}$-$E_{\rm peak}$ relation in the decay phases of these pulses (see Figure 12(b)). Quite all of the pulses followed a narrow $L_{\rm peak}$-$E_{\rm peak}$ relation given by

$$\log L_{\rm peak} \sim (1.42 \pm 0.03) \log E^*_{\rm peak}, \tag{57}$$

with $r = 0.91$ and $P < 10^{-4}$, but the power law index varied. The statistical or observational effects could not account for the large scatter of the power law index, and it was suggested to be an intrinsic feature, indicating that no relation common for all GRB pulses $L_{\rm peak}$-$E_{\rm peak}$ would be expected. However, in the light of *Fermi* observations that revealed deviations from the Band function ([181, 231–234]; see also [235]), it was proposed recently that the GRB spectra should be modeled not with the Band function itself (constituting a nonthermal component), but with additional blackbody (BB, thermal) and power law (PL, nonthermal) components [216, 218, 219, 236]. The nonthermal component was well described within the context of synchrotron radiation from particles in the jet, while the thermal component was interpreted by the emission from the jet photosphere. The PL component was claimed to originate most likely from the inverse-Compton process. The results point toward a universal relation between $L_{\rm peak}$ and $E^*_{\rm peak}$ related to the nonthermal components.

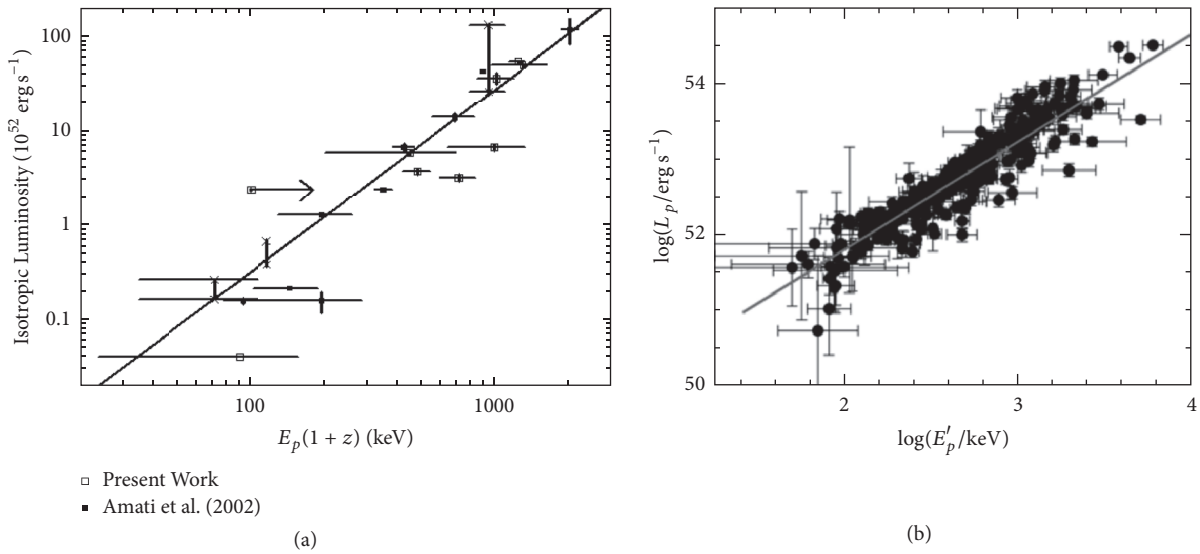

FIGURE 12: (a) The $\log L_{\mathrm{peak}}$- $\log E_{\mathrm{peak}}$ relation. The open squares mark the BATSE data. *BeppoSAX* events, which are converted into the energy range of 30–10000 keV, are shown as filled squares and the cross points. The solid line indicates the best-fit line. (Figure after Yonetoku et al. [116]; see Figure 1 therein. @ AAS. Reproduced with permission.) (b) $\log L_{\mathrm{peak}}$ versus $\log E_{\mathrm{peak}}$ for 276 time-resolved spectra within the decay pulses for the sample. The solid line stands for the best fit to the data. (Figure after Lu and Liang [230]; see Figure 4 therein. Copyright @ 2010 Springer.)

Tsutsui et al. [237] analysed 13 SGRB candidates (i.e., an SGRB with $T^*_{90} < 2$ s), from among which they selected 8 events considering them as secure ones. An SGRB candidate is regarded as a misguided SGRB if it is located within the $3\sigma_{\mathrm{int}}$ dispersion region from the best-fit E^*_{peak}-E_{iso} function of the correlation for LGRBs, while the others are regarded as secure SGRBs. The relation obtained with secure GRBs is the following:

$$\log L_{\mathrm{peak}} = (52.29 \pm 0.066) + (1.59 \pm 0.11) \log E^*_{\mathrm{peak}}, \quad (58)$$

with $r = 0.98$ and $P = 1.5 \times 10^{-5}$, where E^*_{peak} (in units of 774.5 keV) is from the time-integrated spectrum, while L_{peak} (in erg s^{-1}) was taken as the luminosity integrated for 64 ms at the peak considering the shorter duration of SGRBs. Application of this relation to 71 bright BATSE SGRBs resulted in pseudoredshifts distributed in the range $z \in [0.097, 2.258]$, with $\langle z \rangle = 1.05$, which is apparently lower than $\langle z \rangle = 2.2$ for LGRBs. Finally, Yonetoku et al. [238], using 72 SGRBs with well determined spectral features as observed by BATSE, determined their pseudoredshifts and luminosities by employing the L_{peak}-E_{peak} correlation for SGRBs found by Tsutsui et al. [237]. It was found that the obtained redshift distribution for $z \leq 1$ was in agreement with that of 22 *Swift* SGRBs, indicating the reliability of the redshift determination via the E^*_{peak}-L_{peak} relation.

3.6.3. Physical Interpretation of the Luminosity versus Peak Energy Relations. As pointed out by Schaefer et al. [121] and Schaefer [203], E_{peak} and L_{iso} are correlated because of their dependence on Γ. The L_{iso}-E_{peak} relation could shed light on the structure of the ultrarelativistic outflow, the shock acceleration, and the magnetic field generation [239]. However, since only few SGRBs are included in the samples used, the correlations and interpretations are currently only applicable to LGRBs.

Schaefer et al. [121] and Schaefer [203] claimed that the values of E_{peak} are approximately constant for all the bursts with $z \geq 5$. However, with the launch of the *Swift* satellite in the end of 2004 the hunt for "standard candles" via a number of GRB correlations is still ongoing. Thus, the great challenge is to find universal constancy in some GRB parameters, despite the substantial diversity exhibited by their light curves. If this goal is achieved, GRBs might prove to be a useful cosmological tool [240].

Liang et al. [241] defined a parameter $\omega = (L_{\mathrm{iso}}/10^{52}\,\mathrm{erg\,s^{-1}})^{0.5}/(E_{\mathrm{peak}}/200\,\mathrm{keV})$ and discussed possible implications of the E_{peak}-L_{iso} relation for the fireball models. They found that ω is limited to the range $\simeq$ 0.1–1. They constrained some parameters, such as the combined internal shock parameter, ζ_i, for the internal as well as external shock models, with an assumption of uncorrelated model parameters. Their distributions suggest that the production of prompt γ-rays within internal shocks dominated by kinetic energy is in agreement with the standard internal shock model. Similarly in case when the γ-rays come from external shocks dominated by magnetic dissipation. These results imply that both models can provide a physical interpretation of the $L_{\mathrm{iso}} \propto E^2_{\mathrm{peak}}$ relation as well as the parameter ω.

To explain the origin of this correlation, Mendoza et al. [242] considered simple laws of mass and linear momentum conservation on the emission surface to give a full description of the working surface flow parameterized by the initial velocity and mass injection rate. They assumed a source-ejecting matter in a preferred direction x with

a velocity $v(t)$ and a mass ejection rate $\dot{m}(t)$, both dependent on time t as measured from the jet's source; that is, they studied the case of a uniform release of mass and the luminosity was measured considering simple periodic oscillations of the particle velocity, a common assumption in the internal shock model scenario.

Due to the presence of a velocity shear with a considerable variation in Γ at the boundary of the spine and sheath region, a fraction of the injected photons is accelerated via a Fermi-like acceleration mechanism such that a high-energy power law tail is formed in the resultant spectrum. Ito et al. [243] showed in particular that if a velocity shear with a considerable variance in Γ is present, the high-energy part of the observed GRB photon spectrum can be explained by this photon acceleration mechanism. The accelerated photons may also account for the origin of the extra hard power law component above the bump of the thermal-like peak seen in some peculiar GRBs (090510, 090902B, 090926A). It was demonstrated that time-integrated spectra can also reproduce the low energy spectra of GRBs consistently due to a multitemperature effect when time evolution of the outflow is considered.

Regarding the Yonetoku relation, its implications are related to the GRB formation rate and the luminosity function of GRBs. In fact, the analysis of Yonetoku et al. [116] showed that the existence of the luminosity evolution of GRBs, assuming as a function a simple power law dependence on the redshift, such as $g(z) = (1+z)^{1.85}$, may indicate the evolution of GRB progenitor itself (mass) or the jet evolution. To study the evolution of jet-opening angle they considered two assumptions: either the maximum jet-opening angle decreases or the total jet energy increases. In the former case, the GRB formation rate obtained may be an underestimation since the chance probability of observing the high-redshift GRBs will decrease. If so, the evolution of the ratio of the GRB formation rate to the star formation rate becomes more rapid. On the other hand, in the latter case, GRB formation rate provides a reasonable estimate.

Recently Frontera et al. [244], building on the spectral model of the prompt emission of Titarchuk et al. [245], gave a physical interpretation of the origin of the time-resolved $L_{\rm iso}$-$E_{\rm peak}$ relation. The model consists of an expanding plasma shell, result of the star explosion, and a thermal bath of soft photons. Frontera et al. [244] showed analytically that in the asymptotic case of the optical depth $\tau \gg 1$ the relation $\log L_{\rm iso}$- $\log E_{\rm peak}$ indeed has a slope of 1/2. This, in turn, is evidence for the physical origin of the Amati relation (see Section 3.5.2).

3.7. Comparisons between E_{peak}-E_{iso} and E_{peak}-L_{peak} Correlation. For a more complete dissertation we compare the $E_{\rm peak}$-$E_{\rm iso}$ correlation with the $E_{\rm peak}$-$L_{\rm peak}$ correlation. To this end, Ghirlanda et al. [246] derived the $E_{\rm peak}$-$L_{\rm peak}$ relation with a sample of 22 GRBs with known z and well determined spectral properties. This relation has a slope of 0.51, similar to the one proposed by Yonetoku et al. [116] with 12 GRBs, although its scatter is much larger than the one originally found.

Tsutsui et al. [247] investigated these two relations using only data from the prompt phase of 33 low-redshift GRBs with $z \leq 1.6$. In both cases the correlation coefficient was high, but a significant scatter was also present. Next, a partial linear correlation degree, which is the degree of association between two random variables, was found to be $\rho_{L_{\rm peak}, E_{\rm iso}, E_{\rm peak}} = 0.38$. Here, $\rho_{1,2,3}$ means the correlation coefficient between the first and the second parameter after fixing the third parameter. This fact indicates that two distance indicators may be independent from each other even if they are characterized by the same physical quantity, $E_{\rm peak}$, and similar quantities, $L_{\rm peak}$ and $E_{\rm iso}$. To correct the large dispersion of the Yonetoku correlation, Tsutsui et al. [247] introduced a luminosity time constant T_L defined by $T_L = E_{\rm iso}/L_{\rm peak}$ as a third parameter and a new correlation was established in the following form:

$$\log L_{\rm peak} = (-3.87 \pm 0.19) + (1.82 \pm 0.08) \log E_{\rm peak} - (0.34 \pm 0.09) \log T_L, \quad (59)$$

with $r = 0.94$ and $P = 10^{-10}$. Here, $L_{\rm peak}$ is in units of $10^{52}\,{\rm erg\,s^{-1}}$, $E_{\rm peak}$ is in keV, and T_L in seconds. In this way the systematic errors were reduced by about 40%, and the plane represented by this correlation might be regarded as a "fundamental plane" of GRBs.

Later, Tsutsui et al. [248] reconsidered the correlations among $E_{\rm peak}$, $L_{\rm peak}$, and $E_{\rm iso}$, using the database constructed by Yonetoku et al. [229], which consisted of 109 GRBs with known redshifts, and $E_{\rm peak}$, $L_{\rm peak}$, and $E_{\rm iso}$ well determined. The events are divided into two groups by their data quality. One (gold data set) consisted of GRBs with $E_{\rm peak}$ determined by the Band function with four free parameters. GRBs in the other group (bronze data set) had relatively poor energy spectra so that their $E_{\rm peak}$ were determined by the Band function with three free parameters (i.e., one spectral index was fixed) or by the cut-off power law (CPL) model with three free parameters. Using only the gold data set, the intrinsic dispersion, $\sigma_{\rm int}$, in $\log L_{\rm peak}$, is 0.13 for the $E_{\rm peak}$-T_L-$L_{\rm peak}$ correlation and 0.22 for the $E_{\rm peak}$-$L_{\rm peak}$ correlation. In addition, GRBs in the bronze data set had systematically larger $E_{\rm peak}$ than expected by the correlations constructed with the gold data set. This indicates that the quality of the sample is an important issue for the scatter of correlations among $E_{\rm peak}$, $L_{\rm peak}$, and $E_{\rm iso}$.

The difference between the $E_{\rm peak}$-$L_{\rm peak}$ correlation for LGRBs from [180] and the one from [229] is due to the presence of GRB060218. In the former, it was considered an ordinary LGRB, while, in the latter, it was considered an outlier by a statistical argument. Because GRB060218 is located far from the $L_{\rm peak}$-$E_{\rm peak}$ correlation in [229] (more than 8σ), it makes the best-fit line much steeper.

Regarding the high-energetic GRBs, Ghirlanda et al. [180] considered 13 GRBs detected by *Fermi* up to the end of July 2009 and with known redshift. They found a tight relation:

$$\log E^{*}_{\rm peak} \sim 0.4 \log L_{\rm iso}, \quad (60)$$

with a scatter of $\sigma = 0.26$. A similarly tight relation exists between $E^*_{\rm peak}$ and $E_{\rm iso}$:

$$\log E^*_{\rm peak} \sim 0.5 \log E_{\rm iso}. \quad (61)$$

The time-integrated spectra of 8 *Fermi* GRBs with measured redshift were consistent with both the $E_{\rm peak}$-$E_{\rm iso}$ and the $E_{\rm peak}$-$L_{\rm iso}$ correlations defined by 100 pre-*Fermi* bursts.

Regarding the study of SGRBs within the context of these two correlations, Tsutsui et al. [237] used 8 SGRBs out of 13 SGRB candidates to check whether the $E_{\rm peak}$-$E_{\rm iso}$ and $E_{\rm peak}$-$L_{\rm peak}$ correlations exist for SGRBs as well. It was found that the $E_{\rm peak}$-$E_{\rm iso}$ correlation seemed to hold in the following form:

$$\log E_{\rm iso} = (51.42 \pm 0.15) + (1.58 \pm 0.28) \log E^*_{\rm peak}, \quad (62)$$

with $r = 0.91$, $P = 1.5 \times 10^{-3}$, $E_{\rm iso}$ in erg s^{-1} and $E^*_{\rm peak}$ in units of 774.5 keV. They also found that the $E_{\rm peak}$-$L_{\rm peak}$ correlation with a functional form as in (58) is tighter than the $E_{\rm peak}$-$E_{\rm iso}$ one. Both correlations for SGRBs indicate that they are less luminous than LGRBs, for the same $E_{\rm peak}$, by factors $\simeq 100$ (for $E_{\rm peak}$-$E_{\rm iso}$) and $\simeq 5$ (for $E_{\rm peak}$-$L_{\rm peak}$). It was the first time that the existence of distinct $E_{\rm peak}$-$E_{\rm iso}$ and $E_{\rm peak}$-$L_{\rm peak}$ correlations for SGRBs was argued.

3.8. The $L_{X,p}$-T^*_p Correlation and Its Physical Interpretation. Using data gathered by *Swift*, Willingale et al. [81] proposed a unique phenomenological function to estimate some relevant parameters of both the prompt and afterglow emission. Both components are well fitted by the same functional form:

$$f_i(t) = \begin{cases} F_i e^{\alpha_i (1 - t/T_i)} e^{-t_i/t}, & t < T_i, \\ F_i \left(\dfrac{t}{T_i} \right)^{-\alpha_i} e^{-t_i/t}, & t \geq T_i. \end{cases} \quad (63)$$

The index i can take the values p or a to indicate the prompt and afterglow, respectively. The complete light curve, $f_{\rm tot}(t) = f_p(t) + f_a(t)$, is described by two sets of four parameters each: $\{T_i, F_i, \alpha_i, t_i\}$, where α_i is the temporal power law decay index, the time t_i is the initial rise timescale, F_i is the flux, and T_i is the break time. Figure 13 schematically illustrates this function.

Following the same approach as adopted in [131], Qi and Lu [249] investigated the prompt emission properties of 107 GRB light curves detected by the XRT instrument onboard the *Swift* satellite in the X-ray energy band (0.3–10 keV). They found that there is a correlation between $L_{X,p}$ and T^*_p. Among the 107 GRBs, they used only 47, because some of the events did not have a firm redshift and some did not present reliable spectral parameters in the prompt decay phase. Among the 47 GRBs, only 37 had $T^*_p > 2$ s, and 3 of them had $T^*_p > 100$ s.

The functional form for this correlation could be written in the following way:

$$\log L_{X,p} = a + b \log T^*_p, \quad (64)$$

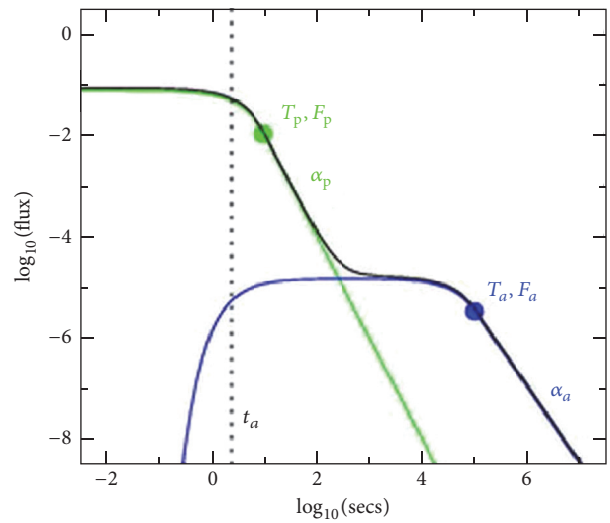

FIGURE 13: Functional form of the decay and the fitted parameters. The prompt component (green curve) has no rise because time zero is set at the peak. The afterglow component (blue curve) rises at time T_a as shown. (Figure after Willingale et al. [81]; see Figure 1 therein. @ AAS. Reproduced with permission.)

where $L_{X,p}$ is in erg s^{-1} and T^*_p is in seconds. The fits were performed via the D'Agostini [153] fitting method applied to the following data sets:

(1) The total sample of 47 GRBs (see Figure 14(a))

(2) 37 GRBs with $T^*_p > 2$ s (see Figure 14(b))

(3) 34 GRBs with $2\text{ s} < T^*_p < 100$ s (see Figure 14(c))

The results of these fittings turned out to give different forms of (64). In case (1), $a = 50.91 \pm 0.23$ and $b = -0.89 \pm 0.19$ were obtained. The slope b is different in cases (2) and (3), $b = -1.73$ and $b = -0.74$, respectively. The best fit with the smallest $\sigma_{\rm int}$ comes from case (3). Remarkably, in this case the slope b is close to the slope $(-0.74^{+0.20}_{-0.19})$ of a similar $\log L_X$-$\log T^*_a$ relation [131].

Qi and Lu [249] noticed a broken linear relation of the $L_{X,p}$-T^*_p correlation. More specifically, an evidence of curvature appears in Figure 14(b). One can see, from Figure 14(a), that if the best-fit line is extended to the range of $T^*_p < 2$ s, all the GRBs with $T^*_p < 2$ s are located below this line. However, the small sample of GRBs used in their analysis is still not sufficient to conclude whether the change in the slope is real or just a selection bias caused by outliers. If there is a change in the slope this may suggest that GRBs could be classified into two groups, long and short, based on their values of T^*_p instead of T_{90}, since T^*_p is an estimate of the GRB duration based on temporal features of the light curves and T_{90} is a measure based on the energy. This idea has actually been proposed for the first time by O'Brien and Willingale [250]. It is worth noting that while T_{90} and T_p are both estimates of the GRB duration, the correlation does not hold if T_p is replaced with T_{90}. For an analysis of an extended sample and comparison of T_{45} versus T_p also, see [251].

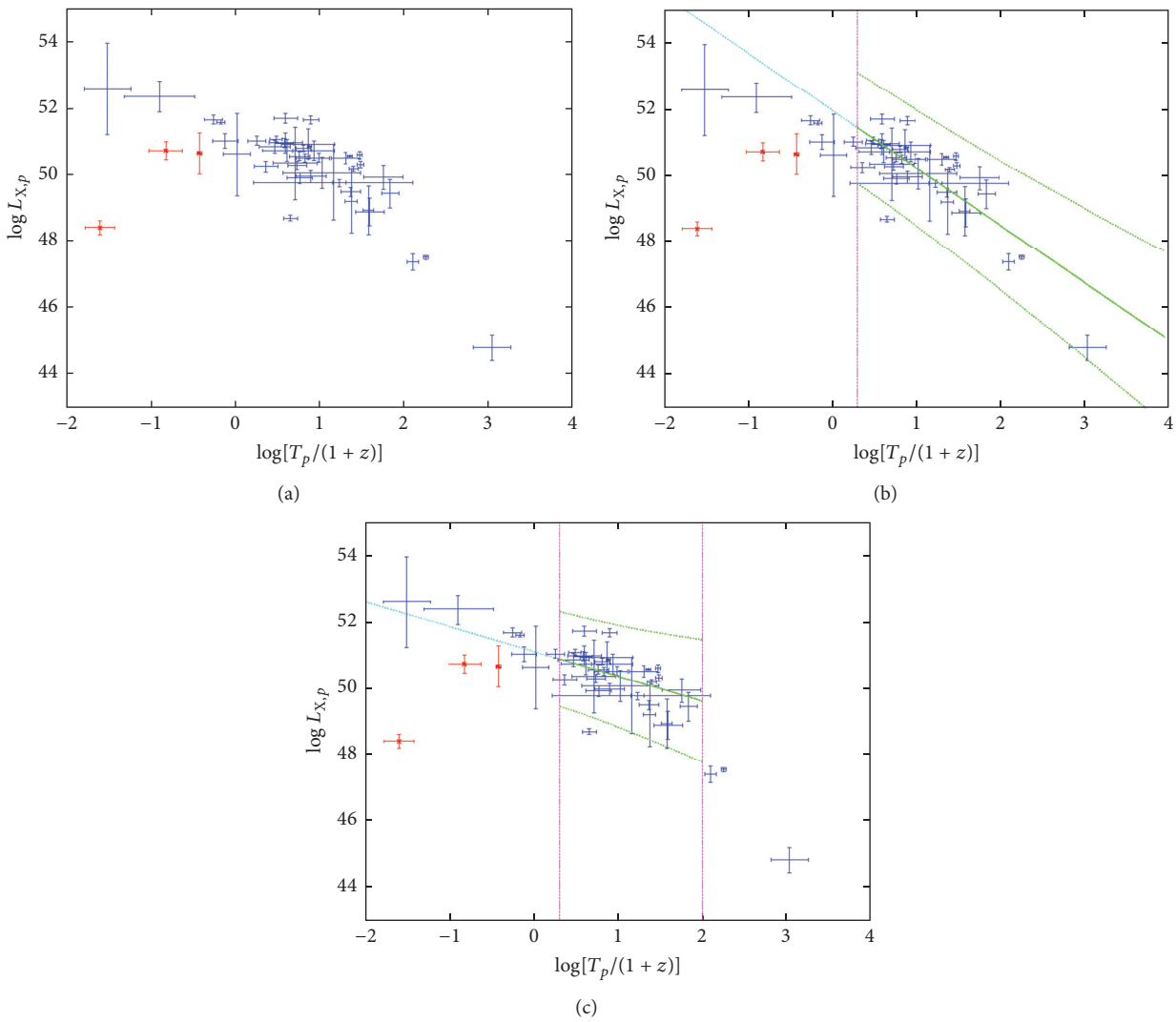

FIGURE 14: (a) $\log L_{X,p}$ (in erg s^{-1}) versus $\log T_p^*$ (in s) for the whole sample of 47 GRBs. The red dots represent SGRBs (i.e., $T_{90} < 2$ s). (Figure after Qi and Lu [249]; see Figure 1 therein. @ AAS. Reproduced with permission.) (b) Best fit of the $\log L_{X,p}$ (in erg s^{-1}) versus $\log T_p^*$ (in s) relation following equation (64) and the corresponding 2σ confidence region. Only GRBs with $T_p^* > 2$ s are included in the fit. (Figure after Qi and Lu [249]; see Figure 2 therein. @ AAS. Reproduced with permission.) (c) Best fit of the $\log L_{X,p}$ (in erg s^{-1}) versus $\log T_p^*$ (in s) relation following equation (64) and the corresponding 2σ confidence region. In this case only the 34 GRBs with 2 s $< T_p^* <$ 100 s are included in the fit. (Figure after Qi and Lu [249]; see Figure 3 therein. @ AAS. Reproduced with permission.)

Regarding the physical interpretation, the change of the slope in the $L_{X,p}$-T_p^* relation at different values of T_p^* in [249] can be due to the presence of few GRBs with a large T_p^*, but it might also be due to different emission mechanisms. Unfortunately, the paucity of the sample prevents putting forward any conclusion due to the presence of (potential) outliers in the data set. A more detailed analysis is necessary to further validate this correlation and better understand its physical interpretation.

3.9. The L_f-T_f Correlation and Its Physical Interpretation. In most GRBs a rapid decay phase (RDP) soon after the prompt emission is observed [89], and this RDP appears to continue smoothly after the prompt, in terms of both temporal and spectral variations [86]. This indicates that the RDP could be the prompt emission's tail and a number of models have been proposed to take it into account (see [88]), in particular the high latitude emission (HLE). This model states that once the prompt emission from a spherical shell turns off at some radius, then the photons reach the observer from angles apparently larger (relative to the line of sight) due to the added path length caused by the curvature of the emitting region. The Doppler factor of these late-arriving photons is smaller.

A successful attempt to individually fit all the distinct pulses in the prompt phase and in the late X-ray flares observed by the complete *Swift*/BAT + XRT light curves has been performed by Willingale et al. [108] using a physically

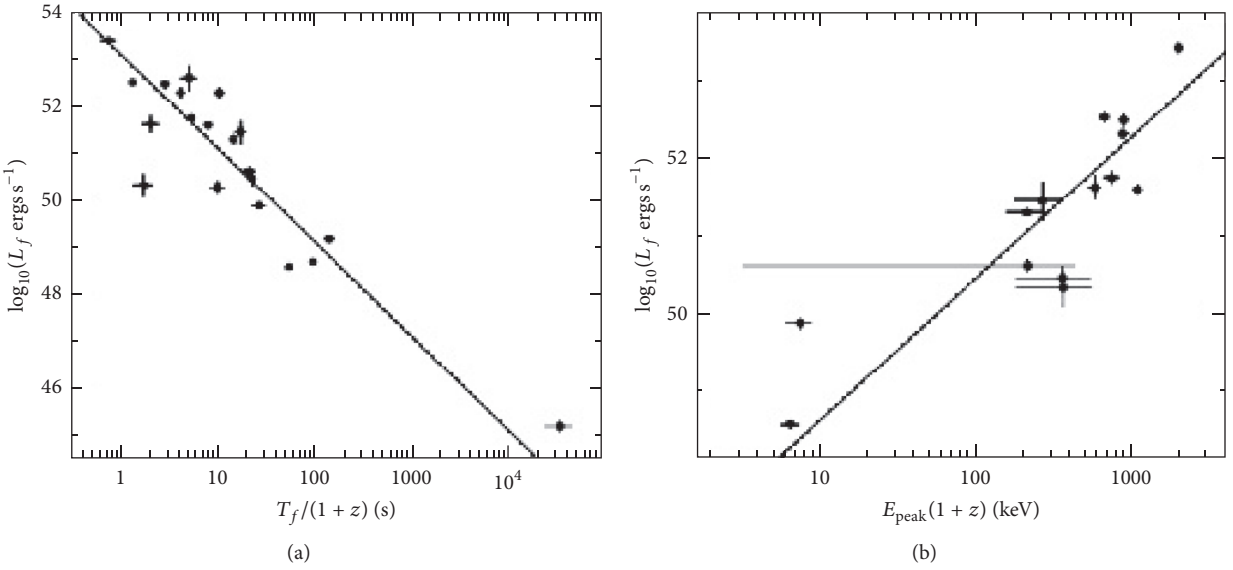

FIGURE 15: (a) L_f (in erg s^{-1}) versus T_f^*. (b) L_f (in erg s^{-1}) versus E_{peak}. (Figures after Willingale et al. [108]; see Figure 16 therein.)

motivated pulse profile. This fitting is an improved procedure compared to the Willingale et al. [81] one. The pulse profile has the following functional form:

$$P = \left\{ \left[\min\left(\frac{T - T_{\text{ej}}}{T_f}, 1 \right)^{\alpha+2} - \left(\frac{T_f - T_{\text{rise}}}{T_f} \right)^{\alpha+2} \right] \cdot \left[1 - \left(\frac{T_f - T_{\text{rise}}}{T_f} \right)^{\alpha+2} \right]^{-1} \right\} \left(\frac{T - T_{\text{ej}}}{T_f} \right)^{-1}, \tag{65}$$

where $T_0 = T_f - T_{\text{rise}}$ (with T_{rise} the rise time of the pulse) is the arrival time of the first photon emitted from the shell. It is assumed here that the emission comes from an ultrarelativistic thin shell spreading over a finite range of radii along the line of sight, in the observer frame measured with respect to the ejection time, T_{ej}. From these assumptions it is possible to model the rise of the pulse through α, T_{rise}, and T_f (see also Figure 1).

The combination of the pulse profile function $P(t, T_f, T_{\text{rise}})$ and the blue shift of the spectral profile $B(x)$ produces the rise and fall of the pulse. $B(x)$ is approximated with the Band function in the following form:

$$B(x) = B_{\text{norm}} \times \begin{cases} x^{(\alpha-1)} e^{-x}, & x \le \alpha - \beta, \\ x^{(\beta-1)} (\alpha - \beta)^{(\alpha-\beta)} e^{-(\alpha-\beta)}, & x > \alpha - \beta, \end{cases} \tag{66}$$

where $x = (E/E_f)[(T - T_{\text{ej}})/T_f]^{-1}$, with E_f being the energy at the spectral break, and B_{norm} is the normalization.

Using this motivated pulse profile, Willingale et al. [108] found that, within a sample of 12 GRBs observed by *Swift* in the BAT and XRT energy bands, L_f is anticorrelated with T_f^* in the following way:

$$\log L_f \sim -(2.0 \pm 0.2) \log T_f^*. \tag{67}$$

Therefore, high-luminosity pulses occur shortly after ejection, while low-luminosity pulses appear at later time (see Figure 15(a)). Moreover, Willingale et al. [108] also found a correlation between L_f and E_{peak} as shown in Figure 15(b). This is in agreement with the known correlation between L_{peak} for the whole burst and E_{peak} of the spectrum during the time T_{90} [116, 237]; for comparison with the L_{peak}-E_{peak} correlation, see also Section 3.6.2.

In the 12 light curves considered by Willingale et al. [108], 49 pulses were analysed. Although several pulses with a hard peak could not be correctly fitted, the overall fitting to the RDP was satisfactory and the HLE model was shown to be able to take into account phase of the GRB emission. However, it is worth mentioning the hard pulse in GRB061121 which requires a spectral index $\beta_S = 2.4$, larger than the value expected for synchrotron emission, that is, $\beta_S = 1$.

Lee et al. [252] and Quilligan et al. [253] discussed analogous correlations, although these authors considered the width of a pulse rather than T_f, which is in fact closely correlated with pulse width. Many authors afterwards [254–264] have used the motivated pulse profile of Willingale et al. [108] for various studies on the prompt emission properties of the pulses.

Regarding the physical interpretation, in [108], the flux density of each prompt emission pulse is depicted by an analytical expression derived under the assumption that the radiation comes from a thin shell, as we have already described. The decay after the peak involves the HLE [265] along the considered shell which is delayed and modified with a different Doppler factor due to the curvature of the surface [266, 267].

4. Summary

In this work we have reviewed the bivariate correlations among a number of GRB prompt phase parameters and their characteristics. It is important to mention that several of these correlations have the problem of double truncation which affects the parameters. Some relations have also been tested to prove their intrinsic nature like the $E_{\rm peak}$-$S_{\rm tot}$, $E_{\rm peak}$-$E_{\rm iso}$, and $L_{\rm peak}$-$E_{\rm peak}$ relations. For the others, we are not aware of their intrinsic forms and consequently how far the use of the observed relations can influence the evaluation of the theoretical models and the "best" cosmological settings. Therefore, the evaluation of the intrinsic correlations is crucial for the determination of the most plausible model to explain the prompt emission. In fact, though there are several theoretical interpretations describing each correlation, in many cases more than one is viable, thus showing that the emission processes that rule GRBs still need to be further investigated. These correlations might also serve as discriminating factors among different GRB classes, as several of them hold different forms for SGRBs and LGRBs, hence providing insight into the generating mechanisms. Hopefully those correlations could lead to new standard candles allowing exploring the high-redshift universe.

Conflicts of Interest

The authors declare that they have no conflicts of interest.

Acknowledgments

M. Tarnopolski acknowledges support in a form of a special scholarship of Marian Smoluchowski Scientific Consortium "Matter-Energy-Future" from KNOW funding, Grant no. KNOW/48/SS/PC/2015. The work of R. Del Vecchio was supported by the Polish National Science Centre through Grant DEC-2012/04/A/ST9/00083.

References

[1] E. Nakar, "Short-hard gamma-ray bursts," *Physics Reports*, vol. 442, no. 1–6, pp. 166–236, 2007.

[2] B. Zhang, "Open questions in GRB physics," *Comptes Rendus Physique*, vol. 12, no. 3, pp. 206–225, 2011.

[3] N. Gehrels and S. Razzaque, "γ-ray bursts in the swift-Fermi era," *Frontiers of Physics*, vol. 8, no. 6, pp. 661–678, 2013.

[4] E. Berger, "Short-duration gamma-ray bursts," *Annual Review of Astronomy and Astrophysics*, vol. 52, no. 1, pp. 43–105, 2014.

[5] P. Kumar and B. Zhang, "The physics of gamma-ray bursts and relativistic jets," *Physics Reports*, vol. 561, pp. 1–109, 2015.

[6] P. Mészáros and M. J. Rees, "Gamma-ray bursts," *General Relativity and Gravitation*.

[7] R. W. Klebesadel, I. B. Strong, and R. A. Olson, "Observations of gamma-ray bursts of cosmic origin," *The Astrophysical Journal*, vol. 182, pp. L85–L88, 1973.

[8] E. P. Mazets, S. V. Golenetskii, V. N. Il'Inskii et al., "Catalog of cosmic gamma-ray bursts from the KONUS experiment data—parts I and II," *Astrophysics and Space Science*, vol. 80, no. 1, pp. 3–83, 1981.

[9] C. Meegan, G. Fishman, R. Wilson et al., "The spatial distribution of gamma-ray bursts observed by BATSE," in *Proceedings of the Compton Gamma-Ray Observatory*, pp. 681–685, USA.

[10] C. Kouveliotou, C. A. Meegan, G. J. Fishman et al., "Identification of two classes of gamma-ray bursts," *The Astrophysical Journal*, vol. 413, no. 2, pp. 101–104, 1993.

[11] B. Paczynski, "On the Galactic origin of gamma-ray bursts," *Acta Astron*, vol. 348, pp. 485–494, 1990.

[12] B. Paczynski, "Cosmological gamma-ray bursts," *Acta Astronomica*, vol. 41:0, pp. 257–267, 1991.

[13] G. J. Fishman, "γ-ray bursts," *Annual Review of Astronomy and Astrophysics*, vol. 33, no. 1, pp. 415–458.

[14] M. S. Briggs, W. S. Paciesas, G. N. Pendleton et al., "BATSE observations of the large-scale isotropy of gamma-ray bursts," *The Astrophysical Journal*, vol. 459, p. 40, 1996.

[15] M. R. Metzger, S. G. Djorgovski, S. R. Kulkarni et al., "Spectral constraints on the redshift of the optical counterpart to the γ-ray burst of 8 May 1997," *Nature*, vol. 387, no. 6636, pp. 878–880, 1997.

[16] L. G. Balazs, A. Meszaros, and I. Horvath, "Anisotropy of the sky distribution of gamma-ray bursts," p. 339, 0 1–6, 339, November 1998.

[17] A. Mészáros, Z. Bagoly, I. Horváth, L. G. Balázs, and R. Vavrek, "A remarkable angular distribution of the intermediate subclass of gamma-ray bursts," *The Astrophysical Journal* , vol. 539, no. 1, pp. 98–101, 2000.

[18] A. Mészáros, Z. Bagoly, and R. Vavrek, "On the existence of the intrinsic anisotropies in the angular distributions of gamma-ray bursts," *Astronomy & Astrophysics* , vol. 354, no. 1, pp. 1–6, 2000.

[19] A. Mészáros and J. Štoček, "Anisotropy in the angular distribution of the long gamma-ray bursts?" *Astronomy & Astrophysics*, vol. 403, no. 2, pp. 443–448, 2003.

[20] M. Magliocchetti, G. Ghirlanda, and A. Celotti, "Evidence for anisotropy in the distribution of short-lived gamma-ray bursts," *Monthly Notices of the Royal Astronomical Society*, vol. 343, no. 1, pp. 255–258, 2003.

[21] A. Bernui, I. S. Ferreira, and C. A. Wuensche, "On the large-scale angular distribution of short gamma-ray bursts," *The Astrophysical Journal* , vol. 673, no. 2, pp. 968–971, 2008.

[22] R. Vavrek, L. G. Balázs, A. Mészáros, I. Horváth, and Z. Bagoly, "Testing the randomness in the sky-distribution of gamma-ray bursts," *Monthly Notices of the Royal Astronomical Society*, vol. 391, no. 4, pp. 1741–1748, 2008.

[23] M. Tarnopolski, "Testing the anisotropy in the angular distribution of Fermi/GBM gamma-ray bursts," *Monthly Notices of the Royal Astronomical Society*, vol. 472, no. 4, pp. 4819–4831, 2017.

[24] A. Mészáros, L. G. Balázs, Z. Bagoly, and P. Veres, "Impact on cosmology of the celestial anisotropy of the short gamma-ray bursts," *Baltic Astronomy*, vol. 18, no. 3-4, pp. 293–296, 2009.

[25] J. Hjorth, J. Sollerman, P. Møller et al., "A very energetic supernova associated with the γ-ray burst of 29 March 2003," *Nature*, vol. 423, no. 6942, pp. 847–850, 2003.

[26] D. Malesani, G. Tagliaferri, G. Chincarini et al., "SN 2003lw and GRB 031203: a bright supernova for a faint gamma-ray burst," *The Astrophysical Journal* , vol. 609, no. 1, pp. L5–L8, 2004.

[27] S. E. Woosley and J. S. Bloom, "The supernova-gamma-ray burst connection," *Annual Review of Astronomy and Astrophysics*, vol. 44, pp. 507–556, 2006.

[28] M. Sparre, J. Sollerman, J. P. U. Fynbo et al., "Spectroscopic evidence for SN 2010ma associated with GRB 101219B," *The Astrophysical Journal Letters*, vol. 735, no. 1, p. L24, 2011.

[29] S. Schulze, D. Malesani, A. Cucchiara et al., "GRB 120422A/SN 2012bz: bridging the gap between low- and high-luminosity gamma-ray bursts," *Astronomy & Astrophysics*, vol. 566, article A102, 2014.

[30] D. Eichler, M. Livio, T. Piran, and D. N. Schramm, "Nucleosynthesis, neutrino bursts and γ-rays from coalescing neutron stars," *Nature*, vol. 340, no. 6229, pp. 126–128, 1989.

[31] R. Narayan, B. Paczyński, and T. Piran, "Gamma-ray bursts as the death throes of massive binary stars," *The Astrophysical Journal*, vol. 395, no. 2, pp. 83–86, 1992.

[32] E. Nakar and T. Piran, "Outliers to the peak energy-isotropic energy relation in gamma-ray bursts," *Monthly Notices of the Royal Astronomical Society*, vol. 360, no. 1, pp. L73–L76, 2005.

[33] B. Zhang, B.-B. Zhang, F. J. Virgili et al., "Discerning the physical origins of cosmological gamma-ray bursts based on multiple observational criteria: the cases of $z = 6.7$ GRB 080913, $z = 8.2$ GRB 090423, and some short/hard GRBs," *The Astrophysical Journal*, vol. 703, no. 2, pp. 1696–1724, 2009.

[34] B. P. Abbott, R. Abbott, T. D. Abbott et al., "Observation of gravitational waves from a binary black hole merger," *Physical Review Letters*, vol. 116, no. 6, 061102, 16 pages, 2016.

[35] V. Connaughton, E. Burns, A. Goldstein et al., "Fermi GBM observations of ligo gravitational-wave event GW150914," *The Astrophysical Journal Letters*, vol. 826, no. 1, article no. L6, 2016.

[36] P. N. Bhat, C. A. Meegan, A. Von Kienlin et al., "The third fermi gbm gamma-ray burst catalog: the first six years," *The Astrophysical Journal Supplement Series*, vol. 223, no. 2, article no. 28, 2016.

[37] V. Savchenko, C. Ferrigno, S. Mereghetti et al., "Integral upper limits on gamma-ray emission associated with the gravitational wave event gw150914," *The Astrophysical Journal Letters*, vol. 820, no. 2, article no. L36, 2016.

[38] P. A. Evans, J. A. Kennea, S. D. Barthelmy et al., "*Swift* follow-up of the gravitational wave source GW150914," *MNRAS Letters*, vol. 460, no. 1, pp. L40–L44, 2016.

[39] M. Lyutikov, "Fermi GBM signal contemporaneous with GW150914—an unlikely association".

[40] X. Li, F.-W. Zhang, Q. Yuan et al., "Implications of the tentative association between gw150914 and a fermi-gbm transient," *The Astrophysical Journal Letters*, vol. 827, no. 1, article no. L16, 2016.

[41] A. Loeb, "Electromagnetic counterparts to black hole mergers detected by ligo," *The Astrophysical Journal Letters*, vol. 819, no. 2, article no. L21, 2016.

[42] R. Perna, D. Lazzati, and B. Giacomazzo, "Short gamma-ray bursts from the merger of two black holes," *The Astrophysical Journal Letters*, vol. 821, no. 1, article no. L18, 2016.

[43] B. J. Morsony, J. C. Workman, and D. M. Ryan, "Modeling the afterglow of the possible Fermi-GBM event associated with GW150914," *The Astrophysical Journal Letters*, vol. 825, no. 2, article no. L24, 2016.

[44] E. Costa, F. Frontera, J. Heise et al., "Discovery of an X-ray afterglow associated with the γ-ray burst of 28 February 1997," *Nature*, vol. 387, no. 6635, pp. 783–785, 1997.

[45] J. van Paradijs, P. J. Groot, T. Galama et al., "Transient optical emission from the error box of the γ-ray burst of 28 february 1997," *Nature*, vol. 386, no. 6626, pp. 686–689, 1997.

[46] I. Horváth, "A third class of gamma-ray bursts?" *The Astrophysical Journal*, vol. 508, no. 2, pp. 757–759, 1998.

[47] I. Horváth, "A further study of the BATSE Gamma-Ray Burst duration distribution," *Astronomy & Astrophysics*, vol. 392, no. 3, pp. 791–793, 2002.

[48] I. Horvath, L. G. Balazs, Z. Bagoly, and P. Veres, "Classification of Swift's gamma-ray bursts," *Astronomy & Astrophysics*, vol. 489, no. 1, pp. L1–L4, 2008.

[49] I. Horváth, "Classification of BeppoSAX's gamma-ray bursts," *Astrophysics and Space Science*, vol. 323, no. 1, pp. 83–86, 2009.

[50] D. Huja, A. Mészáros, and J. Řípa, "A comparison of the gamma-ray bursts detected by BATSE and Swift," *Astronomy & Astrophysics* , vol. 504, no. 1, pp. 67–71, 2009.

[51] J. Řípa, A. Mészáros, C. Wigger, D. Huja, R. Hudec, and W. Hajdas, "Search for gamma-ray burst classes with the RHESSI satellite," *Astronomy & Astrophysics* , vol. 498, no. 2, pp. 399–406, 2009.

[52] S. Mukherjee, E. D. Feigelson, G. J. Babu, F. Murtagh, C. Fralev, and A. Raftery, "Three types of gamma-ray bursts," *The Astrophysical Journal*, vol. 508, no. 1, pp. 314–327, 1998.

[53] I. Horváth, L. G. Balázs, Z. Bagoly, F. Ryde, and A. Mészáros, "A new definition of the intermediate group of gamma-ray bursts," *Astronomy & Astrophysics* , vol. 447, no. 1, pp. 23–30, 2006.

[54] I. Horávth, Z. Bagoly, L. G. Balázs, A. De Ugarte Postigo, P. Veres, and A. Mészáros, "Detailed classification of swift's gamma-ray bursts," *The Astrophysical Journal* , vol. 713, no. 1, pp. 552–557, 2010.

[55] P. Veres, Z. Bagoly, I. Horváth, A. Mészáros, and L. G. Balázs, "A distinct peak-flux distribution of the third class of gamma-ray bursts: a possible signature of X-ray flashes?" *The Astrophysical Journal*, vol. 725, no. 2, pp. 1955–1964, 2010.

[56] C. Koen and A. Bere, "On multiple classes of gamma-ray bursts, as deduced from autocorrelation functions or bivariate duration/hardness ratio distributions," *Monthly Notices of the Royal Astronomical Society*, vol. 420, no. 1, pp. 405–415, 2012.

[57] H. Zitouni, N. Guessoum, W. J. Azzam, and R. Mochkovitch, "Statistical study of observed and intrinsic durations among BATSE and Swift/BAT GRBs," *Astrophysics and Space Science*, vol. 357, no. 1, 2015.

[58] M. Tarnopolski, "Analysis of Fermi gamma-ray burst duration distribution," *Astronomy and Astrophysics*, vol. 581, 2015.

[59] M. Tarnopolski, "Analysis of gamma-ray burst duration distribution using mixtures of skewed distributions," *Monthly Notices of the Royal Astronomical Society*, vol. 458, no. 2, pp. 2024–2031, 2016.

[60] M. Tarnopolski, "Analysis of the observed and intrinsic durations of gamma-ray bursts with known redshift," *Astrophysics and Space Science*, vol. 361, no. 3, article no. 125, 2016.

[61] M. Tarnopolski, "Analysis of the observed and intrinsic durations of Swift/BAT gamma-ray bursts," *New Astronomy*, vol. 46, pp. 54–59, 2016.

[62] O. Bromberg, E. Nakar, T. Piran, and R. Sari, "Short versus long and collapsars versus non-collapsars: a quantitative classification of gamma-ray bursts," *The Astrophysical Journal* , vol. 764, no. 2, article 179, 2013.

[63] M. Tarnopolski, "On the limit between short and long GRBs," *Astrophysics and Space Science*, vol. 359, no. 1, 2015.

[64] H. Gao, Y. Lu, and S. N. Zhang, "A new class of γ-ray bursts from stellar disruptions by intermediate-mass black holes," *The Astrophysical Journal*, vol. 717, no. 1, pp. 268–276, 2010.

[65] J. P. Norris and J. T. Bonnell, "Short gamma-ray bursts with extended emission," *The Astrophysical Journal*, vol. 643, no. 1, article 266, 2006.

[66] M. Boër, B. Gendre, and G. Stratta, "Are ultra-long gamma-ray bursts different?" *The Astrophysical Journal* , vol. 800, no. 1, article no. 16, 2015.

[67] F. J. Virgili, C. G. Mundell, V. Pal'Shin et al., "GRB 091024A and the nature of ultra-long gamma-ray bursts," *The Astrophysical Journal* , vol. 778, no. 1, article 54, 2013.

[68] B.-B. Zhang, B. Zhang, K. Murase, V. Connaughton, and M. S. Briggs, "How long does a burst burst?" *The Astrophysical Journal*, vol. 787, no. 1, article 66, 2014.

[69] A. J. Levan, N. R. Tanvir, R. L. C. Starling et al., "A new population of ultra-long duration gamma-ray bursts," *The Astrophysical Journal*, vol. 781, no. 1, article 13, 2014.

[70] A. J. Levan, "Swift discoveries of new populations of extremely long duration high energy transient," *Journal of High Energy Astrophysics*, vol. 7, pp. 44–55, 2015.

[71] J. Heise, J. I. Zand, R. M. Kippen, and P. M. Woods, "X-ray flashes and X-ray rich gamma ray bursts," *Gamma-Ray Bursts in the Afterglow Era*, pp. 16–21, 2001.

[72] R. M. Kippen, P. M. Woods, J. Heise, J. I. Zand, R. D. Preece, and M. S. Briggs, "BATSE observations of fast X-ray transients detected by BeppoSAX-WFC," in *Gamma-ray Bursts in the Afterglow Era*, E. Costa, F. Frontera, and J. Hjorth, Eds., p. 22, 2001.

[73] D. Grupe, J. A. Nousek, P. Veres, B.-B. Zhang, and N. Gehrels, "Evidence for new relations between gamma-ray burst prompt and x-ray afterglow emission from 9 years of swift," *The Astrophysical Journal Supplement Series*, vol. 209, no. 2, article no. 20, 2013.

[74] J. P. U. Fynbo, D. Watson, C. C. Thöne et al., "No supernovae associated with two long-duration γ-ray bursts," *Nature*, vol. 444, no. 7122, pp. 1047–1049, 2006.

[75] M. Della Valle, D. Malesani, J. S. Bloom et al., "Hypernova signatures in the late rebrightening of GRB 050525A," *The Astrophysical Journal Letters*, vol. 642, no. 2, pp. L103–L106, 2006.

[76] D. A. Perley, N. R. Tanvir, J. Hjorth et al., "The swift GRB host galaxy legacy survey. ii. rest-frame near-ir luminosity distribution and evidence for a near-solar metallicity threshold," *The Astrophysical Journal*, vol. 817, no. 1, article no. 8, 2016.

[77] J. Greiner, P. A. Mazzali, and D. A. Kann, "A very luminous magnetar-powered supernova associated with an ultra-long γ-ray burst," *Nature*, vol. 523, no. 7559, pp. 189–192, 2015.

[78] R. A. M. J. Wijers, M. J. Rees, and P. Mészáros, "Shocked by GRB 970228: the afterglow of a cosmological fireball," *Monthly Notices of the Royal Astronomical Society*, vol. 288, no. 4, pp. L51–L56, 1997.

[79] P. Mészáros, "Theoretical models of gamma-ray bursts," in *Proceedings of the Gamma-Ray BURSTS*, pp. 647–656, Huntsville, Alabama (USA).

[80] P. Mészros, "Gamma-ray bursts," *Reports on Progress in Physics*.

[81] R. Willingale, P. T. O'Brien, J. P. Osborne et al., "Testing the standard fireball model of gamma-ray bursts using late X-ray afterglows measured by Swift," *The Astrophysical Journal* , vol. 662, no. 2 I, pp. 1093–1110, 2007.

[82] A. Melandri, C. G. Mundell, S. Kobayashi et al., "The early-time optical properties of gamma-ray burst afterglows," *The Astrophysical Journal* , vol. 686, no. 2, pp. 1209–1230, 2008.

[83] E. S. Rykoff, F. Aharonian, and C. W. Akerlof, "Looking into the fireball: Rotse-III and *Swift* observations of early gamma-ray burst afterglows," *The Astrophysical Journal*, vol. 702, no. 1, p. 489, 2009.

[84] S. R. Oates, M. J. Page, P. Schady et al., "A statistical comparison of the optical/UV and X-ray afterglows of gamma-ray bursts using the swift ultraviolet optical and X-ray telescopes," *Monthly Notices of the Royal Astronomical Society*, vol. 412, no. 1, pp. 561–579, 2011.

[85] N. Gehrels, G. Chincarini, P. Giommi et al., "The swift gamma-ray burst mission," *The Astrophysical Jornal*, vol. 611, pp. 1005–1020, August 2004.

[86] P. T. O'Brien, R. Willingale, J. Osborne et al., "The early X-ray emission from GRBs," *The Astrophysical Journal Letters*, vol. 647, no. 2, pp. 1213–1237, 2006.

[87] T. Sakamoto, J. E. Hill, R. Yamazaki et al., "Evidence of exponential decay emission in the gamma-ray bursts," *The Astrophysical Journal* , vol. 669, no. 2, pp. 1115–1129, 2007.

[88] B.-B. Zhang, E. N.-W. Liang, and B. Zhang, "A comprehensive analysis of Swift XRT data. I. Apparent spectral evolution of gamma-ray burst X-ray tails," *The Astrophysical Journal* , vol. 666, no. 2 I, pp. 1002–1011, 2007.

[89] J. A. Nousek, C. Kouveliotou, and D. Grupe, "Evidence for a canonical gamma-ray burst afterglow light curve in the *Swift* XRT Data," *The Astrophysical Journal*, vol. 642, no. 1, pp. 389–400, 2006.

[90] A. Cucchiara, A. J. Levan, D. B. Fox et al., "A photometric redshift of $z \sim 9.4$ for GRB 090429B," *The Astrophysical Journal*, vol. 736, no. 1, article 7, 2011.

[91] S. A. Rodney, A. G. Riess, D. M. Scolnic et al., "Erratum: Two SNe Ia at redshift ~2: Improved classification and redshift determination with medium-band infrared imaging," *The Astronomical Journal*, vol. 151, no. 2, 2016.

[92] H. Lin, X. Li, S. Wang, and Z. Chang, "Are long gamma-ray bursts standard candles?" *Monthly Notices of the Royal Astronomical Society*, vol. 453, no. 1, pp. 128–132, 2015.

[93] T. Totani, "Cosmological gamma-ray bursts and evolution of galaxies," *The Astrophysical Journal*, vol. 486, no. 2, pp. L71–L74.

[94] C. Porciani and P. Madau, "On the association of gamma-ray bursts with massive stars: Implications for number counts and lensing statistics," *The Astrophysical Journal* , vol. 548, no. 2, pp. 522–531, 2001.

[95] V. Bromm and A. Loeb, "High-redshift γ-ray bursts from population III progenitors," *The Astrophysical Journal* , vol. 642, no. 1 I, pp. 382–388, 2006.

[96] M. D. Kistler, H. Yüksel, J. F. Beacom, A. M. Hopkins, and J. S. B. Wyithe, "The star formation rate in the reionization era as indicated by gamma-ray bursts," *The Astrophysical Journal* , vol. 705, no. 2, pp. L104–L108, 2009.

[97] R. S. De Souza, N. Yoshida, and K. Ioka, "Populations III.1 and III.2 gamma-ray bursts: constraints on the event rate for future radio and X-ray surveys," *Astronomy & Astrophysics* , vol. 533, article A32, 2011.

[98] R. Barkana and A. Loeb, "Gamma-ray bursts versus quasars: Lyα signatures of reionization versus cosmological infall," *The Astrophysical Journal* , vol. 601, no. 1 I, pp. 64–77, 2004.

[99] K. Ioka and P. Mészáros, "Radio afterglows of gamma-ray bursts and hypernovae at high redshift and their potential for 21 centimeter absorption studies," *The Astrophysical Journal* , vol. 619, no. 2, pp. 684–696, 2005.

[100] S. Inoue, K. Omukai, and B. Ciardi, "The radio to infrared emission of very high redshift gamma-ray bursts: probing early star formation through molecular and atomic absorption lines," *Monthly Notices of the Royal Astronomical Society*, vol. 380, no. 4, pp. 1715–1728, 2007.

[101] R. Salvaterra, "High redshift gamma-ray bursts," *Journal of High Energy Astrophysics*, vol. 7, pp. 35–43, 2015.

[102] D. E. Reichart, D. Q. Lamb, E. E. Fenimore, E. Ramirez-Ruiz, T. L. Cline, and K. Hurley, "A possible cepheid-like luminosity estimator for the long gamma-ray bursts," *The Astrophysical Journal*, vol. 552, no. 1, pp. 57–71, 2001.

[103] G. J. Fishman, C. A. Meegan, R. B. Wilson et al., "The first batse gamma-ray burst catalog," *The Astrophysical Journal Supplement Series*, vol. 92, no. 1, pp. 229–283, 1994.

[104] J. P. Norris, R. J. Nemiroff, and J. T. Bonnell, "Attributes of pulses in long bright gamma-ray bursts," *The Astrophysical Journal*, vol. 459, p. 393, 1996.

[105] B. E. Stern and R. Svensson, "Evidence for "chain reaction" in the time profiles of gamma-ray bursts," *The Astrophysical Journal*, vol. 469, no. 2, pp. L109–L113.

[106] F. Ryde and R. Svensson, "On the variety of the spectral and temporal behavior of long gamma-ray burst pulses," *The Astrophysical Journal* , vol. 566, no. 1 I, pp. 210–228, 2002.

[107] R. Sari, T. Piran, and J. P. Halpern, "Jets in gamma-ray bursts," *The Astrophysical Journal Letters*, vol. 519, no. 1, pp. L17–L20, 1999.

[108] R. Willingale, F. Genet, J. Granot, and P. T. O'Brien, "The spectral-temporal properties of the prompt pulses and rapid decay phase of gamma-ray bursts," *Monthly Notices of the Royal Astronomical Society*, vol. 403, no. 3, pp. 1296–1316, 2010.

[109] J. E. Rhoads, "How to tell a jet from a balloon: a proposed test for beaming in gamma-ray bursts," *The Astrophysical Journal Letters*, vol. 487, no. 1, p. L1, 1997.

[110] R. S. Mallozzi, W. S. Paciesas, G. N. Pendleton et al., "The nu F nu Peak Energy Distributions of Gamma-Ray Bursts Observed by BATSE," *The Astrophysical Journal*, vol. 454, p. 597, 1995.

[111] L. Amati, F. Frontera, M. Tavani et al., "Intrinsic spectra and energetics of BeppoSAX gamma-ray bursts with known redshifts," *Astronomy & Astrophysics*, vol. 390, no. 1, pp. 81–89, 2002.

[112] T. T. Lee and V. Petrosian, "Distributions of peak flux and duration for gamma-ray bursts," *The Astrophysical Journal*, vol. 470, p. 479, 1996.

[113] J. P. Norris, G. F. Marani, and J. T. Bonnell, "Connection between energy-dependent lags and peak luminosity in gamma-ray bursts," *The Astrophysical Journal*, vol. 534, no. 1, pp. 248–257, 2000.

[114] L. Li and B. Paczynski, "Improved correlation between the variability and peak luminosity of gamma-ray bursts," *Monthly Notices of the Royal Astronomical Society*, vol. 366, no. 1, pp. 219–226, 2006.

[115] D. Band, J. Matteson, L. Ford et al., "BATSE observations of gamma-ray burst spectra. I. Spectral diversity," *The Astrophysical Journal Letters*, vol. 413, no. 1, pp. 281–292, 1993.

[116] D. Yonetoku, T. Murakami, T. Nakamura, R. Yamazaki, A. K. Inoue, and K. Ioka, "Gamma-ray burst formation rate inferred from the spectral peak energy-peak luminosity relation," *The Astrophysical Journal*, vol. 609, no. 2, pp. 935–951, 2004.

[117] M. G. Kendall and A. Stuart, *The Advanced Theory of Statistics*, vol. 2 of *Inference and Relationship*, Macmillan, New York, NY, USA, 1973.

[118] P. R. Bevington and D. K. Robinson, *Data Reduction and Error Analysis for the Physical Sciences*, McGraw-Hill, Boston, Mass, USA, 2nd edition, 1992.

[119] C. Spearman, "The proof and measurement of association between two things," *The American Journal of Psychology*, vol. 15, no. 1, p. 72, 1904.

[120] E. Liang and V. Kargatis, "Dependence of the spectral evolution of γ-ray bursts on their photon fluence," *Nature*, vol. 381, no. 6577, pp. 49–51, 1996.

[121] B. E. Schaefer, M. Deng, and D. L. Band, "Redshifts and luminosities for 112 gamma-ray bursts," *The Astrophysical Journal* , vol. 563, no. 2, pp. L123–L127, 2001.

[122] J. D. Salmonson, "On the kinematic origin of the luminosity-pulse lag relationship in gamma-ray bursts," *The Astrophysical Journal*, vol. 544, no. 2, pp. L115–L117, 2000.

[123] F. Daigne and R. Mochkovitch, "The physics of pulses in gamma-ray bursts: Emission processes, temporal profiles and time-lags," *Monthly Notices of the Royal Astronomical Society*, vol. 342, no. 2, pp. 587–592, 2003.

[124] Z. Zhang, G. Z. Xie, J. G. Deng, and W. Jin, "Revisiting the characteristics of the spectral lags in short gamma-ray bursts," *Monthly Notices of the Royal Astronomical Society*, vol. 373, no. 2, pp. 729–732, 2006.

[125] B. E. Schaefer, "Explaining the gamma-ray burst lag/luminosity relation," *The Astrophysical Journal*, vol. 602, no. 1, pp. 306–311, 2004.

[126] D. Kocevski and E. Liang, "The connection between spectral evolution and gamma-ray burst lag," *The Astrophysical Journal*, vol. 594, no. 1, pp. 385–389, 2003.

[127] J. Hakkila, T. W. Giblin, J. P. Norris, P. C. Fragile, and J. T. Bonnell, "Correlations between lag, luminosity, and duration in gamma-ray burst pulses," *The Astrophysical Journal* , vol. 677, no. 2, pp. L81–L84, 2008.

[128] R. Tsutsui, T. Nakamura, D. Yonetoku, T. Murakami, S. Tanabe, and Y. Kodama, "Redshift dependent lag-luminosity relation in 565 baste gamma ray bursts," in *Proceedings of the Santa Fe Conference on Gamma-Ray Bursts 2007, GRB 2007*, pp. 28–31, USA, November 2007.

[129] J. Sultana, D. Kazanas, and K. Fukumura, "Luminosity correlations for gamma-ray bursts and implications for their prompt and afterglow emission mechanisms," *The Astrophysical Journal* , vol. 758, no. 1, p. 32, 2012.

[130] N. Gehrels, J. P. Norris, S. D. Barthelmy et al., "A new γ-ray burst classification scheme from GRB 060614," *Nature*, vol. 444, no. 7122, pp. 1044–1046, 2006.

[131] M. G. Dainotti, V. F. Cardone, and S. Capozziello, "A time-luminosity correlation for γ -ray bursts in the X-rays," *Monthly Notices of the Royal Astronomical Society*, vol. 391, no. 1, pp. L79–L83, 2008.

[132] M. G. Dainotti, R. Willingale, S. Capozziello, V. F. Cardone, and M. Ostrowski, "Discovery of a tight correlation for gamma-ray burst afterglows with "canonical" light curves," *The Astrophysical Journal*, vol. 722, no. 2, pp. L215–L219, 2010.

[133] M. G. Dainotti, V. F. Cardone, S. Capozziello, M. Ostrowski, and R. Willingale, "Study of possible systematics in the L^*_X-T^*_a correlation of gamma-ray bursts," *The Astrophysical Journal*, vol. 730, no. 2, article no. 135, 2011.

[134] M. G. Dainotti, V. F. Cardone, E. Piedipalumbo, and S. Capozziello, "Slope evolution of GRB correlations and cosmology," *Monthly Notices of the Royal Astronomical Society*, vol. 436, no. 1, pp. 82–88, 2013.

[135] M. Dainotti, V. Petrosian, R. Willingale, P. O'Brien, M. Ostrowski, and S. Nagataki, "Luminosity-time and luminosity-luminosity correlations for GRB prompt and afterglow plateau emissions," *Monthly Notices of the Royal Astronomical Society*, vol. 451, no. 4, pp. 3898–3908, 2015.

[136] T. N. Ukwatta, M. Stamatikos, K. S. Dhuga et al., "Spectral lags and the lag-luminosity relation: an investigation with swift bat gamma-ray bursts," *The Astrophysical Journal Letters*, vol. 711, no. 2, pp. 1073–1086, 2010.

[137] T. N. Ukwatta, K. S. Dhuga, M. Stamatikos et al., "The lag-luminosity relation in the GRB source frame: An investigation with Swift BAT bursts," *Monthly Notices of the Royal Astronomical Society*, vol. 419, no. 1, pp. 614–623, 2012.

[138] R. Margutti, C. Guidorzi, G. Chincarini et al., "Lag-luminosity relation in γ-ray burst X-ray flares: a direct link to the prompt emission," *Monthly Notices of the Royal Astronomical Society*, vol. 406, no. 4, pp. 2149–2167, 2010.

[139] A. Panaitescu and P. Kumar, "Properties of relativistic jets in gamma-ray burst afterglows," *The Astrophysical Journal Letters*, vol. 571, no. 2, pp. 779–789, 2002.

[140] E. E. Fenimore, C. D. Madras, and S. Nayakshin, "Expanding relativistic shells and gamma-ray burst temporal structure," *The Astrophysical Journal* , vol. 473, no. 2, pp. 998–1012, 1996.

[141] K. Ioka and T. Nakamura, "Peak luminosity-spectral lag relation caused by the viewing angle of the collimated gamma-ray bursts," *The Astrophysical Journal Letters*, vol. 554, no. 2, pp. L163–L167, 2001.

[142] E.-W. Liang, J. L. Racusin, B. Zhang, B.-B. Zhang, and D. N. Burrows, "A comprehensive analysis of Swift XRT data. III. Jet break candidates in X-ray and optical afterglow light curves," *The Astrophysical Journal* , vol. 675, no. 1, pp. 528–552, 2008.

[143] J. Lü, Y.-C. Zou, W.-H. Lei et al., "Lorentz-factor–isotropic-luminosity/energy correlations of gamma-ray bursts and their interpretation," *The Astrophysical Journal*, vol. 751, no. 1, article no. 49, 2012.

[144] T.-F. Yi, G.-Z. Xie, and F.-W. Zhang, "A close correlation between the spectral lags and redshifts of gamma-ray bursts," *Chinese Journal of Astronomy and Astrophysics*, vol. 8, no. 1, pp. 81–86, 2008.

[145] G. Stratta, D. Guetta, V. D'Elia, M. Perri, S. Covino, and L. Stella, "Evidence for an anticorrelation between the duration of the shallow decay phase of GRB X-ray afterglows and redshift," *Astronomy & Astrophysics* , vol. 494, no. 2, p. -L12, 2009.

[146] G. Ryan, H. van Eerten, A. MacFadyen, and B.-B. Zhang, "Gamma-ray bursts are observed off-axis," *The Astrophysical Journal*, vol. 799, no. 1, article 3, 2015.

[147] Z. L. Uhm and B. Zhang, "Toward an understanding of GRB prompt emission mechanism. I. the origin of spectral lags," *The Astrophysical Journal* , vol. 825, no. 2, article no. 97, 2016.

[148] E. E. Fenimore and E. Ramirez-Ruiz, "Redshifts For 220 BATSE γ-Ray Bursts Determined by Variability and the Cosmological Consequences".

[149] C. Guidorzi, F. Frontera, E. Montanari et al., "The gamma-ray burst variability-peak luminosity correlation: New results," *Monthly Notices of the Royal Astronomical Society*, vol. 363, no. 1, pp. 315–325, 2005.

[150] D. E. Reichart and M. C. Nysewander, "GRB Variability-Luminosity Correlation Confirmed," *ArXiv Astrophysics e-prints*, August 2005.

[151] C. Guidorzi, F. Frontera, E. Montanari et al., "The slope of the gamma-ray burst variability/peak luminosity correlation," *Monthly Notices of the Royal Astronomical Society*, vol. 371, no. 2, pp. 843–851, 2006.

[152] C. Guidorzi, "Testing the gamma-ray burst variability/peak luminosity correlation using the pseudo-redshifts of a large sample of BATSE gamma-ray bursts," *Monthly Notices of the Royal Astronomical Society*, vol. 364, no. 1, pp. 163–168, 2005.

[153] G. D'Agostini, "Fits, and especially linear fits, with errors on both axes," *Extra Variance of The Data Points And Other Complications. Arxiv Physics E-Prints*, November 2005.

[154] D. Rizzuto, C. Guidorzi, P. Romano et al., "Testing the gamma-ray burst variability/peak luminosity correlation on a Swift homogeneous sample," *Monthly Notices of the Royal Astronomical Society*, vol. 379, no. 2, pp. 619–628, 2007.

[155] T. Piran, "The physics of gamma-ray bursts," *Reviews of Modern Physics*, vol. 76, no. 4, pp. 1143–1210, 2004.

[156] J. D. Salmonson and T. J. Galama, "Discovery of a tight correlation between pulse LAG/luminosity and jet-break times: A connection between gamma-ray bursts and afterglow properties," *The Astrophysical Journal* , vol. 569, no. 2 I, pp. 682–688, 2002.

[157] B. E. Schaefer, "The Hubble Diagram to Redshift >6 from 69," *Gamma-Ray Bursts*, vol. 660:0, Article ID 511742, pp. 16–46, May 2007.

[158] B. Schaefer, "Four luminosity indicators for gamma-ray bursts," in *Proceedings of the COSPAR Scientifc Assembly, volume 34 of COSPAR Meeting*, p. 1141, Houston, Texas, USA, Oct 2002.

[159] L. Xiao and B. E. Schaefer, "Estimating redshifts for long gamma-ray bursts," *The Astrophysical Journal* , vol. 707, no. 1, pp. 387–403, 2009.

[160] D. L. Freedman and E. Waxman, "On the energy of gamma-ray bursts," *The Astrophysical Journal*, vol. 547, no. 2, pp. 922–928, 2001.

[161] E. Waxman, "γ-Ray burst afterglow: confirming the cosmological fireball model," *The Astrophysical Journal*, vol. 489, no. 1, pp. L33–L36.

[162] R. A. M. J. Wijers and T. J. Galama, "Physical parameters of GRB 970508 and GRB 971214 from their afterglow synchrotron emission," *The Astrophysical Journal*, vol. 523, no. 1, pp. 177–186, 1999.

[163] J. Granot, T. Piran, and R. Sari, "Images and spectra from the interior of a relativistic fireball," *The Astrophysical Journal*, vol. 513, no. 2, pp. 679–689, 1999.

[164] E.-W. Liang, S.-X. Yi, J. Zhang, H.-J. Lü, and B.-B. Zhang, "Constraining gamma-ray burst initial lorentz factor with the afterglow onset feature and discovery of a tight Γ_0-$E_{gamma,iso}$ Correlation," *The Astrophysical Journal*, vol. 725, pp. 2209–2224, 2010.

[165] G. Ghirlanda, G. Ghisellini, L. Nava, and D. Burlon, "Spectral evolution of Fermi/GBM short gamma-ray bursts," *Monthly Notices of the Royal Astronomical Society*, vol. 410, no. 1, pp. L47–L51, 2011.

[166] R. Sari and T. Piran, "GRB 990123: the optical flash and the fireball model," *The Astrophysical Journal*, vol. 517, no. 2, pp. L109–L112, 1999.

[167] Y. Lithwick and R. Sari, "Lower limits on Lorentz factors in gamma-ray bursts," *The Astrophysical Journal Letters*, vol. 555, no. 1, pp. 540–545, 2001.

[168] Y.-C. Zou and T. Piran, "Lorentz factor constraint from the very early external shock of the gamma-ray burst ejecta," *Monthly Notices of the Royal Astronomical Society*, vol. 402, no. 3, pp. 1854–1862, 2010.

[169] B. Zhang and A. Pe'er, "Evidence of an initially magnetically dominated outflow in GRB 080916C," *The Astrophysical Journal Letters*, vol. 700, no. 2, pp. L65–L68, 2009.

[170] Y. Fan, "The spectrum of γ-ray burst: a clue," *Monthly Notices of the Royal Astronomical Society*, vol. 403, no. 1, pp. 483–490, 2010.

[171] B. Zhang and H. Yan, "The internal-collision-induced magnetic reconnection and turbulence (ICMART) model of gamma-ray bursts," *The Astrophysical Journal*, vol. 726, no. 2, p. 90, 2011.

[172] W. H. Lei, D. X. Wang, L. Zhang, Z. M. Gan, Y. C. Zou, and Y. Xie, "Magnetically torqued neutrino-dominated accretion flows for gamma-ray bursts," *The Astrophysical Journal* , vol. 700, no. 2, pp. 1970–1976, 2009.

[173] N. M. Lloyd, V. Petrosian, and R. S. Mallozzi, "Cosmological versus Intrinsic: The Correlation between Intensity and the Peak of the νF Î¡," *The Astrophysical Journal*, vol. 534, no. 1, pp. 227–238, 2000.

[174] M. G. Kendall, "A New Measure of Rank Correlation," *Biometrika*, vol. 30, no. 1-2, p. 81, 1938.

[175] R. S. Mallozzi, G. N. Pendleton, W. S. Paciesas, R. D. Preece, and M. S. Briggs, "Gamma-ray burst spectra and the hardness-intensity correlation," in *Proceedings of the GAMMA-RAY BURSTS*, vol. 428, pp. 273–277, Huntsville, Alabama (USA).

[176] A. Goldstein, R. D. Preece, and M. S. Briggs, "A new discriminator for gamma-ray burst classification: The $E_{\rm peak}$-fluence energy ratio," *The Astrophysical Journal*, vol. 721, no. 2, pp. 1329–1332, 2010.

[177] R.-J. Lu, J.-J. Wei, E.-W. Liang et al., "A comprehensive analysis of fermi gamma-ray burst data. II. E_p evolution patterns and implications for the observed spectrum-luminosity relations," *The Astrophysical Journal*, vol. 756, no. 2, article no. 112, 2012.

[178] S. V. Golenetskii, E. P. Mazets, R. L. Aptekar, and V. N. Ilyinskii, "Correlation between luminosity and temperature in γ-ray burst sources," *Nature*, vol. 306, no. 5942, pp. 451–453, 1983.

[179] L. Borgonovo and F. Ryde, "On the hardness-intensity correlation in gamma-ray burst pulses," *The Astrophysical Journal* , vol. 548, no. 2, pp. 770–786, 2001.

[180] G. Ghirlanda, L. Nava, and G. Ghisellini, "Spectral-luminosity relation within individual Fermi gamma rays bursts," *Astronomy & Astrophysics*, vol. 511, no. 1, article A43, 2010.

[181] S. Guiriec, M. S. Briggs, V. Connaugthon et al., "Time-resolved spectroscopy of the three brightest and hardest short gamma-ray bursts observed with the fermi gamma-ray burst monitor," *The Astrophysical Journal* , vol. 725, no. 1, pp. 225–241, 2010.

[182] N. M. Lloyd and V. Petrosian, "Distribution of spectral characteristics and the cosmological evolution of gamma-ray bursts," *The Astrophysical Journal*, vol. 511, no. 2, pp. 550–561, 1999.

[183] N. M. Lloyd, V. Petrosian, and R. D. Preece, "Synchrotron emission as the source of GRB spectra, Part II: Observations," in *Proceedings of the The fifth huntsville gamma-ray burst symposium*, pp. 155–159, Huntsville, Alabama (USA).

[184] J. S. Bloom, D. A. Frail, and R. Sari, "The prompt energy release of gamma-ray bursts using a cosmological k-correction," *The Astronomical Journal*, vol. 121, no. 6, pp. 2879–2888, 2001.

[185] L. Amati, F. Frontera, J. M. Castro Cerón et al., "The Prompt and Afterglow Emission of GRB 001109 Measured by BeppoSAX," in *A Workshop Celebrating the First Year of the HETE Mission American Institute of Physics Conference Series*, J. J. M. and R. K. Ricker, Eds., vol. 662, pp. 387–389, April 2003.

[186] D. Q. Lamb, T. Q. Donaghy, and C. Graziani, "A unified jet model of X-ray flashes and γ-ray bursts," *New Astronomy Reviews*, vol. 48, no. 5-6, pp. 459–464, 2004.

[187] T. Sakamoto, D. Q. Lamb, C. Graziani et al., "High energy transient explorer 2 observations of the extremely soft X-ray flash XRF 020903," *The Astrophysical Journal* , vol. 602, no. 2 I, pp. 875–885, 2004.

[188] G. Ghirlanda, G. Ghisellini, and D. Lazzati, "The collimation-corrected gamma-ray burst energies correlate with the peak energy of their νF_ν spectrum," *The Astrophysical Journal*, vol. 616, no. 1, pp. 331–338, 2004.

[189] G. Ghirlanda, G. Ghisellini, and C. Firmani, "Probing the existence of the $E_{\rm peak}$-$E_{\rm iso}$ correlation in long gamma ray bursts," *Monthly Notices of the Royal Astronomical Society*, vol. 361, no. 1, pp. L10–L14, 2005.

[190] L. Amati, "The $E_{p,i}$-E_{iso} correlation in gamma-ray bursts: updated observational status, re-analysis and main implications," *Monthly Notices of the Royal Astronomical Society*, vol. 372, no. 1, pp. 233–245, 2006.

[191] G. Ghirlanda, L. Nava, G. Ghisellini, C. Firmani, and J. I. Cabrera, "The $E_{\rm peak}$-$E_{\rm iso}$ plane of long gamma-ray bursts and selection effects," *Monthly Notices of the Royal Astronomical Society*, vol. 387, no. 1, pp. 319–330, 2008.

[192] L. Amati, F. Frontera, and C. Guidorzi, "Extremely energetic Fermi gamma-ray bursts obey spectral energy correlations," *Astronomy & Astrophysics* , vol. 508, no. 1, pp. 173–180, 2009.

[193] L. Amati, "Cosmology with the $E_{{\rm p},i}$-$E_{\rm iso}$ correlation of gamma-ray bursts," *International Journal of Modern Physics: Conference Series*, vol. 12, pp. 19–27, 2012.

[194] L. Amati, C. Guidorzi, F. Frontera et al., "Measuring the cosmological parameters with the $E_{p,i}$-E_{iso} correlation of gamma-ray bursts," *Monthly Notices of the Royal Astronomical Society*, vol. 391, no. 2, pp. 577–584, 2008.

[195] Y.-P. Qin and Z.-F. Chen, "Statistical classification of gamma-ray bursts based on the amati relation," *Monthly Notices of the Royal Astronomical Society*, vol. 430, no. 1, pp. 163–173, 2013.

[196] V. Heussaff, J.-L. Atteia, and Y. Zolnierowski, "The E_{peak}-E_{iso} relation revisited with fermi GRBs: resolving a long-standing debate?" *Astronomy & Astrophysics*, vol. 557, article 100, 2013.

[197] L. Amati and M. Della Valle, "Measuring cosmological parameters with gamma ray bursts," *International Journal of Modern Physics D*, vol. 22, no. 14, Article ID 1330028, 2013.

[198] R. Basak and A. R. Rao, "Erratum: Correlation between the isotropic energy and the peak energy at zero fluence for the individual pulses of gamma-ray bursts: Toward a universal physical correlation for the prompt emission," *The Astrophysical Journal*, vol. 754, no. 1, article no. 79, 2012.

[199] R. Basak and A. R. Rao, "Pulse-wise Amati correlation in Fermi gamma-ray bursts," *Monthly Notices of the Royal Astronomical Society*, vol. 436, no. 4, pp. 3082–3088, 2013.

[200] F. Frontera, L. Amati, C. Guidorzi, R. Landi, and J. In'T Zand, "Erratum: Broadband time-resolved $E_{{\rm p},i}$-$L_{\rm iso}$ correlation in γ-ray bursts (Astrophysical Journal (2012) 754 (138))," *The Astrophysical Journal*, vol. 757, no. 1, article no. 107, 2012.

[201] D. A. Frail, S. R. Kulkarni, R. Sari et al., "The radio afterglow from grb 980519: a test of the jet and circumstellar models," *The Astrophysical Journal*, vol. 534, no. 2, pp. 559–564, 2000.

[202] S. A. Yost, D. A. Frail, F. A. Harrison et al., "The broadband afterglow of GRB 980329," *The Astrophysical Journal* , vol. 577, no. 1 I, pp. 155–163, 2002.

[203] B. E. Schaefer, "Explaining the gamma-ray burst $E_{\rm peak}$ distribution," *The Astrophysical Journal*, vol. 583, no. 2, pp. L71–L74, 2003.

[204] E. Liang and B. Zhang, "Model-independent multivariable gamma-ray burst luminosity indicator and its possible cosmological implications," *The Astrophysical Journal*, vol. 633, no. 2, pp. 611–623, 2005.

[205] L. Nava, G. Ghisellini, G. Ghirlanda, F. Tavecchio, and C. Firmani, "On the interpretation of spectral-energy correlations in long gamma-ray bursts," *Astronomy & Astrophysics* , vol. 450, no. 2, pp. 471–481, 2006.

[206] G. Ghirlanda, L. Nava, G. Ghisellini, and C. Firmani, "Confirming the γ-ray burst spectral-energy correlations in the era of multiple time breaks," *Astronomy & Astrophysics* , vol. 466, no. 1, pp. 127–136, 2007.

[207] N. M. Lloyd-Ronning and V. Petrosian, "Interpreting the behavior of time-resolved gamma-ray burst spectra," *The Astrophysical Journal Letters*, vol. 565, no. 1, pp. 182–194, 2002.

[208] B. Zhang and P. Mészáros, "An analysis of gamma-ray burst spectral break models," *The Astrophysical Journal*, vol. 581, no. 2, pp. 1236–1247, 2002.

[209] G. Ghirlanda, G. Ghisellini, R. Salvaterra et al., "The faster the narrower: Characteristic bulk velocities and jet opening angles of gamma-ray bursts," *Monthly Notices of the Royal Astronomical Society*, vol. 428, no. 2, pp. 1410–1423, 2013.

[210] M. J. Rees and P. Mészáros, "Dissipative photosphere models of gamma-ray bursts and X-ray flashes," *The Astrophysical Journal*, vol. 628, no. 2, p. 847, 2005.

[211] E. Ramirez-Ruiz, "Photospheric signatures imprinted on the γ-ray burst spectra," *Monthly Notices of the Royal Astronomical Society*, vol. 363, no. 1, pp. L61–L65, 2005.

[212] F. Ryde, "Is thermal emission in gamma-ray bursts ubiquitous?" *The Astrophysical Journal Letters*, vol. 625, no. 2, pp. L95–L98, 2005.

[213] A. M. Beloborodov, "Collisional mechanism for gamma-ray burst emission," *Monthly Notices of the Royal Astronomical Society*, vol. 407, no. 2, pp. 1033–1047, 2010.

[214] S. Guiriec, V. Connaughton, M. S. Briggs et al., "Detection of a thermal spectral component in the prompt emission of GRB 100724B," *The Astrophysical Journal Letters*, vol. 727, no. 2, article L33, 2011.

[215] R. Hascoët, F. Daigne, and R. Mochkovitch, "Prompt thermal emission in gamma-ray bursts," *Astronomy & Astrophysics* , vol. 551, article A124, 2013.

[216] S. Guiriec, F. Daigne, R. Hascoët et al., "Evidence for a photospheric component in the prompt emission of the short GRB 120323a and its effects on the GRB hardness-luminosity relation," *The Astrophysical Journal*, vol. 770, no. 1, article 32, 2013.

[217] I. Vurm and A. M. Beloborodov, "Radiative transfer models for gamma-ray bursts," *The Astrophysical Journal*, vol. 831, no. 2, article no. 175, 2016.

[218] S. Guiriec, C. Kouveliotou, F. Daigne et al., "Toward a better understanding of the grb phenomenon: a new model for grb prompt emission and its effects on the new L_i^{NT}-$E_{peak,i}^{nth,rest}$ relation," *The Astrophysical Journal*, vol. 807, no. 2, article no. 148, 2015.

[219] S. Guiriec, R. Mochkovitch, T. Piran et al., "GRB 131014A: A laboratory for studying the thermal-like and non-thermal emissions in gamma-ray bursts, and the new $L^{nTh}{}_i$-$E^{nTh,rest}{}_{peak,i}$ relation," *The Astrophysical Journal*, vol. 814, no. 1, article no. 10, 2015.

[220] F. Frontera, L. Amati, E. Costa et al., "Prompt and delayed emission properties of γ-ray bursts observed with *BeppoSAX*," *The Astrophysical Journal*, vol. 127, no. 1, pp. 59–78, 2000.

[221] R. D. Preece, M. S. Briggs, R. S. Mallozzi, G. N. Pendleton, W. S. Paciesas, and D. L. Band, "The BATSE gamma-ray Burst spectral catalog. I. High time resolution spectroscopy of bright Bursts using high energy resolution data," *The Astrophysical Journal*, vol. 126, no. 1, pp. 19–36, 2000.

[222] G. Ghirlanda, A. Celotti, and G. Ghisellini, "Extremely hard GRB spectra prune down the forest of emission models," *Astronomy & Astrophysics* , vol. 406, no. 3, pp. 879–892, 2003.

[223] A. Panaitescu, "An external-shock origin of the relation for gamma-ray bursts," *Monthly Notices of the Royal Astronomical Society*, vol. 393, no. 3, pp. 1010–1015, March 2009.

[224] R. Mochkovitch and L. Nava, "The $E_{\rm p}$-$E_{\rm iso}$ relation and the internal shock model. Åp," *Astronomy and Astrophysics*, vol. 557, pp. 10–1051, May 2015.

[225] A. C. Collazzi, B. E. Schaefer, and J. A. Moree, "The total errors in measuring $E_{\rm peak}$ for γ-ray bursts," *The Astrophysical Journal*, vol. 729, no. 2, article 89, 2011.

[226] B. E. Schaefer, "Gamma-ray burst Hubble diagram to z = 4.5," *The Astrophysical Journal Letters*, vol. 583, no. 2, pp. L67–L70, 2003.

[227] L. Nava, R. Salvaterra, G. Ghirlanda et al., "A complete sample of bright Swift long gamma-ray bursts: testing the spectral-energy correlations," *Monthly Notices of the Royal Astronomical Society*, vol. 421, no. 2, pp. 1256–1264, 2012.

[228] G. Ghirlanda, G. Ghisellini, and A. Celotti, "The spectra of short γ-ray bursts," *Astronomy & Astrophysics*, vol. 422, no. 3, pp. L55–L58, 2004.

[229] D. Yonetoku, T. Murakami, R. Tsutsui, T. Nakamura, Y. Morihara, and K. Takahashi, "Possible origins of dispersion of the peak energy-brightness correlations of gamma-ray bursts," *Publications of the Astronomical Society of Japan*, vol. 62, no. 6, pp. 1495–1507, 2010.

[230] R. Lu and E. Liang, "Luminosity-peak energy relation in the decay phases of gamma-ray burst pulses," *Science China Physics, Mechanics & Astronomy*, vol. 53, no. 1, pp. 163–170, 2010.

[231] A. A. Abdo, M. Ackermann, M. Ajello et al., *Fermi Observations of GRB 090902B: A Distinct Spectral Component in the Prompt and Delayed Emission, 706:0 L138L144*, 0 L138–L144, 706, November 2009.

[232] M. Ackermann, K. Asano, W. B. Atwood et al., *A Short-Hard Gamma-ray Burst with an Additional, Hard Power-law Component from 10 keV TO GeV Energies*, vol. 716:0, 0 1178–1190, 716, June 2010.

[233] M. Ackermann, M. Ajello, K. Asano et al., *Detection of a Spectral Break in the Extra Hard Component of GRB 090926A*, 0 114, 729, March 2011.

[234] M. Ackermann, M. Ajello, A. Allafort et al., *The First Fermi-LAT Catalog of Sources above 10 GeV*, 0 34, 209, December.

[235] H.-N. Lin, X. Li, and Z. Chang, "Effect of gamma-ray burst (GRB) spectra on the empirical luminosity correlations and the GRB Hubble diagram," *Monthly Notices of the Royal Astronomical Society*, vol. 459, no. 3, pp. 2501–2512, 2016.

[236] S. Guiriec, M. M. Gonzalez, J. R. Sacahui, C. Kouveliotou, N. Gehrels, and J. McEnery, "CGRO/BATSE Data support the new paradigm for GRB prompt emission and the new L_i^{nth}-$E_{peak,i}^{nth,rest}$ relation," *The Astrophysical Journal*, vol. 819, no. 1, article no. 79, 2016.

[237] R. Tsutsui, D. Yonetoku, T. Nakamura, K. Takahashi, and Y. Morihara, "Possible existence of the E_p-L_p and E_p-E_{iso} correlations for short gamma-ray bursts with a factor 5-100 dimmer than those for long gamma-ray bursts," *Monthly Notices of the Royal Astronomical Society*, vol. 431, no. 2, pp. 1398–1404, 2013.

[238] D. Yonetoku, T. Nakamura, T. Sawano, K. Takahashi, and A. Toyanago, "Short gamma-ray burst formation rate from batse data using E_p-L_p correlation and the minimum gravitational-wave event rate of a coalescing compact binary," *The Astrophysical Journal*, vol. 789, no. 1, article no. 65, 2014.

[239] N. M. Lloyd-Ronning and E. Ramirez-Ruiz, "On the spectral energy dependence of gamma-ray burst variability," *The Astrophysical Journal* , vol. 576, no. 1 I, pp. 101–106, 2002.

[240] F. Wang, Z. Dai, and E. Liang, "Gamma-ray burst cosmology," *New Astronomy Reviews*, vol. 67, pp. 1–17, 2015.

[241] E. W. Liang, Z. G. Dai, and X. F. Wu, "The luminosity-E_p relation within gamma-ray bursts and the implications for fireball models," *The Astrophysical Journal*, vol. 606, no. 1, pp. L29–L32, 2004.

[242] S. Mendoza, J. C. Hidalgo, D. Olvera, and J. I. Cabrera, "Internal shocks in relativistic jets with time-dependent sources," *Monthly Notices of the Royal Astronomical Society*, vol. 395, no. 3, pp. 1403–1408, 2009.

[243] H. Ito, S. Nagataki, M. Ono et al., "Photospheric emission from stratified jets," *The Astrophysical Journal*, vol. 777, no. 1, article 62, 2013.

[244] F. Frontera, L. Amati, R. Farinelli et al., "Possible physical explanation of the intrinsic $E_{p,i}$-"intensity" correlation commonly used to "standardize" GRBs," *International Journal of Modern Physics D*, vol. 25, no. 5, Article ID 1630014, 2016.

[245] L. Titarchuk, R. Farinelli, F. Frontera, and L. Amati, "An upscattering spectral formation model for the prompt emission of gamma-ray bursts," *The Astrophysical Journal* , vol. 752, no. 2, article no. 116, 2012.

[246] G. Ghirlanda, G. Ghisellini, C. Firmani, A. Celotti, and Z. Bosnjak, "The peak luminosity-peak energy correlation in gamma-ray bursts," *Monthly Notices of the Royal Astronomical Society*, vol. 360, no. 1, pp. L45–L49, 2005.

[247] R. Tsutsui, T. Nakamura, D. Yonetoku, T. Murakami, Y. Kodama, and K. Takahashi, "Cosmological constraints from calibrated Yonetoku and Amati relation suggest fundamental plane of gamma-ray bursts," *Journal of Cosmology and Astroparticle Physics*, vol. 2009, no. 8, article no. 015, 2009.

[248] R. Tsutsui, T. Nakamura, D. Yonetoku, T. Murakami, and K. Takahashi, "Intrisic Dispersion of Correlations among Ep, Lp," *and Eiso of Gamma Ray Bursts depends on the quality of Data Set. ArXiv e-prints*, December 2010.

[249] S. Qi and T. Lu, "A new luminosity relation for gamma-ray bursts and its implication," *The Astrophysical Journal* , vol. 717, no. 2, pp. 1274–1278, 2010.

[250] P. T. O'Brien and R. Willingale, "Using Swift observations of prompt and afterglow emission to classify GRBs," *Philosophical Transactions of the Royal Society A: Mathematical, Physical & Engineering Sciences*, vol. 365, no. 1854, pp. 1179–1188, 2007.

[251] M. G. Dainotti, M. Ostrowski, and R. Willingale, "Towards a standard gamma-ray burst: Tight correlations between the prompt and the afterglow plateau phase emission," *Monthly Notices of the Royal Astronomical Society*, vol. 418, no. 4, pp. 2202–2206, 2011.

[252] A. Lee, E. D. Bloom, and V. Petrosian, "Properties of Gamma-Ray Burst Time Profiles Using Pulse Decomposition Analysis," *The Astrophysical Jornal*, vol. 131, November 2000.

[253] F. Quilligan, B. McBreen, L. Hanlon, S. McBreen, K. J. Hurley, and D. Watson, "Temporal properties of gamma ray bursts as signatures of jets from the central engine," *Astronomy & Astrophysics*, vol. 385, no. 2, pp. 377–398, 2002.

[254] O. M. Littlejohns, N. R. Tanvir, R. Willingale, P. A. Evans, P. T. O'Brien, and A. J. Levan, "Are gamma-ray bursts the same at high redshift and low redshift?" *Monthly Notices of the Royal Astronomical Society*, vol. 436, no. 4, Article ID stt1841, pp. 3640–3655, 2013.

[255] Ž. Bošnjak and F. Daigne, "Spectral evolution in gamma-ray bursts: Predictions of the internal shock model and comparison to observations," *Astronomy & Astrophysics* , vol. 568, article no. A45, 2014.

[256] P. A. Evans, R. Willingale, J. P. Osborne et al., "GRB 130925A: an ultralong gamma ray burst with a dust-echo afterglow, and implications for the origin of the ultralong GRBs," *Monthly Notices of the Royal Astronomical Society*, vol. 444, no. 1, pp. 250–267, 2014.

[257] J. Hakkila and R. D. Preece, "Gamma-ray burst pulse shapes: Evidence for embedded shock signatures?" *The Astrophysical Journal* , vol. 783, no. 2, article no. 88, 2014.

[258] T. Laskar, E. Berger, N. Tanvir et al., "GRB 120521C at z ~ 6 and the properties of high-redshift γ-ray bursts," *The Astrophysical Journal* , vol. 781, no. 1, article no. 1, 2014.

[259] O. M. Littlejohns and N. R. Butler, "Investigating signatures of cosmological time dilation in duration measures of prompt gamma-ray burst light curves," *Monthly Notices of the Royal Astronomical Society*, vol. 444, no. 4, pp. 3948–3960, 2014.

[260] A. Roychoudhury, S. K. Sarkar, and A. Bhadra, "Spectral lag features of GRB 060814 from swift bat and Suzaku observations," *The Astrophysical Journal* , vol. 782, no. 2, article no. 105, 2014.

[261] C. Ceccobello and P. Kumar, "Inverse-Compton drag on a highly magnetized GRB jet in stellar envelope," *Monthly Notices of the Royal Astronomical Society*, vol. 449, no. 3, pp. 2566–2575, 2015.

[262] D. Kazanas, J. L. Racusin, J. Sultana, and A. Mastichiadis, "The Statistics of the Prompt-to-Afterglow GRB Flux Ratios and the Supercritical Pile GRB Model".

[263] T. Laskar, E. Berger, R. Margutti et al., "Energy injection in gamma-ray burst afterglows," *The Astrophysical Journal* , vol. 814, no. 1, article no. 1, 2015.

[264] Z. Y. Peng, Y. Yin, T. F. Yi, Y. Y. Bao, and H. Wu, "A comprehensive comparative study of temporal properties between X-ray flares and GRB pulses," *Astrophysics and Space Science*, vol. 355, no. 1, pp. 95–103, 2015.

[265] F. Genet and J. Granot, "Realistic analytic model for the prompt and high-latitude emission in GRBs," *Monthly Notices of the Royal Astronomical Society*, vol. 399, no. 3, pp. 1328–1346, 2009.

[266] F. Ryde and V. Petrosian, "Gamma-ray burst spectra and light curves as signatures of a relativistically expanding plasma," *The Astrophysical Journal* , vol. 578, no. 1 I, pp. 290–303, 2002.

[267] C. D. Dermer, "Rapid X-ray declines and plateaus in Swift GRB light curves explained by a highly radiative blast wave," *The Astrophysical Journal* , vol. 664, no. 1 I, pp. 384–396, 2007.

Hindawi
Advances in Astronomy
Volume 2017, Article ID 8929054, 41 pages
https://doi.org/10.1155/2017/8929054

Review Article

The Observer's Guide to the Gamma-Ray Burst Supernova Connection

Zach Cano,[1,2] Shan-Qin Wang,[3,4] Zi-Gao Dai,[3,4] and Xue-Feng Wu[5,6]

[1] *Centre for Astrophysics and Cosmology, Science Institute, University of Iceland, Dunhagi 5, 107 Reykjavik, Iceland*
[2] *Instituto de Astrofísica de Andalucía (IAA-CSIC), Glorieta de la Astronomía s/n, 18008 Granada, Spain*
[3] *School of Astronomy and Space Science, Nanjing University, Nanjing 210093, China*
[4] *Key Laboratory of Modern Astronomy and Astrophysics (Nanjing University), Ministry of Education, Nanjing, China*
[5] *Purple Mountain Observatory, Chinese Academy of Sciences, Nanjing 210008, China*
[6] *Joint Center for Particle, Nuclear Physics and Cosmology, Nanjing University-Purple Mountain Observatory, Nanjing 210008, China*

Correspondence should be addressed to Zach Cano; zewcano@gmail.com

Received 7 April 2016; Accepted 29 November 2016; Published 11 April 2017

Academic Editor: Josep M. Trigo-Rodríguez

We present a detailed report of the connection between long-duration gamma-ray bursts (GRBs) and their accompanying supernovae (SNe). The discussion presented here places emphasis on how observations, and the modelling of observations, have constrained what we know about GRB-SNe. We discuss their photometric and spectroscopic properties, their role as cosmological probes, including their measured luminosity–decline relationships, and how they can be used to measure the Hubble constant. We present a statistical summary of their bolometric properties and use this to determine the properties of the "average" GRB-SN. We discuss their geometry and consider the various physical processes that are thought to power the luminosity of GRB-SNe and whether differences exist between GRB-SNe and the SNe associated with ultra-long-duration GRBs. We discuss how observations of their environments further constrain the physical properties of their progenitor stars and give a brief overview of the current theoretical paradigms of their central engines. We then present an overview of the radioactively powered transients that have been photometrically associated with short-duration GRBs, and we conclude by discussing what additional research is needed to further our understanding of GRB-SNe, in particular the role of binary-formation channels and the connection of GRB-SNe with superluminous SNe.

1. Introduction

Observations have proved the massive-star origins of long-duration GRBs (LGRBs) beyond any reasonable doubt. The temporal and spatial connection between GRB 980425 and broad-lined type Ic (IcBL) SN 1998bw offered the first clues to their nature [1, 2] (Figure 1). The close proximity of this event ($z = 0.00866$; ~40 Mpc), which is still the closest GRB to date, resulted in it becoming one of the most, if not *the* most, scrutinized GRB-SN in history. It was shown that SN 1998bw had a very large kinetic energy (see Section 4 and Table 3) of ~ 2–5×10^{52} erg, which led it to being referred to as a hypernova [3]. However, given several peculiarities of its γ-ray properties, including its underluminous γ-ray luminosity ($L_{\gamma,\mathrm{iso}} \sim 5 \times 10^{46}\ \mathrm{erg\,s^{-1}}$), it was doubted whether this event was truly representative of the general LGRB population. This uncertainty persisted for almost five years until the spectroscopic association between cosmological/high-luminosity GRB 030329 ($L_{\gamma,\mathrm{iso}} \sim 8 \times 10^{50}\ \mathrm{erg\,s^{-1}}$) and SN 2003dh [4–6]. GRB 030329 had an exceptionally bright optical afterglow (AG; see Figures 2 and 3), and a careful decomposition of the photometric and spectroscopic observations was required in order to isolate the SN features from the dominant AG light [7] (see Section 2.1 and Figure 4). As was seen for SN 1998bw, SN 2003dh was a type IcBL SN, and its kinetic energy was in excess of 10^{52} erg, showing that it too was a hypernova.

The launch of the *Swift* satellite [8] dramatically changed the way we studied GRBs and the GRB-SN association, and the number of events detected by this mission has helped increase the GRB-SN sample size by a factor of three since

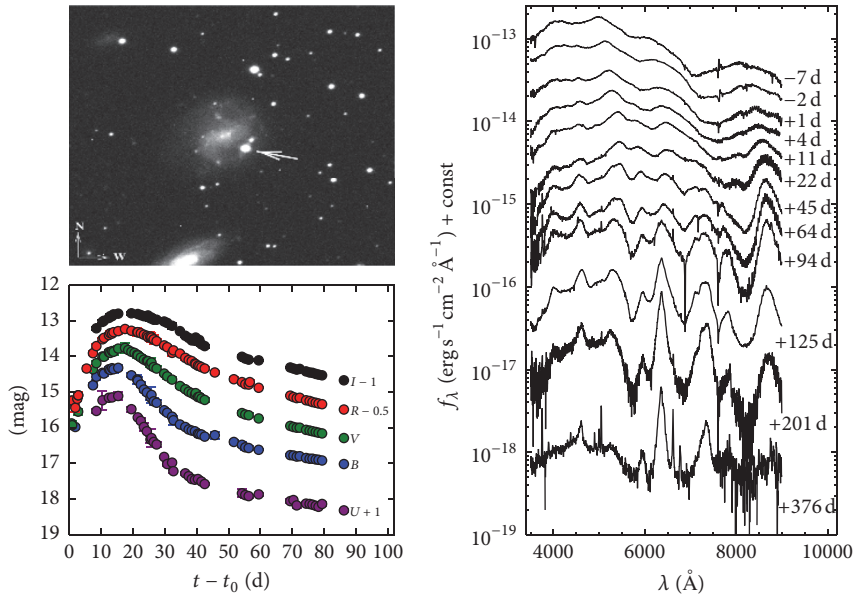

Figure 1: GRB 980425/SN 1998bw: the archetype GRB-SN. Host image (ESO 184-G82) is from [1], where the position of the optical transient is clearly visible. Optical light curves are from [9] and spectra from [2].

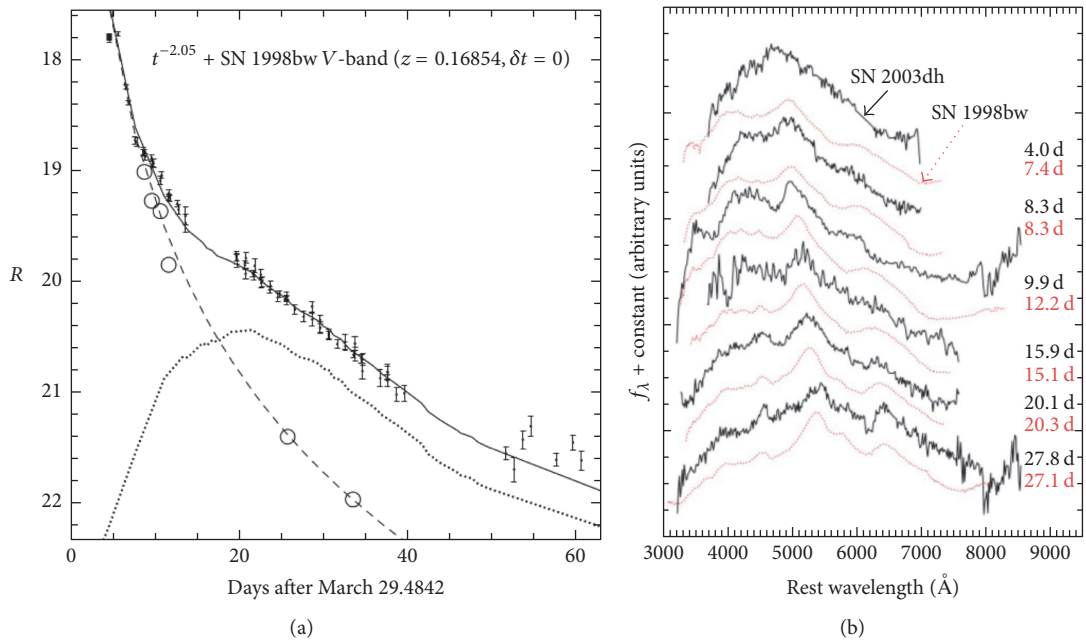

Figure 2: (a) The photometric (R-band) evolution of GRB 030329/SN 2003dh, from [6]; (b) the spectral evolution of GRB 030329/SN 2003dh, as compared with that of SN 1998bw, from [4].

the pre-*Swift* era. This includes, among many others, the well-studied events GRB 060218/SN 2006aj, GRB 100316D/SN 2010bh, GRB 111209A/SN 2011kl, GRB 120422A/SN 2012bz, GRB 130427A/SN 2013cq, and GRB 130702A/SN 2013dx. A full list of the references to these well-studied spectroscopic GRB-SN associations is found in Table 4.

This review paper represents a continuation of other review articles presented to date, including the seminal work by Woosley and Bloom (2006) [11]. As such, we have focused the majority of the content on achievements made in the 10 years since [11] was published. In this review and many others [12–19], thorough historical accounts of the development of the gamma-ray burst supernova (GRB-SN) connection are presented, and we encourage the reader to consult the detailed presentation given in section one of [11] for further details. In Tables 2 and 3 we present the most comprehensive database yet compiled of the observational and physical properties of the GRB prompt emission and

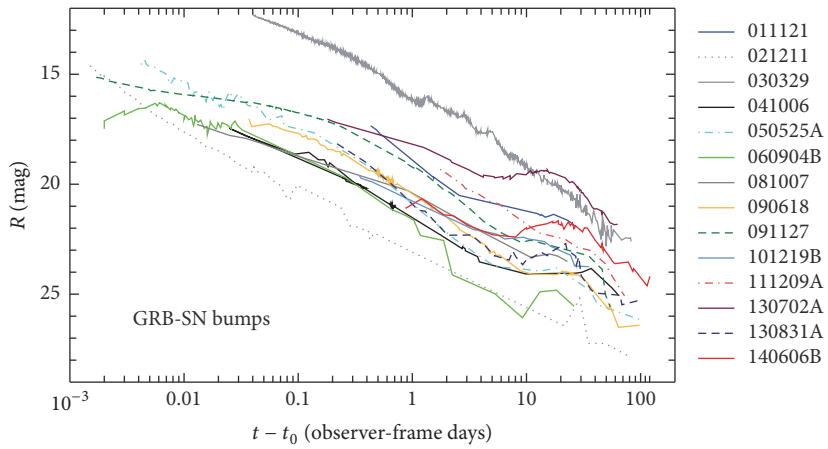

FIGURE 3: A mosaic of GRB-SNe (AG + SN). Clear SN bumps are observed for all events except SN 2003dh, for which the SN's properties had to be carefully decomposed from photometric and spectroscopic observations [7]. The lack of an unambiguous SN bump in this case is not surprising given the brightness of its AG relative to the other GRB-SN in the plot: SN 2013dx was at a comparable redshift ($z = 0.145$, compared with $z = 0.1685$ for 2003dh), but its AG was much fainter (2–5 mag) at a given moment in time. The redshift range probed in this mosaic spans almost an order of magnitude ($0.145 < z < 1.006$) and shows the variation in peak observed magnitude for GRB-SNe. It is important to remember that given the large span of distances probed here, observer-frame R-band samples a wide range of rest-frame SEDs (from U-band to V-band).

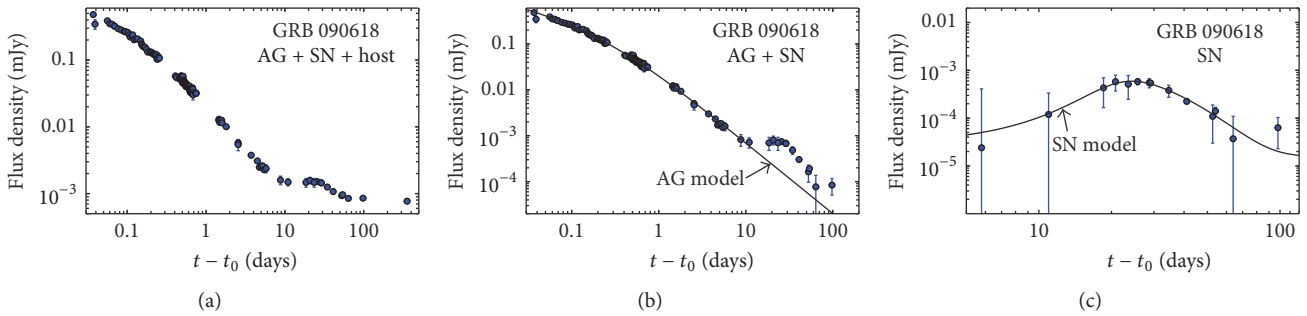

FIGURE 4: An example decomposition of the optical (R-band) light curve of GRB 090618 [10]. (a) For a given GRB-SN event, the single-filter monochromatic flux is attributed as arising from three sources: the AG, the SN, and a constant source of flux from the host galaxy. (b) Once the observations have been dereddened, the host flux is removed, either via the image-subtraction technique or by being mathematically subtracted away. At this point a mathematical model composed of one or more power laws punctuated by break-times is fit to the early light curve to determine the temporal behaviour of the AG. (c) Once the AG model has been determined, it is subtracted from the observations leaving just light from the SN.

GRB-SNe, respectively, which consists of 46 GRB-SNe. It is the interpretation of these data which forms a substantial contribution to this review. We have adopted the grading scheme devised by [17] to assign a significance of the GRB-SN association to each event, where A is strong spectroscopic evidence, B is a clear light curve bump as well as some spectroscopic evidence resembling a GRB-SN, C is a clear bump consistent with other GRB-SNe at the spectroscopic redshift of the GRB, D is a bump, but the inferred SN properties are not fully consistent with other GRB-SNe or the bump was not well sampled or there is no spectroscopic redshift of the GRB, and E is a bump, either of low significance or inconsistent with other GRB-SNe. This is found in Table 3.

Throughout this article we use a ΛCDM cosmology constrained by [20] of $H_0 = 67.3\,\mathrm{km\,s^{-1}\,Mpc^{-1}}$, $\Omega_M = 0.315$, $\Omega_\Lambda = 0.685$. All published data, where applicable, have been renormalized to this cosmological model. Foreground extinctions were calculated using the dust extinction maps of [21, 22]. Unless stated otherwise, errors are statistical only. Nomenclature is as follows: σ denotes the standard deviation of a sample, whereas the root-mean square of a sample is expressed as RMS. A symbol with an overplotted bar denotes an average value. LGRB and SGRB are long- and short-duration GRBs, respectively, while a GRB-SN is implicitly understood to be associated with an LGRB. The term t_0 refers to the time that a given GRB was detected by a GRB satellite.

2. Observational Properties

2.1. Photometric Properties. The observer-frame, optical light curves (LCs) of GRBs span more than 8–10 magnitudes at a given observer-frame postexplosion epoch (see, e.g., Figure 1

in [23]). Similarly, if we inspect the observer-frame R-band LCs of GRB-SNe (redshift range $0.145 < z < 1.006$) shown in Figure 3, they too span a similar range at a given epoch. Indeed, the peak SN brightness during the SN "bump" phase ranges from $R = 19.5$ for GRB 130702A (the brightest GRB-SN bump observed to date) to $R = 25$ for GRB 021211.

For a typical GRB-SN, there are three components of flux being measured: (1) the afterglow (AG), which is associated with the GRB event, (2) the SN, and (3) the constant source of flux coming from the host galaxy. A great deal of information can be obtained from modelling each component, but, for the SN component to be analysed, it needs to be *decomposed* from the optical/NIR LCs (Figure 4). To achieve this task, the temporal behaviour of the AG, the constant source of flux from the host galaxy, and the line of sight extinction, including foreground extinction arising from different sight-lines through the Milky Way (MW) [21, 22], and extinction local to the event itself [10, 23–26], in a given filter need to be modelled and quantified. The host contribution can be considered either by removing it via the image-subtraction technique [27–29], by simple flux-subtraction [30–32], or by including it as an additional component in the fitting routine [33–36]. The AG component is modelled using either a single or a set of broken power laws (SPL/BPL; [37]). This phenomenological approach is rooted in theory however, as standard GRB theory states that the light powering the AG is synchrotron in origin and therefore follows a power law behaviour in both time and frequency ($f_\nu \propto (t - t_0)^{-\alpha}\nu^{-\beta}$, where the respective decay and energy spectral indices are α and β).

Once the SN LC has been obtained, traditionally it is compared to a template supernova, that is, SN 1998bw, where the relative brightness (k) and width (also known as a stretch factor, s) are determined. Such an approach has been used extensively over the years [10, 18, 31–34, 38–43]. Another approach to determining the SN's properties is to fit a phenomenological model to the resultant SN LC [10, 42–44], such as the Bazin function [45], in order to determine the magnitude/flux at peak SN light, the time it takes to rise and fade from peak, and the width of the LC, such as the Δm_{15} parameter (in a given filter, the amount a SN fades in magnitudes from peak light to 15 days later). All published values of these observables are presented in Table 3.

2.2. Spectroscopic Properties. Optical and NIR spectra, of varying levels of quality due to their large cosmological distances, have been obtained for more than a dozen GRB-SNe. Those of the highest quality show broad observation lines of O I, Ca II, Si II, and Fe II near maximum light. The line velocities of two specific transitions (Si II λ6355 and Fe II λ5169; Figure 6) indicate that near maximum light the ejecta that contain these elements move at velocities of order 20,000–40,000 km s^{-1} (Fe II λ5169) and about 15,000–25,000 km s^{-1} (Si II λ6355). The weighted mean absorption velocities at peak V-band light of a sample of SNe IcBL that included GRB-SNe were found to be 23,800 ± 9500 km s^{-1} (Fe II λ5169) by [46] (see as well Table 3). SNe IcBL (including and excluding GRB-SNe) have Fe II λ5169 widths that are ~9,000 km s^{-1} broader than SNe Ic, while

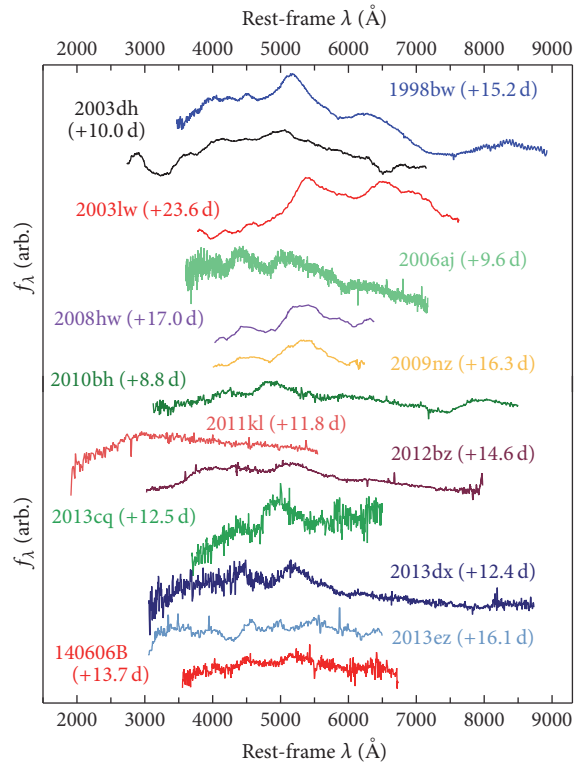

Figure 5: Peak/near-peak spectra of GRB-SNe. The spectra have been arbitrarily shifted in flux for comparison purposes and to exaggerate their main features, and host emission lines have been manually removed. The spectra of SNe 2012bz, 2013cq, and 2013dx have been Kaiser smoothed [31] in order to suppress noise. Most of the spectra are characterized by broad absorption features, while such features are conspicuously absent in the spectra of SN 2013ez and SN 2011kl.

GRB-SNe appear to be, on average, about ~6,000 km s^{-1} more rapid than SNe IcBL at peak light [46]. Si II λ6355 appears to have a tighter grouping of velocities than Fe II λ5169, though SN 2010bh is a notable outlier, being roughly 15,000 to 20,000 km s^{-1} more rapid than the other GRB-SNe. SN 2013ez is also a notable outlier due to its low line velocity (4000–6000 km s^{-1}), and inspection of its spectrum (Figure 5) reveals fewer broad features than other GRB-SNe, where it more closely resembles type Ic SNe rather than type IcBL [31]. Nevertheless, this relative grouping of line velocities may indicate similar density structure(s) in the ejecta of these SN, which in turn could indicate some general similarities in their preexplosion progenitor configurations. For comparison, [46] found that the dispersion of peak SNe Ic Fe II λ5169 line velocities is tighter than those measured for GRB-SNe and SNe IcBL not associated with GRBs (σ = 1500, 9500, 2700 km s^{-1}, resp.). This suggests that GRB-SNe and SNe IcBL have more diversity in their spectral velocities, and in turn their density structures, than SNe Ic. Finally, [46] found no differences in the spectra of *ll*GRB-SNe relative to high-luminosity GRB-SNe.

During the nebular phase of SN 1998bw (one of only a few GRB-SNe that has been spectroscopically observed

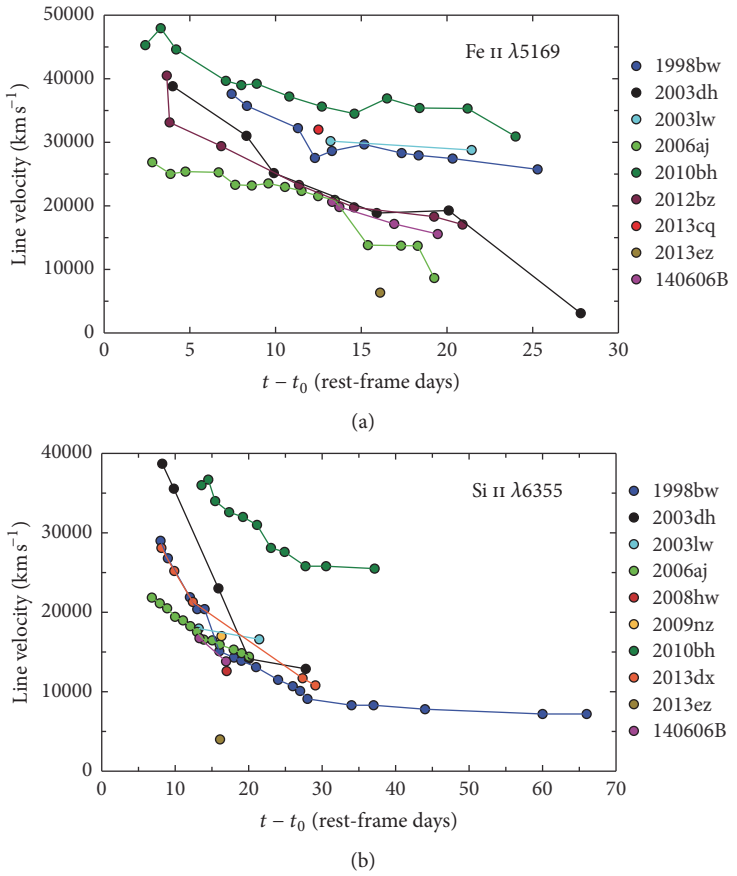

FIGURE 6: Measured line velocities of a sample of GRB-SNe. See Table 4 for their respective references.

during this phase due to its close proximity; see as well Section 5), observed lines include [O I] λ5577, $\lambda\lambda$6300,6364; O [II] λ7322; Ca II $\lambda\lambda$3934,3963, $\lambda\lambda$7291,7324; Mg I] λ4570; Na I $\lambda\lambda$5890,5896; [Fe II] λ4244, λ4276, λ4416, λ4458, λ4814, λ4890, λ5169, λ5261, λ5273, λ5333, λ7155, λ7172, λ7388, λ7452; [Fe III] λ5270; Co II λ7541; C I] λ8727 [47]. Nebular [O I] $\lambda\lambda$6300,6364 was also observed for nearby GRB-SNe 2006aj [48] and 100316D [49], though in the latter case strong lines from the underlying HII are considerably more dominant. For SN 2006aj, [Ni II λ7380] was tentatively detected [48], which, given the short half-life of ^{56}Ni, implies the existence of roughly 0.05 $M_\odot$ of ^{58}Ni. Such a large amount of stable neutron-rich Ni strongly indicates the formation of a neutron star [48]. Moreover, the absence of [Ca II] lines for SN 2006aj also supported the lower kinetic energy of this event relative to other GRB-SNe, which is likely less than that attributed to a hypernova.

3. Phenomenological Classifications of GRB-SNe

Replicating previous works [19, 41], in this review, we divided GRB-SNe into the following subclasses based primarily on their isotropic γ-ray luminosity $L_{\gamma,\mathrm{iso}}$:

(i) *ll*GRB-SNe: GRB-SNe associated with low-luminosity GRBs ($L_{\gamma,\mathrm{iso}} < 10^{48.5}$ erg s^{-1}).

(ii) INT-GRB-SNe: GRB-SNe associated with intermediate-luminosity GRBs ($10^{48.5} < L_{\gamma,\mathrm{iso}} < 10^{49.5}$ erg s^{-1}). (Not to be confused with intermediate-duration GRBs, i.e., those with durations of 2–5 s [50–52].)

(iii) GRB-SNe: GRB-SNe associated with high-luminosity GRBs ($L_{\gamma,\mathrm{iso}} > 10^{49.5}$ erg s^{-1}).

(iv) ULGRB-SNe: ultra-long-duration GRB-SNe, which are classified according to the exceptionally long duration of their γ-ray emission (~10^4 seconds [53, 54]) rather than on their γ-ray luminosities.

Historically, the term X-ray flash (XRF) was used throughout the literature, which has slowly been replaced with the idiom of "low-luminosity." Strictly speaking, the definition of an XRF [55] arises from the detection of soft, X-ray rich events detected by the Wide Field Camera on *BeppoSax* in the energy range 2–25 keV. Here we make no distinction based on the detection of a given satellite and instrumentation, where the "*ll*" nomenclature refers only to the magnitude of a given GRB's $L_{\gamma,\mathrm{iso}}$.

The luminosity, energetics, and shape of the γ-ray pulse of a given GRB can reveal clues to the origin of its high-energy emission and thus its emission process. Of particular importance is whether the γ-rays emitted by *ll*GRBs arise from the same mechanism as high-luminosity GRBs (i.e., from a jet) or whether from a relativistic shock breakout

(SBO) [30, 56–60] (see as well Section 9). It was demonstrated by [61, 62] that a key observable of *ll*GRBs are their single-peaked, smooth, nonvariable γ-ray LCs compared to the more erratic γ-ray LCs of jetted-GRBs, which become softer over time. It was shown by [60] that an SBO is likely present in all LGRB events, but for any realistic configuration the energy in the SBO pulse is lower by many orders of magnitude compared to those observed in the GRB prompt emission ($E_{\rm SBO} = 10^{44}$–10^{47} erg, for reasonable estimates of the ejecta mass and progenitor radii). These low energies (compared with $E_{\gamma,\rm iso}$) suggest that relativistic SBOs are not likely to be detected at redshifts exceeding $z \approx 0.1$. In cases where they are detectable, the SBO may be in the form of a short pulse of photons with energies >1 MeV. Inspection of the E_p values in Table 2 shows that only a few events have photons with peak γ-ray energies close to this value: GRB 140606B has $E_p \approx$ 800 keV [32]; however suspected *ll*GRBs 060218 and 100316D only have $E_p = 5$ keV and 30 keV, respectively. It should be noted that while the SBO model of [60] successfully explains the observed properties (namely, the energetics, temperature, and duration of the prompt emission) of GRBs 980425, 031203, 060218, and 100316D, their SBO origins are still widely debated [63, 64], with no firm consensus yet achieved.

Thermal, black body (BB) components in UV and X-ray spectra have been detected for several events, including GRB 060218 (X-ray: $kT = 0.17$ keV, time averaged from first 10,000 s, [58]); GRB 100316D (X-ray: $kT = 0.14$ keV, time averaged from 144–737 s, [65]); GRB 090618 (X-ray: $kT = 0.3$–1 keV up to first 2500 s, [66]); GRB 101219B (X-ray: $kT = 0.2$ keV, [67]); and GRB 120422A (UV: $kT = 16$ eV at observer-frame $t - t_0 = 0.054$ d, [41]). A sample of LGRBs with associated SNe was analysed by [68] who found that thermal components were present in many events, which could possibly be attributed to thermal emission arising from a cocoon that surrounds the jet [69] or perhaps associated with SBO emission. Reference [67] analysed a larger sample of LGRBs and found that, for several events, a model that included a BB contribution provided better fits than absorbed power laws. Reference [70] found that, in their sample of 28 LGRBs, eight had evidence of thermal emission in their X-ray spectra, indicating such emission may be somewhat prevalent. However, the large inferred BB temperatures (kT ranging from 0.16 keV for 060218 to 3.2 keV for 061007, with an average of ≈1 keV) indicates that the origin of the thermal emission may not be a SBO. Moreover, the large superluminal expansions inferred for the thermal components instead hint at a connection with late photospheric emission. In comparison, some studies indicate a SBO temperature of ~ 1 keV [71], while [60, 72–74] showed that for a short while the region behind the shock is out of thermal equilibrium, and temperatures can reach as high as ~50 keV.

The radius of the fitted BB component offers additional clues. References [58, 59] derived a BB radius of 5–8×10^{12} cm for GRB 060218; [65] found $\approx 8 \times 10^{11}$ cm for GRB 100316D; [41] found $\approx 7 \times 10^{13}$ cm for GRB 120422A; and [75] derived a radius of $\approx 9 \times 10^{13}$ cm for GRB 140606B. The radii inferred for GRBs 060218, 120422A, and 140606B are commensurate with the radii of red supergiants (200–1500 $R_\odot$), while that measured for GRB 100316D is similar to that of the radius of a blue supergiant ($\leq 25\ R_\odot$). These radii, which are much larger than those expected for Wolf-Rayet (WR) stars (of order a few solar radius to a few tens of solar radii), were explained by these authors by the presence of a massive, dense stellar wind surrounding the progenitor star, where the thermal radiation is observed once the shock, which is driven into the wind, reaches a radius where the wind becomes optically thin. An alternative explanation for the large BB radii was presented by [76] (see as well [77]), where the breakout occurs in an extended ($R = 100\ R_\odot$) low-mass ($0.01\ M_\odot$) envelope surrounding the preexplosion progenitor star. The origin of envelope is likely material stripped just prior to explosion, and such an envelope is missing for high-luminosity GRB-SNe [77].

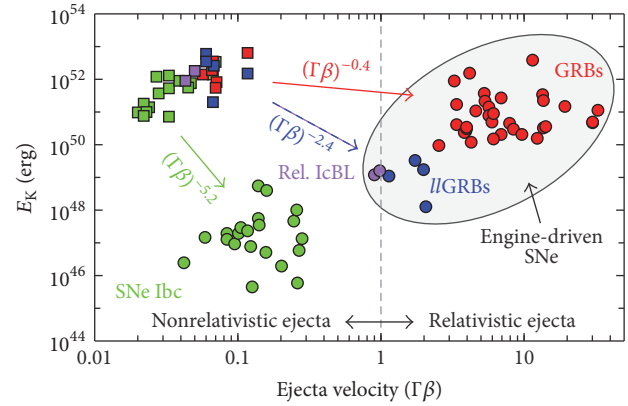

FIGURE 7: The positions of GRBs, SNe Ibc, and GRB-SNe in the $E_{\rm K}$-$\Gamma\beta$ plane [32, 78–81]. Ordinary SNe Ibc are shown in green, *ll*GRBs in blue, relativistic SNe IcBL in purple, and jetted-GRBs in red. Squares are used for the slow-moving SN ejecta, while circles represent the kinetic energy and velocity of the nonthermal radio-emitting ejecta associated with these events (e.g., the GRB jet). The velocities were computed for $t - t_0 = 1$ day (rest-frame), where the value $\Gamma\beta = 1$ denotes the division between relativistic and nonrelativistic ejecta. The solid lines correspond to (green) ejecta kinetic energy profiles of a purely hydrodynamical explosion $E_{\rm K} \propto (\Gamma\beta)^{-5.2}$ [57, 82, 83]; (blue/purple dashed) explosions powered by a short-lived central engine (SBO-GRBs and relativistic IcBL SNe 2009bb and 2012ap: $E_{\rm K} \propto (\Gamma\beta)^{-2.4}$); (red) those arising from a long-lived central engine (i.e., jetted-GRBs; $E_{\rm K} \propto (\Gamma\beta)^{-0.4}$ [84]). Modified, with permission, from Margutti et al. [78, 81].

For a given GRB-SN event there are both relativistic and nonrelativistic ejecta, where the former is responsible for producing the prompt emission, and the latter is associated with the SN itself. The average mass between the two components is large: the ejecta mass of a GRB-SN is of order 2–8 $M_\odot$, while that in the jet that produces the γ-rays is of order $10^{-6}\ M_\odot$, based on arguments for very low baryon loading [88]. A GRB jet decelerates very rapidly, within a few days, because the very low-mass ejecta is rapidly swept up into the comparatively larger mass of the surrounding CSM. Conversely, SNe have much heavier ejecta and can be in free-expansion for many years or even centuries. Measuring the amount of kinetic energy associated with each ejecta component can offer additional clues to the explosion mechanisms operating in these events. Figure 7 shows the position of SNe

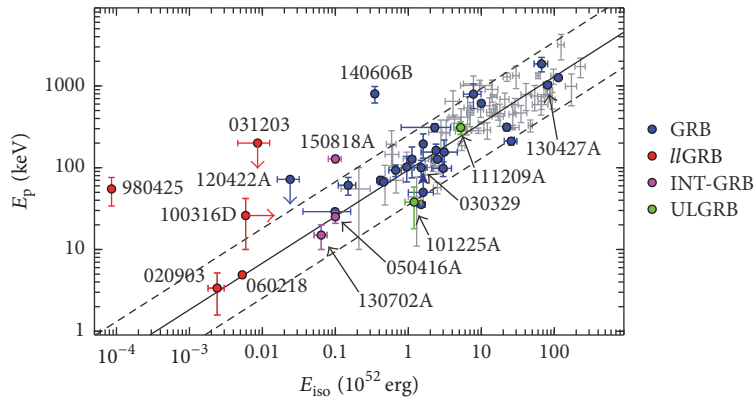

FIGURE 8: Properties of the prompt emission for different classes of GRBs in the $E_{\gamma,\mathrm{iso}}$-E_p plane [85]. Data from [85–87] are shown in grey along with their best fit to a single power law (index of $\alpha = 0.57$) and the 2σ uncertainty in their fit. Notable events that do not appear to follow the Amati relation include *ll*GRBs (980425 and 031203), INT-GRBs (150818A), and high-luminosity GRB 140606B. Both ULGRBs are consistent with the Amati relation, so are GRBs 030329 and 130427A, while GRB 120422A and *ll*GRB 100316D are marginally consistent.

Ibc (green), GRBs (red), *ll*GRBs (blue), and relativistic SNe IcBL (purple) in the E_K-$\Gamma\beta$ plane [32, 78–81], where $\beta = v/c$ (not to be confused with the spectral PL index of synchrotron radiation) and Γ is the bulk Lorentz factor. Squares indicate slow-moving SN ejecta, while circles represent the kinetic energy and velocity of the nonthermal radio-emitting ejecta associated with these events (e.g., the jet in GRBs). The velocities were computed for $t-t_0 = 1$ day (rest-frame), where the value $\Gamma\beta = 1$ denotes the division between relativistic and nonrelativistic ejecta. The solid lines show the ejecta kinetic energy profiles of a purely hydrodynamical explosion (green) $E_\mathrm{K} \propto (\Gamma\beta)^{-5.2}$ [57, 82, 83]; explosions powered by a short-lived central engine (blue/purple dashed), SBO-GRBs and relativistic IcBL SNe 2009bb and 2012ap: $E_\mathrm{K} \propto (\Gamma\beta)^{-2.4}$; and those arising from a long-lived central engine (red), that is, jetted-GRBs: $E_\mathrm{K} \propto (\Gamma\beta)^{-0.4}$ [84].

It is seen that *ll*GRBs and high-luminosity GRBs span a wide range of engine energetics, as indicated by the range of PL indices seen in Figure 7. The two relativistic SNe IcBL considered in this review (SNe 2009bb and 2012ap), which are also thought to be engine-driven SNe [79, 81, 89], occur at the lower-end of central engine energetics. Modelling of GRB 060218 [90] showed that ~10^{48} erg of energy was coupled to the mildly relativistic ejecta ($\Gamma \sim 2$). Reference [78] showed the presence of a very weak central engine for GRB 100316D, where ~10^{49} erg of energy was coupled to mildly relativistic ($\Gamma = 1.5$–2), quasi-spherical ejecta. It was shown by [79] that $\geq 10^{49}$ erg was associated with the relativistic ($v = 0.9c$), radio-emitting ejecta of SN 2009bb. These authors also showed that, unlike GRB jets, the ejecta was in free-expansion, which implied it was baryon loaded. For SN 2012ap, [89] estimated there was ~1.6×10^{49} erg of energy associated with the mildly relativistic ($0.7c$) radio-emitting ejecta. The weak X-ray emission of SN 2012ap [81] implied no late-time activity of its central engine, which led these authors to suggest that relativistic SNe IcBL represent the weakest engine-driven explosions, where the jet is unable to successfully break out of the progenitor. *ll*GRBs then represent events where the jet does not or just barely escapes into space. Note that [91] calculated an estimate to the dividing line between SBO-GRBs and jet-GRBs, finding that for γ-ray luminosities above 10^{48} erg s^{-1} a jet-GRB may be possible.

Next, the distribution of T_{90} (the time over which a burst emits from 5% of its total measured counts to 95%) as measured by the various GRB satellites can be used to infer additional physical properties of the GRB jet duration and progenitor radii. A basic assertion of the collapsar model is that the duration of the GRB prompt phase (where T_{90} is used as a proxy) is the difference of the time that the central engine operates minus the time it takes for the jet to break out of the star: $T_{90} \sim t_\mathrm{engine} - t_\mathrm{breakout}$. A direct consequence of this premise is that there should be a plateau in the distribution of T_{90} for GRBs produced by collapsars when $T_{90} < t_\mathrm{breakout}$ [92]. Moreover, the value of T_{90} found at the upper limit of the plateaus seen for three satellites (*BATSE*, *Swift*, and *Fermi*) was approximately the same ($T_{90} \sim 20$–30 s), which is interpreted as the typical breakout time of the jet. This short breakout time suggests that the progenitor star at the time of explosion is quite compact (~5 $\mathrm{R}_\odot$ [93]). Reference [94] then used these distributions to calculate the probability that a given GRB arises from a collapsar or not based on its T_{90} and hardness ratio. Note however that T_{90} might not always be the best indicator of the engine on-time. For example, [91] showed that while GRB 120422A had $T_{90} = 5$ s, the actual duration of the jet was actually 86 s, as constrained by modelling of the curvature effect. Though see [95] who state that curvature radiation is not from a central engine that is still on but from electrons that were off-axis and hence had a lower Lorentz factor and which are received over a time interval that is long compared to the duration of the burst.

Finally, Figure 8 shows the properties of the prompt emission for the various GRB-SN subclasses in the $E_{\gamma,\mathrm{iso}}$-E_p plane, that is, the Amati relation [85]. Data from [85–87] are shown in grey along with their best fit to a single power law (index of $\alpha = 0.57$) and the 2σ uncertainty in their fit. Several events do not appear to follow the Amati relation, including *ll*GRBs 980425 and 031203, INT-GRB 150818A, and

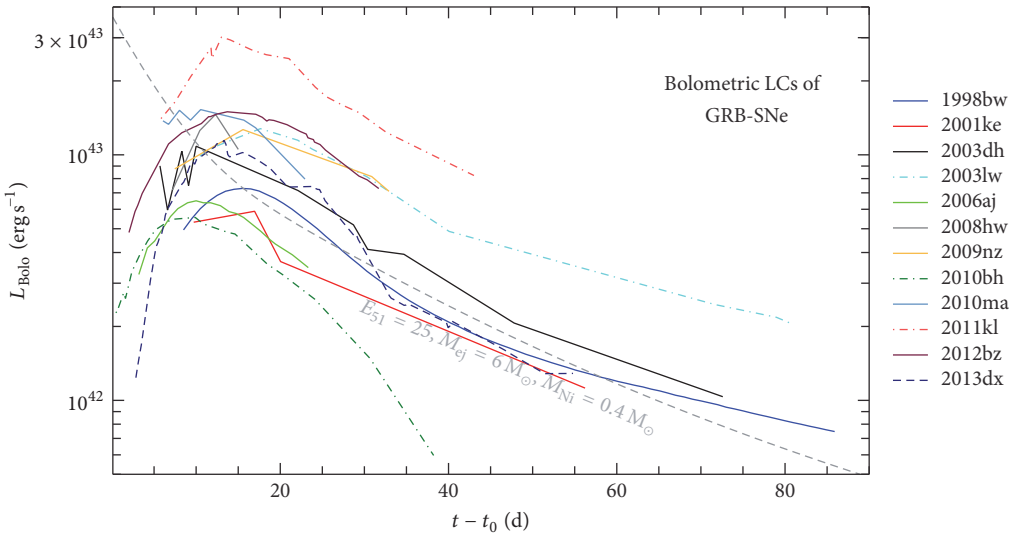

FIGURE 9: Bolometric LCs of a sample of GRB-SNe. Times are given in the rest-frame. The average peak luminosity of all GRB-SNe except SN 2011kl is $\overline{L}_p = 1.0 \times 10^{43}$ erg s^{-1}, with a standard deviation of 0.36×10^{43} erg s^{-1}. The peak luminosity of SN 2011kl is $L_p = 2.9 \times 10^{43}$ erg s^{-1}, which makes it more than 5σ more luminous than the average GRB-SN. The average peak time of the entire sample is $t_p = 13.2$ d, with a standard deviation of 2.6 d. If SN 2011kl is excluded from the sample, this changes to 13.0 d. Plotted for reference is an analytical model that considers the luminosity produced by the average GRB-SN ($E_K = 25 \times 10^{51}$ erg, $M_{ej} = 6\,M_\odot$, and $M_{Ni} = 0.4\,M_\odot$).

high-luminosity GRB 140606B. Both ULGRBs are consistent with the Amati relation, so are GRBs 030329 and 130427A, while GRB 120422A and *ll*GRB 100316D are marginally consistent. It was once supposed that the placement of a GRB in the $E_{\gamma,iso}$-E_K plane could be a discriminant of GRB's origins, where it is seen that SGRBs also do not follow the Amati relation. However, over the years many authors have closely scrutinized the Amati relation, with opinions swinging back and forth as to whether it reflects a physical origin or is simply due to selection effects [96–103]. To date, no consensus has yet been reached.

4. Physical Properties: Observational Constraints

4.1. Bolometrics. The bolometric LCs of a sample of 12 GRB-SNe, which includes *ll*GRB-SNe and ULGRB-SN 2011kl, are shown in Figure 9. The Bazin function was fit to the GRB-SN bolometric LCs in order to determine their peak luminosity (L_p), the time of peak luminosity (t_p), and the amount the bolometric LC fades from peak to 15 days later (Δm_{15}). (*NB.* that SNe 2001ke, 2008hw, and 2009nz were excluded from the fitting and the subsequent calculated averages, as their bolometric LCs contained too few points to be fit with the Bazin function, which has four free parameters. As such, their luminosities and peak times were approximated by eye and are not included in the average GRB-SN properties presented here.) These values are presented in Table 3.

The average peak luminosity of the GRB-SN sample, excluding SN 2011kl, is $\overline{L}_p = 1.0 \times 10^{43}$ erg s^{-1}, with a standard deviation of $\sigma_{L_p} = 0.4 \times 10^{43}$ erg s^{-1}. The peak luminosities of SNe 2003dh and 2013dx are $\approx 1 \times 10^{43}$ erg s^{-1}, meaning that they are perhaps better representatives of a typical GRB-SN than the archetype SN 1998bw ($L_p = 7 \times 10^{42}$ erg s^{-1}). The peak luminosity of SN 2011kl is $L_p = 2.9 \times 10^{43}$ erg s^{-1}, which makes it more than 5σ more luminous than the average GRB-SN. This is not, however, as bright as superluminous supernovae (SLSNe), whose luminosities exceed $>7 \times 10^{43}$ erg s^{-1} [104]. This makes SN 2011kl an intermediate SN event between GRB-SNe and SLSNe and perhaps warrants a classification of a "superluminous GRB-SNe" (SLGRB-SN); however, in this chapter we will stick with the nomenclature ULGRB-SN. When SN 2011kl is included in the sample, $\overline{L}_p = 1.2 \times 10^{43}$ erg s^{-1}, with $\sigma_{\overline{L}_p} = 0.7 \times 10^{43}$ erg s^{-1}. Even using this average value, SN 2011kl is still 2.5σ more luminous than the average GRB-SN.

The average peak time, when SN 2011kl is and is not included in the sample, is $t_p = 13.2$ d ($\sigma_{t_p} = 2.6$ d) and $t_p = 13.0$ d ($\sigma_{t_p} = 2.7$ d), respectively. Similarly, $\Delta m_{15} = 0.7$ mag ($\sigma_{\Delta m_{15}} = 0.1$ mag) and 0.8 mag ($\sigma_{\Delta m_{15}} = 0.1$ mag), respectively. As such, the inclusion/exclusion of SN 2011kl has little effect on these derived values. The fact that SN 2011kl peaks at a similar time as the average GRB-SN, but does so at a much larger luminosity, strongly suggests that ULGRB-SNe do not belong to the same class of standardizable candles as GRB-SNe. This can be readily explained in that SN 2011kl is powered by emission from a magnetar central engine [36, 105–107], whereas GRB-SNe, including *ll*GRB-SNe, are powered by radioactive heating [106]. Whether ULGRB-SNe represent the same set of standardizable candles as type I SLSNe [108, 109], which are also thought to be powered by a magnetar central engine, their own subset, or perhaps none at all, requires additional well-monitored events.

Over the years, and since the discovery of SN 1998bw, the bolometric properties (kinetic energy, E_K, ejecta mass, M_{ej},

Table 1: Average Bolometric properties of GRB-SNe.

Type*					($M_\odot$)			($M_\odot$)						(d, rest)			(mag)			(km s^{-1})	
	N	$E_K^\dagger$	σ	N	M_{ej}	σ	N	M_{Ni}	σ	N	$L_p^\ddagger$	σ	N	t_p	σ	N	Δm_{15}	σ	N	v_{ph}	σ
GRB	19	26.0	18.3	19	5.8	4.0	20	0.38	0.13	2	1.26	0.35	2	12.28	0.67	2	0.85	0.21	6	18400	9700
INT	1	8.2	—	1	3.1	—	1	0.37	—	1	1.08	—	1	12.94	—	1	0.85	—	1	21300	—
LL	6	27.8	19.6	6	6.5	4.0	6	0.35	0.19	5	0.94	0.41	5	13.22	3.53	5	0.75	0.12	4	22800	8200
ULGRB	2	18.8	18.7	2	6.1	2.9	1	0.41	—	1	2.91	—	1	14.80	—	1	0.78	—	1	21000	—
Rel IcBL	2	13.5	6.4	2	3.4	1.0	2	0.16	0.05	2	0.35	0.50	2	12.78	0.84	2	0.90	0.21	2	14000	1400
GRB ALL	28	25.2	17.9	28	5.9	3.8	28	0.37	0.20	9	1.24	0.71	9	13.16	2.61	9	0.79	0.12	12	20300	8100
GRB ALL**	27	25.9	17.9	27	5.9	3.9	28	0.37	0.20	8	1.03	0.36	8	12.95	2.72	8	0.79	0.13	11	20200	8500
Ib	19	3.3	2.6	19	4.7	2.8	12	0.21	0.22	—	—	—	—	—	—	—	—	—	11	8000	1700
Ic	13	3.3	3.3	13	4.6	4.5	7	0.23	0.19	—	—	—	—	—	—	—	—	—	10	8500	1800

*Classifications (Section 3): *ll*GRBs: GRB-SNe associated with low-luminosity GRBs ($L_{\gamma,iso} < 10^{48.5}$ erg s^{-1}); INT-GRBs: GRB-SNe associated with intermediate-luminosity GRBs ($10^{48.5} < L_{\gamma,iso} < 10^{49.5}$ erg s^{-1}); GRBs: GRB-SNe associated with high-luminosity GRBs ($L_{\gamma,iso} > 10^{49.5}$ erg s^{-1}); ULGRBs: GRB-SNe associated with ultra-long-duration GRBs (see Section 3).
**Excluding SN 2011kl.
†Units: 10^{51} erg.
‡Units: 10^{43} erg s^{-1}.
Note: average bolometric properties of SNe Ib and Ic are from [18].

and nickel mass, M_{Ni}) of the best-observed GRB-SNe have been determined by sophisticated numerical simulations (hydrodynamical models coupled with radiative transfer, RT, codes) [3, 7, 36, 47, 48, 107, 110–119] and analytical modelling [10, 18, 31, 32, 40, 41, 43, 106, 120–122]. A summary of the derived bolometric properties for individual GRB-SNe is presented in Table 3, while a summary of the average bolometric properties, broken down by GRB-SN subtype and compared against other subtypes of SNe Ibc, is shown in Table 1. It should be noted that the values presented have been derived over different wavelength ranges: some are observer-frame *BVRI*, while others include UV, *U*-band, and NIR contributions. Further discussion on the effects of including additional filters when constructing a bolometric LC of a given SN can be found in [30, 41, 49, 120, 123], who show that including NIR flux leads to brighter bolometric LCs that decay slower at later times and including UV flux leads to an increase in luminosity at earlier times (during the first couple of weeks, rest-frame) when the UV contribution is nonnegligible.

From this sample of $N = 28$ GRB-SNe we can say that the average GRB-SN (grey-dashed line in Figure 9) has a kinetic energy of $E_K = 2.5 \times 10^{52}$ erg ($\sigma_{E_K} = 1.8 \times 10^{52}$ erg), an ejecta mass of $M_{ej} = 6\,M_\odot$ ($\sigma_{M_{ej}} = 4\,M_\odot$), a nickel mass of $M_{Ni} = 0.4\,M_\odot$ ($\sigma_{M_{Ni}} = 0.2\,M_\odot$), and a peak photospheric velocity of $v_{ph} = 20{,}000$ km s^{-1} ($\sigma_{v_{ph}} = 8{,}000$ km s^{-1}). Here we have assumed that the line velocities of various transitions, namely, Fe II λ5169 and Si II λ6355, are suitable proxies for the photospheric velocities. An in-depth discussion of this assumption and its various caveats can be found in [46]. It has a peak luminosity of $L_p = 1 \times 10^{43}$ erg s^{-1} ($\sigma_{L_p} = 0.4 \times 10^{43}$ erg s^{-1}), reaches peak bolometric light in $t_p = 13$ days ($\sigma_{t_p} = 2.7$ days), and has $\Delta m_{15} = 0.8$ mag ($\sigma_{\Delta m_{15}} = 0.1$ mag). There are no statistical differences in the average bolometric properties, rise times, and decay rates, between the different GRB-SN subtypes, and excluding ULGRB-SN 2011kl, there are no differences in their peak luminosities. As found in previous studies [18, 120], relativistic SNe IcBL are roughly half as energetic as GRB-SNe and contain approximately half as much ejecta mass and nickel content therein. However, we are comparing GRB-SNe against a sample of two relativistic SNe IcBL, meaning we should not draw any firm conclusions as of yet.

There are a few caveats to keep in mind when interpreting these results. The first is the comparison of bolometric properties derived for SNe observed over different filter/wavelength ranges, as discussed above. Secondly, for a GRB-SN to be observed there are several stringent requirements [11], including AGs that fade at a reliably determined rate (e.g., for GRB 030329 the complex AG behaviour led to a range of 1 mag in the peak brightness of accompanying SN 2003dh [4–6]; thus in this case the reported peak brightness was strongly model-dependent), have a host galaxy that can be readily quantified, and are to be at a relatively low redshift ($z \leq 1$ for current 10 m class ground telescopes and *HST*). Moreover, the modelling techniques used to estimate the bolometric properties contain their own caveats and limitations. For example, the analytical Arnett model [208] contains assumptions such as spherical symmetry, homogeneous ejecta distribution, homologous expansion, and a central location for the radioactive elements [18].

4.2. What Powers a GRB-SN? Observations of GRB-SNe can act as a powerful discriminant of the different theoretical models proposed to produce them. The analysis presented in the previous section made the assumption that GRB-SNe are powered by radioactive heating. In this scenario, it is assumed that during the initial core-collapse (see Section 9 for further discussion), roughly 0.1 $M_\odot$ or so of nickel can be created via explosive nucleosynthesis [209] if the stellar material has nearly equal amounts of neutrons and protons (such as silicon and oxygen), and approximately 10^{52} erg of energy is focused

Table 2: GRB-SN master Table 1: γ-ray properties.

					(10^{52} erg)	(keV)	(erg s^{-1})
GRB	SN	Type	z	T_{90} (s)	$E_{\gamma,\mathrm{iso}}$	E_{p}	$L^{\dagger}_{\mathrm{iso}}$
970228		GRB	0.695	56	1.6 (0.12)	195 (64)	4.84×10^{50}
980326		GRB			0.48 (0.09)	935 (36)	
980425	1998bw	*ll*GRB	0.00867	18	0.000086 (0.000002)	55 (21)	4.80×10^{46}
990712		GRB	0.4331	19	0.67 (0.13)	93 (15)	5.05×10^{50}
991208		GRB	0.7063	60	22.3 (1.8)	313 (31)	6.34×10^{51}
000911		GRB	1.0585	500	67 (14)	1859 (371)	2.75×10^{51}
011121	2001ke	GRB	0.362	47	7.8 (2.1)	793 (265)	2.26×10^{51}
020305							
020405		GRB	0.68986	40	10 (0.9)	612 (10)	4.22×10^{51}
020410				>1600			
020903		*ll*GRB	0.2506	3.3	0.0011 (0.0006)	3.37 (1.79)	4.20×10^{48}
021211	2002lt	GRB	1.004	2.8	1.12 (0.13)	127 (52)	8.02×10^{51}
030329	2003dh	GRB	0.16867	22.76	1.5 (0.3)	100 (23)	7.70×10^{50}
030723						<0.023	
030725							
031203	2003lw	*ll*GRB	0.10536	37	0.0086 (0.004)	<200	2.55×10^{48}
040924		GRB	0.858	2.39	0.95 (0.09)	102 (35)	7.38×10^{51}
041006		GRB	0.716	18	3 (0.9)	98 (20)	2.86×10^{51}
050416A		INT	0.6528	2.4	0.1 (0.01)	25.1 (4.2)	6.89×10^{50}
050525A	2005nc	GRB	0.606	8.84	2.5 (0.43)	127 (10)	4.54×10^{51}
050824		GRB	0.8281	25	$0.041 < E < 0.34$	$11 < E < 32$	
060218	2006aj	*ll*GRB	0.03342	2100	0.0053 (0.0003)	4.9 (0.3)	2.60×10^{46}
060729		GRB	0.5428	115	1.6 (0.6)	>50	2.14×10^{50}
060904B		GRB	0.7029	192	2.4 (0.2)	163 (31)	2.12×10^{50}
070419A		INT	0.9705	116	≈0.16		2.71×10^{49}
080319B		GRB	0.9371	124.86	114 (9)	1261 (65)	1.76×10^{52}
081007	2008hw	GRB	0.5295	9.01	0.15 (0.04)	61 (15)	2.54×10^{50}
090618		GRB	0.54	113.34	25.7 (5)	211 (22)	3.49×10^{51}
091127	2009nz	GRB	0.49044	7.42	1.5 (0.2)	35.5 (1.5)	3.01×10^{51}
100316D	2010bh	*ll*GRB	0.0592	1300	>0.0059	26 (16)	4.80×10^{46}
100418A		GRB	0.6239	8	0.0990 (0.0630)	29 (2)	2.00×10^{50}
101219B	2010ma	GRB	0.55185	51	0.42 (0.05)	70 (8)	1.27×10^{50}
101225A		ULGRB	0.847	7000	1.2 (0.3)	38 (20)	3.16×10^{48}
111209A	2011kl	ULGRB	0.67702	10000	58.2 (7.3)	520 (89)	9.76×10^{49}
111211A			0.478				
111228A		GRB	0.71627	101.2	4.2 (0.6)	58.4 (6.9)	7.12×10^{50}
120422A	2012bz	GRB	0.28253	5.4	0.024 (0.008)	<72	5.70×10^{49}
120714B	2012eb	INT	0.3984	159	0.0594 (0.0195)	101.4 (155.7)	5.22×10^{48}
120729A		GRB	0.8	71.5	2.3 (1.5)	310.6 (31.6)	5.79×10^{50}
130215A	2013ez	GRB	0.597	65.7	3.1 (1.6)	155 (63)	7.53×10^{50}
130427A	2013cq	GRB	0.3399	163	81 (10)	1028 (50)	6.65×10^{51}
130702A	2013dx	INT	0.145	58.881	0.064 (0.013)	15 (5)	1.24×10^{49}
130831A	2013fu	GRB	0.479	32.5	0.46 (0.02)	67 (4)	2.09×10^{50}
140606B		GRB	0.384	22.78	0.347 (0.02)	801 (182)	2.10×10^{50}
150518A			0.256				
150818A		INT	0.282	123.3	0.1 (0.02)	128 (13)	1.03×10^{49}

$^{\dagger}L_{\mathrm{iso}} = E_{\mathrm{iso}}(1+z)/T_{90}$.

$^{\ddagger}\gamma$-ray properties calculated by [85] for a redshift range of $0.9 \leq z \leq 1.1$.

*ll*GRB: GRB-SN associated with a low-luminosity GRB ($L_{\gamma,\mathrm{iso}} < 10^{48.5}$ erg s^{-1}); INT: GRB-SN associated with an intermediate-luminosity GRB ($10^{48.5} < L_{\gamma,\mathrm{iso}} < 10^{49.5}$ erg s^{-1}); GRB: GRB-SN associated with a high-luminosity GRB ($L_{\gamma,\mathrm{iso}} > 10^{49.5}$ erg s^{-1}); ULGRB: GRB-SN associated with an ultra-long-duration GRB (see Section 3).

Table 3: GRB-SN master Table 2: SN properties.

GRB	SN	Type	z	S?	Grade	(mag) M_V^*	(mag) $\Delta m_{15,V}$	(d) $t_{V,\mathrm{p}}^*$	(erg s^{-1}) $L_{\mathrm{p,Bol}}$	(d) $t_{\mathrm{p,rest}}$	(mag) $\Delta m_{15,\mathrm{Bol}}$	(10^{51} erg) E_{K}	($\mathrm{M}_\odot$) M_{ej}	($\mathrm{M}_\odot$) M_{Ni}	(km s^{-1}) v_{ph}	$\bar{k}$	$\bar{s}$	Filters
970228		GRB	0.695		C													
980326		GRB			D													
980425	1998bw	*ll*GRB	0.00866	S	A	-19.29 ± 0.08	0.75 ± 0.02	16.09 ± 0.18	7.33×10^{42}	15.16	0.80	20–30	6–10	0.3–0.6	18000	1	1	
990712		GRB	0.4331		C							$26.1^{+24.6}_{-15.0}$	$6.6^{+3.5}_{-2.9}$	0.14 ± 0.04		0.36 ± 0.05	1.10 ± 0.20	R
991208		GRB	0.7063		E							$38.7^{+44.6}_{-26.0}$	$9.7^{+6.8}_{-5.6}$	0.96 ± 0.48		2.11 ± 0.58	1.10 ± 0.20	R
000911		GRB	1.0585		E													
011121	2001ke	GRB	0.362	S	B				$\sim 5.9 \times 10^{42}$	~17		$17.7^{+8.8}_{-6.4}$	4.4 ± 0.8	0.35 ± 0.01		1.13 ± 0.23	0.84 ± 0.17	BV^*
020305					E													
020405		GRB	0.68986		C							$8.9^{+5.4}_{-3.8}$	$2.2^{+0.6}_{-0.5}$	0.23 ± 0.02		0.82 ± 0.14	0.62 ± 0.03	R
020410					D													
020903		*ll*GRB	0.2506	S	B							$28.9^{+32.2}_{-18.9}$	$7.3^{+4.9}_{-4.0}$	0.25 ± 0.13		0.61 ± 0.19	0.98 ± 0.02	R
021211	2002lt	GRB	1.004	S	B							$28.5^{+45.0}_{-13.0}$	$7.2^{+7.4}_{-6.0}$	0.16 ± 0.14		0.40 ± 0.19	0.98 ± 0.26	R
030329	2003dh	GRB	0.16867	S	A	-19.39 ± 0.14	0.90 ± 0.50	10.74 ± 2.57	1.01×10^{43}	12.75	0.70	20–50	5–10	0.4–0.6	20000	1.28 ± 0.28	0.87 ± 0.18	UBV^*
030723					D													
030725					E													
031203	2003lw	*ll*GRB	0.10536	S	A	-19.90 ± 0.16	0.64 ± 0.10	19.94 ± 1.48	1.26×10^{43}	17.33	0.62	60.0 ± 15	13.0 ± 4.0	0.55 ± 0.20	18000	1.65 ± 0.36	1.10 ± 0.24	VRI^*
040924		GRB	0.858		C													
041006		GRB	0.716		C							$76.4^{+39.8}_{-28.7}$	$19.2^{+3.9}_{-3.6}$	0.69 ± 0.07		1.16 ± 0.06	1.47 ± 0.04	R
050416A		INT	0.6528		D													
050525A	2005nc	GRB	0.606	S	B	-18.59 ± 0.31	1.17 ± 0.88	11.08 ± 3.37				$18.9^{+10.7}_{-7.5}$	$4.8^{+1.1}_{-1.0}$	0.24 ± 0.02		0.69 ± 0.03	0.83 ± 0.03	R
050824		GRB	0.8281		E							$5.7^{+9.3}_{-3.7}$	$1.4^{+1.6}_{-0.6}$	0.26 ± 0.17		1.05 ± 0.42	0.52 ± 0.14	R
060218	2006aj	*ll*GRB	0.03342	S	A	-18.85 ± 0.08	1.08 ± 0.06	9.96 ± 0.18	6.47×10^{42}	10.42	0.83	1.0 ± 0.5	2.0 ± 0.5	0.20 ± 0.10	20000	0.58 ± 0.13	0.67 ± 0.14	$UBVR^*$
060729		GRB	0.5428		D							$24.4^{+14.3}_{-9.9}$	$6.1^{+1.6}_{-1.4}$	0.36 ± 0.05		0.94 ± 0.10	0.92 ± 0.04	RI
060904B		GRB	0.7029		C							$9.9^{+5.1}_{-3.7}$	2.5 ± 0.5	0.12 ± 0.01		0.42 ± 0.02	0.65 ± 0.01	R
070419A		GRB	0.9705		D													
080319B		GRB	0.9371		C							$22.7^{+19.1}_{-11.9}$	$5.7^{+2.6}_{-2.2}$	0.86 ± 0.45		2.30 ± 0.90	0.89 ± 0.10	I
081007	2008hw	GRB	0.5295	S	B				$\sim 1.4 \times 10^{43}$	~12		19.0 ± 15.0	2.3 ± 1.0	0.39 ± 0.08	12600	0.71 ± 0.10	0.85 ± 0.11	riz
090618		GRB	0.54		C	-19.34 ± 0.13	0.65 ± 0.17	17.54 ± 1.64				$36.5^{+20.0}_{-14.2}$	$9.2^{+2.1}_{-1.9}$	0.37 ± 0.03		1.11 ± 0.22	0.98 ± 0.20	B^*
091127	2009nz	GRB	0.49044	S	B				$\sim 1.2 \times 10^{43}$	~15	~0.5	13.5 ± 0.4	4.7 ± 0.1	0.33 ± 0.01	17000	0.89 ± 0.01	0.88 ± 0.01	I
100316D	2010bh	*ll*GRB	0.0592	S	A	-18.89 ± 0.10	1.10 ± 0.05	8.76 ± 0.37	5.67×10^{42}	8.76	0.89	15.4 ± 1.4	2.5 ± 0.2	0.12 ± 0.02	35000	0.53 ± 0.15	0.53 ± 0.11	VRI^*
100418A		INT	0.6239		D/E													
101219B	2010ma	GRB	0.55185	S	A/B				1.5×10^{43}	11.80	0.99	10.0 ± 6.0	1.3 ± 0.5	0.43 ± 0.03		1.16 ± 0.63	0.76 ± 0.10	$griz$
101225A		ULGRB	0.847		D							32.0 ± 16.0	8.1 ± 1.5	0.41 ± 0.03		0.96 ± 0.05	1.02 ± 0.03	i
111209A	2011kl	ULGRB	0.67702		A/B				2.91×10^{43}	14.80	0.78	20–90	3–5		21000	1.81 ± 0.19	1.08 ± 0.11	iz
111211A			0.478	S	B/C													
111228A			0.71627		E													
120422A	2012bz	*ll*GRB	0.28253	S	A	-19.50 ± 0.03	0.73 ± 0.06	14.20 ± 0.34	1.48×10^{43}	14.45	0.62	25.5 ± 2.1	6.1 ± 0.5	0.57 ± 0.07	20500	1.13 ± 0.25	0.93 ± 0.19	BV^*
120714B	2012eb		0.3984	S	B													
120729A		GRB	0.8		D/E									0.42 ± 0.11		1.02 ± 0.26	1‡	ri
130215A	2013ez	GRB	0.597	S	B									0.25–0.30	6000	0.6–0.75	1‡	ri
130427A	2013cq	GRB	0.3399	S	B							64.0 ± 7.0	6.3 ± 0.7	0.28 ± 0.02	35000	0.85 ± 0.03	0.77 ± 0.03	r
130702A	2013dx	INT	0.145	S	A	-19.26 ± 0.24	1.05 ± 0.05	13.86 ± 0.70	1.08×10^{43}	12.94	0.85	8.2 ± 0.4	3.1 ± 0.1	0.37 ± 0.01	21300	0.98 ± 0.07	0.78 ± 0.05	$griz$
130831A	2013fu	GRB	0.479	S	A/B							18.7 ± 9.0	4.7 ± 0.8	0.30 ± 0.07		0.95 ± 0.19	0.82 ± 0.19	B^*
140606B		GRB	0.384	S	A/B							19.0 ± 11.0	4.8 ± 1.9	0.42 ± 0.17	19800	1.04 ± 0.24	0.81 ± 0.13	V^*
150518A			0.256		C/D													
150818A		INT	0.282	S	B													
—	2009bb	Rel IcBL	0.009987	S	—	-18.61 ± 0.28	1.13 ± 0.04	13.37 ± 0.32				18.0 ± 8.0	4.1 ± 1.9	0.19 ± 0.03	15000	0.60 ± 0.05	0.73 ± 0.07	$BVRI^*$
—	2012ap	Rel IcBL	0.012141	S		-18.76 ± 0.33	0.92 ± 0.08	14.43 ± 0.19				9.0 ± 3.0	2.7 ± 0.5	0.12 ± 0.02	13000	1.10 ± 0.23	0.82 ± 0.09	$BVRI^*$

S denotes one or more spectra of the SN were obtained.

Grades are from Hjorth and Bloom (2012): A: strong spectroscopic evidence. B: a clear light curve bump as well as some spectroscopic evidence resembling a GRB-SN. C: a clear bump consistent with other GRB-SNe at the spectroscopic redshift of the GRB. D: a bump, but the inferred SN properties are not fully consistent with other GRB-SNe or the bump was not well sampled or there is no spectroscopic redshift of the GRB. E: a bump, either of low significance or inconsistent with other GRB-SNe.

$*$ denotes exact, K-corrected rest-frame filter observable.

‡Values fixed during fit.

$\bar{k}$ and $\bar{s}$ denote the filter-averaged luminosity (k) and stretch (s) factors relative to SN 1998bw.

Table 4: References.

GRB	References(s)
970228	[124, 125]
980326	[126, 127]
980425	[1–3, 9, 18, 42, 44, 47, 110, 111, 120, 128]
990712	[18, 129]
991208	[18, 130]
000911	[131, 132]
011121	[18, 42, 44, 133–136]
020305	[137]
020405	[18, 138]
020410	[139, 140]
020903	[18, 141–143]
021211	[18, 144, 145]
030329	[4–7, 18, 30, 42, 44, 112, 128, 146, 147]
030723	[148, 149]
030725	[150]
031203	[18, 42, 44, 113, 128, 151–156]
040924	[90, 157]
041006	[18, 39, 90, 158]
050416A	[159, 160]
050525A	[18, 44, 128, 161]
050824	[18, 35, 162, 163]
060218	[18, 33, 42, 44, 48, 58, 90, 113, 120, 128, 156, 164–168]
060729	[10, 18, 169, 170]
060904B	[18, 171]
070419A	[172, 173]
080319B	[174–176]
081007	[177–181]
090618	[10, 18, 42, 128]
091127	[18, 181–183]
100316D	[18, 30, 42, 44, 49, 65, 78, 120, 121, 128, 184]
100418A	[185–187]
101219B	[181, 188]
101225A	[34, 53], *here*
111209A	[36, 53, 105–107, 189], *here*
111211A	[190]
111228A	[191]
120422A	[18, 41, 44, 91, 128, 192]
120714B	[193, 194]
120729A	[31]
130215A	[31]
130427A	[40, 195–197]
130702A	[43, 44, 198]
130831A	[31, 42, 199]
140606B	[32, 75]
150518A	[200]
150818A	[201–203]
SN 2009bb	[18, 42, 44, 79, 120, 204, 205]
SN 2012ap	[76, 89, 206, 207], *here*

into ~1% of the star, which occurs in the region between the newly formed compact object and 4×10^9 cm [210]. In this scenario, temperatures in excess of 4×10^9 K can be attained. However, the precise amount of ^{56}Ni that is generated is quite uncertain and depends greatly on how much the star has expanded (or collapsed), prior to energy deposition. The radioactive nickel decays into cobalt with a half-life of 6.077 d and then cobalt into iron with a half-life of 77.236 d: $^{56}_{28}\mathrm{Ni} \rightarrow {}^{56}_{27}\mathrm{Co} \rightarrow {}^{56}_{26}\mathrm{Fe}$ [208, 211]. Given its short half-life, the synthesized nickel must be generated during the explosion itself and not long before core-collapse. Gamma-rays that are emitted during the different radioactive decay processes are thermalised in the optically thick SN ejecta, which heat the ejecta that in turn radiates this energy at longer wavelengths (optical and NIR). This physical process is expected to power other types of SNe, including all type I SNe (Ia, Ib, Ic, and type Ic SLSNe) and the radioactive tail of type IIP SNe.

Observationally, there are hints that suggest that the best-observed GRB-SNe are powered, at least in part [212], by radioactive heating. At late times, the decay of ^{56}Co leads to an exponential decline in the nebular-phase bolometric LC of type I SNe. An example of this is the grey-dashed line in Figure 9, which is an analytical model [122, 213] that considers the luminosity produced by a fiducial SN with a kinetic energy of $E_{\mathrm{K}} = 25 \times 10^{51}$ erg, an ejecta mass of $M_{\mathrm{ej}} = 6\,\mathrm{M}_{\odot}$, and a nickel mass of $M_{\mathrm{Ni}} = 0.4\,\mathrm{M}_{\odot}$ (e.g., the "average" GRB-SN). Such a model and others of this ilk assume full trapping of the emitted γ-rays and thermalised energy. For comparison, the late-time LC of SN 1998bw appears to fade more rapidly than this, presumably because some of the γ-rays escape directly into space without depositing energy into the expanding ejecta. At times later than 500 d [9, 214], the observed flattening seen in the LC can be interpreted in terms of both more of the energy and γ-rays being retained in the ejecta, and more energy input from the radioactive decay of species in addition to cobalt.

In the collapsar model, there are additional physical processes that can lead to the creation of greater masses of radioactive nickel. One potential source of ^{56}Ni arises from the wind emitted by the accretion disk surrounding the newly formed black hole (BH). According to the numerical simulations of [215], the amount of generated nickel depends on the accretion rate as well as the viscosity of the inflow. In theory, at least, the only upper bound on the amount of nickel that can be synthesized by the disk wind is the mass of material that is accreted. In an analytical approach, [216] demonstrated that enough ^{56}Ni can be synthesized (in order to match observations of GRB-SNe), over the course of a few tens of seconds, in the convective accretion flow arising from the initial circularization of the infalling envelope around the BH.

In the millisecond magnetar model, it is more difficult to produce a sufficient amount of ^{56}Ni via energy injection from a central engine. Some simulations suggest that only a few hundredths of a solar mass of nickel can be synthesized in the magnetar model [217]. However it may be possible to generate more nickel by tapping into the initial rotational energy of the magnetar via magnetic stresses, thus enhancing the shocks induced by the collision of the energetic wind emanated by the magnetar with material already processed by the SN shock [218, 219]. Another route would be via a shock

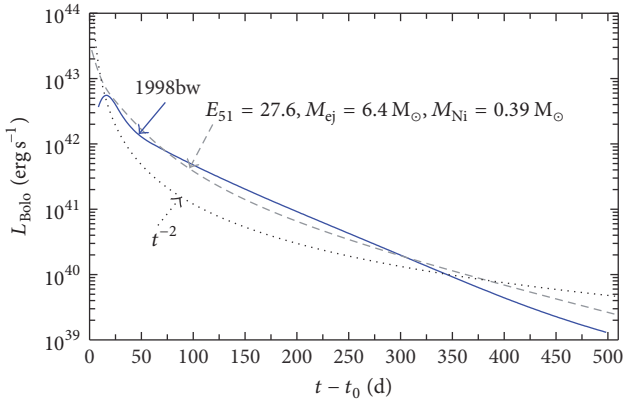

Figure 10: Late-time bolometric LC of SN 1998bw in filters *BVRI*. Two analytical models have been plotted to match the peak luminosity: (1) a single-zone analytical model for a fiducial SN that is powered by radioactive heating, where $E_K = 27.6 \times 10^{51}$ erg, an ejecta mass of $M_{ej} = 6.4\,M_\odot$, and a nickel mass of $M_{Ni} = 0.39\,M_\odot$, and (2) a t^{-2} curve, which is the expected decay rate for luminosity powered by a magnetar central engine. At late times the decay rate of model (1) provides a much better fit than the t^{-2} decay, which grossly overpredicts the bolometric luminosity at times later than 400 d. This is one line of observational evidence that GRB-SNe are powered by radioactive heating and not via dipole-extracted radiation from a magnetar central engine (i.e., a magnetar-driven SN).

wave driven into the ejecta by the magnetar itself, which for certain values of P and B could generate the required nickel masses [220]. However, in this scenario an isotropic-equivalent energy input rate of more than 10^{52} erg is required, and the subsequent procurement of additional nickel mass via explosive nucleosynthesis will inevitably lead to a more rapid spin-down of the magnetar central engine, rendering it unable to produce energy input during the AG phase. It is also worth considering that if a magnetar (and the subsequent GRB) is formed via the accretion-induced collapse of a white dwarf star, or perhaps the merger of two white dwarfs, there is no explosive nucleosynthesis and thus a very low ^{56}Ni yield [221].

The uncertainties unpinning both models mean that neither can be ruled out at this time, though perhaps the collapsar model offers a slightly easier route for producing the necessary quantity of nickel needed to explain the observed luminosities of GRB-SNe. But what if GRB-SNe are not powered by radioactive heating, but instead via another mechanism? Could, instead, GRB-SNe be powered by a magnetar central engine [223, 224], as has been proposed for some type I SLSNe [225–227]? A prediction of the magnetar-driven SN model is that at late times the bolometric LC should decay as t^{-2} [106, 217, 223–225, 228, 229]. Plotted in Figure 10 is the bolometric LC of SN 1998bw to $t - t_0 = 500$ d. Overplotted are two analytical models: (1) a single-zone analytical model for a fiducial SN that is powered by radioactive heating, where $E_K = 27.6 \times 10^{51}$ erg, an ejecta mass of $M_{ej} = 6.4\,M_\odot$, and a nickel mass of $M_{Ni} = 0.39\,M_\odot$, and (2) a t^{-2} curve (i.e., the decay rate expected for luminosity powered by a magnetar central engine). Both have been fitted to the bolometric LC of SN 1998bw to match its peak luminosity. At late times the decay rate of the radioactive-heated analytical LC provides a much better fit than the t^{-2} decay, which grossly overpredicts the bolometric luminosity at times later than 400 d. The difference between observations and the radioactive decay model can be attributed to incomplete trapping of γ-rays produced during the radioactive decay process.

Further evidence against the magnetar model are the observed line velocities as a function of time. In 1D analytical magnetar models [228, 229], a mass shell forms due to the expanding magnetar bubble. This feature of the 1D models has the implication that the observed line velocities will have a flat, plateau-like evolution. Inspection of Figure 6 reveals that this is indeed not the case for all the GRB-SNe of which there are time-series spectra. This particularly applies in the measured Si II λ6355 velocities, where all appear to decrease from a maximum value early on, rather than maintaining a flat evolution throughout. This is a second line of evidence that rules against magnetar heating in GRB-SNe.

However, it appears that not all GRB-SNe subtypes are powered by radioactive heating. Several investigations have provided compelling evidence that ULGRB 111209A/SN 2011kl was powered instead by a magnetar central engine. Reference [36] showed that SN 2011kl could not be powered entirely (or at all) by radioactive heating. Their argument was based primarily on the fact that the inferred ejecta mass ($3.2 \pm 0.5\,M_\odot$), determined via fitting the Arnett model [208] to their constructed bolometric LC, was too low for the amount of nickel needed to explain the observed bolometric luminosity ($1.0 \pm 0.1\,M_\odot$). The ratio of $M_{Ni}/M_{ej} = 0.3$ was much larger than that inferred for the general GRB-SN population ($M_{Ni}/M_{ej} \approx 0.07$; [18]), which rules against radioactive heating powering SN 2011kl. Secondly, the shape and relative brightness of an optical spectrum obtained of SN 2011kl just after peak SN light ($t - t_0 = 20$ d, rest-frame) was entirely unlike the spectra observed for GRB-SNe (Figure 5), including SN 1998bw [2]. Instead, the spectrum more closely resembled those of SLSNe in its shape, including the sharp cut-off at wavelengths bluewards of 3000 Å. Several authors [36, 105–107, 230] modelled different phases of the entire ULGRB event to determine the ejecta mass (M_{ej}), initial spin period (P), and the initial magnetic field strength (B), with some general consensus among the derived values: $M_{ej} = 3$–$5\,M_\odot$ (for various values of the assumed grey opacity), $P = 2$–11 ms, and $B = 0.4$–2×10^{15} G. Note that some models assumed additional heating from some nucleosynthesised nickel ($0.2\,M_\odot$ [105, 107]), while [106] assumed that energy injection from the magnetar central engine was solely responsible for powering the entire event. The general consensus of all the modelling approaches is that SN 2011kl was not powered entirely by radioactive heating, and additional energy, likely arising from a magnetar central engine, was needed to explain the observations of this enigmatic event.

5. Geometry

Measuring the geometry of GRB-SNe can lead to additional understanding of their explosion mechanism(s) and the role and degree of nickel mixing within the ejecta. A starting

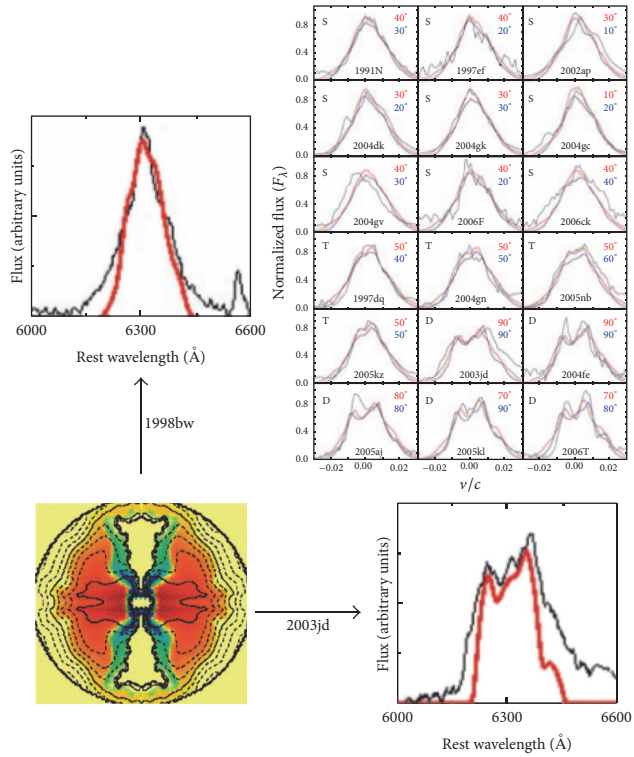

FIGURE 11: Observed [O I] $\lambda\lambda$6300,6364 emission-line profiles for a sample of SNe Ibc. Top right: emission lines classified into characteristic profiles (from [222]): single-peaked (S), transition (T), and double-peaked (D). Model predictions from a bipolar model (red curves) and a less aspherical model (blue), for different viewing directions are shown (directions denoted by the red and blue text). All other panels: nebular line profiles observed for an aspherical explosion model for different viewing angles (from [113]). The figure shows the properties of the explosion model: Fe (coloured in green and blue) is ejected near the jet direction and oxygen (red) in a torus-like structure near the equatorial plane. Synthetic [O I] $\lambda\lambda$6300,6364 emission-line profiles are compared with the spectra of SN 1998bw (top left) and SN 2003jd (bottom right).

point is to understand the geometry of GRB-SNe relative to other types of stripped-envelope core-collapse SNe (CCSNe) and ascertain whether any differences exist. In this section we will recap the results of photometric, spectroscopic, and polarimetric/spectropolarimetry observations of SNe Ibc. The collective conclusion of these studies is that asphericity appears to be ubiquitous to *all* SNe Ibc.

5.1. Non-GRB-SNe Ibc

5.1.1. Spectroscopy. The best way to investigate the inner ejecta geometry of a given SN is through late-time spectroscopy, as done by [110, 111, 222, 231–235]. At ≥200 d after the explosion, expansion makes the density of the ejecta so low that it becomes optically thin, thus allowing optical photons produced anywhere in the ejecta to escape without interacting with the gas. At these epochs the SN spectrum is nebular, showing emission lines mostly of forbidden transitions. Because the expansion velocity is proportional to the radius of any point in the ejecta, the Doppler shift indicates where the photon was emitted: those emitted from the near side of the ejecta are detected at a shorter (blueshifted) wavelengths, while those from the far side of the ejecta are detected at a longer (redshifted) wavelength. The late-time nebular emission profiles thus probe the geometry and the distribution of the emitting gas within the SN ejecta [236, 237]. Importantly for SNe Ibc, nebular spectra allow the observer to look directly into the oxygen core.

One of the strongest emission lines is the [O I] $\lambda\lambda$6300,6364 doublet, which behaves like a single transition if the lines are sufficiently broad (≥0.01c) because the red component is weaker than the blue one by a factor of three; see Figure 11. The appearance of this line can then be used to infer the approximate ejecta geometry: (1) a radially expanding spherical shell of gas produces a square-topped profile; (2) and a filled uniform sphere, where ^{56}Ni is confined in a central high-density region with an inner hole that is surrounded by a low-density O-rich region [238], produces a parabolic profile. These authors also considered a third scenario: (3) a bipolar model [215, 238, 239] characterized by a low-density ^{56}Ni-rich region located near the jet axis, where the jets convert stellar material (mostly O) into Fe-peak elements. The [O I] profile in the bipolar model depends on both the degree of asphericity and the viewing angle. If a bipolar SN explosion is viewed from a direction close to the jet axis, the O-rich material in the equatorial region expands in a direction perpendicular to the line of sight, and the [O I] emission profile is observed to be sharp and single-peaked.

On the other hand, for a near-equatorial view, the profile is broader and double-peaked. It is important to note that a double-peaked profile cannot be accounted for in the spherical model. Furthermore, the separation of the blueshifted and redshifted peaks, which represent the forward and rear portions of an expanding torus of O-rich material, suggests that the two peaks actually originate from the two lines of the doublet from a single emitting source on the front of the SN moving towards the observer. Double emission peaks seen in asymmetric profiles with separations larger or smaller than the doublet spacing do not share this problem. The high incidence of ≈64 Å separation between emission peaks of symmetric profiles plus the lack of redshifted emission peaks in asymmetric profiles suggests that emission from the rear of the SN may be suppressed. This implies that the double-peaked [O I] $\lambda\lambda$6300,6364 line profiles of SNe Ibc are not necessarily signatures of emission from a torus. The underlying cause of the observed predominance of blueshifted emission peaks is unclear but may be due to internal scattering or dust obscuration of emission from far side ejecta [235]. These models are for single-star progenitors, and they do not consider the effects that binary interactions or merger might impart to the observed geometry of the SN ejecta [240].

References [222, 232, 234] found that all SNe Ibc and IIb are aspherical explosions. The degree of asphericity varies in severity, but all studies concluded that most SNe Ibc are not as extremely aspherical as GRB-SNe (specifically SN 1998bw). Interestingly [234] found that, for some SNe Ibc, the [O I] line exhibits a variety of shifted secondary peaks or shoulders, interpreted as blobs of matter ejected at high velocity and possibly accompanied by neutron-star kicks to assure momentum conservation. The interpretation of massive blobs in the SN ejecta is expected to be the signature of very one-sided explosions.

Some notable and relevant nebular spectra analyses include SNe IcBL 2003jd [231], 2009bb [204], and 2012ap [206]. Reference [231] interprets their double-peaked [O I] $\lambda\lambda$6300,6364 nebular lines of SN 2003jd as an indication of an aspherical axisymmetric explosion viewed from near the equatorial plane, and directly perpendicular to the jet axis, and suggested that this asphericity could be caused by an off-axis GRB jet. Reference [204] obtained moderately noisy nebular spectra of SN 2009bb, which nevertheless displayed strong nebular lines of [O I] $\lambda\lambda$6300,6364 and [Ca II] $\lambda\lambda$7291,7324 that had all single-peaked profiles. In their derived synthetic spectra, a single velocity provided a good fit to these lines, thus implying that the ejecta is not overly aspherical. The nebular spectra (>200 d) of SN 2012ap [206] had an asymmetric double-peaked [O I] $\lambda\lambda$6300,6364 emission profile that was attributed to either absorption in the supernova interior or a toroidal ejecta geometry.

5.1.2. Polarimetry. Further enlightening clues to the geometry of SNe Ibc have arisen via polarimetric and spectropolarimetric observations (see [242] for an extensive review and Figure 12). When light scatters through the expanding debris of a SN, it retains information about the orientation of the scattering layers. Since it is not possible to spatially resolve extragalactic SNe through direct imaging, polarization is a powerful tool to determine the morphology of the ejecta. Spectropolarimetry measures both the overall shape of the emitting region and the shape of regions composed of particular chemical elements. Collectively, numerous polarimetric data have provided overwhelming evidence that all CCSNe are intrinsically three-dimensional phenomena with significant departures from spherical symmetry, and they routinely show evidence for strong alignment of the ejecta in single well-defined directions, suggestive of a jet-like flow. As discussed in [242], many of these CCSNe often show a rotation of the position angle with time of 30–40° that is indicative of a jet of material emerging at an angle with respect to the rotational axis of the inner layers. Another recent investigation by [241] showed that all SNe Ibc show nonzero polarization at the wavelength of strong lines. More importantly, they demonstrated that five of the six SNe Ibc they investigated had a "loop" in their Stokes Q-U diagram (where Q is the radiance linearly polarized in the direction parallel or perpendicular to the reference plane and U is the radiance linearly polarized in the directions 45° to the reference plane), which indicates that a nonaxisymmetric, three-dimensional ion distribution is ubiquitous for SNe Ibc ejecta.

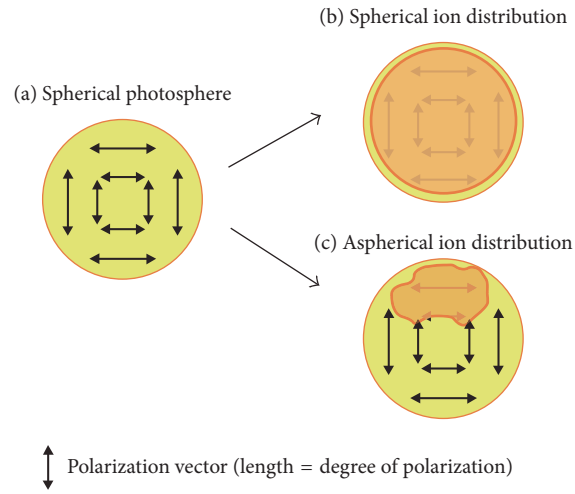

Figure 12: Schematic illustration of polarization in the SN ejecta. (a) When the photosphere is spherical, polarization is canceled out, and no polarization is expected. At the wavelength of a line, polarization produced by the electron scattering is depolarized by the line transition. (b) When the ion distribution is spherical, the remaining polarization is canceled, and no polarization is expected. (c) When the ion distribution is not spherical, the cancelation becomes incomplete, and line polarization could be detected (figure and caption taken from [241]).

The results of [242] suggest that the mechanism that drives CCSNe must produce energy and momentum aspherically from the start, either induced from the preexplosion progenitor star (i.e., rotation and/or magnetic fields) or perhaps arising from the newly formed neutron star (NS) [243–246]. In any case, it appears that the asphericity is permanently frozen into the expanding matter. Collimated outflows might be caused by magnetohydrodynamic jets, as is perhaps the case for GRB-SNe [210, 215, 247, 248], from accretion

flows around the central neutron star, via asymmetric neutrino emission, from magnetoacoustic flux, jittering jets (jets that have their launching direction rapidly change [249]), or by some combination of those mechanisms. Another alternative idea, perhaps intimately related, is that material could be ejected in clumps that block the photosphere in different ways in different lines. It may be that jet-like flows induce clumping so that these effects occur simultaneously. Alternatively, the results of [241] suggest that the global asymmetry of SNe Ibc ejecta may rather arise from convection and preexisting asymmetries in the stellar progenitor before and during the time of core-collapse (e.g., [250, 251]), rather than induced by two-dimensional jet-like asphericity.

In addition to the above analyses, there are more clues which show that asphericity is quite ubiquitous in CCSN ejecta. A jet model was proposed for type Ic SN 2002ap [252], where the jet was buried in the ejecta and did not bore through the oxygen mantle. The lack of Fe polarization suggests that a nickel jet had not penetrated all the way to the surface. For CCSNe, we know that pulsars are somehow kicked at birth in a manner that requires a departure from both spherical and up/down symmetry [253]. The spatial distribution of various elements, including ^{44}Ti in supernova remnants [254], is also consistent with an aspherical explosion, arising from the development of low-mode convective instabilities (e.g., standing accretion shock instabilities [255]) that can produce aspherical or bipolar explosions in CCSNe. The anisotropies inferred by the oxygen distribution instead suggest that large-scale (plume-like) mixing is present, rather than small-scale (Rayleigh-Taylor) mixing, in supernova remnants. Additionally, the Cassiopeia A supernova remnant shows signs of a jet and counterjet that have punched holes in the expanding shell of debris [256], and there are examples of other asymmetric supernova remnants [257, 258] and remnants with indications of being jet-driven explosions or possessing jet-like features [259, 260].

5.1.3. Role of Mixing in the Ejecta. The analytical modelling of late-time (>50–100 d) bolometric LCs of SNe Ibc also implies a departure from spherical symmetry (or perhaps a range grey optical opacities [261]). Modelling performed by [122] showed that the late-time bolometric LC behaviour of a sample of three SNe Ic and IcBL (SNe 1998bw, 1997ef, and 2002ap) was better described by a two-component model (two concentric shells that approximated the behaviour of a high-velocity jet and a dense inner core/torus) than spherical models. Their modelling also showed that there was a large degree of nickel mixing throughout the ejecta. A similar result was inferred by [262] for a sample of SNe Ibc, who showed that the outflow of SNe Ib is thoroughly mixed. Helium lines arise via nonthermal excitation and nonlocal thermodynamic equilibrium [263–266]. High-energy γ-rays produced during the radioactive decay of nickel, cobalt, and iron Compton scatter with free and bound electrons, ultimately producing high-energy electrons that deposit their energy in the ejecta through heating, excitation, and ionization.

To address the question of whether the lack of helium absorption lines for SNe Ic was due to a lack of this element in the ejecta or that the helium was located at large distances from the decaying nickel [266–268], [262] showed that the ejecta of type SN Ic 2007gr was also thoroughly mixed, meaning that the lack of helium lines in this event could not be attributed to poor mixing. A similar conclusion was reached by [46] who demonstrated that He lines cannot be "smeared out" in the spectra of SNe IcBL, that is, blended so much that they disappear; instead He really must be absent in the ejecta (see as well [269]). A prediction of RT models [270] is if the lack of mixing is the only discriminant between SNe Ib and Ic, then well-mixed SNe Ib should have higher ejecta velocities than the less well-mixed SNe Ic. The investigation by [271] tested this prediction with a very large sample of SNe Ibc spectra, finding the opposite to be true: SNe Ic have higher ejecta velocities than SNe Ib, implying that the lack of He lines in the former cannot be attributed entirely to poor mixing in the ejecta. Next, [272] showed that for a sample of SNe Ibc, SNe Ib, Ic, and IcBL have faster rising LCs than SNe Ib, implying that the ejecta in these events are probably well mixed. The collective conclusion of these observational investigations states that the lack of helium features in SNe Ic spectra cannot be attributed to poor mixing but rather the absence of this element in the ejecta, which agrees with the conclusion of [268] that no more than 0.06–0.14 $M_\odot$ of He can be "hidden" in the ejecta of SNe Ic.

5.2. GRB-SNe. The key result presented in the previous sections is that all CCSNe possess a degree of asphericity: either two-dimensional [242] asymmetries where most CCSNe possess a jet or three-dimensional asymmetries [241]. Taken at face value, if all CCSNe possess two-dimensional axisymmetric geometry, then the observation of the 30–40° rotation of the position angle with time is suggestive of a jet of material emerging at an angle with respect to the rotational axis of the inner layers. This observation differs to that expected for GRB-SNe, where the jet angle is expected to be along or very near to the rotation axis of the preexplosion progenitor star. If jets are almost ubiquitous in CCSNe, but they are usually at an angle to the rotational axis, does this suggest that GRB-SNe are different because the jet emerges along, or very near to, the rotational axis? If so, then something is required to maintain that collimation: that is, more rapid rotation of GRB-SN progenitors and/or strong collimation provided by magnetic fields [248]. Moreover, is the difference between *ll*GRBs and high-luminosity GRBs due to less collimation in the former? In turn, perhaps more SNe Ibc arise from central engine that is currently accounted for, but for whatever reason the jets very quickly lose their collimation, perhaps to underenergetic or very short-lived central engines, and deposit their energy in the interior of the star, where perhaps a combination of jets and a neutrino-driven explosion mechanism is responsible for the observed SN. Note that this supposition is also consistent with the study of [273] who looked for off-axis radio emission from GRBs pointed away from Earth, finding <10% of all SNe Ibc are associated with GRBs pointed away from our line of sight. In this scenario, no imprint of the jet in the non-GRB-SNe Ibc is imparted to the ejecta. Nevertheless, the results of [241] need to be kept in mind when considering this speculative scenario, where the asymmetries in SNe Ibc may

not be axisymmetric, but instead may be intrinsically three-dimensional.

More observations are sorely needed of nearby GRB-SNe to help address this outstanding question. To date only two GRB-SNe have occurred at close enough distances that reasonable quality nebular spectra have been obtained: SN 1998bw (~40 Mpc) and SN 2006aj (~150 Mpc). Even SN 2010bh was too distant (~270 Mpc) for the nebular emission lines to be reasonably modelled [49]. In the following section we will present a brief summary of the results of spectroscopic and polarimetric analyses of these two GRB-SNe.

References [47, 110, 111] investigated the nebular spectra of SN 1998bw, which exhibited properties that could not be explained with spherical symmetry. Instead, a model with high-velocity Fe-rich material ejected along the jet axis, and lower-velocity oxygen torus perpendicular to the jet axis, was proposed. From this geometry a strong viewing-angle dependence of nebular line profiles was obtained [110]. Reference [47] noted that the [Fe II] lines were unusually strong for a SN Ic and that lines of different elements have different widths, indicating different expansion velocities, where iron appeared to expand more rapidly than oxygen (i.e., a rapid Fe/Ni-jet and a slower moving O-torus). The [O I] nebular lines declined more slowly than the [Fe II] ones, signalling deposition of γ-rays in a slowly moving O-dominated region. These facts suggest that the explosion was aspherical. The absence of [Fe III] nebular lines can be understood if the ejecta are significantly clumped. Reference [111] noted that their models show an initial large degree (~4 depending on model parameters) of boosting luminosity along the polar/jet direction relative to the equatorial plane, which decreased as the SN approached peak light. After the peak, the factor of the luminosity boost remains almost constant (~1.2) until the supernova entered the nebular phase. This behaviour was attributed to an aspherical ^{56}Ni distribution in the earlier phase and to the disk-like inner low-velocity structure in the later phase.

Early polarization measurements of ≈0.5%, possibly decreasing with time, were detected for SN 1998bw [2, 274], which imply the presence of aspherical ejecta, with an axis ratio of about 2 : 1 [115]. In contrast, radio emission of GRB 980425/SN 1998bw showed no evidence for polarization [56], which suggested that the mildly relativistic ejecta were not highly asymmetric, at least in projection. However it should be noted that internal Faraday dispersion in the ejecta can suppress radio polarization. As mentioned in the previous section, modelling of the late-time bolometric LC of SN 1998bw [9, 117, 214, 275] showed that some degree of asymmetry in the explosion is required to explain its decay behaviour (see as well Figure 10).

For SN 2006aj, the [Fe II] lines were much weaker than those observed for SN 1998bw, which supports its lower luminosity relative to the archetype GRB-SN [113]. Most of the nebular lines had similar widths, and their profiles indicated that no major asymmetries were present in the ejecta at velocities below 8000 km s^{-1}. The modelling results of [48] implied a 1.3 M$_\odot$ oxygen core that was produced by a mildly asymmetric explosion. The mildly peaked [O I] $\lambda\lambda$6300,6364 profile showed an enhancement of the material density at velocities

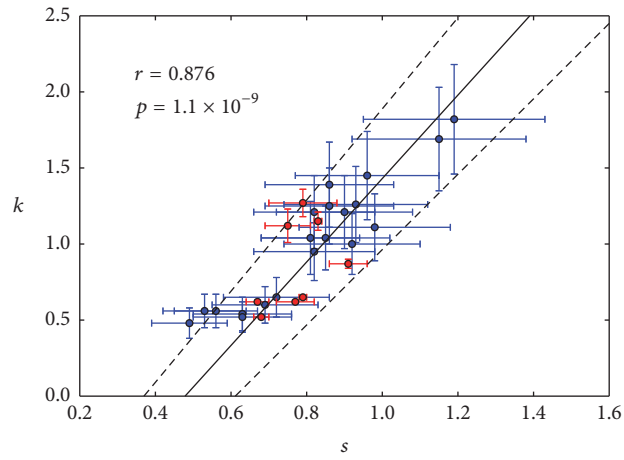

Figure 13: Luminosity (k)-stretch (s) relation for relativistic type IcBL SNe [42]. For all filters from *UBVRI*, and combinations thereof, GRB-SNe are shown in blue, and the two known relativistic type IcBL SNe (2009bb and 2012ap) are shown in red. A bootstrap analysis was performed to fit a straight line to the dataset to find the slope (m) and y-intercept (b), which used Monte-Carlo sampling and $N = 10{,}000$ simulations. The best-fitting values are $m = 2.72 \pm 0.26$ and $b = -1.29 \pm 0.20$. The correlation coefficient is $r = 0.876$, and the two-point probability of a chance correlation is $p = 1.1 \times 10^{-9}$. This shows that the k-s relationship is statistically significant at the 0.001 significance level.

less than <3000 km s^{-1}, which also indicated an asymmetric explosion. If SN 2006aj was a jetted SN explosion, the jet was wider than in SN 1998bw (intrinsically or due to stronger lateral expansion [238]), since the signature is seen only in the innermost part. Linear polarization was detected by [276] between three and 39 days after explosion, which implied the evolution of an asymmetric SN expansion. Reference [277] concluded that their polarization measurements were not very well constrained, and considering the low polarization observed of 6000–6500 Å, the global asymmetry was ≤15%.

6. GRB-SNe as Cosmological Probes

6.1. Luminosity–Stretch/Decline Relationships. In 2014, [42, 44, 128] (see as well [41]) demonstrated, using entirely different approaches, that GRB-SNe (which included *ll*GRB-SNe, INT-GRB-SNe, and high-luminosity GRB-SNe) have a luminosity–decline relationship that is perfectly akin to that measured for type Ia SNe [279]. All approaches investigated decomposed GRB-SN LCs (see Section 2.1). In [42], a template SN LC (1998bw) was created in filters $BVRI(1+z)$ as it would appear at the redshift of the given GRB-SN. A spline function ($g(x)$) was then fit to the template LC, and the relative brightness (k) and width (s) were determined (i.e., $f(x) = k \times g(x/s)$) for each GRB-SN in each rest-frame filter. These were then plotted, and a straight line was fit to the data, where the slope and intercept were constrained via a bootstrap fitting analysis that used Monte-Carlo sampling. An example of the k-s relation is shown in Figure 13, where GRB-SNe are shown in blue points, and the two relativistic SNe IcBL (2009bb and 2012ap) are shown in red. This relation

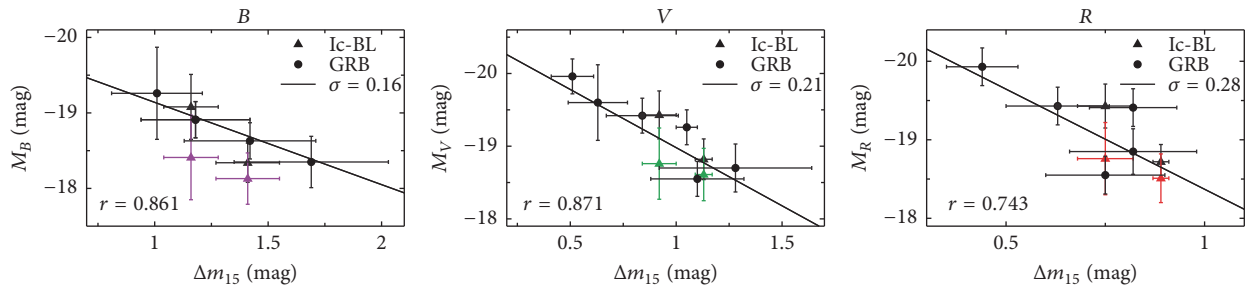

Figure 14: Luminosity–decline relationships of relativistic SNe IcBL (GRB-SNe: filled circles; SNe IcBL: filled triangles) in filters B (purple), V (green), and R (red), from [44]. Solid black lines and points correspond to absolute magnitudes calculated for luminosity distances, while coloured points and lines correspond to absolute magnitudes calculated for those events where independent distance measurements have been made to the SN's host galaxy. The correlation coefficient for each dataset is shown (in black and in their respective colours) as well as the best-fitting luminosity–decline relationship determined using a bootstrap method and the corresponding rms (σ) of the fitted model. It is seen that statistically significant correlations are present for both the GRB-SNe and combined GRB-SN and SN IcBL samples.

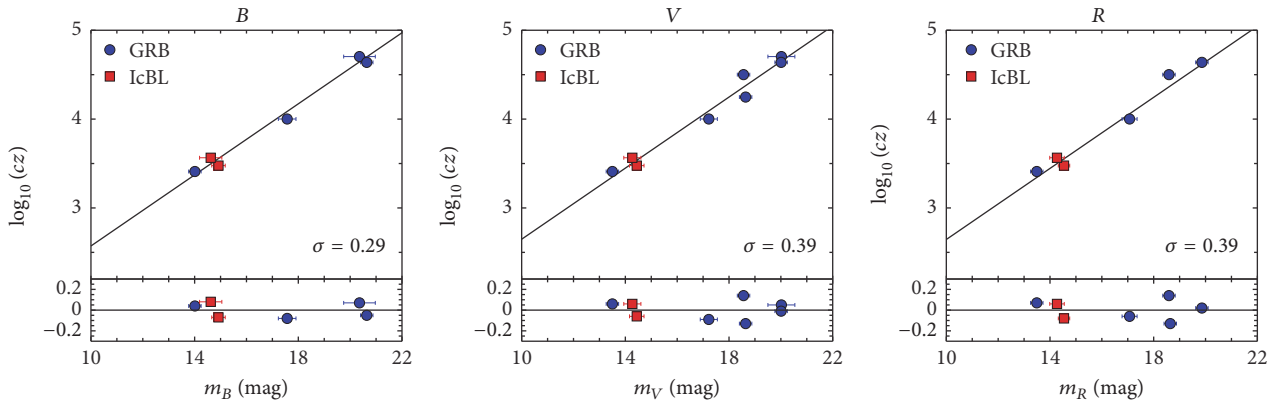

Figure 15: Hubble diagrams of relativistic SNe IcBL in filters BVR, from [44]. GRB-SNe are shown in blue and SNe IcBL (SNe 2009bb and 2012ap) in red. Plotted in each subplot are the uncorrected magnitudes of each subtype and the fitted Hubble ridge line as determined using a bootstrap method. Also plotted are the rms values (σ) and residuals of the magnitudes about the ridge line. In the B-band, the amount of scatter in the combined SNe IcBL sample is the same as that for SNe Ia up to $z = 0.2$ [44, 278], which is $\sigma \approx 0.3$ mag.

shows that GRB-SNe with larger k values also have larger s values; that is, brighter GRB-SNe fade slower. The statistical significance of the fit is shown as Pearson's correlation coefficient, where $r = 0.876$, and the two-point probability of a chance correlation is $p = 1.1 \times 10^{-9}$, which clearly shows that the relationship is significant at more than $p < 0.001$ significance level. This implies that not only are GRB-SNe standardizable candles, but all relativistic type IcBL SNe are.

The result in [42] clearly superseded the results of [30, 33, 39] who searched for correlations in the observer-frame R-band LCs of a sample of GRB-SNe, concluding that none was present. However, the method used in [32, 42, 44] had one key difference to previous methods: they considered precise, K-corrected rest-frame filters. Instead, previous approaches were all sampling different portions of the rest-frame spectral energy distribution (SED), which removed any trace of the k-s relationship. While such a correlation implies that, like SNe Ia, there is a relationship between the brightness of a given GRB-SN and how fast it fades, where brighter GRB-SNe fade slower, this relationship is not very useful if GRB-SNe want to be used for cosmological research: the template LCs of SN 1998bw are created for a specific cosmological model and are therefore model-dependent. Instead, the luminosity–decline relationship presented by [44, 128] relates the same observables as those used in SN Ia-cosmology research: their peak absolute magnitude and Δm_{15} in a given filter. Reference [128] considered rest-frame V-band only, while [44] considered rest-frame BVR. Figure 14 shows the relationships from the latter paper, where the two relativistic SNe IcBL are included in the sample. The amount of RMS scatter increases from blue to red filters and is only statistically significant in B and V (at the $p = 0.02$ level).

6.2. Constraining Cosmological Parameters. Once the luminosity–decline relationship was identified, the logical next step is to use GRB-SNe to constrain cosmological models, in an attempt to determine the rate of universal expansion in the local universe (the Hubble constant, H_0) and perhaps even the mass and energy budget of the cosmos. In a textbook example of how to use any standard(izable) candle to measure H_0 in a Hubble diagram of low-redshift objects (typically $z \ll 1$), [44] followed the procedure outlined in numerous SNe Ia-cosmology papers [280–288]. Figure 15 shows Hubble diagrams of relativistic SNe IcBL in filters BVR (GRB-SNe

in blue, relativistic SNe IcBL in red) for redshifts less than $z = 0.2$. The amount of RMS scatter (shown as σ) is less in the B-filter, ≈0.3 mag, and about 0.4 mag in the redder V and R filters. Compared with the sample of SNe Ia in [278] over the same redshift range, it is seen that SNe Ia in the B-band also have a scatter in their Hubble diagram of 0.3 mag. Moreover, when the large SNe Ia sample ($N = 318$) was decreased to the same sample size of the relativistic SNe IcBL sample, the same amount of scatter was measured, meaning that GRB-SNe and SNe IcBL are as accurate as SNe Ia when used as cosmological probes.

A key observable needed to measure H_0 is independent distance measurements to one or more of the objects being used. However, to date no independent distance has yet been determined for a GRB or GRB-SN. However, relativistic SNe IcBL 2009bb and 2012ap were included in the same sample as the GRB-SNe, which was justified by [44] because both are subtypes of engine-driven SNe (Figure 7), and indeed they also follow the same luminosity–stretch (Figure 13) and luminosity–decline (Figure 14) relationship as GRB-SNe. Thus, one can use the independent distance measurements to their host galaxies (Tully-Fisher distances) and use them as probes of the local Hubble flow to provide a model-independent estimate of H_0. Reference [44] constrained a weighted-average value of $H_{0,w} = 82.5 \pm 8.1\,\mathrm{km\,s^{-1}\,Mpc^{-1}}$. This value is 1σ greater than that obtained using SNe Ia and 2σ larger than that determined by Planck. This difference can be attributed to large peculiar motions of the host galaxies of the two SNe IcBL, which are members of galaxy groups. Interestingly, when the same authors used a sample of SNe Ib, Ic, and IIb, they found an average value of H_0 that had a standard deviation of order $20–40\,\mathrm{km\,s^{-1}\,Mpc^{-1}}$, which demonstrates that these SNe are poor cosmological candles. In a separate analysis, [289] used their sample of GRB-SNe, which did not include non-GRB-SNe IcBL but instead covered a larger redshift range (up to $z = 0.6$), to derive the mass and energy budget of the universe, finding loosely constrained values of $\Omega_M = 0.58^{+0.22}_{-0.25}$ and $\Omega_\Lambda = 0.42^{+0.25}_{-0.22}$.

6.3. Physics of the Luminosity–Decline Relationship. A physical explanation for why GRB-SNe are standardizable candles is not immediately obvious. If the luminosity of GRB-SNe (excluding SN 2011kl) is powered by radioactive heating (see Section 4.2), then more nickel production leads to brighter SNe. So far however, no correlation has been found between the bolometric properties of GRB-SNe and the properties (E_{iso} and T_{90}) of the accompanying γ-ray emission [11, 32, 43]. To a first order, this is at odds with the simplest predictions of the collapsar model, which suggests that more energy input by a central engine should lead to increased nickel production and more relativistic ejecta. However, γ-ray energetics are a poor proxy of the total energy associated with the central engine, so the absence of a correlation is perhaps not surprising. Moreover, as pointed out by [11], one expects large variations in the masses and rotation rates of the pre-explosion progenitor stars, especially when metallicity effects are factored in. Different stellar rotation rates will result in different rotation rates imparted to their cores, leading to different amounts of material being accreted and ultimately

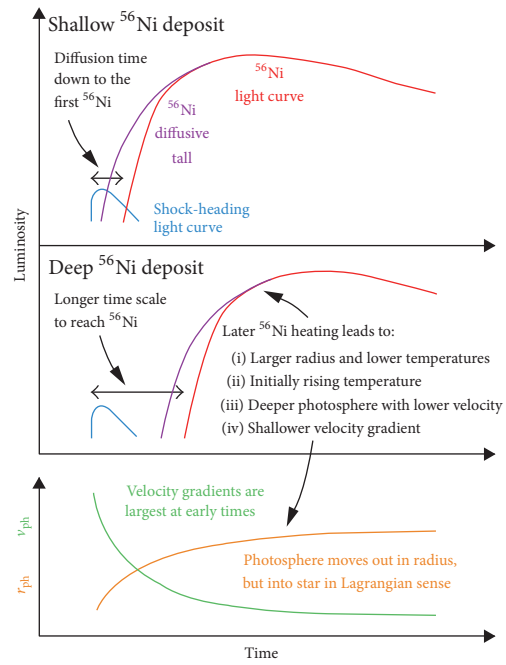

Figure 16: The effect of different degrees of nickel mixing in the ejecta of SNe Ibc on their observed LCs, from [290]. Top and middle panels: how the relative positions of the shock-heating contribution (blue curves), ^{56}Ni diffusive tail contribution (purple curves), and the ^{56}Ni contribution (red curves) to the observed LC can differ depending on the depth and amount of mixing of the ^{56}Ni. The total observed LC is the sum of these three components. When the ^{56}Ni is located deep in the ejecta (middle panel) and the shock-heating light curve (blue curve) is below the detection limits, there can be a significant dark phase between the time of explosion and the moment of first detection. Bottom: temporal evolution of the photospheric radius (orange curve) and velocity (green curve). Depending on the position of the ^{56}Ni LC, different photospheric radii, velocities, and velocity gradients will be present during the rising LC.

resulting in a variation of the final BH masses. Along with variations in the stellar density, all of these factors will result in a range of nickel masses being produced. Moreover, even if the same amount of nickel is produced in each event, SNe that expand at a slower rate will be fainter because their LCs will peak later after which more of the nickel has decayed and suffered adiabatic degradation. Additionally, the location of the nickel in the ejecta will also result in different looking LCs, where nickel that is located deeper in the ejecta takes longer to diffuse out of the optically thick ejecta, leading to later peak times (Figure 16). If the degree of mixing in the early SN is heterogeneous for GRB-SNe, a range of rise times is expected, along with a large variation in the velocity gradients and photospheric radii. However, inspection of Figure 6 shows that, if we naively take a single transition as a proxy of the photospheric velocity, the distribution of say Si II λ6355 shows that the velocity gradient of most GRB-SNe has a similar evolution, though the range of velocities of the Fe II λ5169 transition implies that they still have a wide range of velocities at a given epoch. This similar behaviour might suggest a similar degree of nickel mixing in the SN ejecta.

Nevertheless, it appears from independent studies using different approaches that GRB-SNe *are* standardizable candles. Whether this observation implies similarities in the physical properties of the central engine driving the explosion, or the SNe themselves, is uncertain. For the most part, it is expected that most GRB-SNe are viewed close to the jet axis [42], which also appears to apply to SN 2009bb [204], meaning we are observing SNe more or less with the same approximate geometry. The fact that GRB-SNe are standard*izable* and have a range of brightness implies that different amounts of nickel are being generated. A naive conclusion to be drawn is that the observed luminosity–decline relationships suggest that a correlation exists between the strength and energetics produced by the central engine and the resultant nucleosynthetic yields of ^{56}Ni. Moreover, the lack a luminosity–decline relationship for SNe Ibc [42, 44] implies that the explosion and nucleosynthesis mechanism(s) are not correlated.

In the context of SNe Ia, which are, of course, also standardizable candles, their LCs are also powered solely by the radioactive decay of nickel and cobalt, the amount of which determines the LC's peak brightness and width. The width also depends on the photon diffusion time, which in turn depends on the physical distribution of the nickel in the ejecta, as well as the mean opacity of the ejecta. In general, the opacity increases with increasing temperature and ionization [291], thus implying that more nickel present in the ejecta leads to larger diffusion times. This directly implies that fainter SNe Ia fade faster than brighter SNe Ia, thus satisfying the luminosity–decline relation [279]. This is not the only effect however, as the distribution of nickel in the ejecta also affects how the LC evolves, where nickel located further out has a faster bolometric LC decline. Additionally, following maximum *B*-band light, SNe Ia colours are increasingly affected by the development of Fe II and Co II lines that blanket/suppress the blue *B*-band light. Dimmer SNe are thus cooler, and the onset of Fe III $\rightarrow$ Fe II recombination occurs quicker than in brighter SNe Ia, resulting in a more rapid evolution to redder colours [292]. Therefore the faster *B*-band decline rate of dimmer SNe Ia reflects their faster ionization evolution and provides additional clues as to why fainter SNe Ia fade more rapidly. Thus, as the LCs of GRB-SNe are also powered by radioactive decay, the physics that govern SNe Ia also govern those of GRB-SNe and may go some way to explaining why GRB-SNe are also standardizable candles.

7. Host Environments

Direct observations of the SNe that accompany LGRBs, and their subtypes, provide a rich range of clues as to the physical properties of their preexplosion progenitor stars. LGRBs represent a rare endpoint of stellar evolution, and their production and subsequent properties are likely to be a consequence of environmental factors. As such, many in-depth investigations of their host environments, both their global/galaxy-wide properties and, where possible, host-resolved environmental conditions, have been performed. Indeed, the information gained from this myriad of investigations warrants their own reviews, and the gathered nuances of these studies are beyond the scope of this GRB-SN review. Instead, in this section we highlight what we regard as the most important developments in this branch of GRB phenomenology that have directly furthered our understanding of the GRB-SN connection. For further insight, we refer the reader to excellent reviews and seminal studies by, among others, [293–296], and references therein.

7.1. Global Properties. With the advent of X-ray localizations of GRB AGs came the ability to study the type of galaxies that LGRBs occur in. Over the years, evidence mounted that LGRBs appeared to prefer low-luminosity, low-mass, blue, star-forming galaxies that have higher specific star-formation rates (SFRs) than the typical field galaxy [293, 297–308]. Visual inspection of optical *HST* imaging of LGRB host galaxies [307, 309, 310] showed a high fraction of merging/interacting systems: 30% showed clear signs of interaction, and another 30% showed irregular and asymmetric structure, which may be the result of recent mergers. The position of a GRB within its host also provided additional clues: both [311], who examined the offsets of LGRBs from their host nuclei (see as well [312, 313]), and [309] demonstrated that, within their hosts, LGRBs were more likely to be localized in the brightest UV regions of the galaxy, which are associated with concentrated populations of young massive stars.

At the same time, several early studies were converging towards the idea that LGRBs favoured subsolar, low-metallicity (Z) host/environments [314–317]. As the progenitors of LGRBs are massive stars with short lifetimes (of order a few million years), they are not expected to travel far from their birth in H II regions, and the measured metallicity of the associated H II region at the site of an LGRB can be used as a proxy of the natal metallicity. Reference [305] found that the metallicities of half a dozen low-redshift ($z < 0.3$) LGRB hosts were lower than their equally luminous counterparts in the local star-forming galaxy population and proposed that LGRB formation was limited by a strong metallicity threshold. This was based on the observation that LGRB hosts were placed below the standard L-Z relation for star-forming galaxies, where galaxies with higher masses, and therefore luminosities, generally have higher metallicities [318–321]. A metallicity cut-off for LGRB formation was also proposed by [322]. Reference [323] demonstrated that nearby LGRB host galaxies had systematically lower metallicities than the host galaxies of nearby ($z < 0.14$) SNe IcBL. Reference [205] showed that most LGRB host galaxies fall below the general L-Z relation for star-forming galaxies and are statistically distinct to the host galaxies of SNe Ibc and the larger star-forming galaxy population. LGRB hosts followed their own mass-metallicity relation out to $z \sim 1$ that is offset from the general mass-metallicity relation for star-forming galaxies by an average of 0.4 ± 0.2 dex in metallicity. This marks LGRB hosts as distinct from the host galaxies of SNe Ibc and reinforced the idea that LGRB host galaxies are not representative of the general galaxy population [303, 324, 325].

For the better part of a decade, this general picture became the status-quo for the assumed host properties of LGRBs: blue, low-luminosity, low-mass, star-forming galaxies with low metal content. However, more recently this

previously quite uniform picture of GRB hosts became somewhat more diverse: several metal-rich GRB hosts were discovered [205, 326, 327], which revealed a population of red, high-mass, high-luminosity hosts that were mostly associated with dust-extinguished afterglows [328–331]. Next, the offset of GRB-selected galaxies towards lower metallicities in the mass-metallicity relation [205] could, for example, be partially explained with the dependence of the metallicity of star-forming galaxies on SFR [332, 333]. Moreover, it was shown that LGRBs do not exclusively form in low-metallicity environments [328, 331, 334, 335], where the results of [296] are an excellent example of this notion. Analysing the largest sample of LGRB-selected host spectra yet considered (up to $z = 3.5$), they found that a fraction of LGRBs occur in hosts that contain super-solar ($Z > Z_\odot$) metal content (<20% at $z = 1$). This shows that while some LGRBs can be found in high-Z galaxies, this fraction is significantly less than the fraction of star-forming regions in similar galaxies, indicating GRBs are actually quite scarce in high-metallicity hosts. They found a range of host metallicities of 12 + log(O/H) = 7.9 to 9.0, with a median of 8.5. Reference [296] therefore concluded that GRB host properties at lower redshift ($z < 1$-2) are driven by a given LGRB's preference to occur in lower-metallicity galaxies without fully avoiding metal-rich ones and that one or more mechanism(s) may operate to quench GRB formation at the very highest metallicities. This result supported similar conclusions from numerous other recent studies [205, 326, 331, 335–340] which show that LGRBs seem to prefer environments of lower metallicity, with possibly no strict cut-off in the upper limit of metal content (though see [341]).

Another revealing observation was made by [342] who showed that low-z SNe IcBL and $z < 1.2$ LGRBs (i.e., core-collapse explosions in which a significant fraction of the ejecta moves at velocities exceeding 20,000–30,000 km s^{-1}) preferentially occur in host galaxies of high stellar-mass and star-formation densities when compared with SDSS galaxies of similar mass ($z < 0.2$). Moreover, these hosts are compact for their stellar masses and SFRs compared with SDSS field galaxies. More importantly, [342] showed that the hosts of low-z SNe IcBL and $z < 1.2$ LGRBs have high gas velocity dispersions for their stellar masses. It was shown that core-collapse SNe (types Ibc and II) showed no such preferences. It appears that only SLSNe occur in more extreme environments than GRB-SNe and relativistic SNe IcBL: [343] showed that SLSNe occur in extreme emission-line galaxies, which are on average more extreme than those of LGRBs and that type I SLSNe may result from the very first stars exploding in a starburst, even earlier than LGRBs. Finally, [342] concluded that the preference for SNe IcBL and LGRBs for galaxies with high stellar-mass densities and star-formation densities may be just as important as their preference for low-metallicity environments.

The result of [342] is the latest in a long line of investigations that suggest that LGRBs are useful probes of high-z star formation. This result stems from a long-debated question of whether LGRBs may be good tracers of the universal star-formation rate over all of cosmic history [293, 296, 311, 331, 335, 344–348]. Reference [296] showed that there is an increase in the (median) SFR of their sample of LGRB host galaxies at increasing redshift, where they found 0.6 M$_\odot$ yr^{-1} at $z \approx 0.6$ to 15.0 M$_\odot$ yr^{-1} at $z \approx 2.0$. Moreover, these authors suggest that by $z \sim 3$ GRB hosts will probe a large fraction of the total star formation. In absence of further secondary environmental factors, GRB hosts would then provide an extensive picture of high-redshift star-forming galaxies. However, the connection between LGRBs and low-metallicity galaxies may hinder their utility as unbiased tracers of star formation [305, 317, 323, 349], though if LGRBs do occur in galaxies of all types, as suggested above, then they may be only mildly biased tracers of star formation [350].

7.2. Immediate Environments. Most LGRB host galaxies are too distant for astronomers to discern their spatially resolved properties. These limitations are important to consider when extrapolating LGRB progenitor properties from the global host properties, as it may be possible that the location of a given LGRB may differ to that of the host itself. Where spatially resolved studies have been performed, such as for GRB 980425 [351–354], GRB 060505 [355], GRB 100316D [356], and GRB 120422A [41, 357], it was found that, in at least two of these cases, the metallicity and SFR of other H II regions in their hosts had comparable properties as those associated with the LGRB location (within 3σ). In these studies the host galaxies had a minimal metallicity gradient [355], and there were multiple low-metallicity locations within the host galaxies, where in some cases the location of the LGRB was in that of the lowest metallicity [357]. These studies suggest that, in general, the host-wide metallicity measurement can be used as a first-order approximation of the LGRB site.

Next, the line ratios of [Ne III] to [O II] suggest that H II regions associated with LGRBs are especially hot [358], which may indicate a preference for the hosts of LGRBs to produce very massive stars. Absorption line spectroscopy has revealed some fine-structure lines (e.g., Fe [II]), which could indicate the presence of absorption occurring in fast-moving winds emanated by WR stars (i.e., stars that are highly stripped of their outer layers of hydrogen and helium). The distances implied by variable fine-structure transitions (e.g., their large equivalent widths imply large distances to avoid photoionization) show that the absorption occurs at distances of order tens to hundreds of parsecs from the GRB itself [359–362], which makes sense given that the dust and surrounding stellar material around a GRB is completely obliterated by the explosion. Such absorption must arise from nearby WR stars whose winds dissect the line of sight between the GRB and Earth.

The type of environment in which a given LGRB occurs is also of interest: is it a constant interstellar medium (ISM) or a wind-like medium? Do the progenitors of LGRB carve out large wind-blown bubbles [363, 364], as has been observed for galactic WR stars [365, 366]? Using a statistical approach to the modelling of GRB AGs, [367] demonstrated that the majority of GRBs (L- and SGRBs) in their sample (18/27) were compatible with a constant ISM, and only six showed evidence of a wind profile at late times. They concluded that, observationally, ISM profiles appear to dominate and that most GRB progenitors likely have relatively small wind termination-shock radii, where a variable mass-loss history, binarity of a dense ISM, and a weak wind can bring the

wind termination shock radius closer to the star [368, 369]. A smaller group of progenitors, however, seem to be characterized by significantly more extended wind regions [367]. In this study, the AG is assumed to be powered by the standard forward-shock model, which has been shown to not always be the best physical description for all LGRBs observed in nature [195].

Finally, it appears that LGRBs generally occur in environments that possess strong ionization fields, which likely arise from hot, luminous massive stars in the vicinity of LGRBs. Reference [296] showed that the GRB hosts in their sample occupied a different phase-space than SDSS galaxies in the Baldwin-Phillips-Terlevich (BPT) diagram [370]: they are predominantly above the ridge line that denotes the highest density of local star-forming field galaxies. A similar offset was also observed for galaxies hosting type I SLSNe [343]. This offset is often attributed to harder ionization fields, higher ionization parameters, or changes in the ISM properties [371–373]. This result is consistent with the hypothesis that the difference in the location in the BPT diagram between GRB hosts and $z \sim 0$ star-forming galaxies is caused by an increase in the ionization fraction; that is, for a given metallicity a larger percentage of the total oxygen abundance is present at higher ionization states at higher redshifts. This could be caused by a harder ionization field originating from hot O-type stars [373] that emit a large number of photons capable of ionizing oxygen into [O III].

7.3. Implications for Progenitor Stars. Before LGRBs were conclusively associated with the core-collapse of a massive star, their massive-star origins were indirectly inferred. If LGRBs were instead associated with the merger of binary compact objects, two "kicks" arising from two SN explosions would imply a long delay before coalescence and likely lead to GRBs occurring at large distances from star-forming regions [374–377]. With subarcsecond localization came observations that showed LGRBs, on average, were offset from the apparent galactic centre by roughly 1 kpc [311], which did not agree with a compact object binary-merger scenario. Further statistical studies showed a strong correlation between the location of LGRBs and the regions of bluest light in their host galaxies [309, 310], which implied an association with massive-star formation. Thus result was furthered by [378] that showed that LGRBs and type Ic SNe have similar locations in their host galaxies, providing additional indirect evidence of LGRBs and massive stars.

The general consensus that LGRBs occur, on average, in metal-poor galaxies (or location within more metal-rich hosts), aligned well with theoretical expectations that LGRB formation has a strong dependence on metallicity. In theoretical models [215, 379–383], the progenitors of LGRBs need to be able to lose their outer layers of hydrogen and helium (as these transitions are not observed spectroscopically), but do so in a manner that does not remove angular momentum from the core (to then power the GRB). At high metallicities, high-mass loss rates will decrease the surface rotation velocities of massive stars and, due to coupling between the outer envelopes and the core, will rob the latter of angular momentum and hence the required rapid rotation to produce a GRB. In quasi-chemically homogeneous models [382–384], rapid rotation creates a quasi-homogeneous internal structure, whereby the onion-like structure retained by non- or slowly rotating massive stars is effectively smeared out, and the recycling of material from the outer layers to the core results in the loss of hydrogen and helium in the star because it is fused in the core. Intriguingly, quasi-chemically homogeneous stars do appear to exist in nature. The FLAMES survey [385] observed over 100 O- and B-type stars in the Large Magellanic Cloud (LMC) and the Milky Way galaxy and showed the presence of a group of rapidly rotating stars that were enriched with nitrogen at their surfaces. The presence of nitrogen at the surface could only be due to rotationally triggered internal transport processes that brought nuclear processed material, in this case nitrogen, from the core to the stellar surface. Observations of metal-poor O-type stars in the LMC by [386, 387] show the signature of CNO cycle-processed material at their surfaces, while modelling of the spectra of galactic and extragalactic oxygen-sequence WR stars shows very low surface He mass fractions, thus making them plausible single-star progenitors of SNe Ic [388].

However, other observations of Local Group massive-star populations have revealed that the WR population actually decreases strongly at lower metallicities, particularly the carbon- and oxygen-rich subtypes [389], suggesting that these proposed progenitors may be extremely rare in LGRB host environments. Moreover, the results of [390], based on the analysis of two LGRBs, suggest that some LGRBs may be associated with progenitors that suffer a great degree of mass loss before exploding and hence a great deal of core angular momentum. Moreover, the association of some LGRBs with super-solar metallicity environments also contradicts the predictions of the collapsar model. However, other recent models have considered alternative evolutionary scenarios whereby LGRB progenitors can lose a great deal of mass before exploding, but still retain enough angular momentum to power a GRB [391–393]. Such models consider the complex connection between surface and core angular momentum loss and show that single stars arising from a wide range of metal content can actually produce a GRB. Moreover, the effects of anisotropic stellar winds need to also be considered [205]. Polar mass loss removes considerably less angular momentum than equatorial mass loss [394], which provides the means for the progenitor to lose mass but sustain a high rotation rate. Alternatively, episodic mass loss, as has been observed for luminous blue variable stars may also offer another means of providing a way to lose mass but retain core angular momentum.

8. Kilonovae Associated with SGRBs

To date, the amount of direct and indirect evidence for the massive-star origins of LGRBs is quite comprehensive and thoroughly beyond any conceivable doubt. The same however cannot be stated about the progenitors of SGRBs. For many years, since the discovery that there are two general classes of GRBs [399, 400], general expectations were that they arose from different physical scenarios, where SGRBs are thought to occur via the merger of a binary compact object system

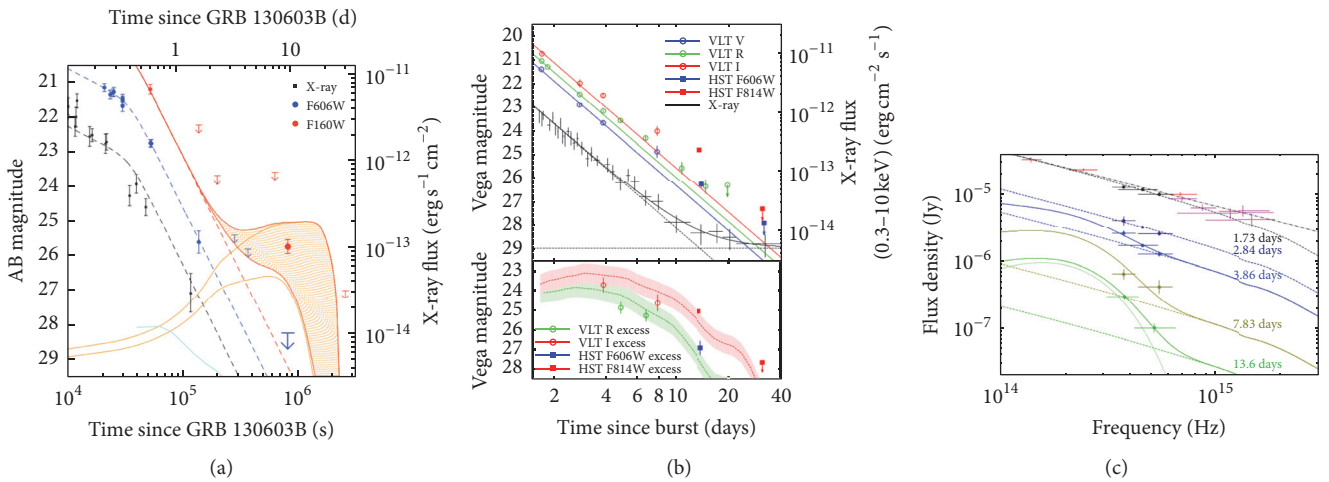

FIGURE 17: Observations of KNe associated with SGRBs: (a) GRB 130603B, from [395]. The decomposed optical and NIR LCs show an excess of flux in the NIR ($F160W$) filter, which is consistent with theoretical predictions of light coming from a KN. (b) GRB 060614, from [396]. Multiband LCs show an excess in the optical LCs (R and I), which once the AG light is removed, the resultant KN LCs match those from hydrodynamic simulations of a BH-NS merger (ejecta velocity of ~0.2c and an ejecta mass of 0.1 $M_\odot$ [397]). (c) SEDs of the multiband observations of GRB 060614, also from [396]. The early SEDs are well described by a power law spectrum, which implies synchrotron radiation. However, at later epochs the SEDs are better described by thermal, black body spectra, with peak temperatures of ~2700 K, which are in good agreement with theoretical expectations [398].

containing at least one neutron star (i.e., NS-NS or NS-BH). Circumstantial evidence for the compact object merger origins of SGRBs [401, 402] includes their locations in elliptical galaxies, the lack of associated supernovae (as observed for LGRBs) [403–406], the distribution of explosion-site offsets relative to their host galaxies (0.5–75 kpc away, median of 5 kpc [407, 408]), and a weak spatial correlation of SGRB locations with star-formation activity within their host galaxies.

The compact coalescence scenario predicts SGRB AGs at longer wavelengths [401, 402, 409–411], which have been observed [412]. As well as the expected AG emission, emission from a SN-like transient was also predicted [413–417], which have been referred to as a "kilonova" (KN), "mergernova," or "macronova" (see the recent review by [418]), where we have adopted the former terminology in this review.

The KN prediction is a natural consequence of the unavoidable decompression of NS material, where a compact binary coalescence provides excellent conditions for the rapid-neutron capture process (r-process [409, 419–422]). The neutron capture process occurs very quickly and is completed in less than a second, and it leaves behind a broad distribution of radioactive nuclei whose decay, once the ejected material becomes transparent, powers an electromagnetic transient in a process similar to that expected to cause GRB-SNe to shine. Hydrodynamic simulations suggest that, during a merger, mass is ejected via two mechanisms: (I) during the merger, surface layers may be tidally stripped and dynamically flung out in tidal tails; (II) following the merger, material that has accumulated into a centrifugally supported disk may be blown off in a neutrino or nuclear-driven wind. In mechanism (I), the amount of material ejected depends primarily on the mass ratio of the compact objects and the equation of state of the nuclear matter. The material is very neutron-rich ($Y_e \sim 0.1$), and the ejecta is expected to assemble into heavy ($Z > 50$) elements (including Lanthanides, $58 < Z < 70$, and Actinides, $90 < Z < 100$) via the r-process. In mechanism (II), however, neutrinos emitted by the accretion disk raise the electron fraction ($Y_e \sim 0.5$) to values where a Lanthanide-free outflow is created [423]. In both cases 10^{-4}–10^{-1} $M_\odot$ of ejecta is expected to be expelled. A direct observational consequence of mechanism (I) is a radioactively powered transient that resembles a SN, but which evolves over a rapid timescale (~1 week, due to less material ejected compared with a typical SN) and whose spectrum peaks at IR wavelengths. In contrast to other types of SNe, for example, SNe Ia whose optical opacity is dictated by the amount of iron-group elements present in the ejecta, r-process ejecta that is composed of Lanthanides has a much larger expansion opacity (≈100 times greater) due to the atoms/ions having a greater degree of complexity in the number of ways in which their electrons can be arranged in their valence shells (relative to iron-group elements).

There have been a handful of observational searches for KN emission: GRB 050709 [424, 425]; GRB 051221A [426]; GRB 060614 [396, 427]; GRB 070724A [428, 429]; GRB 080503 [430, 431]; GRB 080905A [432]; and GRB 130603B [395, 433]. In almost all cases null results were obtained, with the notable exceptions being GRB 130603B, GRB 060614 (see Figure 17), and GRB 050709. In these cases, the optical and NIR LCs required a careful decomposition, and once the AG components were accounted for, an excess of emission was detected. In the case of GRB 130603B, a single NIR datapoint was found to be in excess of the extrapolated AG decay, which was interpreted by [395] as arising from emission from a KN. The (observer-frame) colour term $R_{F606W} - H_{F160W} < 1.7$ mag at +0.6 d, and $R_{F606W} - H_{F160W} < 2.5$ mag at +9 days, which is inconsistent with a colour change due to FS emission and was

argued to be evidence of nonsynchrotron emission arising from a possible KN. The dataset of GRB 060614 considered by [396] is more extensive than that of GRB 130603B, and KN bumps were detected in two filters (observer-frame R and I), which peaked at 4–6 d (rest-frame). The decomposed KN LCs were shown to be consistent with LCs arising from hydrodynamic simulations of a BH-NS merger, which had an ejecta velocity of ~0.2c and an ejecta mass of 0.1 $M_\odot$ [233]. The larger dataset also allowed for the construction of SEDs, which showed a clear transition from a power law spectrum at early epochs (<3 d), which appeared to transition into a thermal, black body spectrum over the next two weeks. Moreover, the inferred temperature of the black body was around 2700 K, which fitted well with theoretical expectations. However, the precise nature of GRB 060614 is still not understood, and it is still uncertain if it is a short or a long GRB.

9. Theoretical Overview

While the focus of this review is geared towards what observations tell us about the GRB-SN connection, a keen understanding of the leading theoretical models is also required. The finer intricacies of each model are presented elsewhere, and we suggest the reader to start with the comprehensive review by [434] (and references therein), which is just one of many excellent reviews of the physics of the prompt emission and AGs. As such, what is presented here is meant only as an overview of the rich and complex field of GRB phenomenology.

9.1. Central-Engine Models: Millisecond Magnetars versus Collapsars. The main consensus of all GRB models is that LGRBs and their associated SNe arise via the collapse of massive stars, albeit ones endowed with physical properties that must arise only seldom in nature, given the fact GRB-SNe are very rare. In the leading theoretical paradigms, after the core-collapse of the progenitor stars, the leftover remnant is either a NS or a BH, and under the correct conditions, both can operate as a central engine to ultimately produce an LGRB.

In reality, very few solid facts are known about the true nature of the central-engine(s) operating to produce LGRBs. Nevertheless, one of the most prevailing models of the central engines of GRBs associated with SNe is the collapsar model [210, 215, 247], where the accretion of material from a centrifugally supported disk onto a BH leads to the launch a bipolar relativistic jet, and material within the jet leads to the production of γ-ray emission. The collapsar model suggests that there is enough kinetic energy ($2–5 \times 10^{52}$ erg) in the accretion disk wind which can be used to explosively disrupt the star, as well as synthesizing ~0.5 $M_\odot$ of ^{56}Ni. In this model, the duration of the prompt emission is directly related to the stellar envelope infall time, and the jet structure is maintained either magnetically or via neutrino-annihilation-driven jets along the rotation axes. The other promising mechanism that could lead to the production of an LGRB and its hypernovae is the millisecond magnetar model [221, 435–437]. In this scenario, the compact remnant is a rapidly rotating ($P \sim 1–10$ ms), highly magnetized ($B \sim 10^{14\text{-}15}$ G) NS, where the relativistic Poynting-flux jets are supported by stellar confinement [436].

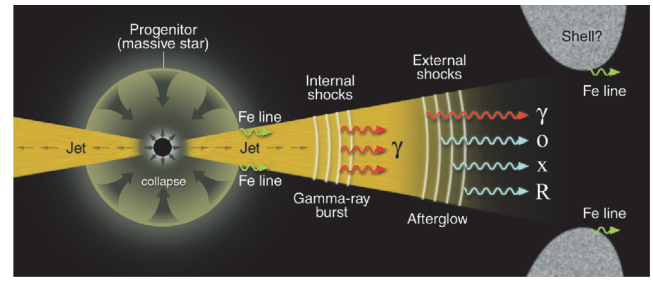

FIGURE 18: The death of a massive star produces a GRB (and its multiband AG) and an energetic and bright SN (from [439]).

A cartoon visualization of the formation of an LGRB, including its AG and associated SN, is shown in Figure 18. In the standard fireball model, shells of material within the jet interact to produce the initial burst of γ-rays, called the prompt emission, via internal shocks. As the jet propagates away from the explosion site, it eventually collides with the surrounding medium producing external shocks that power an AG that is visible across almost the entire electromagnetic spectrum, from X-rays to radio, and which lasts for several weeks to months. In this leptonic model, the prompt and AG radiation is synchrotron or synchrotron-self-Compton in origin [438]. It is interesting to note that this scenario is pretty much independent of the nature of the central engine; all that is required is the formation of an ultra-relativistic jet. It is generally thought that luminous GRBs with bulk Lorentz factors of order $\Gamma_B \sim 300$ must stem from ultra-relativistic collisionless jets produced by millisecond magnetars and/or collapsars. As discussed in Section 3, in order to penetrate the stellar envelope, the active timescale of the jet produced by the central engine ($t_{\rm engine}$) must be longer than the penetrating timescale, where the latter is $\sim R/v_{\rm jet}$. Some *ll*GRBs whose $\Gamma_B \sim 2$ can also be explained by this model, but in these cases, the active timescale is likely to be slightly smaller than the penetrating timescale so that the ultra-relativistic jet from the central engine either just barely or completely fails to completely penetrate the stellar envelope.

The first class of models for the prompt emission of GRBs was the internal-shock model, where synchrotron or synchrotron self-Compton radiation was emitted by electrons that were accelerated by internal shocks [438, 440] in the form of high-energy γ-ray photons. Inverse Compton (IC) scattering and synchrotron self-Compton (SSC) scattering can enhance the seed photons and account for the very high-energy γ-ray photons measured for some GRBs. One prediction of the internal-shock model is the production of high-energy neutrinos, which to date have not been observed by neutrino detectors such as IceCube (only upper limits have been obtained so far, see the review by [441]). Although more detailed calculations performed by [442, 443] have demonstrated that the internal-shock model which includes benchmark parameters (e.g., the bulk Lorentz factor $\Gamma_B = 300$) is consistent with the upper limits obtained by IceCube, these results have posed more stringent constraints on the internal

shocks model because there is a possible correlation between the bulk Lorentz factor Γ_B and the GRB luminosity [444–446]. Instead, alternative scenarios in the context of the ultra-relativistic jet model are the photospheric emission model [447–451] and the Internal-Collision-induced MAgnetic Reconnection and Turbulence (ICMART) model [452, 453]. Photospheric models assume that thermal energy stored in the jet is radiated as prompt emission at the Thomson photosphere [454–456], while ICMART models envisage that collisions between "mini-shells" in a Poynting-flux-dominated outflow distort the ordered magnetic field lines in a runaway manner, which accelerates particles that then radiate synchrotron γ-ray photons at radii of ~10^{15}-10^{16} cm [452, 453].

9.2. Shock Breakout Models. It has long been believed that when the diffusion timescale of photons at the shock-wave front is comparable to the dynamical timescale, a SBO can occur (see as well Section 3). The SBO of a CCSN can produce a brief and bright flash whose spectral energy distribution peaks in the near UV or X-ray regimes [57, 60, 62, 73, 83, 457–464]. When the SN progenitor is a red supergiant whose radius is larger than several hundred $R_\odot$, the SBO is nonrelativistic (Newtonian) [459–461] and the emission is dominated by optical and UV radiation, which is detectable with space telescopes [465–467]. When the explosion is energetic enough, and the progenitor is a WR star whose radius is of order a few solar radii, the SBO emission typically peaks at X-rays or soft γ-rays, with a duration of ~10–2000 s. This class of relativistic SBOs can naturally explain some LGRBs [60, 62, 463, 464]. Reference [62] demonstrated that *ll*GRB jets either fail or just barely pierce through the stellar envelope. This choked/stifled jet can also help accelerate the shock to a mildly relativistic velocities (~30,000–100,000 km s^{-1}). In the shock breakout model, the AG emission is produced when the stellar ejecta collides with the CSM, and [464] showed that the data of the afterglows of GRBs 980425, 031203, 060218, and 100316D are in good agreement with the predictions of this model.

10. Future Research

While considerable progress has been made in the field of GRB-SNe, there are still uncertainties related to several aspects of their true nature. Solidifying their role as standardizable candles and cosmological probes requires both more work and considerably more events. Indeed for GRB-SNe to be used as cosmological probes, independent distance measurements to their host galaxies need to be obtained. Sample studies of GRB-SNe are the ideal way to approach this question, and with the hopeful launch of *JWST* in the next few years, their use over larger redshift ranges than SNe Ia could make them appealing cosmological candles. Additional attention is also required to determine the physical configuration and properties of their preexplosion progenitor stars, to help address the question of whether they arise from single versus binary systems. Moreover, further ULGRB-SNe are needed to address the question of whether all are ultra-luminous compared with typical GRB-SNe, as seen for SN 2011kl, or whether this event is quite anomalous.

10.1. Role of Binarity. Throughout this review, discussions of their stellar progenitors were primarily focused on single-star candidates. However the role of binarity may prove to be one of the most important ingredients to eventually producing a GRB. Theoretically, there are strong motivations for considering a binary evolution. To date, the best theoretical stellar models find it hard to produce enough angular momentum in the core at the time of collapse to make a centrifugally supported disk, though some progress has been made [382, 383, 468]. Instead, it is possible to impart angular momentum into the core of a star through the inspiral of a companion star during a common envelope phase (CEP) [469]: that is, converting orbital angular momentum into core angular momentum. The general idea is to consider a binary system comprised of, among others, a red supergiant and a NS [217], a NS with the He core of a massive star [470], or the merger of two helium stars [471]. During the inspiral of the compact object into the secondary/companion, angular momentum is imparted to the core, which is spun up via disc accretion. During this process, the core of the secondary will increase in mass as well as gain additional angular momentum, while the inspiralling NS will also accrete gas via the Bondi-Hoyle mechanism, which can lead to the NS reaching periods of order milliseconds before it eventually merges with the secondary's core. If a merger of the NS with the core occurs, a collapsar can be created, where a GRB can be produced depending on the initial mass of the secondary, the spin of the newly formed BH, and the amount of angular momentum imparted to the BH.

For the binary model to be a viable route for LGRB formation, one or more mechanism is required to expel the outer envelopes out into space prior to explosion. Generally there are different ways for this to be achieved, either through noncontact methods such as stellar winds, through semi-contact processes such as Roche lobe overflow, or through contact mechanisms that operate during a CEP. The spin-rates of a small sample of O-type star and WR binaries indicate that Roche lobe overflow mass transfer from the WR progenitor companion may play a critical role in the evolution of WR–O-star binaries, where equatorial rotational velocities of 140–500 km s^{-1} have been measured [472]. In the CE scenario, during the inspiral, the orbital separation decreases via drag forces inside the envelope which also results in a loss of kinetic energy. Some of this energy is lost to the surrounding envelope, which heats up and expands. Over a long-enough period the entire envelope can be lost into space. Another mechanism to expel the CE arises via nuclear energy rather than orbital energy [473]. For example, during the slow merger of a massive primary that has completed helium-core burning with a 1–3 $M_\odot$ secondary, H-rich material from the secondary is injected into the He-burning shell of the primary. This leads to nuclear runaway and the explosive ejection of the H and He envelopes and produces a binary comprised of a CO star and the low-mass companion. Should a further merger occur, this could lead to the formation of a GRB. If GRB-SNe arise via this formation channel, then this scenario can naturally explain why GRB-SNe are all of type Ic.

A generalization of the binary-merger model is that the more massive the stars are, the more accretion will occur.

This in turn leads to more convection in the core, which results in larger magnetic fields being generated and hence more magnetic collimation for any jets that are produced. In the case of GRB-SNe versus SNe Ibc, if jets are ubiquitous, then the difference between them may be the mass of the merging stars, where lower masses imply lower magnetic fields and hence less collimation. Moreover, the mass ratio of the secondary to the primary is also important, where higher mass ratios will result in more asymmetric explosions [469].

There is a growing list of observations that show that most massive stars exist in binaries, including [474] who estimated that over 70% of all massive stars will exchange mass with a companion star, which in a third of all cases will lead to a merger of the binary system. Moreover, closely orbiting binaries are more common at lower metallicities [475], where the progenitors of GRBs are normally found (though see [476] who showed that the close binary frequency of WRs is not metallicity dependent). Additional support for the notion that the progenitors of SNe Ibc are massive stars in binary systems has come from [477] who argued that, for a standard initial-mass function, the observed abundances of the different types of CCSNe are not consistent with expectations of single-star evolution. Progenitor nondetection of 10 SNe Ibc strongly indicates that single massive WR stars cannot be their solitary progenitor channel [478]. Reference [479] derived a 15% probability that all SNe Ibc arise from single-star WR progenitors. The large gas velocity dispersions measured for the host galaxies of GRBs by [342] may imply the efficient formation of tight massive binary progenitor systems in dense star-forming regions. Rotationally supported galaxies that are more compact and have dense mass configurations are expected to have higher velocity dispersions. Observations of extra galactic star clusters show evidence that bound-cluster formation efficiency increases with star-formation density [480, 481]. Binaries may form more frequently in bound clusters, and they evolve to become more tightly bound through dynamical interactions with other members of the cluster. Alternatively, if the progenitors of GRBs are actually single stars, but which are more massive than those that produce SNe Ibc and II, a top-heavy initial-mass function (IMF) in dense, highly star-forming regions can also explain their observations. A similar conclusion was made by [343], who suggested that if the progenitors of SLSNe are single stars, the extreme emission-line galaxies in which they occur may indicate a bottom-light IMF in these systems. However, observations of low-mass stars in elliptical galaxies that are thought to have undergone high star-formation densities in their star-forming epochs instead suggest that the IMF is bottom heavy [482, 483].

A major hurdle therefore is finding ways to provide observational evidence to distinguish between single and binary progenitors. One such indication may be idea that the progenitors of GRB-SNe are "runaway" stars: that is, massive stars ejected from compact massive-star clusters [484, 485]. This notation was prompted by the observation that the very nearest GRB-SNe, which can be spatially resolved in their host galaxies, are offset from the nearest sites of star formation by 400–800 pc. If GRB-SNe do arise from runaway stars, the lack of obvious wind-features in AG modelling (Section 7.2) can naturally be explained: simulations [486] suggest that a high density of OB stars is required to produce the r^{-2} wind profile, in the region of 10^4-10^5 OB stars within a few tens of parsecs. This is a much larger density than has been observed in nature, where the densest known cluster is R136 (e.g., [487, 488]) which contains many of the most massive and luminous stars known, including R136a1 ($M \sim 315\,M_\odot$, $L \sim 8.7 \times 10^6\,L_\odot$). Within the central five parsecs of R136 there are 32 of the hottest known type O stars (spectral type O2.0–3.5), 40 other O stars, and 12 Wolf-Rayet stars, mostly of the extremely luminous WNh type (which are still burning hydrogen in their cores and have nitrogen at their surfaces).

For non-GRB related SNe, such as the very nearby peculiar type II SN 1987A (in the LMC, $D \sim 50$ kpc), constraining the nature of its progenitor was made possible due to a combination of a spatially resolved SN remnant and an enormously rich photometric and spectroscopic dataset compiled over a time-span of nearly three decades. These observations have shown that the most likely progenitor of SN 1987A was the merger of a binary system [240, 489], which can explain the triple-ringed structure seen in *HST* images [490], as well as explain the He-enriched outer layers of the blue supergiant progenitor [491]. It was also shown that type IIb SN 1993J (~3.5 Mpc) likely originated from a binary system via analysis of its early LC [492], hydrodynamical modelling [493], and by detection of the preexplosion progenitor star in spatially resolved *HST* images [494] and a possible companion [495]. The direct imaging revealed the progenitor was a red supergiant, where excess of UV and *B*-band flux implied the presence of a hot stellar companion, or it was embedded in an unresolved young stellar cluster. These studies are possible because of the close proximity of the SNe to our vantage point as observers on Earth. However, the nearest GRB to date is GRB 980425, which, at ~40 Mpc, means the progenitor is too distant to be direct imaged. For any progress to be made concerning single versus binary progenitors, nearby events are required that will allow either for exceptionally detailed observations to be obtained and modelled or even the remote chance of directly detecting the progenitor. For lack of better ideas, what we then require is a healthy dose of patience.

10.2. From GRB-SNe to ULGRB-SNe to SLSNe. As discussed previously, the most luminous GRB-SNe to date is SN 2011kl, which had a peak absolute magnitude of ≈−20 mag [496]. This is roughly 0.5–1.0 mag brighter than most GRB-SNe, but still one magnitude fainter than those associated with SLSNe, which peaked at ≈−21 mag [104]. Moreover, it appears that SN 2011kl is not the only object that falls in this gap between ordinary SNe and SLSNe: four objects discovered by PTF and the SNLS have similar peak absolute magnitudes and LC evolution as SN 2011kl [497]. No accompanying γ-ray emission was detected for any of these events, which begs the question of whether they are off-axis ULGRB-SNe or represent yet another type of explosion transient.

In contrast to the cases of GRB-SNe whose optical light curves appear to be mainly powered by heating arising from ^{56}Ni decay, it seems that most SLSNe cannot be explained

by the simple radioactive heat deposition model. Instead the luminosity of SLSNe appears to be either driven by energy input from a magnetar [226, 227] or powered by the interaction between SN ejecta and the CSM, which is the likely mechanism for SNe IIn. Indeed, one could argue that the magnetar model is the most promising model to explain the luminosity of SLSNe-Ic. For the most luminous SNe Ic, such as SN 2010ay [498] and SN 2011kl, if the former event arose from radioactive heating, the ratio of the inferred nickel mass to the total ejecta mass was too large, implying that the radioactive heat deposition model was not a viable model. Instead it is possible that events such as this could be powered by both nickel decay and a magnetar [499]. Then, for true SLSNe-Ic, nickel heating can be ignored, and conversely for SNe Ic, including GRB-SNe, magnetar input is negligible. It is only for SNe Ic (all types) with peak absolute magnitudes that exceed ≈ -20 mag that both energy sources must be considered. Clearly more observations of luminous SNe Ic are needed to test this hypothesis.

One final point of interest is determining whether all ULGRB-SNe are superluminous compared with GRB-SNe or whether GRB 111209A/SN 2011kl is a one-off event. As stated previously, the number of GRB-SNe is very small, and only two are considered here: the aforementioned case and ULGRB 101225A. Modelling of the (observer-frame) i-band LC of the accompanying SN in the latter event showed that its brightness was not exceptional: we found $k = 0.96 \pm 0.05$ and $s = 1.02 \pm 0.03$ (Table 3), which implies that some ULGRB-SNe have luminosities that are similar to those of other GRB-SNe. Moreover, the definition of an ULGRB is important: here we have defined an ULGRB as an event that is still detected after several thousand seconds by a gamma-ray instrument. This definition is inherently detector- and redshift-dependent. Based on this definition alone, it appears that GRB 091127 is also an ULGRB; an inspection of the third version of the *Swift*/BAT catalog [500] reveals that this event was detected by BAT at more than 5000 s. In turn, accompanying SN 2009nz is also quite typical of the general GRB-SN population, with $k = 0.89 \pm 0.01$ and $s = 0.88 \pm 0.01$. However, our definition is of course limited and does not include additional facts of this situation: First, the BAT detection at the late times is very marginal, with a signal-to-noise ratio of just 4.36 (where a value of 7.0 is required in a typical image-trigger threshold). Secondly, the BAT event data value of T_{90} is only 7.42 s, whereas the BAT value in [500] is obtained in survey mode. Thus an alternative interpretation of the extended GRB emission seen in the survey data is that it is soft gamma-rays emitted by the very bright X-ray afterglow and not from the prompt emission. In summary, more unambiguous ULGRB events at redshifts lower than unity are needed in order to measure the properties of their accompanying SN and address the peculiar nature of GRB 111209A/SN 2011kl.

Competing Interests

The authors declare that there is no conflict of interests regarding the publication of this manuscript. This applies both to the scientific content of this work and to their funding.

Acknowledgments

Zach Cano thanks David Alexander "Dr Data" Kann, Steve Schulze, Maryam Modjaz, Jens Hjorth, Jochen Greiner, Elena Pian, Vicki Toy, and Antonio de Ugarte Postigo for sharing their photometric and spectroscopic data and stimulating discussions, which without a doubt led to a much improved manuscript. Some data was extracted using the Dexter applet [501], while others were downloaded from the WiseREP archive [502]. The work of Zach Cano was partially funded by a Project Grant from the Icelandic Research Fund. Shan-Qin Wang, Zi-Gao Dai, and Xue-Feng Wu are supported by the National Basic Research Program (973 Program) of China (Grant nos. 2014CB845800 and 2013CB834900) and the National Natural Science Foundation of China (Grant nos. 11573014 and 11322328). Xue-Feng Wu is partially supported by the Youth Innovation Promotion Association (2011231) and the Strategic Priority Research Program "Multi-Waveband Gravitational Wave Universe" (Grant no. XDB23000000) of the Chinese Academy of Sciences.

References

[1] T. J. Galama, P. M. Vreeswijk, J. van Paradijs et al., "An unusual supernova in the error box of the γ-ray burst of 25 April 1998," *Nature*, vol. 395, no. 6703, pp. 670–672, 1998.

[2] F. Patat, E. Cappellaro, J. Danziger et al., "The metamorphosis of SN 1998bw," *Astrophysical Journal*, vol. 555, no. 2, pp. 900–917, 2001.

[3] K. Iwamoto, P. A. Mazzali, K. Nomoto et al., "A hypernova model for the supernova associated with the γ-ray burst of 25 April 1998," *Nature*, vol. 395, no. 6703, pp. 672–674, 1998.

[4] J. Hjorth, J. Sollerman, P. Møller et al., "A very energetic supernova associated with the γ-ray burst of 29 March 2003," *Nature*, vol. 423, no. 6942, pp. 847–850, 2003.

[5] K. Z. Stanek, T. Matheson, P. M. Garnavich et al., "Spectroscopic discovery of the supernova 2003dh associated with GRB 030329," *The Astrophysical Journal*, vol. 591, no. 1, pp. L17–L20, 2003.

[6] T. Matheson, P. M. Garnavich, K. Z. Stanek et al., "Photometry and spectroscopy of GRB 030329 and its associated supernova 2003dh: the first two months," *The Astrophysical Journal*, vol. 599, no. 1, pp. 394–407, 2003.

[7] J. Deng, N. Tominaga, P. A. Mazzali, K. Maeda, and K. Nomoto, "On the light curve and spectrum of SN 2003dh separated from the optical afterglow of GRB 030329," *Astrophysical Journal*, vol. 624, no. 2, pp. 898–905, 2005.

[8] N. Gehrels, G. Chincarini, P. Giommi et al., "The swift gamma-ray burst mission," *The Astrophysical Journal*, vol. 611, no. 2, pp. 1005–1020, 2004.

[9] A. Clocchiatti, N. B. Suntzeff, R. Covarrubias, and P. Candia, "The ultimate light curve of SN 1998bw/GRB 980425," *Astronomical Journal*, vol. 141, no. 5, article 163, 2011.

[10] Z. Cano, D. Bersier, C. Guidorzi et al., "A tale of two GRB-SNe at a common redshift of $z = 0.54$," *Monthly Notices of the Royal Astronomical Society*, vol. 413, no. 1, pp. 669–685, 2011.

[11] S. E. Woosley and J. S. Bloom, "The supernova-gamma-ray burst connection," *Annual Review of Astronomy and Astrophysics*, vol. 44, pp. 507–556, 2006.

[12] L. Wang and J. C. Wheeler, "The supernova-gamma-ray burst connection," *Astrophysical Journal*, vol. 504, no. 2, pp. L87–L90, 1998.

[13] K. Nomoto, N. Tominaga, M. Tanaka et al., "Diversity of the supernova—gamma-ray burst connection," *Nuovo Cimento B Serie*, vol. 121, pp. 1207–1222, 2006.

[14] E. Bissaldi, F. Calura, F. Matteucci, F. Longo, and G. Barbiellini, "The connection between gamma-ray bursts and supernovae Ib/c," *Astronomy & Astrophysics*, vol. 471, no. 2, pp. 585–597, 2007.

[15] M. D. Valle, "Supernovae and gamma-ray bursts: a decade of observations," *International Journal of Modern Physics D*, vol. 20, no. 10, pp. 1745–1754, 2011.

[16] M. Modjaz, "Stellar forensics with the supernova-GRB connection—ludwig Biermann Award Lecture 2010," *Astronomische Nachrichten*, vol. 332, no. 5, pp. 434–447, 2011.

[17] J. Hjorth and J. S. Bloom, "The gamma-ray burst—supernova connection," in *Gamma-Ray Bursts*, pp. 169–190, Cambridge University Press, Cambridge, UK, 2012.

[18] Z. Cano, "A new method for estimating the bolometric properties of Ibc supernovae," *Monthly Notices of the Royal Astronomical Society*, vol. 434, no. 2, pp. 1098–1116, 2013.

[19] J. Hjorth, "The supernova-gamma-ray burst-jet connection," *Philosophical Transactions of the Royal Society A: Mathematical, Physical and Engineering Sciences*, vol. 371, no. 1992, Article ID 20120275, 2013.

[20] P. A. R. Ade, N. Aghanim, C. Armitage-Caplan et al., "Planck 2013 results. XVI. Cosmological parameters," *A & A*, vol. 571, article A16, 2013.

[21] D. J. Schlegel, D. P. Finkbeiner, and M. Davis, "Maps of dust infrared emission for use in estimation of reddening and cosmic microwave background radiation foregrounds," *The Astrophysical Journal Letters*, vol. 500, no. 2, pp. 525–553, 1998.

[22] E. F. Schlafly and D. P. Finkbeiner, "Measuring reddening with Sloan Digital Sky Survey stellar spectra and recalibrating SFD," *Astrophysical Journal*, vol. 737, no. 2, article no. 103, 2011.

[23] D. A. Kann, S. Klose, B. Zhang et al., "The afterglows of Swift-era gamma-ray bursts. I. Comparing pre-Swift and Swift-era long/soft (type II) GRB optical afterglows," *Astrophysical Journal*, vol. 720, no. 2, pp. 1513–1558, 2010.

[24] D. A. Kann, S. Klose, and A. Zeh, "Signatures of extragalactic dust in PRE-swift GRB afterglows," *The Astrophysical Journal*, vol. 641, no. 2, pp. 993–1009, 2006.

[25] D. A. Kann, S. Klose, B. Zhang et al., "The afterglows of swift-era gamma-ray bursts. II. Type I GRB versus type II GRB optical afterglows," *The Astrophysical Journal*, vol. 734, no. 2, article 96, 2011.

[26] J. Japelj, S. Covino, A. Gomboc et al., "Spectrophotometric analysis of gamma-ray burst afterglow extinction curves with X-Shooter," *Astronomy and Astrophysics*, vol. 579, article no. A74, 2015.

[27] C. Alard and R. H. Lupton, "A method for optimal image subtraction," *Astrophysical Journal*, vol. 503, no. 1, pp. 325–331, 1998.

[28] C. Alard, "Image subtraction using a space-varying kernel," *Astronomy and Astrophysics Supplement Series*, vol. 144, no. 2, pp. 363–370, 2000.

[29] L.-G. Strolger, A. G. Riess, T. Dahlen et al., "The *hubble* higher z supernova search: supernovae to $z \approx 1.6$ and constraints on type Ia progenitor models," *The Astrophysical Journal*, vol. 613, no. 1, pp. 200–223, 2004.

[30] Z. Cano, D. Bersier, C. Guidorzi et al., "XRF 100316D/SN 2010bh and the nature of gamma-ray burst supernovae," *Astrophysical Journal*, vol. 740, no. 1, article no. 41, 2011.

[31] Z. Cano, A. De Ugarte Postigo, A. Pozanenko et al., "A trio of gamma-ray burst supernovae: GRB 120729A, GRB 130215A/SN 2013ez, and GRB 130831A/SN 2013fu," *Astronomy and Astrophysics*, vol. 568, article no. A19, 2014.

[32] Z. Cano, A. de Ugarte Postigo, D. Perley et al., "GRB 140606B/iPTF14bfu: detection of shock-breakout emission from a cosmological γ-ray burst?" *Monthly Notices of the Royal Astronomical Society*, vol. 452, no. 2, pp. 1535–1552, 2015.

[33] P. Ferrero, D. A. Kann, A. Zeh et al., "The GRB 060218/SN 2006aj event in the context of other gamma-ray burst supernovae," *Astronomy & Astrophysics*, vol. 457, no. 3, pp. 857–864, 2006.

[34] C. C. Thöne, A. De Ugarte Postigo, C. L. Fryer et al., "The unusual γ-ray burst GRB 101225A from a helium star/neutron star merger at redshift 0.33," *Nature*, vol. 480, no. 7375, pp. 72–74, 2011.

[35] J. Sollerman, J. P. U. Fynbo, J. Gorosabel et al., "The nature of the X-ray flash of August 24 2005. Photometric evidence for an on-axis z = 0.83 burst with continuous energy injection and an associated supernova?" *Astronomy and Astrophysics*, vol. 466, no. 3, pp. 839–846, 2007.

[36] J. Greiner, P. A. Mazzali, D. A. Kann et al., "A very luminous magnetar-powered supernova associated with an ultra-long γ-ray burst," *Nature*, vol. 523, no. 7559, pp. 189–192, 2015.

[37] K. Beuermann, F. V. Hessman, K. Reinsch et al., "VLT observations of GRB 990510 and its environment," *Astronomy and Astrophysics*, vol. 352, no. 1, pp. L26–L30, 1999.

[38] A. Zeh, S. Klose, and D. H. Hartmann, "A systematic analysis of supernova light in gamma-ray burst afterglows," *Astrophysical Journal*, vol. 609, no. 2, pp. 952–961, 2004.

[39] K. Z. Stanek, P. M. Garnavich, P. A. Nutzman et al., "Deep photometry of grb 041006 afterglow: hypernova bump at redshift $z = 0.716$," *Astrophysical Journal*, vol. 626, no. 1, pp. L5–L9, 2005.

[40] D. Xu, A. De Ugarte Postigo, G. Leloudas et al., "Discovery of the broad-lined type IC SN 2013CQ associated with the very energetic GRB 130427A," *Astrophysical Journal*, vol. 776, no. 2, article no. 98, 2013.

[41] S. Schulze, D. Malesani, A. Cucchiara et al., "GRB 120422A/SN 2012bz: bridging the gap between low- and high-luminosity gamma-ray bursts," *Astronomy & Astrophysics*, vol. 566, article A102, 2014.

[42] Z. Cano, "Gamma-ray burst supernovae as standardizable candles," *Astrophysical Journal*, vol. 794, no. 2, article no. 121, 2014.

[43] V. L. Toy, S. B. Cenko, J. M. Silverman et al., "Optical and near-infrared observations of SN 2013dx associated with GRB 130702A," *Astrophysical Journal*, vol. 818, article 79, 2016.

[44] Z. Cano, P. Jakobsson, and O. Pall Geirsson, "Hubble diagrams of relativistic broad-lined type Ic supernovae," https://arxiv.org/abs/1409.3570.

[45] G. Bazin, V. Ruhlmann-Kleider, N. Palanque-Delabrouille et al., "Photometric selection of type Ia supernovae in the supernova legacy survey," *Astronomy and Astrophysics*, vol. 534, article A43, 2011.

[46] M. Modjaz, Y. Q. Liu, F. B. Bianco, and O. Graur, "The Spectral SN-GRB connection: systematic spectral comparisons between Type Ic Supernovae, and broad-lined Type Ic supernovae with

and without gamma-ray bursts," *The Astrophysical Journal*, vol. 832, no. 2, p. 108, 2015.

[47] P. A. Mazzali, K. Nomoto, F. Patat, and K. Maeda, "The nebular spectra of the hypernova SN 1998bw and evidence for asymmetry," *The Astrophysical Journal*, vol. 559, no. 2, pp. 1047–1053, 2001.

[48] K. Maeda, K. Kawabata, M. Tanaka et al., "SN 2006aj associated with XRF 060218 at late phases: nucleosynthesis signature of a neutron star-driven explosion," *Astrophysical Journal*, vol. 658, no. 1, pp. L5–L8, 2007.

[49] F. Bufano, E. Pian, J. Sollerman et al., "The highly energetic expansion of SN 2010bh associated with GRB 100316D," *The Astrophysical Journal*, vol. 753, no. 1, article 67, 2012.

[50] S. Mukherjee, E. D. Feigelson, G. Jogesh Babu, F. Murtagh, C. Fralev, and A. Raftery, "Three types of gamma-ray bursts," *Astrophysical Journal*, vol. 508, no. 1, pp. 314–327, 1998.

[51] I. Horvath, L. G. Balazs, Z. Bagoly, and P. Veres, "Classification of Swift's gamma-ray bursts," *Astronomy and Astrophysics*, vol. 489, no. 1, pp. L1–L4, 2008.

[52] A. de Ugarte Postigo, I. Horváth, P. Veres et al., "Searching for differences in Swift's intermediate GRBs," *Astronomy & Astrophysics*, vol. 525, article no. A109, 2011.

[53] A. J. Levan, N. R. Tanvir, R. L. C. Starling et al., "A new population of ultra-long duration gamma-ray bursts," *The Astrophysical Journal*, vol. 781, artile 13, 2014.

[54] A. J. Levan, "Swift discoveries of new populations of extremely long duration high energy transient," *Journal of High Energy Astrophysics*, vol. 7, pp. 44–55, 2015.

[55] J. Heise, "X-ray flashes and X-ray counterparts of gamm-ray bursts," in *Proceedings of the Gamma-Ray Burst and Afterglow Astronomy 2001: A Workshop Celebrating the First Year of the HETE Mission*, G. R. Ricker and R. K. Vanderspek, Eds., vol. 662 of *American Institute of Physics Conference Series*, pp. 229–236, April 2003.

[56] S. R. Kulkarni, D. A. Frail, M. H. Wieringa et al., "Radio emission from the unusual supernova 1998bw and its association with the γ-ray burst of 25 April 1998," *Nature*, vol. 395, no. 6703, pp. 663–669, 1998.

[57] J. C. Tan, C. D. Matzner, and C. F. McKee, "Trans-relativistic blast waves in supernovae as gamma-ray burst progenitors," *Astrophysical Journal*, vol. 551, no. 2, pp. 946–972, 2001.

[58] S. Campana, V. Mangano, A. J. Blustin et al., "The association of GRB 060218 with a supernova and the evolution of the shock wave," *Nature*, vol. 442, no. 7106, pp. 1008–1010, 2006.

[59] E. Waxman, P. Mészáros, and S. Campana, "GRB 060218: a relativistic supernova shock breakout," *Astrophysical Journal*, vol. 667, no. 1, pp. 351–357, 2007.

[60] E. Nakar and R. Sari, "Relativistic shock breakouts—a variety of gamma-ray flares: from low-luminosity gamma-ray bursts to type Ia supernovae," *Astrophysical Journal*, vol. 747, no. 2, article 88, 2012.

[61] Y. Kaneko, E. Ramirez-Ruiz, J. Granot et al., "Prompt and afterglow emission properties of gamma-ray bursts with spectroscopically identified supernovae," *The Astrophysical Journal*, vol. 654, no. 1 I, pp. 385–402, 2007.

[62] O. Bromberg, E. Nakar, and T. Piran, "Are low-luminosity gamma-ray bursts generated by relativistic jets?" *The Astrophysical Journal Letters*, vol. 739, no. 2, article L55, 2011.

[63] G. Ghisellini, G. Ghirlanda, and F. Tavecchio, "Did we observe the supernova shock breakout in GRB 060218?" *Monthly Notices of the Royal Astronomical Society: Letters*, vol. 382, no. 1, pp. L77–L81, 2007.

[64] C. M. Irwin and R. A. Chevalier, "Jet or shock breakout? The low-luminosity GRB 060218," *Monthly Notices of the Royal Astronomical Society*, vol. 460, no. 2, pp. 1680–1704, 2016.

[65] R. L. C. Starling, K. Wiersema, A. J. Levan et al., "Discovery of the nearby long, soft GRB 100316D with an associated supernova," *Monthly Notices of the Royal Astronomical Society*, vol. 411, no. 4, pp. 2792–2803, 2011.

[66] K. L. Page, R. L. C. Starling, G. Fitzpatrick et al., "GRB 090618: detection of thermal X-ray emission from a bright gamma-ray burst," *Monthly Notices of the Royal Astronomical Society*, vol. 416, no. 3, pp. 2078–2089, 2011.

[67] M. Sparre and R. L. C. Starling, "A search for thermal X-ray signatures in gamma-ray bursts—II. The swift sample," *Monthly Notices of the Royal Astronomical Society*, vol. 427, no. 4, pp. 2965–2974, 2012.

[68] R. L. C. Starling, K. L. Page, A. Pe'er, A. P. Beardmore, and J. P. Osborne, "A search for thermal X-ray signatures in gamma-ray bursts—I. Swift bursts with optical supernovae," *Monthly Notices of the Royal Astronomical Society*, vol. 427, no. 4, pp. 2950–2964, 2012.

[69] A. Pe'er, P. Mészáros, and M. J. Rees, "Radiation from an expanding cocoon as an explanation of the steep decay observed in GRB early afterglow light curves," *Astrophysical Journal*, vol. 652, no. 1 I, pp. 482–489, 2006.

[70] M. Friis and D. Watson, "Thermal emission in the early X-ray afterglows of gamma-ray bursts: following the prompt phase to late times," *The Astrophysical Journal*, vol. 771, no. 1, article 15, 2013.

[71] L.-X. Li, "Shock breakout in Type Ibc supernovae and application to GRB 060218/SN 2006aj," *Monthly Notices of the Royal Astronomical Society*, vol. 375, no. 1, pp. 240–256, 2007.

[72] T. A. Weaver, "The structure of supernova shock waves," *The Astrophysical Journal Supplement Series*, vol. 32, pp. 233–282, 1976.

[73] B. Katz, R. Budnik, and E. Waxman, "Fast radiation mediated shocks and supernova shock breakouts," *Astrophysical Journal*, vol. 716, no. 1, pp. 781–791, 2010.

[74] Y. Ohtani, A. Suzuki, and T. Shigeyama, "Generation of high-energy photons at ultra-relativistic shock breakout in supernovae," *The Astrophysical Journal*, vol. 777, no. 2, article 113, 2013.

[75] L. P. Singer, M. M. Kasliwal, S. B. Cenko et al., "The needle in the 100 $\deg^2$ haystack: uncovering afterglows of *Fermi* GRBs with the palomar transient factory," *The Astrophysical Journal*, vol. 806, no. 1, article 52, 2015.

[76] R. Margutti, C. Guidorzi, D. Lazzati et al., "Dust in the wind: the role of recent mass loss in long gamma-ray bursts," *Astrophysical Journal*, vol. 805, no. 2, article 159, 2015.

[77] E. Nakar, "A unified picture for low-luminosity and long gamma-ray bursts based on the extended progenitor of llGRB 060218/SN 2006aj," *The Astrophysical Journal*, vol. 807, p. 172, 2015.

[78] R. Margutti, A. M. Soderberg, M. H. Wieringa et al., "The signature of the central engine in the weakest relativistic explosions: GRB 100316D," *Astrophysical Journal*, vol. 778, no. 1, article no. 18, 2013.

[79] A. M. Soderberg, S. Chakraborti, G. Pignata et al., "A relativistic type Ibc supernova without a detected γ-ray burst," *Nature*, vol. 463, no. 7280, pp. 513–515, 2010.

[80] D. Xu, D. Watson, J. Fynbo et al., "Mildly relativistic X-ray transient 080109 and SN 2008D: towards a continuum from energetic GRB/XRF to ordinary Ibc SN," in *Proceedings of the*

37th COSPAR Scientific Assembly, vol. 37 of *COSPAR Meeting*, p. 3512, 2008.

[81] R. Margutti, D. Milisavljevic, A. M. Soderberg et al., "Relativistic supernovae have shorter-lived central engines or more extended progenitors: the case of SN 2012ap," *The Astrophysical Journal*, vol. 797, article 107, 2014.

[82] A. Sakurai, "On the problem of a shock wave arriving at the edge of a gas," *Communications on Pure and Applied Mathematics*, vol. 13, pp. 353–370, 1960.

[83] C. D. Matzner and C. F. Mckee, "The expulsion of stellar envelopes in core-collapse supernovae," *Astrophysical Journal*, vol. 510, no. 1, pp. 379–403, 1999.

[84] D. Lazzati, B. J. Morsony, C. H. Blackwell, and M. C. Begelman, "Unifying the zoo of jet-driven stellar explosions," *Astrophysical Journal*, vol. 750, no. 1, article no. 68, 2012.

[85] L. Amati, F. Frontera, M. Tavani et al., "Intrinsic spectra and energetics of BeppoSAX Gamma-Ray Bursts with known redshifts," *Astronomy & Astrophysics*, vol. 390, pp. 81–89, 2002.

[86] L. Amati, M. Della Valle, F. Frontera et al., "On the consistency of peculiar GRBs 060218 and 060614 with the E p,i—E iso correlation," *Astronomy and Astrophysics*, vol. 463, no. 3, pp. 913–919, 2007.

[87] L. Amati, C. Guidorzi, F. Frontera et al., "Measuring the cosmological parameters with the $E_{p,i}$–E_{iso} correlation of gamma-ray bursts," *Monthly Notices of the Royal Astronomical Society*, vol. 391, no. 2, pp. 577–584, 2008.

[88] A. Shemi and T. Piran, "The appearance of cosmic fireballs," *Astrophysical Journal*, vol. 365, no. 2, pp. L55–L58, 1990.

[89] S. Chakraborti, A. Soderberg, L. Chomiuk et al., "A missing-link in the supernova-GRB connection: the case of SNp," *The Astrophysical Journal*, vol. 805, no. 2, p. 187, 2015.

[90] A. M. Soderberg, S. R. Kulkarni, E. Nakar et al., "Relativistic ejecta from X-ray flash XRF 060218 and the rate of cosmic explosions," *Nature*, vol. 442, no. 7106, pp. 1014–1017, 2006.

[91] B.-B. Zhang, Y.-Z. Fan, R.-F. Shen et al., "GRB 120422A: a low-luminosity gamma-ray burst driven by a central engine," *The Astrophysical Journal*, vol. 756, article 190, 2012.

[92] O. Bromberg, E. Nakar, T. Piran, and R. Sari, "An observational imprint of the Collapsar model of long gamma-ray bursts," *Astrophysical Journal*, vol. 749, no. 2, article no. 110, 2012.

[93] T. Piran, O. Bromberg, E. Nakar, and R. Sari, "The long, the short and the weak: the origin of gamma-ray bursts," *Philosophical Transactions of the Royal Society A*, vol. 371, no. 1992, 2013.

[94] O. Bromberg, E. Nakar, T. Piran, and R. Sari, "Short versus long and collapsars versus non-collapsars: a quantitative classification of gamma-ray bursts," *The Astrophysical Journal*, vol. 764, no. 2, article 179, 2013.

[95] P. Kumar and A. Panaitescu, "Afterglow emission from naked gamma-ray bursts," *The Astrophysical Journal*, vol. 541, no. 2, pp. L51–L54, 2000.

[96] E. Nakar and T. Piran, "Outliers to the peak energy-isotropic energy relation in gamma-ray bursts," *Monthly Notices of the Royal Astronomical Society: Letters*, vol. 360, no. 1, pp. L73–L76, 2005.

[97] C. Firmani, J. I. Cabrera, V. Avila-Reese et al., "Time-resolved spectral correlations of long-duration γ-ray bursts," *Monthly Notices of the Royal Astronomical Society*, vol. 393, no. 4, pp. 1209–1218, 2009.

[98] A. Shahmoradi and R. J. Nemiroff, "Hardness as a spectral peak estimator for gamma-ray bursts," *Monthly Notices of the Royal Astronomical Society*, vol. 407, no. 4, pp. 2075–2090, 2010.

[99] A. Shahmoradi and R. J. Nemiroff, "The possible impact of gamma-ray burst detector thresholds on cosmological standard candles," *Monthly Notices of the Royal Astronomical Society*, vol. 411, no. 3, pp. 1843–1856, 2011.

[100] G. Ghirlanda, L. Nava, and G. Ghisellini, "Spectral-luminosity relation within individual Fermi gamma rays bursts," *Astronomy & Astrophysics*, vol. 511, no. 1, article A43, 2010.

[101] G. Ghirlanda, "Gamma Ray Bursts Spectral-Energy correlations: recent results," in *Proceedings of the Jets at All Scales*, G. E. Romero, R. A. Sunyaev, and T. Belloni, Eds., vol. 275 of *IAU Symposium*, pp. 344–348, 2011.

[102] A. C. Collazzi, B. E. Schaefer, A. Goldstein, and R. D. Preece, "A significant problem with using the Amati relation for cosmological purposes," *The Astrophysical Journal*, vol. 747, no. 1, article 39, 2012.

[103] R. Preece, A. Goldstein, N. Bhat et al., "Which E peak?-the characteristic energy of gamma-ray burst spectra," *The Astrophysical Journal*, vol. 821, no. 1, article 12, 2016.

[104] A. Gal-Yam, "Luminous supernovae," *Science*, vol. 337, no. 6097, pp. 927–932, 2012.

[105] B. D. Metzger, B. Margalit, D. Kasen, and E. Quataert, "The diversity of transients from magnetar birth in core collapse supernovae," *Monthly Notices of the Royal Astronomical Society* , vol. 454, no. 3, pp. 3311–3316, 2015.

[106] Z. Cano, K. G. Johansson Andreas, and K. Maeda, "A self-consistent analytical magnetar model: the luminosity of γ-ray burst supernovae is powered by radioactivity," *Monthly Notices of the Royal Astronomical Society*, vol. 457, no. 3, Article ID stw122, pp. 2761–2772, 2016.

[107] M. C. Bersten, O. G. Benvenuto, M. Orellana, and K. Nomoto, "The unusual super-luminous supernovae SN 2011KL and asassn-15LH," *Astrophysical Journal Letters*, vol. 817, no. 1, article L8, 2016.

[108] C. Inserra and S. J. Smartt, "Superluminous supernovae as standardizable candles and high-redshift distance probes," *The Astrophysical Journal*, vol. 796, no. 2, p. 87, 2014.

[109] J.-J. Wei, X.-F. Wu, and F. Melia, "Testing cosmological models with type Ic super luminous supernovae," *Astronomical Journal*, vol. 149, no. 5, article no. 165, 2015.

[110] K. Maeda, T. Nakamura, K. Nomoto, P. A. Mazzali, F. Patat, and I. Hachisu, "Explosive nucleosynthesis in aspherical hypernova explosions and late-time spectra of SN 1998bw," *Astrophysical Journal*, vol. 565, no. 1, pp. 405–412, 2002.

[111] K. Maeda, "Three-dimensional simulation of gamma-ray emission from asymmetric supernovae and hypernovae," *Astrophysical Journal*, vol. 644, no. 1, pp. 385–399, 2006.

[112] S. E. Woosley and A. Heger, "The light curve of the unusual supernova SN 2003dh," https://arxiv.org/abs/astro-ph/0309165.

[113] P. A. Mazzali, J. Deng, K. Nomoto et al., "A neutron-star-driven X-ray flash associated with supernova SN 2006aj," *Nature*, vol. 442, no. 7106, pp. 1018–1020, 2006.

[114] S. E. Woosley, R. G. Eastman, and B. P. Schmidt, "Gamma-ray bursts and type Ic supernova SN 1998bw," *The Astrophysical Journal*, vol. 516, no. 2, pp. 788–796, 1999.

[115] P. Höflich, J. C. Wheeler, and L. Wang, "Aspherical explosion models for SN 1998bw/GRB 980425," *Astrophysical Journal*, vol. 521, no. 1, pp. 179–189, 1999.

[116] K. Iwamoto, "On the radio-to-X-ray light curves of SN 1998bw and GRB 980425," *Astrophysical Journal*, vol. 512, no. 1, pp. L47–L50, 1999.

[117] T. Nakamura, P. A. Mazzali, K. Nomoto, and K. Iwamoto, "Light curve and spectral models for the hypernova SN 1998bw associated with GRB 980425," *Astrophysical Journal*, vol. 550, no. 2, pp. 991–999, 2001.

[118] P. A. Mazzali, J. Deng, N. Tominaga et al., "The type Ic hypernova SN 2003dh/GRB 030329," *The Astrophysical Journal*, vol. 599, no. 2, pp. L95–L98, 2003.

[119] S. Nagataki, A. Mizuta, and K. Sato, "Explosive nucleosynthesis in GRB jets accompanied by hypernovae," *Astrophysical Journal*, vol. 647, no. 2, pp. 1255–1268, 2006.

[120] J. D. Lyman, D. Bersier, P. A. James et al., "Bolometric light curves and explosion parameters of 38 stripped-envelope core-collapse supernovae," *Monthly Notices of the Royal Astronomical Society*, vol. 457, no. 1, pp. 328–350, 2016.

[121] E. F. Olivares, J. Greiner, P. Schady et al., "The fast evolution of SN 2010bh associated with XRF 100316D," *Astronomy and Astrophysics*, vol. 539, article no. A76, 2012.

[122] K. Maeda, P. A. Mazzali, J. Deng et al., "A two-component model for the light curves of hypernovae," *The Astrophysical Journal*, vol. 593, no. 2, pp. 931–940, 2003.

[123] M. Modjaz, W. Li, N. Butler et al., "From shock breakout to peak and beyond: extensive panchromatic observations of the type Ib supernova 2008D associated with swift x-ray transient 080109," *Astrophysical Journal*, vol. 702, no. 1, pp. 226–248, 2009.

[124] D. E. Reichart, "GRB 970228 revisited: evidence for a supernova in the light curve and late spectral energy distribution of the afterglow," *Astrophysical Journal*, vol. 521, no. 2, pp. L111–L115, 1999.

[125] T. J. Galama, N. Tanvir, P. M. Vreeswijk et al., "Evidence for a supernova in reanalyzed optical and near-infrared images of GRB 970228," *The Astrophysical Journal*, vol. 536, no. 1, pp. 185–194, 2000.

[126] J. S. Bloom, S. R. Kulkarni, S. G. Djorgovski et al., "The unusual afterglow of the γ-ray burst of 26 March 1998 as evidence for a supernova connection," *Nature*, vol. 401, no. 6752, pp. 453–456, 1999.

[127] A. J. Castro-Tirado and J. Gorosabel, "Optical observations of GRB afterglows: GRB 970508 and GRB 980326 revisited," *Astronomy and Astrophysics Supplement Series*, vol. 138, no. 3, pp. 449–450, 1999.

[128] X. Li and J. Hjorth, "Light curve properties of supernovae associated with gamma-ray bursts," https://arxiv.org/abs/1407.3506.

[129] G. Björnsson, J. Hjorth, P. Jakobsson, L. Christensen, and S. Holland, "The jet and the supernova in GRB 990712," *The Astrophysical Journal*, vol. 552, no. 2, pp. L121–L124, 2001.

[130] A. J. Castro-Tirado, V. V. Sokolov, J. Gorosabel et al., "The extraordinarily bright optical afterglow of GRB 991208 and its host galaxy," *Astronomy & Astrophysics*, vol. 370, no. 2, pp. 398–406, 2001.

[131] D. Lazzati, S. Covino, G. Ghisellini et al., "The optical afterglow of GRB 000911: evidence for an associated supernova?" *Astronomy and Astrophysics*, vol. 378, no. 3, pp. 996–1002, 2001.

[132] N. Masetti, E. Palazzi, E. Pian et al., "Late-epoch optical and near-infrared observations of the GRB 000911 afterglow and its host galaxy," *Astronomy and Astrophysics*, vol. 438, no. 3, pp. 841–853, 2005.

[133] J. S. Bloom, S. R. Kulkarni, P. A. Price et al., "Detection of a supernova signature associated with GRB 011121," *Astrophysical Journal*, vol. 572, no. 1, pp. L45–L49, 2002.

[134] P. A. Price, E. Berger, D. E. Reichart et al., "GRB 011121: a massive star progenitor," *The Astrophysical Journal Letters*, vol. 572, no. 1, pp. L51–L55, 2002.

[135] P. M. Garnavich, K. Z. Stanek, L. Wyrzykowski et al., "Discovery of the low-redshift optical afterglow of GRB 011121 and its progenitor supernova sn 2001ke," *Astrophysical Journal*, vol. 582, no. 2, pp. 924–932, 2003.

[136] J. Greiner, S. Klose, M. Salvato et al., "GRB 011121: a collimated outflow into wind-blown surroundings," *Astrophysical Journal*, vol. 599, no. 2 I, pp. 1223–1237, 2003.

[137] J. Gorosabel, J. P. U. Fynbo, A. Fruchter et al., "A possible bright blue supernova in the afterglow of GRB 020305," *The Astronomy and Astrophysics*, vol. 437, no. 2, pp. 411–418, 2005.

[138] P. A. Price, S. R. Kulkarni, E. Berger et al., "Discovery of GRB 020405 and its late red bump," *The Astrophysical Journal*, vol. 589, no. 2, pp. 838–843, 2003.

[139] L. Nicastro, J. J. M. In't Zand, L. Amati et al., "Multiwavelength study of the very long GRB 020410," *Astronomy and Astrophysics*, vol. 427, no. 2, pp. 445–452, 2004.

[140] A. Levan, P. Nugent, A. Fruchter et al., "GRB 020410: a gamma-ray burst afterglow discovered by its supernova light," *Astrophysical Journal*, vol. 624, no. 2, pp. 880–888, 2005.

[141] G. Ricker, J.-L. Atteia, N. Kawai et al., "GRB020903(=H2314): an X-ray flash localized by HETE," *GRB Coordinates Network*, vol. 1530, article 1, 2002.

[142] A. M. Soderberg, S. R. Kulkarni, D. B. Fox et al., "An HST search for supernovae accompanying X-ray flashes," *Astrophysical Journal*, vol. 627, no. 2, pp. 877–887, 2005.

[143] D. Bersier, A. S. Fruchter, L.-G. Strolger et al., "Evidence for a supernova associated with the X-ray flash 020903," *Astrophysical Journal*, vol. 643, no. 1, pp. 284–291, 2006.

[144] M. D. Valle, D. Malesani, S. Benetti et al., "Evidence for supernova signatures in the spectrum of the late-time bump of the optical afterglow of GRB 021211," *The Astronomy and Astrophysics*, vol. 406, no. 2, pp. L33–L37, 2003.

[145] S. B. Pandey, G. C. Anupama, R. Sagar et al., "The optical afterglow of the not so dark GRB 021211," *Astronomy and Astrophysics*, vol. 408, no. 3, pp. L21–L24, 2003.

[146] J. S. Bloom, P. G. Van Dokkum, C. D. Bailyn, M. M. Buxton, S. R. Kulkarni, and B. P. Schmidt, "Optical-infrared ANDICAM observations of the transient associated with GRB 030329," *Astronomical Journal*, vol. 127, no. 1, pp. 252–263, 2004.

[147] Y. M. Lipkin, E. O. Ofek, A. Gal-Yam et al., "The detailed optical light curve of GRB 030329," *Astrophysical Journal*, vol. 606, no. 1, pp. 381–394, 2004.

[148] J. P. U. Fynbo, J. Sollerman, J. Hjorth et al., "On the afterglow of the X-ray flash of 2003 July 23: photometric evidence for an off-axis gamma-ray burst with an associated supernova?" *Astrophysical Journal*, vol. 609, no. 2, pp. 962–971, 2004.

[149] N. Tominaga, J. Deng, P. A. Mazzali et al., "Supernova light-curve models for the bump in the optical counterpart of X-ray flash 030723," *Astrophysical Journal*, vol. 612, no. 2, pp. L105–L108, 2004.

[150] G. Pugliese, P. Møller, J. Gorosabel et al., "The red optical afterglow of GRB 030725," *Astronomy and Astrophysics*, vol. 439, no. 2, pp. 527–532, 2005.

[151] D. Malesani, G. Tagliaferri, G. Chincarini et al., "SN 2003lw and GRB 031203: a bright supernova for a faint gamma-ray burst," *Astrophysical Journal*, vol. 609, no. 1, pp. L5–L8, 2004.

[152] A. M. Soderberg, S. R. Kulkarni, E. Berger et al., "The sub-energetic γ-ray burst GRB 031203 as a cosmic analogue to the nearby GRB 980425," *Nature*, vol. 430, no. 7000, pp. 648–650, 2004.

[153] A. Gal-Yam, D.-S. Moon, D. B. Fox et al., "The J-band light curve of SN 20031w, associated with GRB 031203," *Astrophysical Journal*, vol. 609, no. 2, pp. L59–L62, 2004.

[154] D. Watson, J. Hjorth, A. Levan et al., "A very low luminosity X-ray flash: XMM-Newton observations of GRB 031203," *Astrophysical Journal*, vol. 605, no. 2, pp. L101–L104, 2004.

[155] B. Thomsen, J. Hjorth, D. Watson et al., "The supernova 2003lw associated with X-ray flash 031203," *Astronomy and Astrophysics*, vol. 419, no. 2, pp. L21–L25, 2004.

[156] B. E. Cobb, C. D. Bailyn, P. G. Van Dokkum, and P. Natarajan, "SN 2006aj and the nature of low-luminosity gamma-ray bursts," *Astrophysical Journal*, vol. 645, no. 2, pp. L113–L116, 2006.

[157] K. Wiersema, A. J. Van Der Horst, D. A. Kann et al., "Spectroscopy and multiband photometry of the afterglow of intermediate duration γ-ray burst GRB 040924 and its host galaxy," *Astronomy and Astrophysics*, vol. 481, no. 2, pp. 319–326, 2008.

[158] K. Misra, L. Resmi, S. B. Pandey, D. Bhattacharya, and R. Sagar, "Optical observations and multiband modelling of the afterglow of GRB 041006: evidence of a hard electron energy spectrum," *Bulletin of the Astronomical Society of India*, vol. 33, no. 4, pp. 487–497, 2005.

[159] T. Sakamoto, L. Barbier, S. D. Barthelmy et al., "Confirmation of the E^{src}_{peak}-Eiso (Amati) relation from the X-ray flash XRF 050416A observed by the Swift burst alert telescope," *Astrophysical Journal*, vol. 636, no. 2, pp. L73–L76, 2006.

[160] A. M. Soderberg, E. Nakar, S. B. Cenko et al., "A spectacular radio flare from XRF 050416a at 40 days and implications for the nature of X-ray flashes," *Astrophysical Journal*, vol. 661, no. 2 I, pp. 982–994, 2007.

[161] M. Della Valle, D. Malesani, J. S. Bloom et al., "Hypernova signatures in the late rebrightening of GRB 050525A," *Astrophysical Journal*, vol. 642, no. 2, pp. L103–L106, 2006.

[162] H. Krimm, L. Barbier, S. Barthelmy et al., "GRB 050824: BAT refined analysis of a soft weak burst," *GRB Coordinates Network, Circular Service*, vol. 3871, article 1, 2005.

[163] G. Crew, G. Ricker, J.-L. Atteia et al., "GRB050824, HETE-2 observation," GRB Coordinates Network 3890, 2005.

[164] N. Mirabal, J. P. Halpern, D. An, J. R. Thorstensen, and D. M. Terndrup, "GRB 060218/SN 2006aj: a gamma-ray burst and prompt supernova at z = 0.0335," *The Astrophysical Journal Letters*, vol. 643, no. 2, pp. L99–L102, 2006.

[165] M. Modjaz, K. Z. Stanek, P. M. Garnavich et al., "Early-time photometry and spectroscopy of the fast evolving SN 2006aj associated with GRB 060218," *Astrophysical Journal*, vol. 645, no. 1, pp. L21–L24, 2006.

[166] E. Pian, P. A. Mazzali, N. Masetti et al., "An optical supernova associated with the X-ray flash XRF 060218," *Nature*, vol. 442, pp. 1011–1013, 2006.

[167] J. Sollerman, A. O. Jaunsen, J. P. U. Fynbo et al., "Supernova 2006aj and the associated X-Ray Flash 060218," *Astronomy and Astrophysics*, vol. 454, no. 2, pp. 503–509, 2006.

[168] K. Misra, A. S. Fruchter, and P. Nugent, "Late-time HST observations of XRF 060218/SN 2006aj," in *AIP Conference Proceedings*, J. E. McEnery, J. L. Racusin, and N. Gehrels, Eds., vol. 1358 of *American Institute of Physics Conference Series*, pp. 299–302, 2011.

[169] D. Grupe, C. Gronwall, X.-Y. Wang et al., "SWIFT and *XMM-Newton* observations of the extraordinary gamma-ray burst 060729: more than 125 days of X-ray afterglow," *Astrophysical Journal*, vol. 662, no. 1 I, pp. 443–458, 2007.

[170] N. R. Butler and D. Kocevski, "X-ray hardness evolution in GRB afterglows and flares: late-time GRB activity without NH variations," *Astrophysical Journal*, vol. 663, no. 1, pp. 407–419, 2007.

[171] C. Markwardt, L. Barbier, S. D. Barthelmy et al., "GRB 060904B: Swift-BAT refined analysis," GRB Coordinates Network 5520, 2006.

[172] S. B. Cenko, S. Gezari, T. Small, D. B. Fox, and R. Chornock, "GRB 070419: Keck/LRIS absorption redshift," GRB Coordinates Network 6322, 2007.

[173] J. Hill, P. Garnavich, O. Kuhn et al., "GRB 070419A, deep LBT photometry and possible supernova detection," GRB Coordinates Network 6486, 2007.

[174] D. A. Kann, S. Schulze, and A. C. Updike, "GRB 080319B: jet break, energetics, supernova," GRB Coordinates Network 7627, 2008.

[175] J. S. Bloom, D. A. Perley, W. Li et al., "Observations of the naked-eye GRB 080319B: implications of nature's brightest explosion," *Astrophysical Journal*, vol. 691, no. 1, pp. 723–737, 2009.

[176] N. R. Tanvir, E. Rol, A. J. Levan et al., "Late-time observations of GRB 080319B: jet break, host galaxy, and accompanying supernova," *The Astrophysical Journal*, vol. 725, no. 1, pp. 625–632, 2010.

[177] A. Soderberg, E. Berger, and D. Fox, "GRB 081007: detection of a supernova," GRB Coordinates Network 8662, 2008.

[178] E. Berger, D. B. Fox, A. Cucchiara, and S. B. Cenko, "GRB 081007: Gemini-south redshift," GRB Coordinates Network 8335, 2008.

[179] M. Della Valle, S. Benetti, P. Mazzali et al., "Supernova 2008hw and GRB 081007," Central Bureau Electronic Telegrams 1602, 2008.

[180] Z.-P. Jin, S. Covino, M. Della Valle et al., "GRB 081007 and GRB 090424: the surrounding medium, outflows, and supernovae," *The Astrophysical Journal*, vol. 774, no. 2, p. 114, 2013.

[181] E. F. Olivares, J. Greiner, P. Schady et al., "Multiwavelength analysis of three supernovae associated with gamma-ray bursts observed by GROND," *Astronomy & Astrophysics*, vol. 577, article A44, 2015.

[182] B. E. Cobb, J. S. Bloom, D. A. Perley, A. N. Morgan, S. B. Cenko, and A. V. Filippenko, "Discovery of sn 2009nz associated with grb 091127," *Astrophysical Journal Letters*, vol. 718, no. 2, pp. L150–L155, 2010.

[183] E. Berger, R. Chornock, T. R. Holmes et al., "The spectroscopic classification and explosion properties of SN 2009nz associated with GRB 091127 AT $z = 0.490$," *Astrophysical Journal*, vol. 743, no. 2, article 204, 2011.

[184] R. Chornock, E. Berger, E. M. Levesque et al., "Spectroscopic discovery of the broad-lined type Ic supernova 2010bh associated with the low-redshift GRB 100316D," https://arxiv.org/abs/1004.2262.

[185] S. T. Holland, F. E. Marshall, M. Page, M. de Pasquale, and M. H. Siegel, "GRB 100418A: possible evidence for a supernova," GRB Coordinates Network 10661, 2010.

[186] F. E. Marshall, L. A. Antonelli, D. N. Burrows et al., "The late peaking afterglow of GRB 100418A," *Astrophysical Journal*, vol. 727, no. 2, 2011.

[187] A. De Ugarte Postigo, C. C. Thöne, P. Goldoni, and J. P. U. Fynbo, "Time resolved spectroscopy of GRB 100418A and its host galaxy with X-shooter," *Astronomische Nachrichten*, vol. 332, no. 3, pp. 297–298, 2011.

[188] M. Sparre, J. Sollerman, J. P. U. Fynbo et al., "Spectroscopic evidence for SN 2010ma associated with GRB 101219B," *The Astrophysical Journal Letters*, vol. 735, no. 1, p. L24, 2011.

[189] S. Golenetskii, R. Aptekar, E. Mazets et al., "Konus-wind observation of GRB 111209A," GRB Coordinates Network 12663, 2011.

[190] A. de Ugarte Postigo, C. C. Thoene, and J. Gorosabel, "GRB 111211A: detection of the SN with the 10.4m GTC," GRB Coordinates Network 12802, 2012.

[191] P. D'Avanzo, A. Melandri, E. Palazzi et al., "GRB 111228A: possible detection of the SN with the TNG," GRB Coordinates Network 13069, 2012.

[192] A. Melandri, E. Pian, P. Ferrero et al., "The optical SN 2012bz associated with the long GRB 120422A," *Astronomy and Astrophysics*, vol. 547, article no. A82, 2012.

[193] S. Klose, J. Greiner, J. Fynbo et al., "Supernova 2012eb = GRB 120714B," Central Bureau Electronic Telegrams 3200, 2012.

[194] J. R. Cummings, S. D. Barthelmy, W. H. Baumgartner et al., "GRB 120714B: swift-BAT refined analysis," GRB Coordinates Network 13481, 2012.

[195] M. De Pasquale, M. J. Page, D. A. Kann et al., "The 80 Ms follow-up of the X-ray afterglow of GRB 130427A challenges the standard forward shock model," *Monthly Notices of the Royal Astronomical Society*, vol. 462, no. 1, pp. 1111–1122, 2016.

[196] A. J. Levan, N. R. Tanvir, A. S. Fruchter et al., "Hubble space telescope observations of the afterglow, supernova, and host galaxy associated with the extremely bright GRB 130427A," *The Astrophysical Journal*, vol. 792, no. 2, article 115, 2014.

[197] A. Melandri, E. Pian, V. D'Elia et al., "Diversity of gamma-ray burst energetics vs. supernova homogeneity: SN 2013cq associated with GRB 130427A," *Astronomy and Astrophysics*, vol. 567, article A29, 2014.

[198] V. D'Elia, E. Pian, A. Melandri et al., "SN 2013dx associated with GRB 130702A: A detailed photometric and spectroscopic monitoring and a study of the environment," *Astronomy and Astrophysics*, vol. 577, article A116, 2015.

[199] S. Klose, A. Nicuesa Guelbenzu, T. Kruehler et al., "Supernova 2013fu = GRB 130831A," Central Bureau Electronic Telegrams 3677, 2013.

[200] A. Pozanenko, E. Mazaeva, A. Sergeev et al., "GRB 150518A: possible SN observations," GRB Coordinates Network 17903, 2015.

[201] A. de Ugarte Postigo, Z. Cano, D. A. Perley et al., "GRB 150818A: spectroscopic confirmation of the SN from GTC," GRB Coordinates Network 18213, 2015.

[202] S. Golenetskii, R. Aptekar, D. Frederiks et al., "Konus-Wind observation of GRB 150818A," GRB Coordinates Network 18198, 2015.

[203] D. M. Palmer, S. D. Barthelmy, J. R. Cummings et al., "GRB 150818A: Swift-BAT refined analysis," GRB Coordinates Network 18157, 2015.

[204] G. Pignata, M. Stritzinger, A. Soderberg et al., "SN 2009bb: a peculiar broad-lined Type Ic supernova," *Astrophysical Journal*, vol. 728, no. 1, 2011.

[205] E. M. Levesque, L. J. Kewley, E. Berger, and H. J. Zahid, "The host galaxies of gamma-ray bursts. II. A mass-metallicity relation for long-duration gamma-ray burst host galaxies," *Astronomical Journal*, vol. 140, no. 5, pp. 1557–1566, 2010.

[206] D. Milisavljevic, R. Margutti, J. T. Parrent et al., "The broad-lined type Ic SN 2012ap and the nature of relativistic supernovae lacking a gamma-ray burst detection," *The Astrophysical Journal*, vol. 799, no. 1, article 51, 2015.

[207] Z. Liu, X.-L. Zhao, F. Huang et al., "Optical observations of the broad-lined type Ic supernova SN 2012ap," *Research in Astronomy and Astrophysics*, vol. 15, no. 2, article 007, pp. 225–236, 2015.

[208] W. D. Arnett, "Type I supernovae. I—analytic solutions for the early part of the light curve," *The Astrophysical Journal*, vol. 253, pp. 785–797, 1982.

[209] K. Maeda and N. Tominaga, "Nucleosynthesis of 56Ni in wind-driven supernova explosions and constraints on the central engine of gamma-ray bursts," *Monthly Notices of the Royal Astronomical Society*, vol. 394, no. 3, pp. 1317–1324, 2009.

[210] A. I. Macfadyen, S. E. Woosley, and A. Heger, "Supernovae, jets, and collapsars," *Astrophysical Journal*, vol. 550, no. 1, pp. 410–425, 2001.

[211] S. E. Woosley and T. A. Weaver, "The physics of supernova explosions," *Annual Review of Astronomy & Astrophysics*, vol. 24, pp. 205–253, 1986.

[212] C. L. Fryer, P. A. Mazzali, J. Prochaska et al., "Constraints on Type Ib/c supernovae and gamma-ray burst progenitors," *Publications of the Astronomical Society of the Pacific*, vol. 119, no. 861, pp. 1211–1232, 2007.

[213] K. Takaki, K. S. Kawabata, M. Yamanaka et al., "A luminous and fast-expanding type Ib supernova SN 2012au," *Astrophysical Journal Letters*, vol. 772, no. 2, article no. L17, 2013.

[214] J. Sollerman, S. T. Holland, P. Challis et al., "Supernova 1998bw—the final phases," *Astronomy and Astrophysics*, vol. 386, no. 3, pp. 944–956, 2002.

[215] A. I. MacFadyen and S. E. Woosley, "Collapsars: gamma-ray bursts and explosions in 'failed supernovae'," *The Astrophysical Journal*, vol. 524, no. 1, pp. 262–289, 1999.

[216] M. Milosavljević, C. C. Lindner, R. Shen, and P. Kumar, "Supernovae powered by collapsar accretion in gamma-ray burst sources," *Astrophysical Journal*, vol. 744, no. 2, article no. 103, 2012.

[217] M. V. Barkov and S. S. Komissarov, "Recycling of neutron stars in common envelopes and hypernova explosions," *Monthly Notices of the Royal Astronomical Society*, vol. 415, no. 1, pp. 944–958, 2011.

[218] T. A. Thompson, "Assessing millisecond proto-magnetars as GRB central engines," *Revista Mexicana de Astronomia y Astrofisica*, vol. 27, pp. 80–90, 2007.

[219] T. A. Thompson, B. D. Metzger, and N. Bucciantini, "Proto-magnetars as GRB central engines: uncertainties, limitations, & particulars," in *Proceedings of the American Institute of Physics Conference Series*, N. Kawai and S. Nagataki, Eds., vol. 1279 of *American Institute of Physics Conference Series*, pp. 81–88, 2010.

[220] Y. Suwa and N. Tominaga, "How much can ^{56}Ni be synthesized by the magnetar model for long gamma-ray bursts and hypernovae?" *Monthly Notices of the Royal Astronomical Society*, vol. 451, no. 1, pp. 282–287, 2015.

[221] B. D. Metzger, T. A. Thompson, and E. Quataert, "Proto-neutron star winds with magnetic fields and rotation," *The Astrophysical Journal*, vol. 659, no. 1 I, pp. 561–579, 2007.

[222] K. Maeda, K. Kawabata, P. A. Mazzali et al., "Asphericity in supernova explosions from late-time spectroscopy," *Science*, vol. 319, no. 5867, pp. 1220–1223, 2008.

[223] J. P. Ostriker and J. E. Gunn, "Do pulsars make supernovae?" *The Astrophysical Journal*, vol. 164, pp. L95–L104, 1971.

[224] B. Zhang and P. Mészáros, "Gamma-ray burst afterglow with continuous energy injection: signature of a highly magnetized millisecond pulsar," *Astrophysical Journal*, vol. 552, no. 1, pp. L35–L38, 2001.

[225] E. Chatzopoulos, J. C. Wheeler, J. Vinko et al., "SN 2008am: a super-luminous type IIn supernova," *The Astrophysical Journal*, vol. 729, article 143, 2011.

[226] C. Inserra, S. J. Smartt, A. Jerkstrand et al., "Super-luminous type Ic supernovae: catching a magnetar by the tail," *The Astrophysical Journal*, vol. 770, no. 2, p. 128, 2013.

[227] M. Nicholl, S. J. Smartt, A. Jerkstrand et al., "Slowly fading super-luminous supernovae that are not pair-instability explosions," *Nature*, vol. 502, pp. 346–349, 2013.

[228] D. Kasen and L. Bildsten, "Supernova light curves powered by young magnetars," *Astrophysical Journal*, vol. 717, no. 1, pp. 245–249, 2010.

[229] S. E. Woosley, "Bright supernovae from magnetar birth," *Astrophysical Journal Letters*, vol. 719, no. 2, pp. L204–L207, 2010.

[230] P. A. Mazzali, M. Sullivan, E. Pian, J. Greiner, and D. A. Kann, "Spectrum formation in superluminous supernovae (Type I)," *Monthly Notices of the Royal Astronomical Society*, vol. 458, no. 4, pp. 3455–3465, 2016.

[231] P. A. Mazzali, K. S. Kawabata, K. Maeda et al., "An asymmetric energetic type Ic supernova viewed off-axis, and a link to gamma ray bursts," *Science*, vol. 308, no. 5726, pp. 1284–1287, 2005.

[232] M. Modjaz, R. P. Kirshner, S. Blondin, P. Challis, and T. Matheson, "Double-peaked oxygen lines are not rare in nebular spectra of core-collapse Supernovae," *The Astrophysical Journal Letters*, vol. 687, pp. L9–L12, 2008.

[233] M. Tanaka, N. Tominaga, K. Nomoto et al., "Type Ib supernova 2008D associated with the luminous X-ray transient 080109: an energetic explosion of a massive helium star," *The Astrophysical Journal*, vol. 692, no. 2, pp. 1131–1142, 2009.

[234] S. Taubenberger, S. Valenti, S. Benetti et al., "Nebular emission-line profiles of Type Ib/c supernovae—probing the ejecta asphericity," *Monthly Notices of the Royal Astronomical Society*, vol. 397, no. 2, pp. 677–694, 2009.

[235] D. Milisavljevic, R. A. Fesen, C. L. Gerardy, R. P. Kirshner, and P. Challis, "Doublets and double peaks: late-time [O I] $\lambda\lambda$6300, 6364 line profiles of stripped-envelope, core-collapse supernovae," *The Astrophysical Journal*, vol. 709, no. 2, pp. 1343–1355, 2010.

[236] C. Fransson and R. A. Chevalier, "Late emission from SN 1987A," *The Astrophysical Journal*, vol. 322, no. 1, pp. L15–L20, 1987.

[237] E. M. Schlegel and R. P. Kirshner, "The type Ib supernova 1984L in NGC 991," *Astronomical Journal*, vol. 98, pp. 577–589, 1989.

[238] K. Maeda and K. Nomoto, "Bipolar supernova explosions: nucleosynthesis and implications for abundances in extremely metal-poor stars," *The Astrophysical Journal*, vol. 598, no. 2, pp. 1163–1200, 2003.

[239] A. M. Khokhlov, P. A. Höflich, E. S. Oran, J. C. Wheeler, L. Wang, and A. Y. Chtchelkanova, "Jet-induced explosions of core collapse supernovae," *Astrophysical Journal*, vol. 524, no. 2, pp. L107–L110, 1999.

[240] T. Morris and P. Podsiadlowski, "The triple-ring nebula around SN 1987A: fingerprint of a binary merger," *Science*, vol. 315, no. 5815, pp. 1103–1106, 2007.

[241] M. Tanaka, K. S. Kawabata, T. Hattori et al., "Three-dimensional explosion geometry of stripped-envelope core-collapse supernovae. I. Spectropolarimetric observations," *The Astrophysical Journal*, vol. 754, no. 1, p. 63, 2012.

[242] L. Wang and J. C. Wheeler, "Spectropolarimetry of supernovae," *Annual Review of Astronomy & Astrophysics*, vol. 46, pp. 433–474, 2008.

[243] S. Akiyama, J. C. Wheeler, D. L. Meier, and I. Lichtenstadt, "The magnetorotational instability in core-collapse supernova explosions," *The Astrophysical Journal*, vol. 584, no. 2, pp. 954–970, 2003.

[244] T. A. Thompson, P. Chang, and E. Quataert, "Magnetar spin-down, hyperenergetic supernovae, and gamma-ray bursts," *Astrophysical Journal*, vol. 611, no. 1, pp. 380–393, 2004.

[245] Y. Masada, T. Sano, and H. Takabe, "Nonaxisymmetric magnetorotational instability in proto-neutron stars," *The Astrophysical Journal*, vol. 641, no. 1, pp. 447–457, 2006.

[246] D. A. Uzdensky and A. I. MacFadyen, "Magnetar-driven magnetic tower as a model for gamma-ray bursts and asymmetric supernovae," *Astrophysical Journal*, vol. 669, no. 1, pp. 546–560, 2007.

[247] S. E. Woosley, "Gamma-ray bursts from stellar mass accretion disks around black holes," *The Astrophysical Journal*, vol. 405, no. 1, pp. 273–277, 1993.

[248] P. Mösta, C. D. Ott, D. Radice, L. F. Roberts, E. Schnetter, and R. Haas, "A large-scale dynamo and magnetoturbulence in rapidly rotating core-collapse supernovae," *Nature*, vol. 528, no. 7582, pp. 376–379, 2015.

[249] O. Papish and N. Soker, "Exploding core collapse supernovae with jittering jets," *Monthly Notices of the Royal Astronomical Society*, vol. 416, no. 3, pp. 1697–1702, 2011.

[250] S. M. Couch and E. P. O'Connor, "High-resolution three-dimensional simulations of core-collapse supernovae in multiple progenitors," *The Astrophysical Journal*, vol. 785, no. 2, p. 123, 2014.

[251] S. M. Couch and C. D. Ott, "The role of turbulence in neutrino-driven core-collapse supernova explosions," *The Astrophysical Journal*, vol. 799, no. 1, article 5, 2015.

[252] L. Wang, D. Baade, P. Höflich, and J. C. Wheeler, "Spectropolarimetry of the type Ic supernova SN 2002ap in M74: more evidence for asymmetric core collapse," *Astrophysical Journal*, vol. 592, no. 1, pp. 457–466, 2003.

[253] A. G. Lyne and D. R. Lorimer, "High birth velocities of radio pulsars," *Nature*, vol. 369, no. 6476, pp. 127–129, 1994.

[254] B. W. Grefenstette, F. A. Harrison, S. E. Boggs et al., "Asymmetries in core-collapse supernovae from maps of radioactive ^{44}Ti in Cassiopeia A," *Nature*, vol. 506, no. 7488, pp. 339–342, 2014.

[255] J. M. Blondin, A. Mezzacappa, and C. Demarino, "Stability of standing accretion shocks, with an eye toward core-collapse supernovae," *Astrophysical Journal*, vol. 584, no. 2 I, pp. 971–980, 2003.

[256] S. Orlando, M. Miceli, M. L. Pumo, and F. Bocchino, "Modeling SNR cassiopeia a from the supernova explosion to its current age: the role of post-explosion anisotropies of Ejecta," *Astrophysical Journal*, vol. 822, no. 1, article 22, 2016.

[257] R. A. Fesen, "An optical survey of outlying ejecta in Cassiopeia A: evidence for a turbulent, asymmetric explosion," *The Astrophysical Journal, Supplement Series*, vol. 133, no. 1, pp. 161–186, 2001.

[258] J. C. Wheeler, J. R. Maund, and S. M. Couch, "The shape of Cas A," *The Astrophysical Journal*, vol. 677, no. 2, pp. 1091–1099, 2008.

[259] L. A. Lopez, E. Ramirez-Ruiz, D. Castro, and S. Pearson, "The galactic supernova remnant W49B likely originates from a jet-driven, core-collapse explosion," *The Astrophysical Journal*, vol. 764, no. 1, p. 50, 2013.

[260] R. A. Fesen and D. Milisavljevic, "An HST survey of the highest-velocity Ejecta in cassiopeia A," *Astrophysical Journal*, vol. 818, no. 1, article 17, 2016.

[261] J. C. Wheeler, V. Johnson, and A. Clocchiatti, "Analysis of late-time light curves of type IIb, Ib and Ic supernovae," *Monthly Notices of the Royal Astronomical Society*, vol. 450, no. 2, pp. 1295–1307, 2015.

[262] Z. Cano, K. Maeda, and S. Schulze, "Type Ib SN 1999dn as an example of the thoroughly mixed ejecta of Ib supernovae," *Monthly Notices of the Royal Astronomical Society*, vol. 438, no. 4, pp. 2924–2937, 2014.

[263] R. P. Harkness, J. C. Wheeler, B. Margon et al., "The early spectral phase of type Ib supernovae—evidence for helium," *The Astrophysical Journal*, vol. 317, pp. 355–367, 1987.

[264] L. B. Lucy, "Nonthermal excitation of helium in type Ib supernovae," *The Astrophysical Journal*, vol. 383, no. 1, pp. 308–313, 1991.

[265] H. Li and R. McCray, "The He I emission lines of SN 1987A," *The Astrophysical Journal*, vol. 441, pp. 821–829, 1995.

[266] C. Li, D. J. Hillier, and L. Dessart, "Non-thermal excitation and ionization in supernovae," *Monthly Notices of the Royal Astronomical Society*, vol. 426, no. 2, pp. 1671–1686, 2012.

[267] S. E. Woosley, N. Langer, and T. A. Weaver, "The presupernova evolution and explosion of helium stars that experience mass loss," *Astrophysical Journal*, vol. 448, no. 1, pp. 315–338, 1995.

[268] S. Hachinger, P. A. Mazzali, S. Taubenberger, W. Hillebrandt, K. Nomoto, and D. N. Sauer, "How much H and He is 'hidden' in SNe Ib/c? - I. Low-mass objects," *Monthly Notices of the Royal Astronomical Society*, vol. 422, no. 1, pp. 70–88, 2012.

[269] L. H. Frey, C. L. Fryer, and P. A. Young, "Can stellar mixing explain the lack of type ib supernovae in long-duration gamma-ray bursts?" *Astrophysical Journal Letters*, vol. 773, no. 1, article no. L7, 2013.

[270] L. Dessart, D. J. Hillier, C. Li, and S. Woosley, "On the nature of supernovae Ib and Ic," *Monthly Notices of the Royal Astronomical Society*, vol. 424, no. 3, pp. 2139–2159, 2012.

[271] Y. Liu, M. Modjaz, F. B. Bianco, and O. Graur, "Analyzing the largest spectroscopic data set of stripped supernovae to improve their identifications and constrain their progenitors," *The Astrophysical Journal*, vol. 827, no. 2, 2016.

[272] F. Taddia, J. Sollerman, G. Leloudas et al., "Early-time light curves of Type Ib/c supernovae from the SDSS-II Supernova Survey," *Astronomy & Astrophysics*, vol. 574, article A60, 2015.

[273] A. M. Soderberg, E. Nakar, E. Berger, and S. R. Kulkarni, "Late-time radio observations of 68 type Ibc supernovae: strong constraints on off-axis gamma-ray bursts," *Astrophysical Journal*, vol. 638, no. 2 I, pp. 930–937, 2006.

[274] L. E. Kay, J. P. Halpern, K. M. Leighly et al., "Spectropolarimetry of the peculiar Type IC supernovae 1998bw and 1997ef," *Bulletin of the American Astronomical Society*, vol. 30, article 1323, 1998.

[275] E. H. McKenzie and B. E. Schaefer, "The late-time light curve of SN 1998bw associated with GRB 980425," *Publications of the Astronomical Society of the Pacific*, vol. 111, no. 762, pp. 964–968, 1999.

[276] J. Gorosabel, V. Larionov, A. J. Castro-Tirado et al., "Detection of optical linear polarization in the SN 2006aj/XRF 060218 non-spherical expansion," *Astronomy & Astrophysics*, vol. 459, no. 3, pp. L33–L36, 2006.

[277] J. R. Maund, J. C. Wheeler, F. Patat, D. Baade, L. Wang, and P. Höflich, "Spectropolarimetry of SN 2006aj at 9.6 days," *Astronomy and Astrophysics*, vol. 475, no. 1, pp. L1–L4, 2007.

[278] M. Betoule, R. Kessler, J. Guy et al., "Improved cosmological constraints from a joint analysis of the SDSS-II and SNLS supernova samples," *Astronomy & Astrophysics*, vol. 568, article A22, 2014.

[279] M. M. Phillips, "The absolute magnitudes of type IA supernovae," *Astrophysical Journal*, vol. 413, no. 2, pp. L105–L108, 1993.

[280] C. T. Kowal, "Absolute magnitudes of supernovae," *The Astronomical Journal*, vol. 73, pp. 1021–1024, 1968.

[281] D. Branch and G. A. Tammann, "Type IA supernovae as standard candles," *Annual Review of Astronomy & Astrophysics*, vol. 30, pp. 359–389, 1992.

[282] A. Sandage and G. A. Tammann, "The Hubble diagram in V for supernovae of Type IA and the value of H(0) therefrom," *The Astrophysical Journal*, vol. 415, no. 1, pp. 1–9, 1993.

[283] M. Hamuy, M. M. Phillips, J. Maza, N. B. Suntzeff, R. A. Schommer, and R. Avilés, "A hubble diagram of distant Type Ia supernovae," *Astronomical Journal*, vol. 109, no. 1, pp. 1–13, 1995.

[284] M. Hamuy, M. M. Phillips, N. B. Suntzeff, R. A. Schommer, J. Maza, and R. Avilés, "The absolute luminosities of the calan/tololo type IA supernovae," *Astronomical Journal*, vol. 112, no. 6, pp. 2391–2397, 1996.

[285] M. Hamuy, M. M. Phillips, N. B. Suntzeff, R. A. Schommer, J. Maza, and R. Avilés, "The hubble diagram of the calan/tololo type IA supernovae and the value of HO," *Astronomical Journal*, vol. 112, no. 6, p. 2398, 1996.

[286] A. G. Riess, A. V. Filippenko, P. Challis et al., "Observational evidence from supernovae for an accelerating universe and a cosmological constant," *The Astronomical Journal*, vol. 116, no. 3, pp. 1009–1038, 1998.

[287] S. Perlmutter, G. Aldering, G. Goldhaber et al., "Measurements of Ω and Λ from 42 high-redshift supernovae," *The Astrophysical Journal*, vol. 517, no. 2, pp. 565–586, 1999.

[288] W. L. Freedman, B. F. Madore, B. K. Gibson et al., "Final results from the Hubble Space Telescope key project to measure the Hubble constant," *Astrophysical Journal Letters*, vol. 553, no. 1, pp. 47–72, 2001.

[289] X. Li, J. Hjorth, and R. Wojtak, "Cosmological parameters from supernovae associated with gamma-ray bursts," *The Astrophysical Journal*, vol. 796, no. 1, article L4, 2014.

[290] A. L. Piro and E. Nakar, "What can we learn from the rising light curves of radioactively powered supernovae?" *The Astrophysical Journal*, vol. 769, no. 1, article 67, 2013.

[291] S. E. Woosley and W. Zhang, "Models for GRBs and diverse transients," *Philosophical Transactions of the Royal Society A: Mathematical, Physical and Engineering Sciences*, vol. 365, no. 1854, pp. 1129–1139, 2007.

[292] D. Kasen and S. E. Woosley, "On the origin of the type Ia supernova width-luminosity relation," *The Astrophysical Journal*, vol. 656, no. 2, pp. 661–665, 2007.

[293] S. Savaglio, K. Glazebrook, and D. Le Borgne, "The galaxy population hosting gamma-ray bursts," *The Astrophysical Journal*, vol. 691, no. 1, pp. 182–211, 2009.

[294] P. Jakobsson, D. Malesani, J. Hjorth, J. P. U. Fynbo, and B. Milvang-Jensen, "Host galaxies of long gamma-ray bursts," in *Proceedings of the Gamma Ray Bursts 2010, GRB 2010*, pp. 265–270, usa, November 2010.

[295] E. M. Levesque, "The host galaxies of long-duration gamma-ray bursts," *Publications of the Astronomical Society of the Pacific*, vol. 126, no. 935, pp. 1–14, 2014.

[296] T. Krühler, D. Malesani, J. P. U. Fynbo et al., "GRB hosts through cosmic time: VLT/X-shooter emission-line spectroscopy of 96 γ-ray-burst-selected galaxies at $0.1 < z < 3.6$," *The Astronomy and Astrophysics*, vol. 581, article A125, 2015.

[297] S. Mao and H. J. Mo, "The nature of the host galaxies for gamma-ray bursts," *Astronomy and Astrophysics*, vol. 339, no. 1, pp. L1–L4, 1998.

[298] D. W. Hogg and A. S. Fruchter, "The faint-galaxy hosts of gamma-ray bursts," *Astrophysical Journal*, vol. 520, no. 1, pp. 54–58, 1999.

[299] S. G. Djorgovski, D. A. Frail, S. R. Kulkarni, J. S. Bloom, S. C. Odewahn, and A. Diercks, "The afterglow and the host galaxy of the dark burst GRB 970828," *The Astrophysical Journal*, vol. 562, no. 2, pp. 654–663, 2001.

[300] S. G. Djorgovski, J. S. Bloom, and S. R. Kulkarni, "The redshift and the host galaxy of GRB 980613: a gamma-ray burst from a merger-induced starburst?" *Astrophysical Journal*, vol. 591, no. 1, pp. L13–L16, 2003.

[301] E. Le Floc'h, P.-A. Duc, I. F. Mirabel et al., "Are the hosts of gamma-ray bursts sub-luminous and blue galaxies?" *Astronomy and Astrophysics*, vol. 400, no. 2, pp. 499–510, 2003.

[302] L. Christensen, J. Hjorth, and J. Gorosabel, "UV star-formation rates of GRB host galaxies," *Astronomy and Astrophysics*, vol. 425, no. 3, pp. 913–926, 2004.

[303] N. R. Tanvir, V. E. Barnard, A. W. Blain et al., "The submillimetre properties of gamma-ray burst host galaxies," *Monthly Notices of the Royal Astronomical Society*, vol. 352, no. 3, pp. 1073–1080, 2004.

[304] C. J. Conselice, J. A. Blackburne, and C. Papovich, "The luminosity, stellar mass, and number density evolution of field galaxies of known morphology from z = 0.5 to 3," *Astrophysical Journal*, vol. 620, no. 2, pp. 564–583, 2005.

[305] K. Z. Stanek, O. Y. Gnedin, J. F. Beacom et al., "Protecting life in the Milky Way: metals keep the GRBs away," *Acta Astronomica*, vol. 56, no. 4, pp. 333–345, 2006.

[306] J. M. C. Cerón, M. J. MichaŁowski, J. Hjorth, D. Watson, J. P. U. Fynbo, and J. Gorosabel, "Star formation rates and stellar masses in $z \sim 1$ gamma-ray burst hosts," *Astrophysical Journal*, vol. 653, no. 2, pp. L85–L88, 2006.

[307] C. Wainwright, E. Berger, and B. E. Penprase, "A morphological study of gamma-ray burst host galaxies," *The Astrophysical Journal*, vol. 657, no. 1 I, pp. 367–377, 2007.

[308] J. M. Castro Cerón, M. J. Michallowski, J. Hjorth et al., "On the distribution of stellar masses in gamma-ray burst host galaxies," *The Astrophysical Journal*, vol. 721, no. 2, pp. 1919–1927, 2010.

[309] A. S. Fruchter, A. J. Levan, L. Strolger et al., "Long γ-ray bursts and core-collapse supernovae have different environments," *Nature*, vol. 441, pp. 463–468, 2006.

[310] K. M. Svensson, A. J. Levan, N. R. Tanvir, A. S. Fruchter, and L.-G. Strolger, "The host galaxies of core-collapse supernovae and gamma-ray bursts," *Monthly Notices of the Royal Astronomical Society*, vol. 405, no. 1, pp. 57–76, 2010.

[311] J. S. Bloom, S. R. Kulkarni, and S. G. Djorgovski, "The observed offset distribution of gamma-ray bursts from their host galaxies: a robust clue to the nature of the progenitors," *Astronomical Journal*, vol. 123, no. 3, pp. 1111–1148, 2002.

[312] A. De Ugarte Postigo, J. P. U. Fynbo, C. C. Thöne et al., "The distribution of equivalent widths in long GRB afterglow spectra," *Astronomy and Astrophysics*, vol. 548, article no. A11, 2012.

[313] P. K. Blanchard, E. Berger, and W.-F. Fong, "The offset and host light distributions of long gamma-ray bursts: a new view from hst observations of swift bursts," *The Astrophysical Journal*, vol. 817, no. 2, article 144, 2016.

[314] J. X. Prochaska, J. S. Bloom, H.-W. Chen et al., "The host galaxy of GRB 031203: implications of its low metallicity, low redshift, and starburst nature," *The Astrophysical Journal*, vol. 611, no. 1, p. 200, 2004.

[315] J. Gorosabel, D. Pérez-Ramírez, J. Sollerman et al., "The GRB 030329 host: a blue low metallicity subluminous galaxy with intense star formation," *Astronomy and Astrophysics*, vol. 444, no. 3, pp. 711–721, 2005.

[316] J. Sollerman, G. Östlin, J. P. U. Fynbo, J. Hjorth, A. Fruchter, and K. Pedersen, "On the nature of nearby GRB/SN host galaxies," *New Astronomy*, vol. 11, no. 2, pp. 103–115, 2005.

[317] L. J. Kewley, W. R. Brown, M. J. Geller, S. J. Kenyon, and M. J. Kurtz, "SDSS 0809+1729: connections between extremely metal-poor galaxies and gamma-ray burst hosts," *Astronomical Journal*, vol. 133, no. 3, pp. 882–888, 2007.

[318] J. Lequeux, M. Peimbert, J. F. Rayo, A. Serrano, and S. Torres-Peimbert, "Chemical composition and evolution of irregular and blue compact galaxies," *Astronomy & Astrophysics*, vol. 80, pp. 155–166, 1979.

[319] E. D. Skillman, R. C. Kennicutt, and P. W. Hodge, "Oxygen abundances in nearby dwarf irregular galaxies," *The Astrophysical Journal*, vol. 347, pp. 875–882, 1989.

[320] D. Zaritsky, R. C. Kennicutt Jr., and J. P. Huchra, "H II regions and the abundance properties of spiral galaxies," *Astrophysical Journal*, vol. 420, no. 1, pp. 87–109, 1994.

[321] C. A. Tremonti, T. M. Heckman, G. Kauffmann et al., "The origin of the mass-metallicity relation: insights from 53,000 star-forming galaxies in the sloan digital sky survey," *The Astrophysical Journal*, vol. 613, no. 2, p. 898, 2004.

[322] C. Wolf and P. Podsiadlowski, "The metallicity dependence of the long-duration gamma-ray burst rate from host galaxy luminosities," *Monthly Notices of the Royal Astronomical Society*, vol. 375, no. 3, pp. 1049–1058, 2007.

[323] M. Modjaz, L. Kewley, R. P. Kirshner et al., "Measured metallicities at the sites of nearby broad-lined type Ic supernovae and implications for the supernovae gamma-ray burst connection," *Astronomical Journal*, vol. 135, no. 4, pp. 1136–1150, 2008.

[324] E. Le Floc'h, V. Charmandaris, W. J. Forrest, I. F. Mirabel, L. Armus, and D. Devost, "Probing cosmic star formation using long gamma-ray bursts: new constraints from the Spitzer Space Telescope," *Astrophysical Journal*, vol. 642, no. 2 I, pp. 636–652, 2006.

[325] M. J. Michałowski, J. Hjorth, J. M. Castro Cerón, and D. Watson, "The nature of GRB-selected submillimeter galaxies: hot and young," *Astrophysical Journal*, vol. 672, no. 2, pp. 817–824, 2008.

[326] J. Elliott, T. Krühler, J. Greiner et al., "The low-extinction afterglow in the solar-metallicity host galaxy of γ-ray burst 110918A," *Astronomy and Astrophysics*, vol. 556, article A23, 2013.

[327] P. Schady, T. Krühler, J. Greiner et al., "Super-solar metallicity at the position of the ultra-long GRB 130925A," *Astronomy and Astrophysics*, vol. 579, article no. A126, 2015.

[328] T. Krühler, J. Greiner, P. Schady et al., "The SEDs and host galaxies of the dustiest GRB afterglows," *Astronomy and Astrophysics*, vol. 534, article no. A108, 2011.

[329] J. Hjorth, D. Malesani, P. Jakobsson et al., "The optically unbiased gamma-ray burst host (tough) survey. I. Survey design and catalogs," *Astrophysical Journal*, vol. 756, no. 2, article no. 187, 2012.

[330] A. Rossi, S. Klose, P. Ferrero et al., "A deep search for the host galaxies of gamma-ray bursts with no detected optical

afterglow," *Astronomy and Astrophysics*, vol. 545, article no. A77, 2012.

[331] D. A. Perley, A. J. Levan, N. R. Tanvir et al., "A population of massive, luminous galaxies hosting heavily dust-obscured gamma-ray bursts: implications for the use of GRBs as tracers of cosmic star formation," *Astrophysical Journal*, vol. 778, no. 2, article no. 128, 2013.

[332] F. Mannucci, R. Salvaterra, and M. A. Campisi, "The metallicity of the long GRB hosts and the fundamental metallicity relation of low-mass galaxies," *Monthly Notices of the Royal Astronomical Society*, vol. 414, no. 2, pp. 1263–1268, 2011.

[333] D. Kocevski and A. A. West, "On the origin of the mass-metallicity relation for gamma-ray burst host galaxies," *The Astrophysical Journal Letters*, vol. 735, no. 1, article L8, 2011.

[334] E. Berger, D. B. Fox, S. R. Kulkarni, D. A. Frail, and S. G. Djorgovski, "The ERO host galaxy of GRB 020127: implications for the metallicity of GRB progenitors," *The Astrophysical Journal*, vol. 660, no. 1, pp. 504–508, 2007.

[335] D. A. Perley, R. A. Perley, J. Hjorth et al., "Connecting GRBs and ULIRGs: a sensitive, unbiased survey for radio emission from gamma-ray burst host galaxies at $0 < z < 2.5$," *Astrophysical Journal*, vol. 801, no. 2, article 102, 2015.

[336] D. Kocevski, A. A. West, and M. Modjaz, "Modeling the GRB host galaxy mass distribution: are GRBs unbiased tracers of star formation?" *Astrophysical Journal*, vol. 702, no. 1, pp. 377–385, 2009.

[337] J. F. Graham and A. S. Fruchter, "The metal aversion of long-duration gamma-ray bursts," *Astrophysical Journal*, vol. 774, no. 2, article no. 119, 2013.

[338] S. D. Vergani, R. Salvaterra, J. Japelj et al., "Are long gamma-ray bursts biased tracers of star formation? Clues from the host galaxies of the *Swift*/BAT6 complete sample of LGRBs: I. Stellar mass at $z < 1$," *The Astronomy and Astrophysics*, vol. 581, article A102, 2015.

[339] M. Trenti, R. Perna, and R. Jimenez, "The luminosity and stellar mass functions of GRB host galaxies: insight into the metallicity bias," *Astrophysical Journal*, vol. 802, no. 2, article no. 103, 2015.

[340] S. Schulze, R. Chapman, J. Hjorth et al., "The Optically Unbiased GRB Host (TOUGH) Survey. VII. The host galaxy luminosity function: probing the relationship between GRBs and star formation to redshift 6," *The Astrophysical Journal*, vol. 808, p. 73, 2015.

[341] J. F. Graham and A. S. Fruchter, "The relative rate of LGRB formation as a function of metallicity," https://arxiv.org/abs/1511.01079.

[342] P. L. Kelly, A. V. Filippenko, M. Modjaz, and D. Kocevski, "The host galaxies of fast-ejecta core-collapse supernovae," *Astrophysical Journal*, vol. 789, no. 1, article no. 23, 2014.

[343] G. Leloudas, S. Schulze, T. Krühler et al., "Spectroscopy of superluminous supernova host galaxies. A preference of hydrogen-poor events for extreme emission line galaxies," *Monthly Notices of the Royal Astronomical Society*, vol. 449, no. 1, pp. 917–932, 2015.

[344] C. Firmani, V. Avila-Reese, G. Ghisellini, and A. V. Tutukov, "Formation rate, evolving luminosity function, jet structure, and progenitors for long gamma-ray bursts," *Astrophysical Journal*, vol. 611, no. 2 I, pp. 1033–1040, 2004.

[345] P. A. Price and B. P. Schmidt, "Towards measuring the cosmic gamma-ray burst rate," in *Gamma-Ray Bursts: 30 Years of Discovery*, E. Fenimore and M. Galassi, Eds., vol. 727 of *American Institute of Physics Conference Series*, pp. 503–507, 2004.

[346] P. Natarajan, B. Albanna, J. Hjorth, E. Ramirez-Ruiz, N. Tanvir, and R. Wijers, "The redshift distribution of gamma-ray bursts revisited," *Monthly Notices of the Royal Astronomical Society*, vol. 364, no. 1, pp. L8–L12, 2005.

[347] R. Chary, E. Berger, and L. Cowie, "Spitzer observations of gamma-ray burst host galaxies: a unique window into high-redshift chemical evolution and star formation," *The Astrophysical Journal*, vol. 671, no. 1, pp. 272–277, 2007.

[348] J. Greiner, D. B. Fox, P. Schady et al., "Gamma-ray bursts trace uv metrics of star formation over $3 < z < 5$," *Astrophysical Journal*, vol. 809, no. 1, article 76, 2015.

[349] F. Y. Wang and Z. G. Dai, "Long GRBs are metallicity-biased tracers of star formation: evidence from host galaxies and redshift distribution," *The Astrophysical Journal*, vol. 213, no. 1, p. 15, 2014.

[350] J. Japelj, S. D. Vergani, R. Salvaterra et al., "Are LGRBs biased tracers of star formation? Clues from the host galaxies of the Swift/BAT6 complete sample of bright LGRBs. II: star formation rates and metallicities at $z < 1$," *Astronomy & Astrophysics*, vol. 590, article A129, 2016.

[351] L. Christensen, P. M. Vreeswijk, J. Sollerman, C. C. Thöne, E. Le Floc'H, and K. Wiersema, "IFU observations of the GRB 980425/SN 1998bw host galaxy: emission line ratios in GRB regions," *The Astronomy and Astrophysics*, vol. 490, no. 1, pp. 45–59, 2008.

[352] E. Le Floc'H, V. Charmandaris, K. Gordon et al., "The first infrared study of the close environment of a long gamma-ray burst," *The Astrophysical Journal*, vol. 746, no. 1, article 7, 2012.

[353] M. J. Michałowski, L. K. Hunt, E. Palazzi et al., "Spatially-resolved dust properties of the GRB 980425 host galaxy," *Astronomy & Astrophysics*, vol. 562, article A70, 2014.

[354] M. Arabsalmani, S. Roychowdhury, M. A. Zwaan, N. Kanekar, and M. J. Michałowski, "First measurement of H I 21 cm emission from a GRB host galaxy indicates a post-merger system," *Monthly Notices of the Royal Astronomical Society: Letters*, vol. 454, no. 1, pp. L51–L55, 2015.

[355] C. C. Thöne, J. P. U. Fynbo, G. Östlin et al., "Spatially resolved properties of the GRB 060505 host: implications for the nature of the progenitor," *Astrophysical Journal*, vol. 676, no. 2, pp. 1151–1161, 2008.

[356] E. M. Levesque, E. Berger, A. M. Soderberg, and R. Chornock, "Metallicity in the GRB 100316D/SN 2010bh host complex," *The Astrophysical Journal*, vol. 739, no. 1, p. 23, 2011.

[357] E. M. Levesque, R. Chornock, A. M. Soderberg, E. Berger, and R. Lunnan, "Host galaxy properties of the subluminous GRB 120422A/SN 2012bz," *The Astrophysical Journal*, vol. 758, no. 2, article 92, 2012.

[358] J. S. Bloom, S. G. Djorgovski, and S. R. Kulkarni, "The redshift and the ordinary host galaxy of GRB 970228," *Astrophysical Journal*, vol. 554, no. 2, pp. 678–683, 2001.

[359] J. X. Prochaska, H.-W. Chen, and J. S. Bloom, "Dissecting the circumstellar environment of γ-ray burst progenitors," *Astrophysical Journal*, vol. 648, no. 1, pp. 95–110, 2006.

[360] P. M. Vreeswijk, C. Ledoux, A. Smette et al., "Rapid-response mode VLT/UVES spectroscopy of GRB 060418. Conclusive evidence for UV pumping from the time evolution of Fe II and Ni II excited- and metastable-level populations," *Astronomy & Astrophysics*, vol. 468, no. 1, pp. 83–96, 2007.

[361] V. D'Elia, F. Fiore, E. J. A. Meurs et al., "UVES/VLT high resolution spectroscopy of GRB 050730 afterglow: probing the features of the GRB environment," *Astronomy and Astrophysics*, vol. 467, no. 2, pp. 629–639, 2007.

[362] J. P. U. Fynbo, T. Krühler, K. Leighly et al., "The mysterious optical afterglow spectrum of GRB140506A at $z = 0.889$," *Astronomy & Astrophysics*, vol. 572, article A12, 2014.

[363] R. A. Chevalier and Z.-Y. Li, "Wind interaction models for gamma-ray burst afterglows: the case for two types of progenitors," *The Astrophysical Journal*, vol. 536, no. 1, pp. 195–212, 2000.

[364] N. Mirabal, J. P. Halpern, R. Chornock et al., "GRB 021004: a possible shell nebula around a Wolf-Rayet star gamma-ray burst progenitor," *Astrophysical Journal*, vol. 595, no. 2, pp. 935–949, 2003.

[365] R. R. Treffers and Y.-H. Chu, "Galactic ring nebulae associated with Wolf-Rayet stars. V—the stellar wind-blown bubbles," *The Astrophysical Journal*, vol. 254, pp. 569–577, 1982.

[366] J. A. Toalá, M. A. Guerrero, G. Ramos-Larios, and V. Guzmán, "WISE morphological study of Wolf-Rayet nebulae," *The Astronomy and Astrophysics*, vol. 578, article A66, 2015.

[367] S. Schulze, S. Klose, G. Björnsson et al., "The circumburst density profile around GRB progenitors: a statistical study," *Astronomy & Astrophysics*, vol. 526, no. 3, article A23, 2011.

[368] A. J. Van Marie, N. Langer, and G. García-Segura, "Constraints on gamma-ray burst and supernova progenitors through circumstellar absorption lines," *Astronomy and Astrophysics*, vol. 444, no. 3, pp. 837–847, 2005.

[369] A. J. Van Marle, N. Langer, A. Achterberg, and G. García-Segura, "Forming a constant density medium close to long gamma-ray bursts," *Astronomy and Astrophysics*, vol. 460, no. 1, pp. 105–116, 2006.

[370] J. A. Baldwin, M. M. Phillips, and R. Terlevich, "Classification parameters for the emission-line spectra of extragalactic objects," *Publications of the Astronomical Society of the Pacific*, vol. 93, pp. 5–19, 1981.

[371] J. Brinchmann, M. Pettini, and S. Charlot, "New insights into the stellar content and physical conditions of star-forming galaxies at z = 2-3 from spectral modelling," *Monthly Notices of the Royal Astronomical Society*, vol. 385, no. 2, pp. 769–782, 2008.

[372] L. J. Kewley, C. Maier, K. Yabe et al., "The cosmic BPT diagram: confronting theory with observations," *Astrophysical Journal Letters*, vol. 774, no. 1, article no. L10, 2013.

[373] C. C. Steidel, G. C. Rudie, A. L. Strom et al., "Strong nebular line ratios in the spectra of $z \sim 2$-3 star forming galaxies: first results from KBSS-mosfire," *Astrophysical Journal*, vol. 795, no. 2, article 165, 2014.

[374] B. Paczyński, "Are gamma-ray bursts in star-forming regions?" *The Astrophysical Journal*, vol. 494, no. 1, pp. L45–L48, 1998.

[375] J. S. Bloom, S. Sigurdsson, and O. R. Pols, "The spatial distribution of coalescing neutron star binaries: implications for gamma-ray bursts," *Monthly Notices of the Royal Astronomical Society*, vol. 305, no. 4, pp. 763–769, 1999.

[376] C. L. Fryer, S. E. Woosley, and D. H. Hartmann, "Formation rates of black hole accretion disk gamma-ray bursts," *The Astrophysical Journal*, vol. 526, no. 1, pp. 152–177, 1999.

[377] K. Belczyński, T. Bulik, and W. Zbijewski, "Distribution of black hole binaries around galaxies," *Astronomy & Astrophysics*, vol. 355, no. 2, pp. 479–484, 2000.

[378] P. L. Kelly, R. P. Kirshner, and M. Pahre, "Long γ-ray bursts and Type Ic core-collapse supernovae have similar locations in hosts," *Astrophysical Journal*, vol. 687, no. 2, pp. 1201–1207, 2008.

[379] R.-P. Kudritzki and J. Puls, "Winds from hot stars," *Annual Review of Astronomy and Astrophysics*, vol. 38, no. 1, pp. 613–666, 2000.

[380] G. Meynet and A. Maeder, "Stellar evolution with rotation XI. Wolf-Rayet star populations at different metallicities," *Astronomy and Astrophysics*, vol. 429, no. 2, pp. 581–598, 2005.

[381] R. Hirschi, G. Meynet, and A. Maeder, "Yields of rotating stars at solar metallicity," *The Astronomy and Astrophysics*, vol. 433, no. 3, pp. 1013–1022, 2005.

[382] S.-C. Yoon and N. Langer, "Evolution of rapidly rotating metal-poor massive stars towards gamma-ray bursts," *Astronomy and Astrophysics*, vol. 443, no. 2, pp. 643–648, 2005.

[383] S. E. Woosley and A. Heger, "The progenitor stars of gamma-ray bursts," *The Astrophysical Journal*, vol. 637, no. 2, pp. 914–921, 2006.

[384] H. F. Song, G. Meynet, A. Maeder, S. Ekström, and P. Eggenberger, "Massive star evolution in close binaries: conditions for homogeneous chemical evolution," *Astronomy and Astrophysics*, vol. 585, article no. A120, 2016.

[385] I. Hunter, I. Brott, D. J. Lennon et al., "The VLT flames survey of massive stars: rotation and nitrogen enrichment as the key to understanding massive star evolution," *The Astrophysical Journal*, vol. 676, no. 1, p. L29, 2008.

[386] J.-C. Bouret, T. Lanz, D. J. Hillier et al., "Quantitative spectroscopy of O stars at low metallicity: O dwarfs in NGC 346," *The Astrophysical Journal*, vol. 595, no. 2, pp. 1182–1205, 2003.

[387] N. R. Walborn, N. I. Morrell, I. D. Howarth et al., "A CNO dichotomy among O2 giant spectra in the magellanic clouds," *Astrophysical Journal*, vol. 608, no. 2 I, pp. 1028–1038, 2004.

[388] F. Tramper, S. M. Straal, D. Sanyal et al., "Massive stars on the verge of exploding: the properties of oxygen sequence Wolf-Rayet stars," *Astronomy and Astrophysics*, vol. 581, article A110, 2015.

[389] P. Massey, "Massive stars in the local group: implications for stellar evolution and star formation," *Annual Review of Astronomy and Astrophysics*, vol. 41, pp. 15–56, 2003.

[390] B. A. Zauderer, E. Berger, R. Margutti et al., "Illuminating the darkest gamma-ray bursts with radio observations," *The Astrophysical Journal*, vol. 767, no. 2, article 161, 2013.

[391] S. Ekström, C. Georgy, P. Eggenberger et al., "Grids of stellar models with rotation I. Models from 0.8 to 120 $M_\odot$ at solar metallicity ($Z = 0.014$)," *Astronomy and Astrophysics*, vol. 537, article no. A146, 2012.

[392] C. Georgy, S. Ekström, G. Meynet et al., "Grids of stellar models with rotation: II. WR populations and supernovae/GRB progenitors at Z = 0.014," *The Astronomy and Astrophysics*, vol. 542, article A29, 2012.

[393] J. H. Groh, G. Meynet, C. Georgy, and S. Ekström, "Fundamental properties of core-collapse supernova and GRB progenitors: predicting the look of massive stars before death," *Astronomy and Astrophysics*, vol. 558, article no. A131, 2013.

[394] A. Maeder, "Stellar evolution with rotation IX. The effects of the production of asymmetric nebulae on the internal evolution," *Astronomy and Astrophysics*, vol. 392, no. 2, pp. 575–584, 2002.

[395] N. R. Tanvir, A. J. Levan, A. S. Fruchter et al., "A 'kilonova' associated with the short-duration γ-ray burst GRB 130603B," *Nature*, vol. 500, no. 7464, pp. 547–549, 2013.

[396] Z.-P. Jin, X. Li, Z. Cano, S. Covino, Y.-Z. Fan, and D.-M. Wei, "The light curve of the macronova associated with the long-short burst GRB 060614," *Astrophysical Journal Letters*, vol. 811, no. 2, article L22, 2015.

[397] M. Tanaka, K. Hotokezaka, K. Kyutoku et al., "Radioactively powered emission from black hole-neutron star mergers," *Astrophysical Journal*, vol. 780, no. 1, article no. 31, 2014.

[398] D. Kasen, N. R. Badnell, and J. Barnes, "Opacities and spectra of the *r*-process ejecta from neutron star mergers," *The Astrophysical Journal*, vol. 774, no. 1, article 25, 2013.

[399] E. P. Mazets, S. V. Golenetskii, V. N. Il'Inskii et al., "Catalog of cosmic gamma-ray bursts from the KONUS experiment data—parts I and II," *Astrophysics and Space Science*, vol. 80, no. 1, pp. 3–83, 1981.

[400] C. Kouveliotou, C. A. Meegan, G. J. Fishman et al., "Identification of two classes of gamma-ray bursts," *Astrophysical Journal*, vol. 413, no. 2, pp. L101–L104, 1993.

[401] E. Nakar, "Short-hard gamma-ray bursts," *Physics Reports*, vol. 442, no. 1-6, pp. 166–236, 2007.

[402] E. Berger, "Short-duration gamma-ray bursts," *Annual Review of Astronomy and Astrophysics*, vol. 52, pp. 43–105, 2014.

[403] J. Hjorth, J. Sollerman, J. Gorosabel et al., "GRB 050509B: constraints on short gamma-ray burst models," *Astrophysical Journal*, vol. 630, no. 2, pp. L117–L120, 2005.

[404] M. Della Valle, G. Chincarini, N. Panagia et al., "An enigmatic long-lasting γ-ray burst not accompanied by a bright supernova," *Nature*, vol. 444, no. 7122, pp. 1050–1052, 2006.

[405] J. P. Fynbo, D. Watson, C. C. Thöne et al., "No supernovae associated with two long-duration γ-ray bursts," *Nature*, vol. 444, no. 7122, pp. 1047–1049, 2006.

[406] N. Gehrels, J. P. Norris, S. D. Barthelmy et al., "A new γ-ray burst classification scheme from GRB 060614," *Nature*, vol. 444, no. 7122, pp. 1044–1046, 2006.

[407] W. Fong, E. Berger, and D. B. Fox, "Hubble space telescope observations of short gammaray burst host galaxies: morphologies, offsets, and local environments," *Astrophysical Journal*, vol. 708, pp. 9–25, 2010.

[408] W. Fong and E. Berger, "The locations of short gamma-ray bursts as evidence for compact object binary progenitors," *Astrophysical Journal*, vol. 776, no. 1, article 18, 2013.

[409] D. Eichler, M. Livio, T. Piran, and D. N. Schramm, "Nucleosynthesis, neutrino bursts and γ-rays from coalescing neutron stars," *Nature*, vol. 340, no. 6229, pp. 126–128, 1989.

[410] R. Narayan, B. Paczyński, and T. Piran, "Gamma-ray bursts as the death throes of massive binary stars," *The Astrophysical Journal*, vol. 395, no. 2, pp. L83–L86, 1992.

[411] W. H. Lee and E. Ramirez-Ruiz, "The progenitors of short gamma-ray bursts," *New Journal of Physics*, vol. 9, no. 1, p. 1, 2007.

[412] N. Gehrels, C. L. Sarazin, P. T. O'Brien et al., "A short big γ-ray burst apparently associated with an elliptical galaxy at redshift $z = 0.225$," *Nature*, vol. 437, pp. 851–854, 2005.

[413] L.-X. Li and B. Paczyński, "Transient events from neutron star mergers," *Astrophysical Journal*, vol. 507, no. 1, 1998.

[414] S. R. Kulkarni, "Modeling supernova-like explosions associated with gamma-ray bursts with short durations," https://arxiv.org/abs/astro-ph/0510256.

[415] S. Rosswog, "Mergers of neutron star-black hole binaries with small mass ratios: nucleosynthesis, gamma-ray bursts, and electromagnetic transients," *The Astrophysical Journal*, vol. 634, no. 2, pp. 1202–1213, 2005.

[416] B. D. Metzger, G. Martínez-Pinedo, S. Darbha et al., "Electromagnetic counterparts of compact object mergers powered by the radioactive decay of r-process nuclei," *Monthly Notices of the Royal Astronomical Society*, vol. 406, no. 4, pp. 2650–2662, 2010.

[417] B. D. Metzger and E. Berger, "What is the most promising electromagnetic counterpart of a neutron star binary merger?" *Astrophysical Journal*, vol. 746, no. 1, article no. 48, 2012.

[418] M. Tanaka, "Kilonova/macronova emission from compact binary mergers," *Advances in Astronomy*, vol. 2016, Article ID 6341974, 12 pages, 2016.

[419] J. M. Lattimer and D. N. Schramm, "Black-hole-neutron-star collisions," *The Astrophysical Journal*, vol. 192, pp. L145–L147, 1974.

[420] S. E. Woosley, J. R. Wilson, G. J. Mathews, R. D. Hoffman, and B. S. Meyer, "The r-process and neutrino-heated supernova ejecta," *The Astrophysical Journal*, vol. 433, no. 1, pp. 229–246, 1994.

[421] C. Freiburghaus, S. Rosswog, and F.-K. Thielemann, "R-process in neutron star mergers," *Astrophysical Journal*, vol. 525, no. 2, pp. L121–L124, 1999.

[422] J. Lippuner and L. F. Roberts, "R-process lanthanide production and heating rates in kilonovae," *The Astrophysical Journal*, vol. 815, article 82, 2015.

[423] B. D. Metzger and R. Fernández, "Red or blue? A potential kilonova imprint of the delay until black hole formation following a neutron star merger," *Monthly Notices of the Royal Astronomical Society*, vol. 441, no. 4, pp. 3444–3453, 2014.

[424] J. Hjorth, D. Watson, J. P. U. Fynbo et al., "The optical afterglow of the short γ-ray burst GRB 050709," *Nature*, vol. 437, no. 7060, pp. 859–861, 2005.

[425] Z.-P. Jin, K. Hotokezaka, X. Li et al., "The Macronova in GRB 050709 and the GRB-macronova connection," *Nature Communications*, vol. 7, Article ID 12898, 2016.

[426] A. M. Soderberg, E. Berger, M. Kasliwal et al., "The afterglow, energetics, and host galaxy of the short-hard gamma-ray burst 051221a," *Astrophysical Journal*, vol. 650, no. 1 I, pp. 261–271, 2006.

[427] B. Yang, Z.-P. Jin, X. Li et al., "A possible macronova in the late afterglow of the long-short burst GRB 060614," *Nature Communications*, vol. 6, article no. 7323, 2015.

[428] E. Berger, S. B. Cenko, D. B. Fox, and A. Cucchiara, "Discovery of the very red near-infrared and optical afterglow of the short-duration GRB 070724A," *Astrophysical Journal*, vol. 704, no. 1, pp. 877–882, 2009.

[429] D. Kocevski, C. C. Thöne, E. Ramirez-Ruiz et al., "Limits on radioactive powered emission associated with a short-hard GRB 070724A in a star-forming galaxy," *Monthly Notices of the Royal Astronomical Society*, vol. 404, no. 2, pp. 963–974, 2010.

[430] D. A. Perley, B. D. Metzger, J. Granot et al., "GRB 080503: implications of a naked short gamma-ray burst dominated by extended emission," *Astrophysical Journal*, vol. 696, no. 2, pp. 1871–1885, 2009.

[431] H. Gao, X. Ding, X.-F. Wu, Z.-G. Dai, and B. Zhang, "GRB 080503 late afterglow re-brightening: signature of a magnetar-powered merger-nova," *Astrophysical Journal*, vol. 807, no. 2, 2015.

[432] A. Rowlinson, K. Wiersema, A. J. Levan et al., "Discovery of the afterglow and host galaxy of the low-redshift short GRB 080905A," *Monthly Notices of the Royal Astronomical Society*, vol. 408, no. 1, pp. 383–391, 2010.

[433] E. Berger, W. Fong, and R. Chornock, "An r-process kilonova associated with the short-hard GRB 130603B," *Astrophysical Journal Letters*, vol. 774, no. 2, article no. L23, 2013.

[434] T. Piran, "The physics of gamma-ray bursts," *Reviews of Modern Physics*, vol. 76, no. 4, pp. 1143–1210, 2004.

[435] V. V. Uso, "Millisecond pulsars with extremely strong magnetic fields as a cosmological source of γ-ray bursts," *Nature*, vol. 357, no. 6378, pp. 472–474, 1992.

[436] N. Bucciantini, E. Quataert, J. Arons, B. D. Metzger, and T. A. Thompson, "Relativistic jets and long-duration gamma-ray bursts from the birth of magnetars," *Monthly Notices of the Royal Astronomical Society: Letters*, vol. 383, no. 1, pp. L25–L29, 2008.

[437] B. D. Metzger, D. Giannios, T. A. Thompson, N. Bucciantini, and E. Quataert, "The protomagnetar model for gamma-ray bursts," *Monthly Notices of the Royal Astronomical Society*, vol. 413, no. 3, pp. 2031–2056, 2011.

[438] M. J. Rees and P. Mészáros, "Unsteady outflow models for cosmological γ-ray bursts," *The Astrophysical Journal*, vol. 430, no. 2, pp. L93–L96, 1994.

[439] P. Mészáros, "Gamma-ray bursts: accumulating afterglow implications, progenitor clues, and prospects," *Science*, vol. 291, no. 5501, pp. 79–84, 2001.

[440] R. Sari, T. Piran, and R. Narayan, "Spectra and light curves of γ-ray burst afterglows," *The Astrophysical Journal*, vol. 497, no. 1, pp. L17–L20, 1998.

[441] S. Hümmer, P. Baerwald, and W. Winter, "Neutrino emission from gamma-ray burst fireballs, revised," *Physical Review Letters*, vol. 108, no. 23, Article ID 231101, 2012.

[442] Z. Li, "Note on the normalization of predicted gamma-ray burst neutrino flux," *Physical Review D*, vol. 85, no. 2, Article ID 027301, 2012.

[443] H.-N. He, R.-Y. Liu, X.-Y. Wang, S. Nagataki, K. Murase, and Z.-G. Dai, "Icecube nondetection of gamma-ray bursts: constraints on the fireball properties," *Astrophysical Journal*, vol. 752, article 29, 2012.

[444] E.-W. Liang, S.-X. Yi, J. Zhang, H.-J. Lü, B.-B. Zhang, and B. Zhang, "Constraining γ-ray burst initial lorentz factor with the afterglow onset feature and discovery of a tight Γ0-E γ, iso correlation," *The Astrophysical Journal*, vol. 725, no. 2, pp. 2209–2224, 2010.

[445] G. Ghirlanda, L. Nava, G. Ghisellini et al., "Gamma-ray bursts in the comoving frame," *Monthly Notices of the Royal Astronomical Society*, vol. 420, no. 1, pp. 483–494, 2012.

[446] J. Lü, Y.-C. Zou, W.-H. Lei et al., "Lorentz-factor-isotropic-luminosity/energy correlations of gamma-ray bursts and their interpretation," *Astrophysical Journal*, vol. 751, no. 1, article no. 49, 2012.

[447] A. Pe'er and F. Ryde, "A theory of multicolor blackbody emission from relativistically expanding plasmas," *The Astrophysical Journal*, vol. 732, no. 1, article 49, 2011.

[448] C. Lundman, A. Pe'er, and F. Ryde, "A theory of photospheric emission from relativistic, collimated outflows," *Monthly Notices of the Royal Astronomical Society*, vol. 428, no. 3, pp. 2430–2442, 2013.

[449] H. Ito, J. Matsumoto, S. Nagataki, D. C. Warren, and M. V. Barkov, "Photospheric emission from collapsar jets in 3D relativistic hydrodynamics," *Astrophysical Journal Letters*, vol. 814, no. 2, article no. L29, 2015.

[450] R. Santana, P. Crumley, R. A. Hernández, and P. Kumar, "Monte carlo simulations of the photospheric process," *Monthly Notices of the Royal Astronomical Society*, vol. 456, no. 1, pp. 1049–1065, 2016.

[451] A. Pe'er and F. Ryde, "Photospheric emission in gamma-ray bursts," https://arxiv.org/abs/1603.05058.

[452] B. Zhang and H. Yan, "The internal-collision-induced magnetic reconnection and turbulence (ICMART) model of gamma-ray bursts," *The Astrophysical Journal*, vol. 726, article 90, 2011.

[453] W. Deng, H. Zhang, B. Zhang, and H. Li, "Collision-induced magnetic reconnection and a unified interpretation of polarization properties of GRBs and blazars," *Astrophysical Journal Letters*, vol. 821, no. 1, article no. L12, 2016.

[454] B. Paczynski, "Gamma-ray bursters at cosmological distances," *The Astrophysical Journal*, vol. 308, pp. L43–L46, 1986.

[455] C. Thompson, "A model of gamma-ray bursts," *Monthly Notices of the Royal Astronomical Society*, vol. 270, no. 3, pp. 480–498, 1994.

[456] P. Mészáros and M. J. Rees, "Steep slopes and preferred breaks in γ-ray burst spectra: the role of photospheres and comptonization," *The Astrophysical Journal*, vol. 530, no. 1, pp. 292–298, 2000.

[457] S. A. Colgate, "Prompt gamma rays and X rays from supernovae," *Canadian Journal of Physics*, vol. 46, no. 10, pp. S476–S480, 1968.

[458] S. A. Colgate, "Early gamma rays from supernovae," *The Astrophysical Journal*, vol. 187, pp. 333–336, 1974.

[459] R. I. Klein and R. A. Chevalier, "X-ray bursts from Type II supernovae," *The Astrophysical Journal Letters*, vol. 223, pp. L109–L112, 1978.

[460] S. W. Falk, "Shock steepening and prompt thermal emission in supernovae," *The Astrophysical Journal Letters*, vol. 225, pp. L133–L136, 1978.

[461] L. Ensman and A. Burrows, "Shock breakout in SN 1987A," *Astrophysical Journal*, vol. 393, no. 2, pp. 742–755, 1992.

[462] X.-Y. Wang, Z. Li, E. Waxman, and P. Mészáros, "Nonthermal γ-ray/x-ray flashes from shock breakout in γ-ray burst-associated supernovae," *The Astrophysical Journal*, vol. 664, no. 2 I, pp. 1026–1032, 2007.

[463] C. D. Matzner, Y. Levin, and S. Ro, "Oblique shock breakout in supernovae and gamma-ray bursts. I. Dynamics and observational implications," *Astrophysical Journal*, vol. 779, no. 1, article no. 60, 2013.

[464] R. Barniol Duran, E. Nakar, T. Piran, and R. Sari, "The afterglow of a relativistic shock breakout and low-luminosity GRBs," *Monthly Notices of the Royal Astronomical Society*, vol. 448, pp. 417–428, 2015.

[465] K. Schawinski, S. Justham, C. Wolf et al., "Supernova shock breakout from a red supergiant," *Science*, vol. 321, no. 5886, pp. 223–226, 2008.

[466] S. Gezari, D. O. Jones, N. E. Sanders et al., "Galex detection of shock breakout in type IIP supernova PS1-13arp: implications for the progenitor star wind," *The Astrophysical Journal*, vol. 804, no. 1, p. 28, 2015.

[467] P. M. Garnavich, B. E. Tucker, A. Rest et al., "Shock breakout and early light curves of type II-P supernovae observed with *Kepler*," *Astrophysical Journal*, vol. 820, no. 1, 2016.

[468] A. Heger, C. L. Fryer, S. E. Woosley, N. Langer, and D. D. H. Hartmann, "How massive single stars end their life," *The Astrophysical Journal*, vol. 591, no. 1, pp. 288–300, 2003.

[469] R. A. Chevalier, "Common envelope evolution leading to supernovae with dense interaction," *Astrophysical Journal Letters*, vol. 752, no. 1, article L2, 2012.

[470] W. Zhang and C. L. Fryer, "The merger of a helium star and a black hole: gamma-ray bursts," *The Astrophysical Journal*, vol. 550, no. 1, pp. 357–367, 2001.

[471] C. L. Fryer and A. Heger, "Binary merger progenitors for gamma-ray bursts and hypernovae," *The Astrophysical Journal*, vol. 623, no. 1, pp. 302–313, 2005.

[472] M. M. Shara, S. M. Crawford, D. Vanbeveren, A. F. Moffat, D. Zurek, and L. Crause, "The spin rates of O stars in WR + O binaries – I. Motivation, methodology, and first results from SALT," *Monthly Notices of the Royal Astronomical Society*, vol. 464, no. 2, pp. 2066–2074, 2016.

[473] P. Podsiadlowski, N. Ivanova, S. Justham, and S. Rappaport, "Explosive common-envelope ejection: implications for γ-ray bursts and low-mass black-hole binaries," *Monthly Notices of the Royal Astronomical Society*, vol. 406, no. 2, pp. 840–847, 2010.

[474] H. Sana, S. E. de Mink, A. de Koter et al., "Binary interaction dominates the evolution of massive stars," *Science*, vol. 337, no. 6093, pp. 444–446, 2012.

[475] T. Linden, V. Kalogera, J. F. Sepinsky, A. Prestwich, A. Zezas, and J. S. Gallagher, "The effect of starburst metallicity on bright X-ray binary formation pathways," *The Astrophysical Journal*, vol. 725, no. 2, pp. 1984–1994, 2010.

[476] K. F. Neugent and P. Massey, "The close binary frequency of wolf-Rayet stars as a function of metallicity in M31 and M33," *Astrophysical Journal*, vol. 789, no. 1, article no. 10, 2014.

[477] N. Smith, W. Li, A. V. Filippenko, and R. Chornock, "Observed fractions of core-collapse supernova types and initial masses of their single and binary progenitor stars," *Monthly Notices of the Royal Astronomical Society*, vol. 412, no. 3, pp. 1522–1538, 2011.

[478] S. J. Smartt, "Progenitors of core-collapse supernovae," *Annual Review of Astronomy and Astrophysics*, vol. 47, pp. 63–106, 2009.

[479] J. J. Eldridge, M. Fraser, S. J. Smartt, J. R. Maund, and R. Mark Crockett, "The death of massive stars—II. Observational constraints on the progenitors of type Ibc supernovae," *Monthly Notices of the Royal Astronomical Society*, vol. 436, no. 1, pp. 774–795, 2013.

[480] Q. E. Goddard, N. Bastian, and R. C. Kennicutt, "On the fraction of star clusters surviving the embedded phase," *Monthly Notices of the Royal Astronomical Society*, vol. 405, no. 2, pp. 857–869, 2010.

[481] E. Silva-Villa, A. Adamo, and N. Bastian, "A variation of the fraction of stars that form in bound clusters within M83," *Monthly Notices of the Royal Astronomical Society*, vol. 436, pp. L69–L73, 2013.

[482] P. G. van Dokkum and C. Conroy, "A substantial population of low-mass stars in luminous elliptical galaxies," *Nature*, vol. 468, no. 7326, pp. 940–942, 2010.

[483] C. Conroy and P. G. Van Dokkum, "The stellar initial mass function in early-type galaxies from absorption line spectroscopy. II. Results," *Astrophysical Journal*, vol. 760, no. 1, article no. 71, 2012.

[484] F. Hammer, H. Flores, D. Schaerer, M. Dessauges-Zavadsky, E. Le Floc'h, and M. Puech, "Detection of Wolf-Rayet stars in host galaxies of gamma-ray bursts (GRBs): are GRBs produced by runaway massive stars ejected from high stellar density regions?" *Astronomy and Astrophysics*, vol. 454, no. 1, pp. 103–111, 2006.

[485] J. J. Eldridge, N. Langer, and C. A. Tout, "Runaway stars as progenitors of supernovae and gamma-ray bursts," *Monthly Notices of the Royal Astronomical Society*, vol. 414, no. 4, pp. 3501–3520, 2011.

[486] N. Yadav, D. Mukherjee, P. Sharma, and B. B. Nath, "Supernovae under microscope: how supernovae overlap to form superbubbles," https://arxiv.org/abs/1603.00815.

[487] P. A. Crowther, O. Schnurr, R. Hirschi et al., "The R136 star cluster hosts several stars whose individual masses greatly exceed the accepted 150 M. stellar mass limit," *Monthly Notices of the Royal Astronomical Society*, vol. 408, no. 2, pp. 731–751, 2010.

[488] P. A. Crowther, S. M. Caballero-Nieves, K. A. Bostroem et al., "The R136 star cluster dissected with Hubble Space Telescope/STIS. I. Far-ultraviolet spectroscopic census and the origin of He II λ1640 in young star clusters," *Monthly Notices of the Royal Astronomical Society*, vol. 458, no. 1, pp. 624–659, 2016.

[489] P. Podsiadlowski, P. C. Joss, and J. J. L. Hsu, "Presupernova evolution in massive interacting binaries," *Astrophysical Journal*, vol. 391, no. 1, pp. 246–264, 1992.

[490] C. J. Burrows, J. Krist, J. J. Hester et al., "Hubble space telescope observations of the SN 1987A triple ring nebula," *The Astrophysical Journal*, vol. 452, no. 2, p. 680, 1995.

[491] G. Sonneborn, C. Fransson, P. Lundqvist et al., "The evolution of ultraviolet emission lines from circumstellar material surrounding SN 1987A," *The Astrophysical Journal*, vol. 477, no. 2, pp. 848–864, 1997.

[492] P. Podsiadlowski, J. J. L. Hsu, P. C. Joss, and R. R. Ross, "The progenitor of supernova 1993J: a stripped supergiant in a binary system?" *Nature*, vol. 364, no. 6437, pp. 509–511, 1993.

[493] S. E. Woosley, R. G. Eastman, T. A. Weaver, and P. A. Pinto, "SN 1993J: a type IIb supernova," *Astrophysical Journal*, vol. 429, no. 1, pp. 300–318, 1994.

[494] J. R. Maund, S. J. Smartt, R. P. Kudritzki, P. Podsiadlowski, and G. F. Gilmore, "The massive binary companion star to the progenitor of supernova 1993J," *Nature*, vol. 427, no. 6970, pp. 129–131, 2004.

[495] O. D. Fox, K. Azalee Bostroem, S. D. Van Dyk et al., "Uncovering the putative B-star binary companion of the SN 1993J progenitor," *The Astrophysical Journal*, vol. 790, no. 1, p. 17, 2014.

[496] D. A. Kann, P. Schady, F. Olivares et al., "Highly Luminous Supernovae associated with Gamma-Ray Bursts I.: GRB 111209A/SN 2011kl in the Context of Stripped-Envelope and Superluminous Supernovae," https://arxiv.org/abs/1606.06791.

[497] I. Arcavi, W. M. Wolf, D. A. Howell et al., "Rapidly rising transients in the supernova—superluminous supernova gap," *Astrophysical Journal*, vol. 819, no. 1, article no. 35, 2016.

[498] N. E. Sanders, A. M. Soderberg, S. Valenti et al., "SN 2010ay is a luminous and broad-lined type ic supernova within a low-metallicity host galaxy," *The Astrophysical Journal*, vol. 756, no. 2, article 184, 2012.

[499] S. Q. Wang, L. J. Wang, Z. G. Dai, and X. F. Wu, "A unified energy-reservoir model containing contributions from 56Ni and neutron stars and its implication for luminous type Ic supernovae," *The Astrophysical Journal*, vol. 807, no. 2, p. 147, 2015.

[500] A. Lien, T. Sakamoto, S. D. Barthelmy et al., "The third swift burst alert telescope gamma-ray burst catalog," *The Astrophysical Journal*, vol. 829, no. 1, article 7, 2016.

[501] M. Demleitner, A. Accomazzi, G. Eichhorn et al., "ADS's dexter data extraction applet," in *Astronomical Data Analysis Software and Systems X*, F. R. Harnden Jr., F. A. Primini, and H. E. Payne, Eds., vol. 238 of *Astronomical Society of the Pacific Conference Series*, p. 321, 2001.

[502] O. Yaron and A. Gal-Yam, "WISeREP-an interactive supernova data repository," *Publications of the Astronomical Society of the Pacific*, vol. 124, no. 917, pp. 668–681, 2012.

Hindawi Publishing Corporation
Advances in Astronomy
Volume 2016, Article ID 2967813, 13 pages
http://dx.doi.org/10.1155/2016/2967813

Review Article

Gamma-Ray Bursts: A Radio Perspective

Poonam Chandra

National Centre for Radio Astrophysics, Tata Institute of Fundamental Research, Pune University Campus, P.O. Box 3, Pune 411007, India

Correspondence should be addressed to Poonam Chandra; poonam@ncra.tifr.res.in

Received 13 July 2016; Revised 28 September 2016; Accepted 10 October 2016

Academic Editor: WeiKang Zheng

Gamma-ray bursts (GRBs) are extremely energetic events at cosmological distances. They provide unique laboratory to investigate fundamental physical processes under extreme conditions. Due to extreme luminosities, GRBs are detectable at very high redshifts and potential tracers of cosmic star formation rate at early epoch. While the launch of *Swift* and *Fermi* has increased our understanding of GRBs tremendously, many new questions have opened up. Radio observations of GRBs uniquely probe the energetics and environments of the explosion. However, currently only 30% of the bursts are detected in radio bands. Radio observations with upcoming sensitive telescopes will potentially increase the sample size significantly and allow one to follow the individual bursts for a much longer duration and be able to answer some of the important issues related to true calorimetry, reverse shock emission, and environments around the massive stars exploding as GRBs in the early Universe.

1. Introduction

Gamma-ray bursts (GRBs) are nonrecurring bright flashes of γ-rays lasting from seconds to minutes. As we currently understand, in the standard GRB model a compact central engine is responsible for accelerating and collimating the ultra-relativistic jet-like outflows. The isotropic energy release in prompt γ-rays ranges from $\sim 10^{48}$ to $\sim 10^{54}$ ergs; see, for example, [1]. While the prompt emission spectrum is mostly nonthermal, presence of thermal or quasithermal components has been suggested for a handful of bursts [2]. Since the initial discovery of GRBs [3] till the discovery of GRB afterglows at X-ray, optical, and radio wavelengths three decades later [4–7], the origin of GRBs remained elusive. The afterglow emission confirmed that GRBs are cosmological in origin, ruling out multiple theories proposed favouring Galactic origin of GRBs; see, for example, [8].

In the *BATSE* burst population, the durations of GRBs followed bimodal distribution, short GRBs with duration less than 2 s and long GRBs lasting for more than 2 s [9]. Long GRBs are predominantly found in star forming regions of late type galaxies [10], whereas short bursts are seen in all kinds of galaxies [11]. Based on these evidences, the current understanding is that the majority of long GRBs originate in the gravitational collapse of massive stars [12], whereas at least a fraction of short GRBs form as a result of the merger of compact object binaries (see Berger [13] for a detailed review).

GRBs are detectable at very high redshifts. The highest redshift GRB is GRB 090429B with a photometric redshift of $z = 9.4$ [14]. However, the farthest known spectroscopically confirmed GRB is GRB 090423 at a redshift of $z = 8.23$ [15], indicating star formation must be taking place at such early epoch in the Universe [16]. At the same time, some GRBs at lower redshifts have revealed association with type Ib/c broad lined supernovae, for example, GRB 980425 associated with SN 1998bw [17].

Since the launch of the *Swift* satellite in November 2004 [18], the field of GRB has undergone a major revolution. Burst Alert Telescope (BAT) [19] on-board *Swift* has been localizing ~100 GRBs per year [20]. X-ray Telescope (XRT [21]) and Ultraviolet/Optical Telescope (UVOT [22]) on-board *Swift* slew towards the BAT localized position within minutes and provide uninterrupted detailed light curve at these bands. Before the launch of the *Swift*, due to the lack of dedicated instruments at X-ray and optical bands the afterglow coverage was sparse, which is no longer the case. *Swift*-XRT has revealed that central engine is capable of injecting energy into the forward shock at late times [23–25].

GRBs are collimated events. An achromatic jet break seen in all frequencies is an undisputed signature of it. However,

the jet breaks are seen only in a few *Swift* bursts, for example, GRB 090426 [26], GRB 130603B [27], and GRB 140903A [28]. Many of the bursts have not shown jet breaks. It could be because *Swift* is largely detecting fainter bursts with an average redshift of >2, much larger than the detected by previous instruments [20]. The faintness of the bursts makes it difficult to see jet breaks. Some of the GRBs have also revealed chromatic jet breaks, for example, GRB 070125 [29].

An additional issue is the narrow coverage of the *Swift*-BAT in 15–150 keV range. Due to the narrow bandpass, the uncertainties associated in energetics are much larger since one needs to extrapolate to 1–10,000 keV bandpass to estimate the $E_{\rm iso}$, which is a key parameter to evaluate the total released energy and other relations. Due to this constraint, it has been possible to catch only a fraction of traditional GRBs.

The *Swift* drawback was overcome by the launch of *Fermi* in 2008, providing observation over a broad energy range of over seven decades in energy coverage (8 keV–300 GeV). Large Area Telescope (LAT [30]) on-board *Fermi* is an imaging gamma-ray detector in 20 MeV–300 GeV range with a field of view of about 20% of the sky and Gamma-ray Burst Monitor (GBM) [31] on-board *Fermi* works in 150 keV–30 MeV and can detect GRBs across the whole of the sky. The highest energy photon detected from a GRB puts a stricter lower limit on the outflow Lorentz factor. *Fermi* has provided useful constraints on the initial Lorentz factor owing to its high energy coverage, for example, short GRB 090510 [32]. This is because to avoid pair production, the GRB jet must be moving towards the observer with ultra-relativistic speeds. Some of the key observations by *Fermi* had been (i) the delayed onset of high energy emission for both long and short GRBs [33–35], (ii) long lasting LAT emission [36], (iii) very high Lorentz factors (~1000) inferred for the detection of LAT high energy photons [33], (iv) significant detection of multiple emission components such as thermal component in several bright bursts [37–39], and (v) power-law [35] or spectral cut-off at high energies [40], in addition to the traditional band function [41].

While the GRB field has advanced a lot after nearly 5 decades of extensive research since the first discovery, there are many open questions about prompt emission, content of the outflow, afterglow emission, microphysics involved, detectability of the afterglow emission, and so forth. Resolving them would enable us to understand GRBs in more detail and also use them to probe the early Universe as they are detectable at very high redshifts. With the recent discoveries of gravitational waves (GWs) [42, 43], a new era of Gravitational Wave Astronomy has opened. GWs are ideal to probe short GRBs as they are the most likely candidates of GW sources with earth based interferometers.

In this paper, we aim to understand the GRBs with a radio perspective. Here we focus on limited problems which can be answered with more sensitive and extensive radio observations and modeling. By no means, this review is exhaustive in nature. In Section 2, we review the radio afterglow in general and out current understanding. In Section 3, we discuss some of the open issues in GRB radio afterglows. Section 4 lists the conclusion.

2. Afterglow Physics: A Radio Perspective and Some Milestones

In the standard afterglow emission model, the relativistic ejecta interacting with the circumburst medium gives rise to a forward shock moving into the ambient circumburst medium and a reverse shock going back into the ejecta. The jet interaction with the circumburst medium gives rise to mainly synchrotron emission in X-ray, optical, and radio bands. The peak of the spectrum moves from high to low observing frequencies over time due to the deceleration of the forward shock [44] (e.g., see Figure 1). Because of the relativistic nature of the ejecta, the spectral peak is typically below optical frequencies when the first observations commence, resulting in declining light curves at optical and X-ray frequencies. However, optically rising light curve has been seen in a handful of bursts after the launch of the *Swift* [45], for example, GRB 060418 [46].

The first radio afterglow was detected from GRB 970508 [7]. Since then the radio studies of GRB afterglows have increased our understanding of the afterglows significantly, for example, [47–49]. A major advantage of radio afterglow emission is that, due to slow evolution, it peaks in much later time and lasts longer, for months or even years (e.g., [50–52]). Thus unlike short-lived optical or X-ray afterglows, radio observations present the possibility of following the full evolution of the fireball emission from the very beginning till the nonrelativistic phase (see, e.g., [50–52]); also see GRB 030329 [53, 54]. Therefore, the radio regime plays an important role in understanding the full broadband spectrum. This constrains both the macrophysics of the jet, that is, the energetics and the circumburst medium density, as well as the microphysics, such as energy imparted in electrons and magnetic fields necessary for synchrotron emission [55]. Some of the phenomena routinely addressed through radio observations are interstellar scintillation, synchrotron self-absorption, forward shocks, reverse shocks, jet breaks, nonrelativistic transitions, and obscured star formation.

The inhomogeneities in the local interstellar medium manifest themselves in the form of interstellar scintillations and cause modulations in the radio flux density of a point source whose angular size is less than the characteristic angular size for scintillations [56]. GRBs are compact objects and one can see the signatures of interstellar scintillation at early time radio observations, when the angular size of the fireball is smaller than the characteristic angular scale for interstellar scintillation. This reflects influx modulations seen in the radio observations. Eventually due to relativistic expansion, the fireball size exceeds the characteristic angular scale for scintillations and the modulations quench. This can be utilised in determining the source size and the expansion speed of the blast wave [7]. In GRB 970508 and GRB 070125, the initial radio flux density fluctuations were interpreted as interstellar scintillations, which lead to an estimation of the upper limit on the fireball size [7, 29, 57]. In GRB 070125, the scintillation time scale and modulation intensity were consistent with those of diffractive scintillations, putting a tighter constraint on the fireball size [29].

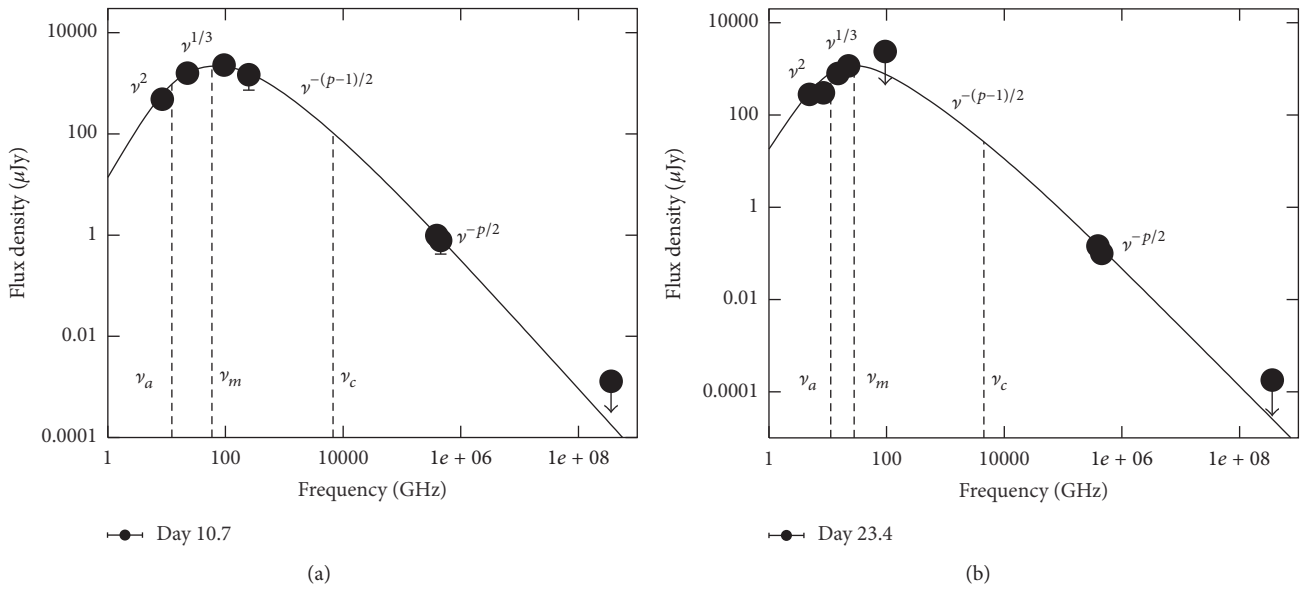

Figure 1: Multiwaveband spectra of GRB 070125 on day 10.7 and day 23.4. The spectra are in fast cooling regime. One can see that, between the spectra on day 10.7 and day 23.4, the peak has shifted to lower frequency. The figure is reproduced from Chandra et al. [29].

Very Long Baseline Interferometry (VLBI) radio observations also play a key role by providing evidence for the relativistic expansion of the jet using for bright GRBs. This provides microarcsecond resolution and directly constrains the source size and its evolution. So far this has been possible for a nearby ($z = 0.16$) GRB 030329 [58]. In this case, the source size measurements were combined with its long term light curves to better constrain the physical parameters [53, 54]. In addition, GRB 030329 also provided the first spectroscopic evidence for association of a GRB with a supernova. This confirmed massive stars origin of at least a class of GRBs.

Radio observations are routinely used in broadband modeling of afterglows and used to derive blast-wave parameters [1, 29, 59–61] (also see Figure 1). Early radio emission is synchrotron self-absorbed; radio observations uniquely constrain the density of the circumburst medium. Radio studies have also proven useful for inferring the opening angles of the GRB jets as their observational signature differs from those at higher wavelengths [50, 62–64]. Recently GRB 130427A, a nearby, high-luminosity event, was followed at all wavebands rigorously. It provided extremely good temporal (over 10 orders of magnitude) and spectral coverage (16 orders of magnitude in observing frequency [65, 66]). Radio observations started as early as 8 hours [67]. One witnessed reverse shock and its peak moving from high to low radio frequencies over time [67–70]. The burst is an ideal example to show how early to late-time radio observations can contribute significantly to our understanding of the physics of both the forward and reverse shocks.

Radio afterglows can be detected at high redshifts [16, 71] owing to the negative k-correction effect [72]. GRB 090423 at a redshift of 8.3 is the highest redshift (spectroscopically confirmed) known object in the Universe [15]. It was detected in radio bands for several tens of days [16]. The multiwaveband modeling indicated the $n\,1\,\mathrm{cm}^{-3}$ density medium and the massive star origin of the GRB. This suggested that the star formation was taking place even at a redshift of 8.3.

The radio afterglow, due to its long-lived nature, is able to probe the time when the jet expansion has become subrelativistic and geometry has become quasispherical [50, 52, 73] and thus can constrain energetics independent of geometry. This is possible only in radio bands as it lasts for months or even years (e.g., [50–52]). GRB 970508 remained bright more than a year after the discovery, when the ejecta had reached subrelativistic speeds. This gave the most accurate estimate of the kinetic energy of the burst [50].

Reverse shock probes the ejecta and thus can potentially put constraints on the Lorentz factor and contents of the jet (e.g., [68, 69]). The shock moving into the ejecta will result in an optical flash in the first tens of seconds after the GRB under right conditions. The radio regime is also well suited to probe the reverse shock emission as well. Short-lived radio flares, most likely due to reverse shock, have also been detected from radio observations [16, 74–76] and seem more common in radio bands than in the optical bands. GRB 990123 was the first GRB in which the reverse shock was detected in optical [77] as well as in radio bands [74].

From the radio perspective, GRB 030329 holds a very important place. It was the first high-luminosity burst at low redshift with a spectroscopic confirmation of a supernova associated with it. So far this is the only GRB for which the source size has been measured with VLBI. The radio afterglow of GRB 030329 was bright and long lasting and has been detected for almost a decade at radio frequencies [52, 78]. This enabled one to perform broadband modeling in the different phases and has led to tighter constraints on the physical parameters [53, 54]. However, the absence of a counter

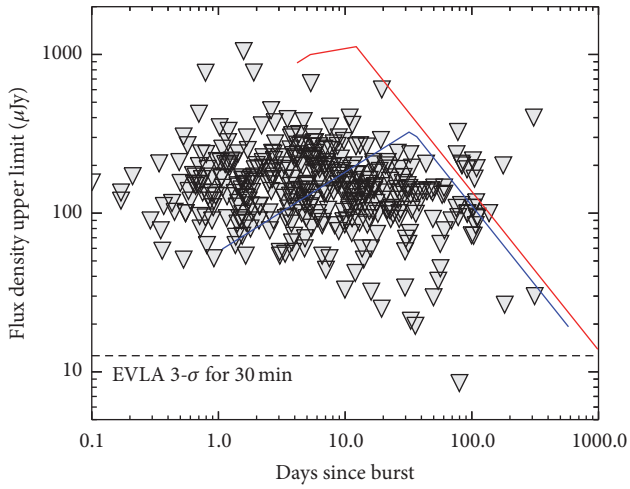

FIGURE 2: Plot of 3-σ upper limits at 8.5 GHz frequency band for all GRBs for which no afterglow was detected. The red line shows light curve of a rare, bright event GRB 980703 and the blue line shows the light curve of a more typical event GRB 980329. The detection fraction of radio afterglows in the first 10 days certainly appears to be mainly limited by the sensitivity. The black dashed line indicates 3-σ sensitivity of the JVLA in its full capacity for a 30-minute integration time. The figure is reproduced from [48].

jet poses serious question in our understanding of GRBs [79].

3. Open Problems in GRB Radio Afterglows

With various high sensitivity new and refurbished telescopes, for example, Atacama Large Millimetre Array (ALMA), Karl J. Jansky Very Large Array (JVLA), upgraded Giant Metrewave Radio Telescope (uGMRT), and upcoming telescopes, for example, Square Kilometre Array (SKA), the radio afterglow physics of GRBs is entering into new era, where we can begin to answer some of the open questions in the field, answers to which are long awaited. In this section, I discuss only some of those open problems in GRB science where radio measurements can play a crucial role.

This review is not expected to be exhaustive. We concentrate on only a few major issues.

3.1. Are GRBs Intrinsically Radio Weak? Since the launch of the *Swift*, the fractions of X-ray and optically detected afterglows have increased tremendously; that is, almost 93% of GRBs have a detected X-ray afterglow [80] and ~75% have detected optical afterglows [81, 82]. However, what is disconcerting is that the radio detection fraction has remained unchanged with only one-third of all GRBs being detected in radio bands [47, 48]. Chandra and Frail [48] attributed it to sensitivity limitation of the current telescopes (see Figure 2). This is because radio detected GRBs have flux densities typically ranging from a few tens of μJy to a few hundreds of μJy [48]. Even the largest radio telescopes have had the sensitivities close to a few tens of μJy, making the radio afterglow detection sensitivity limited. The newer generation radio telescopes should dramatically improve statistics of radio afterglows. For example, using numerical simulation of the forward shock, Burlon et al. [83] predict that the SKA-1 (SKA first phase) Mid band will be able to detect around 400–500 radio afterglows per $\mathrm{sr}^{-1}\ \mathrm{yr}^{-1}$.

The Five-hundred-meter Aperture Spherical radio Telescope (FAST) [84–86] is the largest worldwide single-dish radio telescope, being built in Guizhou province of China with an expected first light in Sep. 2016. FAST will continuously cover the radio frequencies between 70 MHz and 3 GHz. The radio afterglow of GRBs is one of the main focuses of FAST. Zhang et al. [84] have estimated the detectability with FAST of various GRBs like failed GRBs, low-luminosity GRBs, high-luminosity GRBs, and standard GRBs. They predict that FAST will be able to detect most of the GRBs other than subluminous ones up to a redshift of $z \leq 10$.

However, Hancock et al. [87] used stacking of radio visibility data of many GRBs and their analysis still resulted in nondetection. Based on this they proposed a class of GRBs which will produce intrinsically faint radio afterglow emission and have black holes as their central engine. GRBs with magnetars as central engine will produce radio bright afterglow emission. This is because the magnetar driven GRBs will have lower radiative efficiency and produce radio bright GRBs, whereas the black hole driven GRBs with their high radiative efficiency will use most of their energy budget in prompt emission and will be radio-faint. This is a very important aspect and may need to be addressed. And if true, it may reflect the nature of the central engine through radio measurements. JVLA at high radio frequencies and the uGMRT at low radio frequencies test this hypothesis. SKA will eventually be the ultimate instrument to distinguish between the sensitivity limitation and the intrinsic dimness of radio bursts [83].

3.2. Hyperenergetic GRBs. Accurate calorimetry is very important to understand the true nature of the GRBs. This includes prompt radiation energy in the form of γ-rays and kinetic energy in the form of shock powering the afterglow emission. Empirical constraints from models require that all long duration GRBs have the kinetic energies $\leq 10^{51}$ ergs. GRBs are collimated events; thus the jet opening angle is crucial to measure the true budget of the energies. While isotropic energies range of energies spread in four orders of magnitude (see Figure 3), the collimated nature of the jet makes the actual energies in much tighter range clustered around 10^{51} ergs [75, 88, 89]. However, it is becoming increasingly evident that the clustering may not be as tight as envisaged and the actual energy range may be much wider than anticipated earlier. A population of nearby GRBs have relativistic energy orders of magnitude smaller than a typical cosmological GRB; these are called subluminous GRBs, for example, GRB 980425 [25, 90]. *Fermi* has provided evidence for a class of hyperenergetic GRBs. These GRBs have total prompt and kinetic energy release, inferred via broadband modeling [61, 91], to be at least an order of magnitude above the canonical value of 10^{51} erg [1, 29, 48, 92]. The total energy budget of these hyperenergetic GRBs poses a significant challenge for some accepted progenitor models. The maximum energy release in magnetar models [93] is

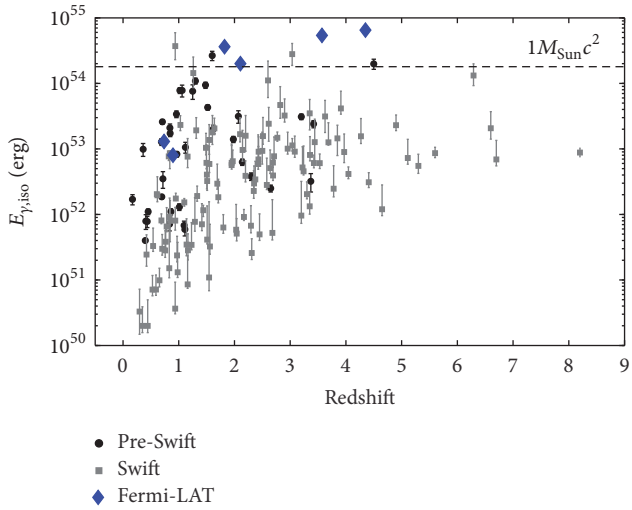

FIGURE 3: Isotropic prompt gamma-ray energy release ($E_{\gamma,\mathrm{iso}}$, in rest frame 1 keV–10 MeV bandpass) of GRBs with measured redshift. One can see a large range of $E_{\gamma,\mathrm{iso}}$. Reproduced from Cenko et al. [1].

3×10^{52} erg, set by the rotational energy of a maximally rotating stable neutron star [94, 95].

It has been very difficult to constrain the true prompt energy budget of the GRBs, mainly, for the following reasons. So far, *Swift* has been instrumental in detecting majority of the GRBs. However, peaks of the emission for various GRBs lie outside the narrow energy coverage of *Swift*-BAT (15–150 keV). In addition, extrapolation of 15–150 keV to 1–10,000 keV bandpass causes big uncertainties in the determination of prompt isotropic energies. With its huge energy coverage (8 keV–300 GeV), *Fermi* has overcome some of these limitations and provided unparalleled constraints on the spectral properties of the prompt emission. *Fermi* has been able to distinguish the true hyperenergetic bursts (such as GRB 090323, GRB 090902B, and GRB 090926A [1]; also see Figure 3). While *Swift* sample is biased towards faint bursts, *Fermi* sample is biased towards GRBs with very large isotropic energy releases (10^{54} erg), which even after collimation correction reach very high energies, for example, [1, 96], and provide some of the strongest constraints on possible progenitor models.

The uncertainty in jet structure in GRBs pose additional difficulty in constraining the energy budget of GRBs. Even after a jet break is seen, to convert it into opening angle, one needs density to convert it into the collimation angle. While some optical light curves can be used to constrain the circumburst density (e.g., Liang et al. [45]), radio SSA peak is easier to detect due to slow evolution in radio bands. With only one-third of sample being radio bright, this has been possible for only a handful of bursts. A larger radio sample at lower frequencies, at early times when synchrotron self-absorption (SSA) is still playing a major role, could be very useful. The uGMRT after upgrade will be able to probe this regime as SSA will be affecting the radio emission at longer wavelength for a longer time. However, the this works on the assumption that the entire relativistic outflow is collimated into a single uniform jet. While the proposed double-jet models for GRB 030329 [97, 98] and GRB 080319B [99] ease out the extreme efficiency requirements, it has caused additional concerns.

The ALMA also has an important role to play since GRB spectrum at early times peak at mm wavelengths, when it is the brightest. ALMA with its high sensitivity can detect such events at early times and give better estimation of the kinetic energy of the burst.

While X-ray and optical afterglows stay above detection limits only for weeks or months, radio afterglows of nearby bursts can be detected up to years [50, 100]. The longevity of radio afterglows also makes them interesting laboratories to study the dynamics and evolution of relativistic shocks. At late stages, the fireball would have expanded sideways so much that it would essentially make transition into nonrelativistic regime and become quasispherical and independent of the jet geometry; calorimetry can be employed to obtain the burst energetics [50, 52]. These estimates will be free of relativistic effects and collimation corrections. This regime is largely unexplored due to limited number of bursts staying above detection limit beyond subrelativistic regime. Several numerical calculations exist for the afterglow evolution starting from the relativistic phase and ending in the deep nonrelativistic phase [79, 101]. SKA with its μJy level sensitivity will be able to extend the current limits of afterglow longevity. This will provide us with an unprecedented opportunity to study the nonrelativistic regime of afterglow dynamics and thereby will be able to refine our understanding of relativistic to nonrelativistic transition of the blast-wave and changing shock microphysics and calorimetry in the GRBs. Burlon et al. [83] have computed that SKA1-MID will be able to observe 2% afterglows till the nonrelativistic (NR) transition but that the full SKA will routinely observe 15% of the whole GRB afterglow population at the NR transition.

3.3. Can Jet Breaks Be Chromatic? After the launch of *Swift*, one obtained a far better sampled optical and X-ray light curves, thus expected to witness achromatic jet breaks across the electromagnetic spectrum, a robust signature associated with a collimated outflow. Several groups conducted a comprehensive analysis of a large sample of light curves of *Swift* bursts in the X-rays [102–105] and optical [106] bands. Surprisingly fewer *Swift* bursts have shown this unambiguous signature of the jet collimation. Without these collimation angles, the true energy release from *Swift* events has remained highly uncertain. A natural explanation for absence of the jet breaks can be attributed to the high sensitivity of *Swift*. Due to its high sensitivity *Swift* is preferentially selecting GRBs with smaller isotropic gamma-ray energies and larger redshifts. This dictates that typical *Swift* events will have large opening angles, thus causing jet breaks to occur at much time than those of pre-*Swift* events. Since afterglow is already weak at later times, making jet break measurements is quite difficult [103, 107].

There have been some cases where chromatic jet breaks are also seen. For example, in GRB 070125, the X-ray jet break occurred around day 10, whereas the optical jet break

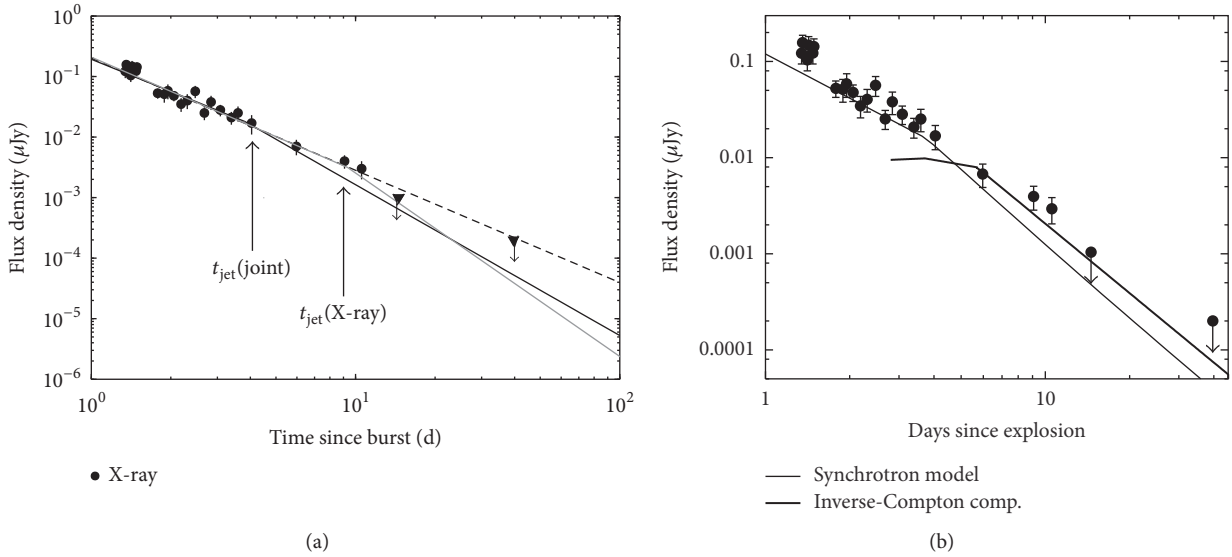

FIGURE 4: (a) X-ray light curve of GRB 070125. Best-fit single power-law models are shown with dashed lines, while the broken power-law models are shown in solid lines. The t_{jet}(joint) is the joint fit to optical and X-ray data and grey solid line t_{jet}(X-ray) is the independent fit. The independent fit shifts the jet break to ~9-10 days, which was found to be day 3 for optical bands. (b) Contribution of IC in the synchrotron model for the X-ray light curve of GRB 070125. The thin line represents the broadband model with the synchrotron component only. The thick line represents the IC light curve. One can see that IC effect can delay the jet breaks in X-ray bands [29].

occurred on day 3. Chandra et al. [29] attributed it to inverse Compton (IC) effect, which does not affect the photons at low energies but shifts the X-ray jet break at a later time (see Figure 4, [29]). As IC effects are dominant in high density medium, radio observations are an important indicator of the effectiveness of the IC effect. Chandra et al. [29] showed that, for a given density of GRB 070125, the estimated delay in X-ray jet break due to the IC effect is consistent with the observed delay. However, this area needs to be explored further for other GRBs. While high density bursts are likely to be brighter in radio bands, it may cause a burst to be a dark one in optical wavelength (Xin et al. [108] and references therein), which then make it difficult to detect the jet break simultaneously in several wavelengths. uGMRT and JVLA will be ideal instruments to probe IC effect and will potentially be able to explain the cause of chromaticity in some of the *Swift* bursts.

3.4. High-z GRBs and PoP III Stars. One of the major challenges of the observational cosmology is to understand the reionization of the Universe, when the first luminous sources were formed. So far quasar studies of the Gunn-Peterson absorption trough, the luminosity evolution of Lyman galaxies, and the polarization isotropy of the cosmic microwave background have been used as diagnostics. But they have revealed a complicated picture in which reionization took place over a range of redshifts.

The ultraviolet emission from young, massive stars (see Fan et al. [109] and references therein) appears to be the dominant source of reionization. However, none of these massive stars have been detected so far. Long GRBs, which are explosions of massive stars, are detectable out to large distances due to their extreme luminosities and thus are the potential signposts of the early massive stars. GRBs are predicted to occur at redshifts beyond those where quasars are expected; thus they could be used to study both the reionization history and the metal enrichment of the early Universe [110]. They could potentially reveal the stars that form from the first dark matter halos through the epoch of reionization [72, 111, 112]. The radio, infrared, and X-ray afterglow emission from GRBs are in principle observable out to $z = 30$ [72, 111–114]. Thus GRB afterglows make ideal sources to probe the intergalactic medium as well as the interstellar medium in their host galaxies at high z.

The fraction of detectable GRBs that lie at high redshift ($z > 6$) is, however, expected to be less than 10% [115, 116]. So far there are only 3 GRBs with confirmed measured redshifts higher than 6. These are GRB 050904 [117], GRB 080913 [118], and GRB 090423 [15]. Radio bands are ideal to probe GRB circumburst environments at high redshift because radio flux density show only a weak dependence on the redshift, due to the negative k-correction effect [72] (also see [47] and Figure 5). In k-correction effect, the afterglow flux density remains high because of the dual effects of spectral and temporal redshift, offsetting the dimming due to the increase in distance [111] (see Figure 5). GRB 050904 and GRB 090423 were detected in radio bands and radio observations of these bursts allowed us to put constraints on the density of the GRB environments at such high redshifts. While the density of GRB 090423 was $n \sim 1\,\mathrm{cm}^{-3}$ [16] (Figure 5), the density of GRB 050904 was ~100 cm^{-3}, indicating dense molecular cloud surrounding the GRB 050904 [119]. This revealed that these two high-z GRBs exploded in a very different environment.

ALMA will be a potential tool for selecting potential high-z bursts that would be suitable for intense follow-up across

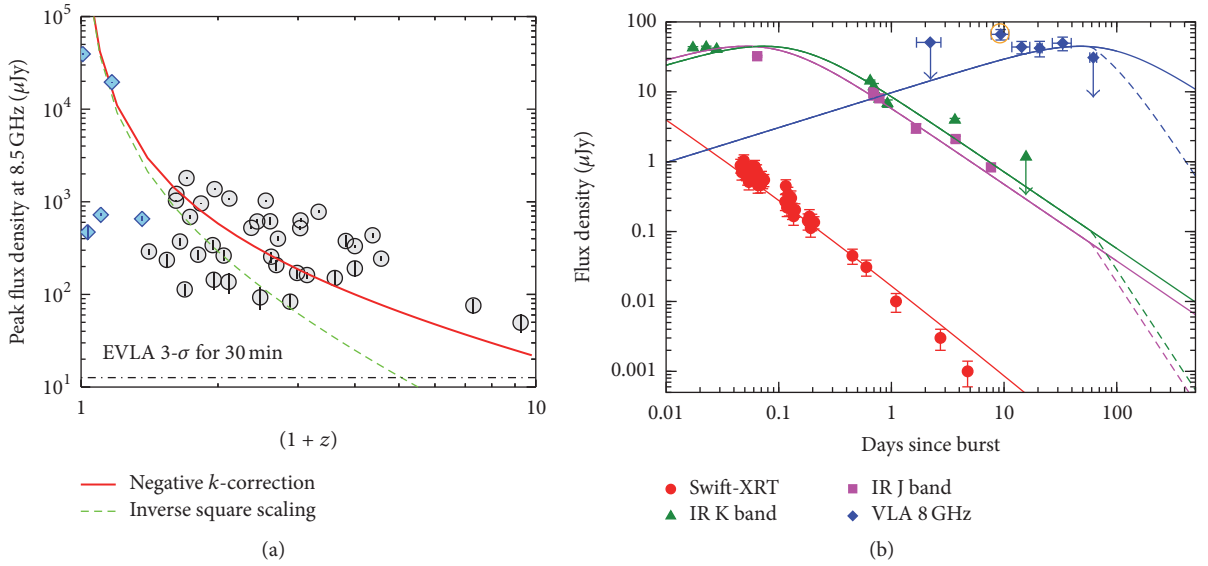

FIGURE 5: (a) The 8.5 GHz radio peak flux density versus $(1 + z)$ plot for radio afterglows with known redshifts. Blue diamonds are GRBs associated with supernovae, while the grey circles denote cosmological GRBs. The green dashed line indicates if the flux density scales as the inverse square of the luminosity distance. The red thick line is the flux density scaling in the canonical afterglow model which includes a negative k-correction effect, offsetting the diminution in distance (reproduced from [48]). (b) Multiwaveband afterglow modeling of highest redshift GRB 090423 at $z = 8.23$ (reproduced from [16]).

the electromagnetic spectrum. With an order of magnitude enhanced sensitivity the JLA will be able to study a high-z GRB for a longer timescale. For example, VLA can detect GRB 090423-like burst for almost 2 years. The uGMRT can also detect bright bursts up to a redshift of $z \sim 9$. These measurements will therefore obtain better density measurements and reveal the environments where massive stars were forming in the early Universe.

3.5. Reverse Shock. In a GRB explosion, there is a forward shock moving forward into the circumburst medium, as well as a reverse shock moving backwards into the ejecta [120]. The nearly self-similar behavior of a forward shock means that little information is preserved about the central engine properties that gave rise to the GRB. In contrast, the brightness of the short-lived reverse shock depends on the initial Lorentz factor and the magnetization of the ejecta. Thus, multifrequency observations of reverse shocks tell about the acceleration, the composition, and the strength and orientation of any magnetic fields in the relativistic outflows from GRBs [68, 69, 121–123]. In general, the reverse shock is expected to result in an optical flash in the first tens of seconds after the GRB [77], which makes it difficult to detect as robotic telescopes are required for fast triggers.

The discovery of a bright optical flash from GRB 990123 [77] leads to extensive searches for reverse shocks [124–127] in optical bands. One expected to see more evidences of reverse shocks in optical bands due to *Swift*-UVOOT; however, based on these efforts it seems that the incidence of optical reserve shocks is low. Since the peak of this emission moves to lower frequencies over time and can be probed at radio frequencies on a time scale of hours to days [74], the radio regime is well suited for studying early time reverse shock phenomena.

There have been several observational as well as theoretical studies of radio reverse shock emission in the literature after the first reverse shock detection in GRB 990123 [74]. Gao et al. [128], Kopač et al. [129], and Resmi and Zhang [130] have done comprehensive analytical and numerical calculations of radio reverse shock emissions and about their detectability. It has been shown [48, 67] that deep and fast monitoring campaigns of radio reverse shock emission could be achieved with the VLA for a number of bursts. JVLA radio frequencies are well suited as reverse shock emission is brighter in higher radio frequencies where self-absorption effects are relatively lesser. Radio afterglow monitoring campaigns in higher SKA bands (e.g., SKA1-Mid Band-4 and Band-5) will definitely be useful in exploring reverse shock characteristics [83].

Reverse shock is detectable in high redshift GRBs ($z \geq 6$) as well. Inoue et al. [131] have predicted that at mm bands the effects of time dilation almost compensate for frequency redshift, thus resulting in a near-constant observed peak frequency at a few hours after event and a flux density at this frequency that is almost independent of redshift. Thus ALMA mm band is ideal to look for reverse shock signatures at high redshifts. Burlon et al. [83] predict that SKA1-Mid will be able to detect a reverse shock from a GRB990123 like GRB at a redshift of ~10.

3.6. Connecting Prompt and Afterglow Physics. *Swift* is an ideal instrument for quick localization of GRBs and rapid follow-up and consequently redshift measurement [20, 132] and *Fermi* for the wideband spectral measurement during the prompt emission. However, good spectral and timing measurement covering early prompt to late afterglow phase is available for a few sources and rarely available for the short GRBs. Some of the key problems that can be addressed by

the observation of the radio afterglows in connection with the prompt emission are (i) comparing the Lorentz factor estimation with both LAT detected GeV photons as well as from the reverse shock [133, 134]; (ii) comparison between nonthermal emission of both the prompt and afterglow emission, which would enable one to constrain the microphysics of the shocks accelerating electrons to ultra-relativistic energies eventually producing the observed radiation; (iii) detailed modeling of the afterglow observation of both long and short GRBs, which will enhance our knowledge about the circumburst medium surrounding the progenitors; (iv) current refurbished and upcoming radio telescopes with their finer sensitivity, which would play a key role in constraining the energetics of GRBs which is crucial in estimating the radiation efficiency of the prompt emission of GRBs. This would strengthen the understanding of the hardness-intensity correlation [135].

The recently launched *AstroSAT* satellite [136] carries several instruments enabling multiwavelength studies. The Cadmium Zinc Telluride Imager (CZTI) on-board *AstroSAT* can provide time resolved polarization measurements for bright GRBs and can act as a monitor above 80 keV [137, 138]. So far no other instrument has such capability to detect polarization. Hence, for a few selected bright GRBs, CZTI, in conjunction with ground based observatories like uGMRT and JVLA, and other space based facilities can provide a complete observational picture of a few bright GRBs from early prompt phase to late afterglow. This will provide us with a comprehensive picture of GRBs, thus enabling a good understanding of the emission mechanisms.

3.7. Some Other Unresolved Issues. So far I have discussed only that small fraction of on-axis GRBs, in which the jet is oriented along our line of sight. Due to large Lorentz factors, small opening angles of the collimated jets, we only detect a small fraction of GRBs [139]. Ghirlanda et al. [140] have estimated that, for every GRB detected, there must be 260 GRBs which one is not able to detect. However, their existence can be witnessed as "orphan afterglow" at late times when the GRB jet is decelerated and spread laterally to come into our line of sight. At such late times, the emission is expected to come only in radio bands. So far attempts to find such orphan radio afterglows have been unsuccessful [75, 141, 142]. Even if detected, disentangling the orphan afterglow emission from other classes will be very challenging. Soderberg et al. [141] carried out a survey towards the direction of 68 Type Ib/c supernovae looking for the orphan afterglows and put limit on GRB opening angles, $\theta_j > 0.8$ d. The detection of population of orphan afterglows with upcoming sensitive radio facilities is promising. This will give a very good handle on jet opening angles and on the total GRB rate whether beamed towards us or not.

The inspiral and merger of binary systems with black holes or neutron stars have been speculated as primary source of gravitational waves (GWs) for the ground based GW interferometers [143, 144]. The discovery of GWs from GW 150914 [42] and GW 151226 [43] with the Advanced LIGO detectors have provided the first observational evidence of the binary black hole systems inspiraling and merging. At least some of the compact binaries involving a neutron star are expected to give rise to radio afterglows of short GRBs. Electromagnetic counterparts of GW source, including emission in the radio bands, are highly awaited as they will, for the first time, confirm the hypothesis of binary merger scenario for GW waves. If localized at high energies, targeted radio observations can be carried out to study these events at late epochs.

Short GRBs arising from mergers of two neutron stars eject significant amount of mass in several components, including subrelativistic dynamical ejecta, mildly relativistic shock-breakout, and a relativistic jet [145]. Hotokezaka and Piran [145] have calculated the expected radio signals produced between the different components of the ejecta and the surrounding medium. The nature of radio emission years after GRB will provide invaluable information on the merger process [145] and the central products [146]. Fong et al. [146] have predicted that the formation of stable magnetar of energy 10^{53} erg during merger process will give rise to a radio transient a year later. They carried out search for radio emission from 9 short GRBs in rest frame times of 1–8 years and concluded that such a magnetar formation can be ruled out in at least half their sample.

In addition, radio observations can also probe the star formation and the metallicity of the GRB host galaxies when optical emissions are obscured by dust [147, 148].

4. Conclusions

In this article, I have reviewed the current status of the *Swift*/*Fermi* GRBs in context of their radio emission. With improved sensitivity of the refurbished radio telescopes, such as JVLA and uGMRT and upcoming telescopes like SKA, it will be possible to answer many open questions. The most crucial of them is the accurate calorimetry of the GRBs. Even after observing a jet break in the GRB afterglow light curves, which is an unambiguous signature of the jet collimation, one needs density estimation to convert the jet break epoch to collimation angle. The density information can be more effectively provided by the early radio measurements when the GRBs are still synchrotron self-absorbed. So far it has been possible for very limited cases because only one-third of the total GRBs have been detected in radio bands [48]. Sensitive radio measurements are needed to understand whether the low detection rate of radio afterglows is intrinsic to GRBs or the sensitivity limitations of the current telescopes are playing a major role. In the era of JVLA, uGMRT, ALMA, and upcoming SKA, this issue should be resolved. In addition, these sensitive radio telescopes will be crucial to detect radio afterglows at very high redshifts and provide unique constraints on the environments of the exploding massive stars in the early Universe. If GRBs are not intrinsically dim in radio bands and the sample is indeed sensitivity limited, then SKA is expected to detect almost 100% GRBs [83]. SKA will be able to study the individual bursts in great detail. This will also allow us to carry out various statistical analyses of the radio sample and drastically increase our overall understanding of the afterglow evolution from very early time to nonrelativistic regime. Detection of the orphan afterglow is due any time and will be novel in itself.

Competing Interests

The author declared that there are no competing interests.

Acknowledgments

The author thanks L. Resmi, Shabnam Iyyanni, A. R. Rao, Kuntal Misra, and D. Frail for many useful discussions in the past, which helped shape this article. The author acknowledges support from the Department of Science and Technology via SwarnaJayanti Fellowship Award (File no. DST/SJF/ PSA-01/2014-15). The author also acknowledges SKA Italy handbook (http://pos.sissa.it/cgi-bin/reader/conf.cgi?confid=215), where many of the SKA numbers on sensitivity, GRB detection rates, and so forth are taken.

References

[1] S. B. Cenko, D. A. Frail, F. A. Harrison et al., "Afterglow observations of Fermi large area telescope gamma-ray bursts and the emerging class of hyper-energetic events," *The Astrophysical Journal*, vol. 732, no. 1, p. 29, 2011.

[2] P. Kumar and B. Zhang, "The physics of gamma-ray bursts & relativistic jets," *Physics Reports*, vol. 561, pp. 1–109, 2015.

[3] R. W. Klebesadel, I. B. Strong, and R. A. Olson, "Observations of gamma-ray bursts of cosmic origin," *Astrophysical Journal*, vol. 182, article L85, 1973.

[4] E. Costa, F. Frontera, J. Heise et al., "Discovery of an X-ray afterglow associated with the γ-ray burst of 28 February 1997," *Nature*, vol. 387, no. 6635, pp. 783–785, 1997.

[5] J. van Paradijs, P. J. Groot, T. Galama et al., "Transient optical emission from the error box of the γ-ray burst of 28 February 1997," *Nature*, vol. 386, no. 6626, pp. 686–689, 1997.

[6] R. A. M. J. Wijers, M. J. Rees, and P. Meszaros, "Shocked by GRB 970228: the afterglow of a cosmological fireball," *Monthly Notices of the Royal Astronomical Society*, vol. 288, no. 4, pp. L51–L56, 1997.

[7] D. A. Frail, S. R. Kulkarnit, L. Nicastro, M. Feroci, and G. B. Taylor, "The radio afterglow from the γ-ray burst of 8 May 1997," *Nature*, vol. 389, no. 6648, pp. 261–263, 1997.

[8] G. J. Fishman and C. A. Meegan, "Gamma-ray bursts," *Annual Review of Astronomy & Astrophysics*, vol. 33, pp. 415–458, 1995.

[9] C. Kouveliotou, C. A. Meegan, G. J. Fishman et al., "Identification of two classes of gamma-ray bursts," *The Astrophysical Journal*, vol. 413, no. 2, pp. L101–L104, 1993.

[10] A. S. Fruchter, A. J. Levan, L. Strolger et al., "Long big γ-ray bursts and core-collapse supernovae have different environments," *Nature*, vol. 441, pp. 463–468, 2006.

[11] W. Fong, E. Berger, and D. B. Fox, "*Hubble Space Telescope* observations of short gamma-ray burst host galaxies: morphologies, offsets, and local environments," *The Astrophysical Journal*, vol. 708, no. 1, p. 9, 2010.

[12] S. E. Woosley and J. S. Bloom, "The supernova-γ-ray burst connection," *Annual Review of Astronomy and Astrophysics*, vol. 44, pp. 507–566, 2006.

[13] E. Berger, "Short-duration gamma-ray bursts," *Annual Review of Astronomy and Astrophysics*, vol. 52, no. 1, pp. 43–105, 2014.

[14] A. Cucchiara, A. J. Levan, D. B. Fox et al., "A photometric redshift of $z \sim 9.4$ for GRB 090429B," *The Astrophysical Journal*, vol. 736, no. 1, p. 7, 2011.

[15] N. R. Tanvir, D. B. Fox, A. J. Levan et al., "A big γ-ray burst at a redshift of $z \approx 8.2$," *Nature*, vol. 461, pp. 1254–1257, 2009.

[16] P. Chandra, D. A. Frail, D. Fox et al., "Discovery of radio afterglow from the most distant cosmic explosion," *The Astrophysical Journal Letters*, vol. 712, no. 1, pp. L31–L35, 2010.

[17] S. R. Kulkarni, D. A. Frail, M. H. Wieringa et al., "Radio emission from the unusual supernova 1998bw and its association with the γ-ray burst of 25 April 1998," *Nature*, vol. 395, no. 6703, pp. 663–669, 1998.

[18] N. Gehrels, G. Chincarini, P. Giommi et al., "The *Swift* γ-ray burst mission," *The Astrophysical Journal*, vol. 611, no. 2, p. 1005, 2004.

[19] S. D. Barthelmy, L. M. Barbier, J. R. Cummings et al., "The burst alert telescope (BAT) on the SWIFT midex mission," *Space Science Reviews*, vol. 120, no. 3-4, pp. 143–164, 2005.

[20] N. Gehrels, E. Ramirez-Ruiz, and D. B. Fox, "Gamma-ray bursts in the *Swift* era," *Annual Review of Astronomy and Astrophysics*, vol. 47, pp. 567–617, 2009.

[21] D. N. Burrows, J. E. Hill, J. A. Nousek et al., "The wift X-ray telescope," *Space Science Reviews*, vol. 120, no. 3-4, pp. 165–195, 2005.

[22] P. W. A. Roming, T. E. Kennedy, K. O. Mason et al., "The *Swift* ultra-violet/optical telescope," *Space Science Reviews*, vol. 120, no. 3, pp. 95–142, 2005.

[23] Z. G. Dai and T. Lu, "γ-ray burst afterglows and evolution of postburst fireballs with energy injection from strongly magnetic millisecond pulsars," *Astronomy and Astrophysics*, vol. 333, no. 3, pp. L87–L90, 1998.

[24] B. Zhang and P. Mészáros, "Gamma-ray bursts with continuous energy injection and their afterglow signature," *The Astrophysical Journal*, vol. 566, no. 2, pp. 712–722, 2002.

[25] E.-W. Liang, B.-B. Zhang, and B. Zhang, "A comprehensive analysis of *Swift* XRT data. II. Diverse physical origins of the shallow decay segment," *The Astrophysical Journal*, vol. 670, no. 1, pp. 565–583, 2007.

[26] A. N. Guelbenzu, S. Klose, A. Rossi et al., "GRB 090426: discovery of a jet break in a short burst afterglow," *Astronomy and Astrophysics*, vol. 531, article L6, 2011.

[27] W. Fong, E. Berger, B. D. Metzger et al., "short GRB 130603B: discovery of a jet break in the optical and radio afterglows, and a mysterious late-time x-ray excess," *The Astrophysical Journal*, vol. 780, no. 2, p. 118, 2014.

[28] E. Troja, T. Sakamoto, S. B. Cenko et al., "An achromatic break in the afterglow of the short GRB 140903A: evidence for a narrow jet," *The Astrophysical Journal*, vol. 827, no. 2, p. 102, 2016.

[29] P. Chandra, S. B. Cenko, D. A. Frail et al., "A comprehensive study of GRB 070125, a most energetic gamma-ray burst," *The Astrophysical Journal*, vol. 683, no. 2, p. 924, 2008.

[30] W. B. Atwood, A. A. Abdo, M. Ackermann et al., "The large area telescope on the *Fermi Gamma-Ray Space Telescope* mission," *The Astrophysical Journal*, vol. 697, no. 2, p. 1071, 2009.

[31] C. Meegan, G. Lichti, P. N. Bhat et al., "The fermi γ-ray burst monitor," *Astrophysical Journal*, vol. 702, no. 1, pp. 791–804, 2009.

[32] M. Ackermann, K. Asano, W. B. Atwood et al., "Fermi observations of GRB 090510: a short-hard γ-ray burst with an additional, hard power-law component from 10 Kev to GeV energies," *The Astrophysical Journal*, vol. 716, no. 2, p. 1178, 2010.

[33] A. A. Abdo, M. Ackermann, M. Ajello et al., "A limit on the variation of the speed of light arising from quantum gravity effects," *Nature*, vol. 462, pp. 331–334, 2009.

[34] A. A. Abdo, M. Ackermann, M. Arimoto et al., "Fermi observations of high-energy gamma-ray emission from GRB 080916C," *Science*, vol. 323, no. 5922, pp. 1688–1693, 2009.

[35] A. A. Abdo, M. Ackermann, M. Ajello et al., "*FERMI* observations of GRB 090902b: a distinct spectral component in the prompt and delayed emission," *The Astrophysical Journal Letters*, vol. 706, no. 1, p. L138, 2009.

[36] M. Ackermann, M. Ajello, K. Asano et al., "The first *Fermi*-LAT gamma-ray burst catalog," *The Astrophysical Journal Supplement Series*, vol. 209, no. 1, p. 11, 2013.

[37] S. Guiriec, V. Connaughton, M. S. Briggs et al., "Detection of a thermal spectral component in the prompt emission of GRB 100724B," *The Astrophysical Journal Letters*, vol. 727, no. 2, p. L33, 2011.

[38] M. Axelsson, L. Baldini, G. Barbiellini et al., "GRB110721A: an extreme peak energy and signatures of the photosphere," *The Astrophysical Journal Letters*, vol. 757, no. 2, p. L31, 2012.

[39] J. M. Burgess, R. D. Preece, V. Connaughton et al., "Time-resolved analysis of *FERMI* gamma-ray bursts with fast- and slow-cooled synchrotron photon models," *The Astrophysical Journal*, vol. 784, no. 1, p. 17, 2014.

[40] M. Ackermann, M. Ajello, K. Asano et al., "Detection of a spectral break in the extra hard component of GRB 090926A," *The Astrophysical Journal*, vol. 729, no. 2, p. 114, 2011.

[41] D. Band, J. Matteson, L. Ford et al., "BATSE observations of gamma-ray burst spectra. I—spectral diversity," *The Astrophysical Journal*, vol. 413, no. 1, pp. 281–292, 1993.

[42] B. P. Abbott, R. Abbott, T. D. Abbott et al., "GW150914: implications for the stochastic gravitational-wave background from binary black holes," *Physical Review Letters*, vol. 116, no. 13, Article ID 131102, 12 pages, 2016.

[43] B. P. Abbott, R. Abbott, T. D. Abbott et al., "Observation of gravitational waves from a binary black hole merger," *Physical Review Letters*, vol. 116, no. 6, Article ID 061102, 16 pages, 2016.

[44] R. Sari, T. Piran, and R. Narayan, "Spectra and light curves of gamma-ray burst afterglows," *The Astrophysical Journal*, vol. 497, no. 1, pp. L17–L20, 1998.

[45] E.-W. Liang, L. Li, H. Gao et al., "A comprehensive study of gamma-ray burst optical emission. II. Afterglow onset and late re-brightening components," *The Astrophysical Journal*, vol. 774, no. 1, p. 13, 2013.

[46] E. Molinari, S. D. Vergani, D. Malesani et al., "REM observations of GRB060418 and GRB 060607A: the onset of the afterglow and the initial fireball Lorentz factor determination," *Astronomy and Astrophysics*, vol. 469, no. 1, pp. L13–L16, 2007.

[47] P. Chandra and D. A. Frail, "Gamma ray bursts and their afterglow properties," *Bulletin of the Astronmical Society of India*, vol. 39, no. 3, pp. 451–470, 2011.

[48] P. Chandra and D. A. Frail, "A radio-selected sample of gamma-ray burst afterglows," *The Astrophysical Journal*, vol. 746, no. 2, p. 156, 2012.

[49] J. Granot and A. J. Van Der Horst, "Gamma-ray burst jets and their radio observations," *Publications of the Astronomical Society of Australia*, vol. 31, no. 1, article e008, 2014.

[50] D. A. Frail, E. Waxman, and S. R. Kulkarni, "A 450 day light curve of the radio afterglow of GRB 970508: fireball calorimetry," *The Astrophysical Journal*, vol. 537, no. 1, pp. 191–204, 2000.

[51] E. Berger, S. R. Kulkarni, and D. A. Frail, "The nonrelativistic evolution of GRBs 980703 and 970508: beaming-independent calorimetry," *Astrophysical Journal*, vol. 612, no. 2, pp. 966–973, 2004.

[52] A. J. van der Horst, A. Kamble, L. Resmi et al., "Detailed study of the GRB 030329 radio afterglow deep into the non-relativistic phase," *Astronomy & Astrophysics*, vol. 480, no. 1, pp. 35–43, 2008.

[53] J. Granot, E. Ramirez-Ruiz, and A. Loeb, "Implications of the measured image size for the radio afterglow of GRB 030329," *Astrophysical Journal*, vol. 618, no. 1, pp. 413–425, 2005.

[54] R. A. Mesler and Y. M. Pihlström, "Calorimetry of GRB 030329: simultaneous model fitting to the broadband radio afterglow and the observed image expansion rate," *The Astrophysical Journal*, vol. 774, no. 1, p. 77, 2013.

[55] R. A. M. J. Wijers and T. J. Galama, "Physical parameters of GRB 970508 and GRB 971214 from their afterglow synchrotron emission," *The Astrophysical Journal*, vol. 523, no. 1, p. 177, 1999.

[56] J. Goodman, "Radio scintillation of gamma-ray-burst afterglows," *New Astronomy*, vol. 2, no. 5, pp. 449–460, 1997.

[57] E. Waxman, S. R. Kulkarni, and D. A. Frail, "Implications of the radio afterglow from the gamma-ray burst of 1997 MAY 8," *Astrophysical Journal*, vol. 497, no. 1, pp. 288–293, 1998.

[58] G. Taylor, D. Frail, E. Berger, and S. Kulkarni, "High resolution observations of GRB 030329," *AIP Conference Proceedings*, vol. 727, pp. 324–327, 2004.

[59] F. A. Harrison, S. A. Yost, R. Sari et al., "Broadband observations of the afterglow of GRB 000926: observing the effect of inverse compton scattering," *The Astrophysical Journal*, vol. 559, no. 1, p. 123, 2001.

[60] A. Panaitescu and P. Kumar, "Fundamental physical parameters of collimated gamma-ray burst afterglows," *The Astrophysical Journal*, vol. 560, no. 1, pp. L49–L53, 2001.

[61] S. A. Yost, F. A. Harrison, R. Sari, and D. A. Frail, "A study of the afterglows of four gamma-ray bursts: constraining the explosion and fireball model," *The Astrophysical Journal*, vol. 597, no. 1, pp. 459–473, 2003.

[62] F. A. Harrison, J. S. Bloom, D. A. Frail et al., "Optical and radio observations of the afterglow from GRB 990510: evidence for a jet," *The Astrophysical Journal Letters*, vol. 523, no. 2, p. L121, 1999.

[63] E. Berger, R. Sari, D. A. Frail et al., "A jet model for the afterglow emission from GRB 000301C," *The Astrophysical Journal*, vol. 545, no. 1, p. 56, 2000.

[64] E. Berger, A. Diercks, D. A. Frail et al., "GRB 000418: a hidden jet revealed," *The Astrophysical Journal*, vol. 556, no. 2, p. 556, 2001.

[65] M. Ackermann, M. Ajello, K. Asano et al., "Fermi-LAT observations of the gamma-ray burst GRB 130427A," *Science*, vol. 343, no. 6166, pp. 42–47, 2014.

[66] A. Maselli, A. Melandri, L. Nava et al., "GRB 130427A: a nearby ordinary monster," *Science*, vol. 343, no. 6166, pp. 48–51, 2014.

[67] T. Laskar, E. Berger, B. A. Zauderer et al., "A reverse shock in GRB 130427A," *The Astrophysical Journal*, vol. 776, no. 2, p. 119, 2013.

[68] G. E. Anderson, A. J. van der horst, T. D. Staley et al., "Probing the bright radio flare and afterglow of GRB 130427A with the arcminute microkelvin imager," *Monthly Notices of the Royal Astronomical Society*, vol. 440, no. 3, pp. 2059–2065, 2014.

[69] D. A. Perley, S. B. Cenko, A. Corsi et al., "The afterglow of GRB 130427A from 1 to 10^{16} GHz," *The Astrophysical Journal*, vol. 781, no. 1, p. 37, 2014.

[70] A. J. van der Horst, Z. Paragi, A. G. de Bruyn et al., "A comprehensive radio view of the extremely bright gamma-ray burst 130427A," *Monthly Notices of the Royal Astronomical Society*, vol. 444, no. 4, pp. 3151–3163, 2014.

[71] D. A. Frail, P. B. Cameron, M. Kasliwal et al., "An energetic afterglow from a distant stellar explosion," *The Astrophysical Journal Letters*, vol. 646, no. 2, pp. L99–L102, 2006.

[72] B. Ciardi and A. Loeb, "Expected number and flux distribution of gamma-ray burst afterglows with high redshifts," *The Astrophysical Journal*, vol. 540, no. 2, pp. 687–696, 2000.

[73] D. A. Frail, A. M. Soderberg, S. R. Kulkarni et al., "Accurate calorimetry of GRB 030329," *Astrophysical Journal*, vol. 619, no. 2 I, pp. 994–998, 2005.

[74] S. R. Kulkarni, D. A. Frail, R. Sari et al., "Discovery of a radio flare from GRB 990123," *The Astrophysical Journal Letters*, vol. 522, no. 2, p. L97, 1999.

[75] E. Berger, S. R. Kulkarni, D. A. Frail, and A. M. Soderberg, "A radio survey of type Ib and Ic supernovae: searching for engine-driven supernovae," *The Astrophysical Journal*, vol. 599, no. 1, pp. 408–418, 2003.

[76] E. Nakar and T. Piran, "GRB 990123 revisited: further evidence of a reverse shock," *The Astrophysical Journal*, vol. 619, no. 2, pp. L147–L150, 2005.

[77] C. Akerlof, R. Balsano, S. Barthelmy et al., "Observation of contemporaneous optical radiation from a γ-ray burst," *Nature*, vol. 398, no. 6726, pp. 400–402, 1999.

[78] R. A. Mesler, Y. M. Pihlström, G. B. Taylor, and J. Granot, "VLBI and archival VLA and WSRT observations of the GRB 030329 radio afterglow," *The Astrophysical Journal*, vol. 759, no. 1, p. 4, 2012.

[79] F. De Colle, E. Ramirez-Ruiz, J. Granot, and D. Lopez-Camara, "Simulations of gamma-ray burst jets in a stratified external medium: dynamics, afterglow light curves, jet breaks, and radio calorimetry," *The Astrophysical Journal*, vol. 751, no. 1, article 57, 2012.

[80] P. A. Evans, A. P. Beardmore, K. L. Page et al., "Methods and results of an automatic analysis of a complete sample of *Swift*-XRT observations of GRBs," *Monthly Notices of the Royal Astronomical Society*, vol. 397, no. 3, pp. 1177–1201, 2009.

[81] D. A. Kann, S. Klose, B. Zhang et al., "The afterglows of *Swift*-era gamma-ray bursts. I. Comparing pre-*Swift* and *Swift*-era long/soft (type II) GRB optical afterglows," *The Astrophysical Journal*, vol. 720, no. 2, p. 1513, 2010.

[82] D. A. Kann, S. Klose, B. Zhang et al., "THE afterglows of *Swift*-era gamma-ray bursts. II. Type I GRB versus type II GRB optical afterglows," *The Astrophysical Journal*, vol. 734, no. 2, p. 96, 2011.

[83] D. Burlon, G. Ghirlanda, A. van der Horst et al., "The SKA view of gamma-ray bursts," https://arxiv.org/abs/1501.04629.

[84] Z.-B. Zhang, S.-W. Kong, Y.-F. Huang, D. Li, and L.-B. Li, "Detecting radio afterglows of gamma-ray bursts with FAST," *Research in Astronomy and Astrophysics*, vol. 15, no. 2, pp. 237–251, 2015.

[85] R. Nan, D. Li, C. Jin et al., "The five-hundred-meter aperture spherical radio telescope (FAST) project," *International Journal of Modern Physics D*, vol. 20, no. 6, pp. 989–1024, 2011.

[86] D. Li, R. Nan, and Z. Pan, "The five-hundred-meter aperture spherical radio telescope project and its early science opportunities," *Proceedings of the International Astronomical Union: Neutron Stars and Pulsars: Challenges and Opportunities after 80 Years*, vol. 8, no. 291, pp. 325–330, 2012.

[87] P. J. Hancock, B. M. Gaensler, and T. Murphy, "Two populations of gamma-ray burst radio afterglows," *Astrophysical Journal*, vol. 776, no. 2, article 106, 2013.

[88] D. A. Frail, S. R. Kulkarni, R. Sari et al., "Beaming in gamma-ray bursts: evidence for a standard energy reservoir," *The Astrophysical Journal Letters*, vol. 562, no. 1, p. L55, 2001.

[89] J. S. Bloom, D. A. Frail, and S. R. Kulkarni, "Gamma-ray burst energetics and the gamma-ray burst Hubble diagram: promises and limitations," *The Astrophysical Journal*, vol. 594, no. 2, pp. 674–683, 2003.

[90] A. M. Soderberg, S. R. Kulkarni, E. Berger et al., "The sub-energetic γ-ray burst GRB 031203 as a cosmic analogue to the nearby GRB 980425," *Nature*, vol. 430, no. 7000, pp. 648–650, 2004.

[91] A. Panaitescu and P. Kumar, "Properties of relativistic jets in gamma-ray burst afterglows," *The Astrophysical Journal*, vol. 571, no. 2 I, pp. 779–789, 2002.

[92] S. B. Cenko, D. A. Frail, F. A. Harrison et al., "The collimation and energetics of the brightest *Swift* gamma-ray bursts," *The Astrophysical Journal*, vol. 711, no. 2, p. 641, 2010.

[93] V. V. Usov, "Millisecond pulsars with extremely strong magnetic fields as a cosmological source of γ-ray bursts," *Nature*, vol. 357, no. 6378, pp. 472–474, 1992.

[94] T. A. Thompson, P. Chang, and E. Quataert, "Magnetar spin-down, hyperenergetic supernovae, and gamma-ray bursts," *Astrophysical Journal*, vol. 611, no. 1, pp. 380–393, 2004.

[95] B. D. Metzger, T. A. Thompson, and E. Quataert, "Proto-neutron star winds with magnetic fields and rotation," *The Astrophysical Journal*, vol. 659, no. 1, pp. 561–579, 2007.

[96] S. B. Cenko, M. Kasliwal, F. A. Harrison et al., "Multiwavelength observations of GRB 050820A: an exceptionally energetic event followed from start to finish," *The Astrophysical Journal*, vol. 652, no. 1, p. 490, 2006.

[97] E. Berger, S. R. Kulkarni, G. Pooley et al., "A common origin for cosmic explosions inferred from calorimetry of GRB030329," *Nature*, vol. 426, no. 6963, pp. 154–157, 2003.

[98] A. J. van der Horst, E. Rol, R. A. M. J. Wijers, R. Strom, L. Kaper, and C. Kouveliotou, "The radio afterglow of GRB 030329 at centimeter wavelengths: evidence for a structured jet or nonrelativistic expansion," *Astrophysical Journal*, vol. 634, no. 2 I, pp. 1166–1172, 2005.

[99] J. L. Racusin, S. V. Karpov, M. Sokolowski et al., "Broadband observations of the naked-eye big γ-ray burst GRB 080319B," *Nature*, vol. 455, pp. 183–188, 2008.

[100] L. Resmi, C. H. Ishwara-Chandra, A. J. Castro-Tirado et al., "Radio, millimeter and optical monitoring of GRB 030329 afterglow: constraining the double jet model," *Astronomy & Astrophysics*, vol. 440, no. 2, pp. 477–485, 2005.

[101] H. J. Van Eerten and A. I. MacFadyen, "Gamma-ray burst afterglow scaling relations for the full blast wave evolution," *Astrophysical Journal Letters*, vol. 747, article L30, 2012.

[102] A. Panaitescu, "Jet breaks in the X-ray light-curves of Swift gamma-ray burst afterglows," *Monthly Notices of the Royal Astronomical Society*, vol. 380, no. 1, pp. 374–380, 2007.

[103] D. Kocevski and N. Butler, "γ-ray burst energetics in the Swift ERA," *Astrophysical Journal*, vol. 680, no. 1, pp. 531–538, 2008.

[104] J. L. Racusin, E. W. Liang, D. N. Burrows et al., "Jet breaks and energetics of *Swift* gamma-ray burst X-ray afterglows," *The Astrophysical Journal*, vol. 698, no. 1, p. 43, 2009.

[105] N. Liang, W. K. Xiao, Y. Liu, and S. N. Zhang, "A cosmology-independent calibration of gamma-ray burst luminosity relations and the hubble diagram," *The Astrophysical Journal*, vol. 685, no. 1, pp. 354–360, 2008.

[106] X.-G. Wang, B. Zhang, E.-W. Liang et al., "How bad or good are the external forward shock afterglow models of gamma-ray bursts?" *The Astrophysical Journal Supplement Series*, vol. 219, no. 1, p. 9, 2015.

[107] R. Perna, R. Sari, and D. Frail, "Jets in γ-ray bursts: tests and predictions for the structured jet model," *The Astrophysical Journal*, vol. 594, no. 1 I, pp. 379–384, 2003.

[108] L. P. Xin, W. K. Zheng, J. Wang et al., "GRB 070518: a gamma-ray burst with optically dim luminosity," *Monthly Notices of the Royal Astronomical Society*, vol. 401, no. 3, pp. 2005–2011, 2010.

[109] X. Fan, C. L. Carilli, and B. Keating, "Observational constraints on cosmic reionization," *Annual Review of Astronomy and Astrophysics*, vol. 44, pp. 415–462, 2006.

[110] T. Totani, N. Kawai, G. Kosugi et al., "Implications for cosmic reionization from the optical afterglow spectrum of the gamma-ray burst 050904 at $z = 6.3$," *Publications of the Astronomical Society of Japan*, vol. 58, no. 3, pp. 485–498, 2006.

[111] D. Q. Lamb and D. E. Reichart, "Gamma-ray bursts as a probe of the very high redshift universe," *The Astrophysical Journal*, vol. 536, no. 1, pp. 1–18, 2000.

[112] L. J. Gou, P. Mészáros, T. Abel, and B. Zhang, "Detectability of long gamma-ray burst afterglows from very high redshifts," *The Astrophysical Journal*, vol. 604, no. 2, pp. 508–520, 2004.

[113] J. Miralda-Escudé, "Reionization of the intergalactic medium and the damping wing of the gunn-peterson trough," *The Astrophysical Journal*, vol. 501, no. 1, pp. 15–22, 1998.

[114] K. Ioka and P. Mészáros, "Radio afterglows of gamma-ray bursts and hypernovae at high redshift and their potential for 21 centimeter absorption studies," *Astrophysical Journal*, vol. 619, no. 2, pp. 684–696, 2005.

[115] D. A. Perley, S. B. Cenko, J. S. Bloom et al., "The host galaxies of Swift dark gamma-ray bursts: observational constraints on highly obscured and very high redshift GRBs," *Astronomical Journal*, vol. 138, no. 6, pp. 1690–1708, 2009.

[116] V. Bromm and A. Loeb, "High-redshift γ-ray bursts from population III progenitors," *Astrophysical Journal*, vol. 642, no. 1 I, pp. 382–388, 2006.

[117] N. Kawai, G. Kosugi, K. Aoki et al., "An optical spectrum of the afterglow of a γ-ray burst at a redshift of z = 6.295," *Nature*, vol. 440, no. 7081, pp. 184–186, 2006.

[118] J. Greiner, T. Krühler, J. P. U. Fynbo et al., "GRB 080913 at redshift 6.7," *The Astrophysical Journal*, vol. 693, no. 2, p. 1610, 2009.

[119] L.-J. Gou, D. B. Fox, and P. Mészáros, "Modeling GRB 050904: autopsy of a massive stellar explosion at $z = 6.29$," *The Astrophysical Journal*, vol. 668, no. 2, pp. 1083–1102, 2007.

[120] R. Sari and T. Piran, "GRB 990123: the optical flash and the fireball model," *Astrophysical Journal*, vol. 517, no. 2, pp. L109–L112, 1999.

[121] S. Kobayashi, "Light curves of gamma-ray burst optical flashes," *The Astrophysical Journal*, vol. 545, no. 2, pp. 807–812, 2000.

[122] B. Zhang, S. Kobayashi, and P. Mészáros, "γ-ray burst early optical afterglows: Implications for the initial lorentz factor and the central engine," *The Astrophysical Journal*, vol. 595, no. 2 I, pp. 950–954, 2003.

[123] E. Nakar and T. Piran, "Early afterglow emission from a reverse shock as a diagnostic tool for gamma-ray burst outflows," *Monthly Notices of the Royal Astronomical Society*, vol. 353, no. 2, pp. 647–653, 2004.

[124] C. Akerlof, R. Balsano, S. Barthelmy et al., "Prompt optical observations of gamma-ray bursts," *The Astrophysical Journal Letters*, vol. 532, no. 1, p. L25, 2000.

[125] P. W. A. Roming, P. Schady, D. B. Fox et al., "Very early optical afterglows of gamma-ray bursts: evidence for relative paucity of detection," *The Astrophysical Journal*, vol. 652, no. 2, p. 1416, 2006.

[126] E. S. Rykoff, F. Aharonian, C. W. Akerlof et al., "Looking into the fireball: Rotse-III AND *Swift* observations of early gamma-ray burst afterglows," *The Astrophysical Journal*, vol. 702, no. 1, p. 489, 2009.

[127] A. Gomboc, S. Kobayashi, C. G. Mundell et al., "Optical flashes, reverse shocks and magnetization," *AIP Conference Proceedings*, vol. 1133, pp. 145–150, 2009.

[128] H. Gao, W.-H. Lei, Y.-C. Zou, X.-F. Wu, and B. Zhang, "A complete reference of the analytical synchrotron external shock models of gamma-ray bursts," *New Astronomy Reviews*, vol. 57, no. 6, pp. 141–190, 2013.

[129] D. Kopač, C. G. Mundell, S. Kobayashi et al., "Radio flares from gamma-ray bursts," *The Astrophysical Journal*, vol. 806, no. 2, p. 179, 2015.

[130] L. Resmi and B. Zhang, "Gamma-ray burst reverse shock emission in early radio afterglows," *The Astrophysical Journal*, vol. 825, no. 1, p. 48, 2016.

[131] S. Inoue, K. Omukai, and B. Ciardi, "The radio to infrared emission of very high redshift gamma-ray bursts: probing early star formation through molecular and atomic absorption lines," *Monthly Notices of the Royal Astronomical Society*, vol. 380, no. 4, pp. 1715–1728, 2007.

[132] N. Gehrels and P. Mészáros, "γ-ray bursts," *Science*, vol. 337, no. 6097, pp. 932–936, 2012.

[133] L. Kidd and E. Troja, "The nature of the most extreme cosmic explosions: broadband studies of fermi LAT GRB afterglows," *American Astronomical Society Meeting Abstracts*, vol. 223, no. 223, 352.14, 2014.

[134] S. Iyyani, F. Ryde, M. Axelsson et al., "Variable jet properties in GRB 110721A: time resolved observations of the jet photosphere," *Monthly Notices of the Royal Astronomical Society*, vol. 433, no. 4, pp. 2739–2748, 2013.

[135] L. Amati, F. Frontera, M. Tavani et al., "Intrinsic spectra and energetics of BeppoSAX γ-ray bursts with known redshifts," *Astronomy and Astrophysics*, vol. 390, no. 1, pp. 81–89, 2002.

[136] K. P. Singh, S. N. Tandon, P. C. Agrawal et al., "ASTROSAT mission," in *Space Telescopes and Instrumentation: Ultraviolet to Gamma Ray*, vol. 9144 of *Proceedings of SPIE*, Montréal, Canada, June 2014.

[137] A. R. Rao, "Hard X-ray spectro-polarimetry of Black Hole sources?" in *Proceedings of the Recent Trends in the Study of Compact Objects (RETCO-II): Theory and Observation*, I. Chattopadhyay, A. Nandi, S. Das, and S. Mandal, Eds., vol. 12 of *ASI Conference Series*, 2015.

[138] V. Bhalerao, D. Bhattacharya, A. R. Rao, and S. Vadawale, "GRB 151006A: astrosat CZTI detection," *GRB Coordinates Network, Circular Service*, no. 18422, p. 1, 2015.

[139] J. E. Rhoads, "How to tell a jet from a balloon: a proposed test for beaming in gamma-ray bursts," *The Astrophysical Journal Letters*, vol. 487, no. 1, p. L1, 1997.

[140] G. Ghirlanda, D. Burlon, G. Ghisellini et al., "GRB orphan afterglows in present and future radio transient surveys," *Publications of the Astronomical Society of Australia*, vol. 31, article e022, 2014.

[141] A. M. Soderberg, E. Nakar, E. Berger, and S. R. Kulkarni, "Late-time radio observations of 68 type Ibc supernovae: strong constraints on off-axis gamma-ray bursts," *Astrophysical Journal*, vol. 638, no. 2, pp. 930–937, 2006.

[142] M. F. Bietenholz, F. De Colle, J. Granot, N. Bartel, and A. M. Soderberg, "Radio limits on off-axis grb afterglows and vlbi observations of sn 2003 gk," *Monthly Notices of the Royal Astronomical Society*, vol. 440, no. 1, pp. 821–832, 2014.

[143] K. S. Thorne, "Gravitational radiation," in *Three Hundred Years of Gravitation*, S. W. Hawking and W. Israel, Eds., pp. 330–458, Cambridge University Press, Cambridge, UK, 1987.

[144] B. F. Schutz, "Sources of gravitational radiation: coalescing binaries," *Advances in Space Research*, vol. 9, no. 9, pp. 97–101, 1989.

[145] K. Hotokezaka and T. Piran, "Mass ejection from neutron star mergers: different components and expected radio signals," *Monthly Notices of the Royal Astronomical Society*, vol. 450, no. 2, pp. 1430–1440, 2015.

[146] W.-F. Fong, B. D. Metzger, E. Berger, and F. Ozel, "Radio constraints on long-lived magnetar remnants in short gamma-ray bursts," https://arxiv.org/abs/1607.00416.

[147] J. F. Graham, A. S. Fruchter, E. M. Levesque et al., "High metallicity LGRB hosts," https://arxiv.org/abs/1511.00667.

[148] J. Greiner, M. J. Michałowski, S. Klose et al., "Probing dust-obscured star formation in the most massive gamma-ray burst host galaxies," *Astronomy & Astrophysics*, vol. 593, article A17, 12 pages, 2016.

Hindawi Publishing Corporation
Advances in Astronomy
Volume 2016, Article ID 1928465, 12 pages
http://dx.doi.org/10.1155/2016/1928465

Research Article

A Decade of GRB Follow-Up by BOOTES in Spain (2003–2013)

Martin Jelínek,[1,2] Alberto J. Castro-Tirado,[2,3] Ronan Cunniffe,[2] Javier Gorosabel,[2,4,5] Stanislav Vítek,[6] Petr Kubánek,[7,8] Antonio de Ugarte Postigo,[2] Sergey Guziy,[2] Juan C. Tello,[2] Petr Páta,[6] Rubén Sánchez-Ramírez,[2] Samantha Oates,[2] Soomin Jeong,[2,9] Jan Štrobl,[1] Sebastián Castillo-Carrión,[10] Tomás Mateo Sanguino,[11] Ovidio Rabaza,[12] Dolores Pérez-Ramírez,[13] Rafael Fernández-Muñoz,[14] Benito A. de la Morena Carretero,[15] René Hudec,[1,6] Víctor Reglero,[8] and Lola Sabau-Graziati[16]

[1] *Astronomický Ústav AV ČR, Ondřejov (ASÚ AV ČR), Ondřejov, Czech Republic*
[2] *Instituto de Astrofísica de Andalucía- (IAA-) CSIC, 18008 Granada, Spain*
[3] *Departamento de Ingeniería de Sistemas y Automática (Unidad Asociada al CSIC), Universidad de Málaga, 29010 Málaga, Spain*
[4] *Unidad Asociada Grupo Ciencia Planetarias UPV/EHU-IAA/CSIC, Departamento de Física Aplicada I, E.T.S. de Ingeniería, Universidad del País Vasco (UPV)/EHU, Alameda de Urquijo s/n, 48013 Bilbao, Spain*
[5] *Ikerbasque, Basque Foundation for Science, Alameda de Urquijo 36-5, 48008 Bilbao, Spain*
[6] *České Vysoké Učení Technické, Fakulta Elektrotechnická (ČVUT-FEL), Praha, Czech Republic*
[7] *Fyzikální ústav AV ČR, Na Slovance 2, 182 21 Praha 8, Czech Republic*
[8] *Image Processing Laboratory, Universidad de Valencia, Burjassot, Valencia, Spain*
[9] *Institute for Science and Technology in Space, Natural Science Campus, Sungkyunkwan University, Suwon 440-746, Republic of Korea*
[10] *Universidad de Málaga, Campus de Teatinos, Málaga, Spain*
[11] *Departamento de Ingeniería de Sistemas y Automática, Universidad de Huelva, E.P.S. de La Rábida, Huelva, Spain*
[12] *Department of Civil Engineering, University of Granada, 18071 Granada, Spain*
[13] *Universidad de Jaén, Campus las Lagunillas, 23071 Jaén, Spain*
[14] *Instituto de Hortofruticultura Subtropical y Mediterránea "La Mayora" (IHSM-CSIC), Algarrobo, 29750 Málaga, Spain*
[15] *Estación de Sondeos Atmosféricos (ESAt) de El Arenosillo (CEDEA-INTA), Mazagón, Huelva, Spain*
[16] *División de Ciencias del Espacio, INTA, Torrejón de Ardoz, Madrid, Spain*

Correspondence should be addressed to Martin Jelínek; mates@iaa.es

Received 11 March 2016; Accepted 17 August 2016

Academic Editor: Dean Hines

This article covers ten years of GRB follow-ups by the Spanish BOOTES stations: 71 follow-ups providing 23 detections. Follow-ups by BOOTES-1B from 2005 to 2008 were given in a previous article and are here reviewed and updated, and additional detection data points are included as the former article merely stated their existence. The all-sky cameras CASSANDRA have not yet detected any GRB optical afterglows, but limits are reported where available.

Dedicated to the memory of Dolores Pérez-Ramírez and Javier Gorosabel, who passed away while this paper was in preparation

1. Introduction

Ever since the discovery of Gamma-ray bursts (GRB) in 1967 [1], it was hoped to discover their counterparts at other wavelengths. The early GRB-related transient searching methods varied (wide-field optical systems as well as deep searches were being employed) but, given the coarse gamma-ray-based GRB localizations provided, generally lacked either

sensitivity or good reaction time. The eventual discovery of GRB optical counterparts was done only when an X-ray follow-up telescope was available on the BeppoSAX satellite [2]. The optical afterglow could then be searched for with a large telescope in a small errorbox provided by the discovery of the X-ray afterglow. The first optical afterglow of a gamma-ray burst was discovered this way in 1997 [3].

Since then, astronomers have been trying to minimize the time delay between receiving the position and the start of observations—by both personal dedication and by automating the telescope reaction. The ultimate step in automation, to minimize the time delay, is a full robotization of the observatory to eliminate any human intervention in the follow-up process. This way, the reaction time can be minimized from ~10-minute limit that can be achieved with a human operated telescope to below 10 seconds. With improvements in computational methods and in image processing speed, blind (non-follow-up) wide-field methods are starting to be practical in the search for optical transients. Although limited in magnitude range, they have already provided important observations of the optical emission simultaneous to the gamma-ray production of a GRB [4].

Since 1997, the robotic telescope network BOOTES has been part of the effort to follow up gamma-ray burst events [5]. As of now, the network of robotic telescopes BOOTES consists of six telescopes around the globe, dedicated primarily to GRB afterglow follow-up. We present the results of our GRB follow-up programme by two telescopes of the network—BOOTES-1B and BOOTES-2—and by the respective stationary very-wide-field cameras (CASSANDRA). This text covers eleven years of GRB follow-ups: 71 follow-ups providing 21 detections.

Different instruments have been part of BOOTES during the years in question: a 30 cm telescope which was used for most of the time at BOOTES-1 station but at periods also at BOOTES-2, the fast-moving 60 cm telescope at BOOTES-2 (Telma), and also two all-sky cameras, CASSANDRA1 at BOOTES-1 and CASSANDRA2 at BOOTES-2. Results from CASSANDRAs are included where available, without paying attention to the complete sample.

This article is a follow-up of a previous article, that is, Jelínek et al. [6], which provided detailed description of evolution of BOOTES-1B, and analysis of efficiency of a system dedicated to GRB follow-up based on real data obtained during four years between 2005 and 2008. This work is a catalogue of BOOTES-1B and BOOTES-2 GRB observations between 2003 and 2013; it is complete in providing information about successfully followed up events but does not provide analysis of missed triggers as did the previous article.

1.1. BOOTES-1B. BOOTES-1 observatory is located at the atmospheric sounding station at El Arenosillo, Huelva, Spain (at lat.: $37^\circ 06' 14''$N, long.: $06^\circ 44' 02''$W). Over time, distinct system configurations were used, including also two 8-inch S-C telescopes, as described in Jelínek et al. [6]; the primary instrument of BOOTES-1B is a $D = 30$ cm Schmidt-Cassegrain optical tube assembly with a CCD camera. Prior to June 15, 2007, Bessel *VRI* filters were being used as noted with the observations, any observations obtained after this date have been obtained without filter (*C* or clear). We calibrate these observations against *R*-band, which, in the case of no color evolution of the optical counterpart, is expected to result in a small (~0.1 mag) constant offset in magnitude.

1.2. BOOTES-2. BOOTES-2 is located at CSIC's experimental station La Mayora (Instituto de Hortofruticultura Subtropical y Mediterránea- (IHSM-) CSIC) (at lat.: $36^\circ 45' 33''$N, long.: $04^\circ 02' 27''$W), 240 km from BOOTES-1. It was originally equipped with an identical 30 cm Schmidt-Cassegrain telescope to that at BOOTES-1B. In 2007 the telescope was upgraded to a lightweight 60 cm Ritchey-Chrètien telescope on a fast-slewing NTM-500 mount, both provided by Astelco. The camera was upgraded at the same time to an Andor iXon 1024×1024 EMCCD, and in 2012 the capabilities were extended yet again to low resolution spectroscopy, by the installation of the imaging spectrograph COLORES of our own design and construction [7]. Bessel magnitudes are calibrated to Vega system, SDSS to AB.

2. Optical Follow-Up of GRB Events

Here we will detail the individual results for each of the 23 events followed up and detected in 2003–2013. Each GRB is given a short introductory paragraph as a reminder of the basic observational properties of the event. Although we do not discuss the properties at other wavelengths, we try to include a comprehensive reference of literature relevant to each burst. As GCN reports usually summarise the relevant GCN circular traffic, we have omitted the raw GCN circulars except for events for which a GCN report or other more exhaustive paper is unavailable.

Further 48 follow-ups which resulted in detection limits are included in Tables 1 and 2 but are not given any further attention.

One by one, we show all the successful follow-ups that these telescopes have performed during the first ten years of the *Swift* era and since the transition of the BOOTES network to the RTS-2 [14] observatory control system, which was for the first time installed at BOOTES-2 in 2003 and during the summer of 2004 at BOOTES-1.

GRB 050525A (A Bright Low-Redshift ($z = 0.606$) Localized by Swift [15]). Plenty of optical observations were obtained, including the signature of the associated supernova sn2005nc [8, 16].

GRB 050525A was the first BOOTES-1B burst for which a detection was obtained. The telescope started the first exposure 28 s after receiving the notice, 383 s after the GRB trigger. An optical afterglow with $V \simeq 16$ was detected. A weak detection of a bright GRB implied a reexamination of observing strategies employed by BOOTES. The largest, 30 cm telescope was changed to make *R*-band imaging instead of using the field spectrograph to greatly improve sensitivity in terms of limiting magnitude. The 20 cm telescopes were still observing with $V + I$ filters (for details see [6]); see Table 3.

Table 1: BOOTES-1B GRBs in a table.

GRB	ΔT	Number of points	Result	Ref.
030913	2 h		$V > 17.5, C > 12$	
050215B	22 m		$V > 16.5, I > 15.0$	
050505	47 m		$V > 19$	
050509A	64 m		$V > 14.9$	
050509B	62 s		$V > 11.5$	
050525A	12 m†	1	16.5 ± 0.4	[8]
050528	71 s		$V > 13.8, I > 13.0$	
050824	10 m	4	$R = 18.2 \pm 0.3$	[9]
050904	2 m		$R > 18.2$	[10]
050922C	4 m	3	$R = 14.6 \pm 0.4$	
051109A	55 s	6	$R = 15.7 \pm 0.4$	
051211B	42 s		$R > 14$	
051221B	4 m		$R > 16$	
060421	61 s		$R > 14$	
061110B	11 m		$R > 18$	
071101	55 s		$C > 17.0$	
071109	59 s		$C > 13.0$	
080330	6 m	6	$C = 16.5 \pm 0.2$	
080413A	61 s	61	$C \simeq 13.3$	
080430	34 s	1	$C \simeq 15.5$	
080603B	1 h	11	$C \simeq 17.4$	[11]
080605	44 s	28	$C \simeq 14.7$	[12]
081003B	41 s		$C > 17.6$	
090313	12 h	1	$C \simeq 18.3$	
090519	99 s		$C > 17.6$	
090813	53 s	1	$C \simeq 17.9$	
090814A	3 m†		$C > 15.8$	
090814B	53 s†		$C > 17.5$	
090817	24 m		$C > 16.7$	
100906A	106 s		$C > 16.5$	
110205A	102 s	16	$C \sim 14$	[13]
110212A	50 s		$C > 13.0$	
110213A	15 h	1	$C = 18.3 \pm 0.2$	
110411A	24 s		$C > 17.8$	
111016A	1.25 h		$C > 17.8$	
120326A	40 m	1	$C \sim 19.5$	
120327A	41 m†	6	$C = 17.5$	
120328A	7.5 m		$C > 16$	
120521C	11.7 m		$C > 20.5$	
120711B	107 s		$C > 18.2$	
120729A	10 h		$C > 19.0$	
121017A	79 s		$C > 19.0$	
121024A	40 m	1	$C = 18.2 \pm 0.5$	
121209A	42 s†		$C > 16.5$	
130122A	28 m		$C > 18.4$	

Note. † marks alerts covered in real time by wide-field camera CASSANDRA-1.

This burst was covered in real time by both all-sky cameras of BOOTES (CASSANDRA1 and CASSANDRA2), providing an unfiltered limit of >9.0 [17].

Table 2: BOOTES-2 GRBs in a table.

GRB	ΔT	Number of points	Result	Ref.
080603B		20	$R \simeq 17.4$	[11]
080605		5	$R \simeq 14.7$	[12]
090817	145 s		$R > 18.3$	
090904A	86 s		$R > 16.1$	
091202	5.5 h		$R > 18.3$	
100219A	6.3 h		$C > 18.3$	
100418A	1.8 h	11	$C = 19.3$	
100522A	625 s		$C > 15.5$	
100526A	4 h		$r' > 14$	
100614A	6.9 m		$C > 18$	
100901A	10 h	10	$C = 17.52 \pm 0.08$	
100915A	106 s		$C > 16.5$	
101020A	5.1 h		$r' > 18.0$	
101112A	595 s	15	$C = 15.5$	
110106B	10.3 m		$C > 16.5$	
110205A	15 m	13	$R \sim 14$	[13]
110212A	32 m		$R > 16.5$	
110223A	228 s		$R > 17.6$	
120729A	13.25 h		$R > 19.4$	
120805A	25 m		$R > 18.5$	
120816A	66 m		$R > 18$	
121001A	32 m		$I > 19.7$	
121017A	3 m		$C > 18.5, i' > 19.5$	
130418A	1.5 h	21	$C = 16.8 \pm 0.06$	
130505A	11.94 h	1	$R_C = 19.26 \pm 0.06$	
130606A	13 m	21	$i' = 16.7 \pm 0.3$	
130608A	2.3 h		$C > 18.8$	
130612A	4.8 m		$C > 18.6$	
130806A	40 s		$C > 18.3$	
131202A	4.25 h		$i' > 19.7$	

Table 3: GRB 050525A: observing log of BOOTES-1B.

ΔT [h]	exp [s]	mag	dmag	Filter
0.195	39×10 s	16.51	0.39	R

Note. Published by Resmi et al. [8].

BOOTES observation of this GRB is included in Resmi et al. [8].

GRB 050824 (A Dim Burst Detected by Swift). The optical afterglow of this GRB is discovered with the 1.5 m telescope at OSN; redshift $z = 0.83$ as determined by VLT [9].

BOOTES-1B was the first telescope to observe this optical transient, starting 636 s after the trigger with $R \simeq 17.5$. The weather was not stable and the focus not perfect, but BOOTES-1B worked as expected. In the end, several hours of data were obtained. BOOTES observation of this GRB is included in Sollerman et al. [9]; see Table 4 and Figure 1.

GRB 050922C. A *Swift* short and intense long burst [18, 19] was observed also by *HETE2* [20]. Optical afterglow is mag ~ 15; $z = 2.198$ [21].

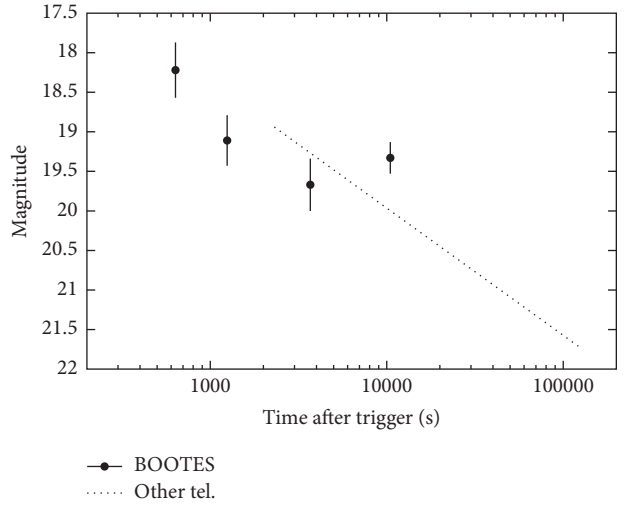

Figure 1: The optical light curve of GRB 050824; the optical light curve represents the behaviour seen by Sollerman et al. [9].

Table 4: GRB 050824: observing log of BOOTES-1B.

ΔT [h]	exp [s]	mag	dmag	Filter
0.1763	2×300 s	18.22	0.35	*R*
0.3462	8×300 s	19.11	0.32	*R*
1.0249	22×300 s	19.67	0.33	*R*
2.9091	31×300 s	19.33	0.20	*R*

Note. Published by Sollerman et al. [9].

Table 5: GRB 050922C: observing log of BOOTES-1B.

ΔT [h]	exp [s]	mag	dmag	Filter
0.0694	40	14.58	0.35	*R*
0.3752	900	17.01	0.39	*R*
0.6193	900	18.53	0.59	*R*

Due to clouds, the limiting magnitude of BOOTES-1B dropped from ~17.0 for a 30 s exposure to merely 12.9. The afterglow was eventually detected with the *R*-band camera (at the 30 cm telescope) during gaps between passing clouds. The first weak detection was obtained 228 s after the GRB trigger and gave $R \simeq 14.6$; see Table 5.

GRB 051109A (A Burst Detected by Swift [23]). The optical afterglow was mag $\sim$ 15, and the redshift was determined to be $z = 2.346$ [24]. The optical lightcurve was published by Mirabal et al. [22].

At BOOTES-1B the image acquisition started 54.8 s after the burst with the 30 cm telescope in *R*-band and one of the 20 cm telescopes in *I*-band [25]. There were still a number of performance problems—most importantly synchronization between cameras such that when the telescope position was to be changed, both cameras had to be idle. As the 30 cm telescope was taking shorter exposures, extra exposures could have been made while waiting for the longer exposures being taken at the 20 cm to finish. The 20 cm detection is, after critical revision, only at the level of 2-σ. The *R*-band

Table 6: GRB 051109A: observing log of BOOTES-1B.

ΔT [s]	exp [s]	mag	dmag	Filter
59.7	10	15.67	0.35	*R*
122.2	74	16.02	0.19	*R*
257.9	41	16.65	0.41	*R*
756.6	205	17.18	0.22	*R*
1021.5	313	17.68	0.26	*R*
508.4	908	16.98	0.54	*I*

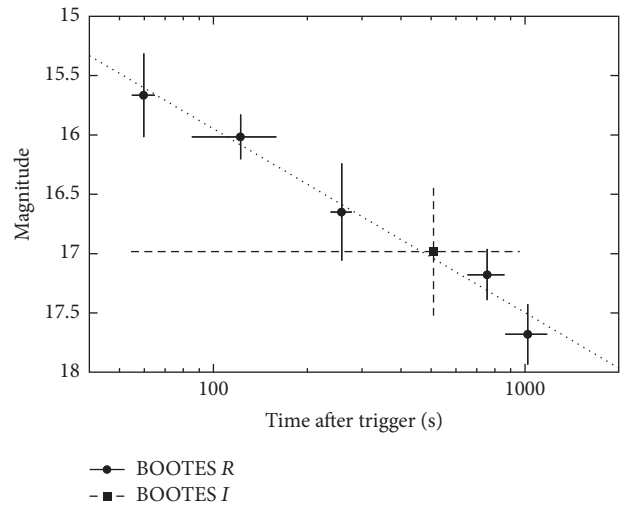

Figure 2: The optical light curve of GRB 051109A. The dotted line represents the optical decay observed by Mirabal et al. [22].

observation shows the object until about 20 minutes after the GRB, when it becomes too dim to measure in the vicinity of a 17.5 m nearby star. Mean decay rate observed by BOOTES is $\alpha = 0.63 \pm 0.06$ ($F_{\text{opt}} \sim t^{-\alpha}$).

The relatively shallow decay observed by BOOTES is in close agreement with what was observed several minutes later by the 2.4 m MDM ($\alpha = 0.62 \pm 0.03$) and according to an unofficial report [26] there was a decay change later, by about 3 h after the burst to $\alpha = 0.89 \pm 0.05$; see Table 6 and Figure 2.

GRB 080330 (A Rather Bright Long Burst Detected by Swift). Afterglow was reported to be detected by UVOT, TAROT, ROTSE-III, Liverpool Telescope, and GROND. Spectroscopic redshift was measured as $z = 1.51$ by the NOT [28].

This GRB happened during the first day recommissioning of BOOTES-1B after its move from the BOOTES-2 site at La Mayora. The GCN client was not yet operational and at the time of the GRB we were focusing the telescope. The first image was obtained 379 s after the GRB trigger and the optical afterglow was detected with magnitude ~16.3 on the first image. A bug in the centering algorithm caused a loss of part subsequent data. Further detections were obtained starting 21 min after the GRB when the problem was fixed.

The light curve (as seen by [27]) seems to show an optical flare and then a possible hydrodynamic peak. The data of BOOTES, however, trace only the final part of this

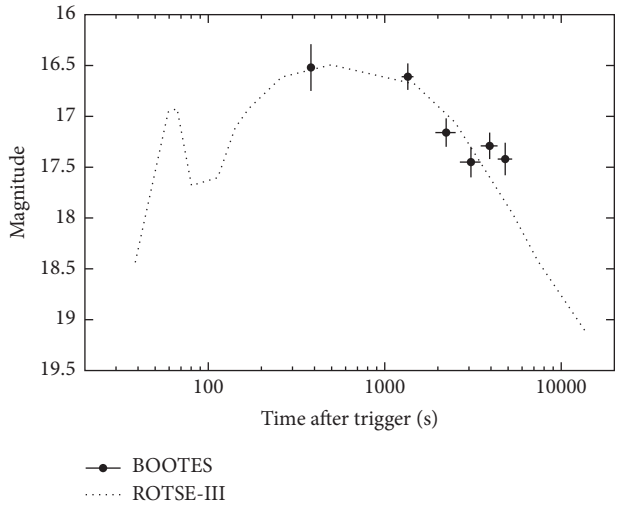

Figure 3: The optical light curve of GRB 080330. The dotted line shows the light curve as seen by ROTSE-III [27].

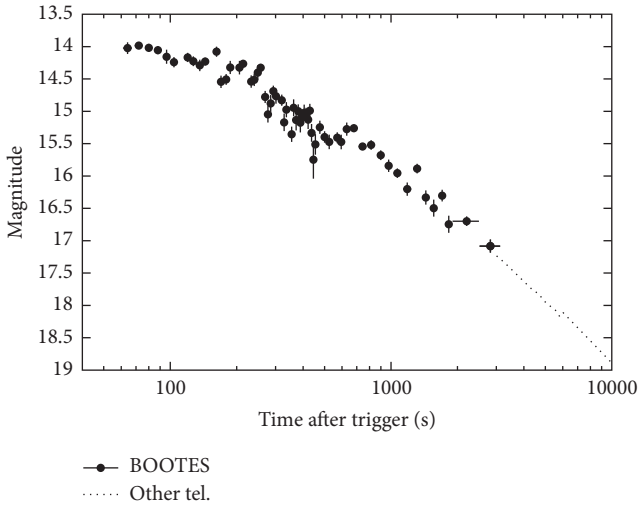

Figure 4: The optical light curve of GRB 080413A.

Table 7: GRB 080330: observing log of BOOTES-1B.

ΔT [h]	exp [s]	mag	dmag	Filter
0.1061	7	16.52	0.23	Clear
0.3752	210	16.61	0.13	Clear
0.6193	588	17.16	0.14	Clear
0.8547	825	17.45	0.15	Clear
1.0915	862	17.29	0.13	Clear
1.3384	905	17.42	0.16	Clear

behaviour, where the decay accelerates after passing through the hydrodynamic peak; see Table 7 and Figure 3.

GRB 080413A. A rather bright GRB was detected by *Swift* and also by *Suzaku*-WAM; optical afterglow was detected by ROTSE-III [27]; and redshift $z = 2.433$ was detected by VLT+UVES [29].

BOOTES-1B started obtaining images of the GRB 080413A just 60.7 s after the trigger (46.3 s after reception of the alert). An $R \simeq 13.3$ magnitude decaying optical afterglow was found ([30], *Jelínek et al., in prep.*); see Figure 4.

GRB 080430 (A Burst Detected by Swift). It was a widely observed, low-redshift $z \simeq 0.75$ optical afterglow with a slowly decaying optical afterglow [31]. It was observed also at very high energies by *MAGIC* without detection [32].

BOOTES-1B obtained the first image of this GRB 34.4 s after the trigger. An optical transient was detected on combined unfiltered images with a magnitude $\simeq 15.5$ [33].

GRB 080603B. A long GRB localized by *Swift* is detected also by *Konus*-Wind and by *INTEGRAL* [34]. Bright optical afterglow was observed. Extensive follow-up was carried out. Redshift is $z = 2.69$ [35].

This GRB happened in Spain during sunset. We obtained first useful images starting one hour after the trigger. An

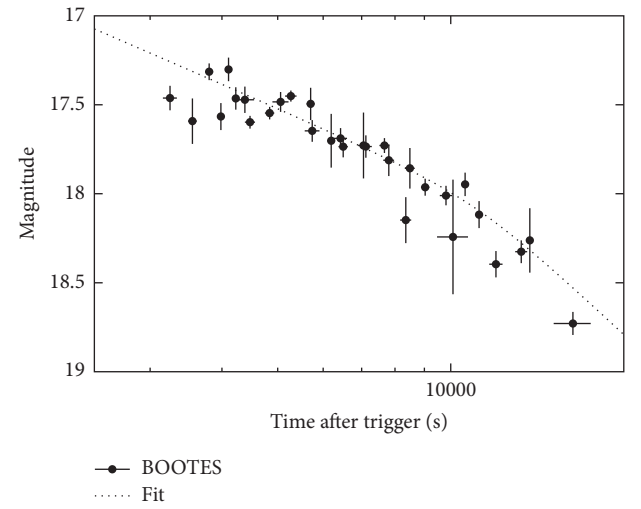

Figure 5: The optical light curve of GRB 080603B [11].

$R \simeq 17.4$ optical transient was detected with both BOOTES-1B and BOOTES-2; see Figure 5. BOOTES observation of this GRB is included in Jelínek et al. [11]; see Figure 5.

GRB 080605 (A Long Burst Detected by Swift [36]). The host was found to be a metal enriched star forming galaxy at redshift $z = 1.64$ [37] and exhibited the 2175 Å extinction feature [38].

GRB 080605 was observed by both BOOTES-1B (28 photometric points) and BOOTES-2 (5 photometric points) starting 44 s after the trigger. A rapidly decaying optical afterglow ($\alpha = 1.27 \pm 0.04$) with $R = 14.7$ on the first images was found; see Figure 6. All BOOTES data are included in Jelínek et al. [12]; see Figure 5.

GRB 090313 (GRB by Swift, No Prompt X-Rays [40]). An optical afterglow peaked at $R \sim 15.6$. Extensive optical + infrared follow-up was carried out. The first GRB to be observed

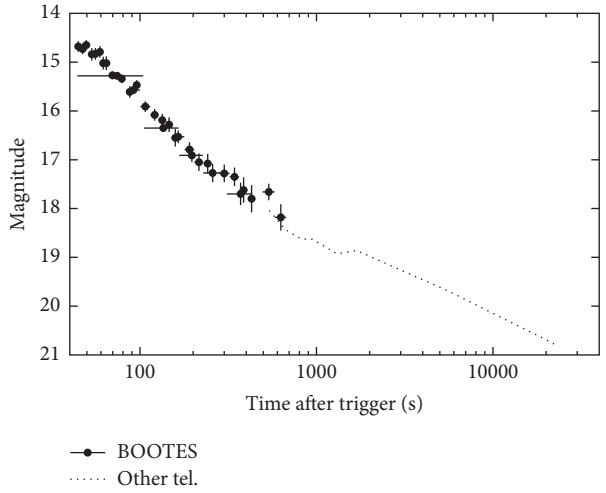

Figure 6: The optical light curve of GRB 080605 [12]; the dotted line is behaviour observed by Rumyantsev and Pozanenko [39] and Zafar et al. [38].

Table 8: GRB 090813: observing log of BOOTES-1B.

ΔT [h]	exp [s]	mag	dmag	Filter
0.175	10×10	17.9	0.3	Clear

was detected by X-Shooter. Also it was detected by various observatories in radio. Redshift is $z = 3.375$ [41, 42].

The GRB happened during daytime for BOOTES-1B and it was followed up manually. Due to the proximity of the moon and limitations of then-new CCD camera driver, many 2 s exposures were taken to be combined later. The optical afterglow was detected with magnitude ~18.3 ± 0.4 on a 635×2 s (=21 min) exposure with the midtime 11.96 h after the GRB trigger.

GRB 090813. A long GRB by *Swift*, suspected of being higher-z, observed also by *Konus*-Wind and *Fermi*-GBM [43]. Optical counterpart was observed by the 1.23 m telescope at Calar Alto with a magnitude of $I = 17.0$ [44].

BOOTES-1B started observation 53 s after the GRB, taking 10 s unfiltered exposures. The optical transient was weakly detected on a combined image of 10×10 s whose exposure mean time was 630 s after the burst. The optical counterpart was found having $R = 17.9 \pm 0.3$. Given that the previous and subsequent images did not show any OT detection, we might speculate about the optical emission peaking at about this time. Also the brightness is much weaker than what might be expected from the detection by Gorosabel et al. [44], supporting the high-redshift origin; see Table 8.

GRB 100418A. A weak long burst was detected by *Swift* [45] with a peculiar, late-peaking optical afterglow with $z = 0.6239$ [46]. Also it was detected in radio [47].

The first image of the GRB location was taken by BOOTES-2 at 21:50 UT (40 min after the GRB trigger). The rising optical afterglow was detected for the first time on an image obtained as a sum of 23 images, with an exposure

Table 9: GRB 100418A: observing log of BOOTES-2.

ΔT [h]	exp [s]	mag	dmag	Filter
1.78	1638	19.785	0.215	Clear
2.09	597	19.127	0.127	Clear
2.55	534	18.774	0.087	Clear
2.72	656	18.668	0.073	Clear
3.10	239	18.706	0.106	Clear
3.43	238	18.759	0.189	Clear
4.70	3908	19.067	0.108	Clear
6.19	4328	18.897	0.115	Clear
7.39	551	18.493	0.078	Clear
77.3	14830	20.475	0.202	Clear
125.6	12482	20.970	0.208	Clear

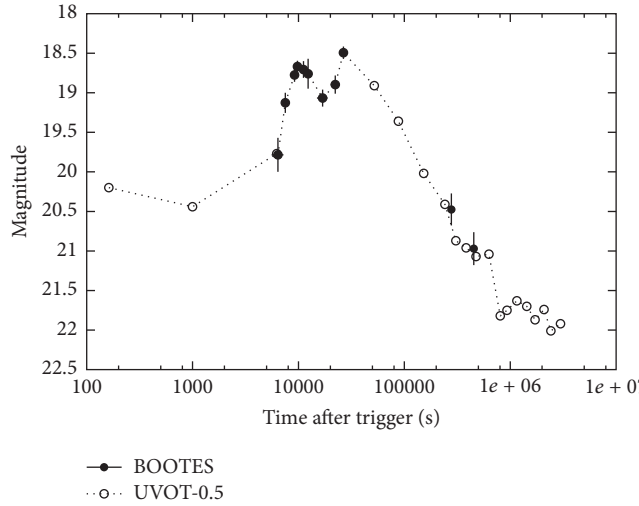

Figure 7: The bizarre optical light curve of GRB 100418A. Combination of BOOTES and UVOT data [45]. UVOT points were shifted by an arbitrary constant.

midtime 107 minutes after the GRB trigger. The optical emission peaked at magnitude $R = 18.7$ another hour later, at an image with the midtime 163 min after the trigger. A slow decay followed, which permitted us to detect the optical counterpart until 8 days after the GRB.

Because of a mount problem, many images were lost (pointed somewhere else) and the potential of the telescope was not fully used. Eventually, after combining images when appropriate, 11 photometric points were obtained. A rising part of the optical afterglow was seen that way; see Table 9 and Figure 7.

GRB 100901A (A Long Burst from Swift). Bright, slowly decaying optical afterglow was discovered by UVOT. Redshift is $z = 1.408$. It was detected also by SMA at 345 GHz [48–50].

The burst happened in daytime in Spain and the position became available only almost ten hours later after the sunset. The afterglow was still well detected with magnitude $R \simeq 17.5$ at the beginning. BOOTES-2 had some problems with CCD cooling, and some images were useless. The afterglow was

Table 10: GRB 100901A: observing log of BOOTES-2.

ΔT [h]	exp [s]	mag	dmag	Filter
10.202	268	17.52	0.08	*R*
10.719	415	17.61	0.07	*R*
11.230	354	17.67	0.09	*R*
11.734	238	17.99	0.16	*R*
12.346	730	17.78	0.13	*R*
12.980	759	17.68	0.12	*R*
13.239	759	17.82	0.16	*R*
13.971	997	18.21	0.12	*R*
14.611	1101	18.32	0.14	*R*
33.791	4012	19.35	0.19	*R*

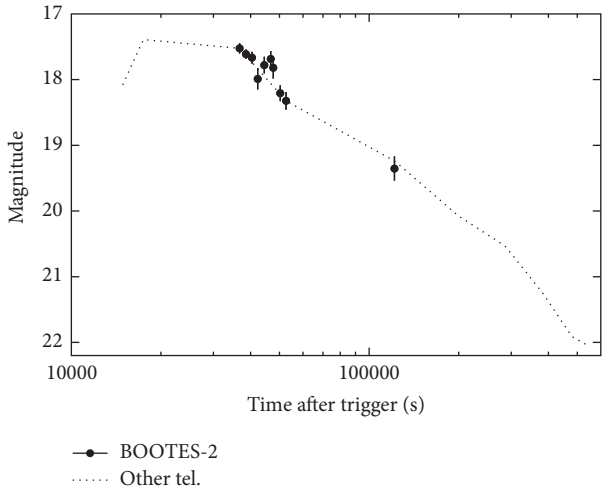

Figure 8: The optical light curve of GRB 100901A. The dotted line representing burst behaviour is based on observations by Gorbovskoy et al. [49], Kann et al. [51], and Rumyantsev et al. [52].

detected also the following night with $R = 19.35$; see Table 10 and Figure 8.

GRB 101112A. An *INTEGRAL*-localized burst [53] was also detected by *Fermi*-GBM [54], *Konus*-Wind [55], and *Swift*-XRT [56]. Optical afterglow was discovered independently by BOOTES-2 and Liverpool Telescope [57]. It was detected also in radio [58].

BOOTES-2 reacted to the GRB 101112A and started to observe 47 s after the GRB. A set of 3 s exposures was taken, but due to technical problems with the mount a significant amount of observing time was lost. An optical afterglow was discovered and reported [59]. The optical light curve exhibited first a decay, then a sudden rise to a peak at about 800 s after the trigger, and finally a surprisingly fast decay with $\alpha \simeq -4$. This behaviour seemed more like an optical flare than a "proper" GRB afterglow, but there does not seem to be contemporaneous high-energy data to make a firm statement; see Table 11 and Figure 9.

GRB 110205A (A Very Long and Bright Burst by Swift). Detected also by *Konus*-Wind and *Suzaku*-WAM, optical

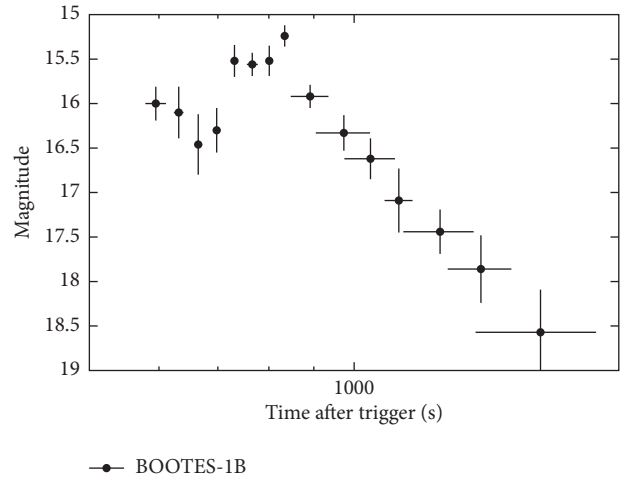

Figure 9: The optical light curve of GRB 101112A.

Table 11: GRB 101112A: observing log of BOOTES-2.

ΔT [s]	exp [s]	mag	dmag	Filter
595.0	16	16.00	0.19	r'
631.8	8	16.10	0.29	r'
664.9	7	16.46	0.34	r'
697.8	7	16.30	0.25	r'
731.0	7	15.52	0.18	r'
766.1	11	15.56	0.13	r'
800.9	7	15.52	0.17	r'
833.8	7	15.24	0.12	r'
891.2	44	15.92	0.13	r'
973.7	69	16.33	0.20	r'
1044.0	69	16.62	0.23	r'
1124.2	41	17.09	0.36	r'
1252.7	115	17.44	0.25	r'
1393.8	116	17.86	0.38	r'
1629.5	255	18.57	0.48	r'

afterglow peaked at $R \sim 14.0$, with extensive multiwavelength follow-up; $z = 2.22$ *"Textbook burst"* [13, 60].

BOOTES-1B reacted automatically to the *Swift* trigger. First 10 s unfiltered exposure was obtained 102 s after the beginning of the GRB (with $T_{90} = 257$ s), that is, while the gamma-ray emission was still taking place. After taking 18 images, the observatory triggered on a false alarm from the rain detector, which caused the observation to be stopped for 20 minutes. After resuming the observation, 3×30 s images were obtained and another false alert struck over. This alert was remotely overridden by Kubánek, so that all 20 minutes was not lost. From then on, the observation continued until sunrise. The afterglow is well detected in the images until 2.2 hours after the GRB. 16 photometric points from combined images were eventually published.

BOOTES-2 started observations 15 min after the trigger, clearly detecting the afterglow in *R*-band until 3.2 hours after the burst. 13 photometric points were obtained. The delay was

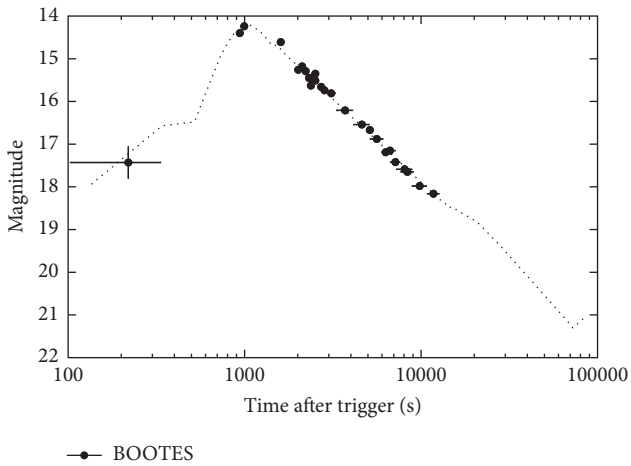

Figure 10: The optical light curve of GRB 110205A.

Table 12: GRB 110213A: observing log of BOOTES-1B.

ΔT [h]	exp [s]	mag	dmag	Filter
15.5	100×30	18.29	0.30	Clear

caused by technical problems. BOOTES observations of this GRB are included in Zheng et al. [13]; see Figure 10.

GRB 110213A. A bright burst was detected by *Swift*; it was detected also by *Konus*-Wind and *Fermi*-GBM. Optical afterglow is $R \sim 14.6$, with extensive follow-up [61].

BOOTES-1B started to observe 15 hours after the GRB (the position was below horizon at the time of the trigger) and continued for an hour; eventually, 100×30 s unfiltered images were combined; the OT brightness calibrated against USNO-A2 is 18.3 ± 0.3 at the exposure midtime of 15.5 h after the GRB trigger; see Table 12.

GRB 120326A (A Swift-Detected Burst). Afterglow was discovered by Tarot [62]. It is long-lived optical emission; redshift is $z = 1.78$ by GTC. It was detected also by *Fermi*-GBM and *Suzaku*-WAM (see [63] and the references therein).

At BOOTES-1B the mount failed, because of the serial port communication failure. After a manual recovery, 40 minutes after the GRB, images were taken in hope for a detection, but the counterpart with the brightness of $R \sim 19.5$ was detected only at about 2σ level.

GRB 120327A. A bright burst by *Swift* with an afterglow is discovered by UVOT [64]. Redshift is $z = 2.813$ [65]. Extensive optical follow-up was carried out.

BOOTES-1B reacted in 41 min (similar failure as the day before: the mount failed, because of the serial port communication failure), obtaining a series of 20 s exposures. These images were combined to get 600 s effective exposures and permitted detection of the afterglow on six such images. The brightness was decaying from $R = 17.5$ to $R = 18.6$; see Table 13.

Table 13: GRB 120327A: observing log of BOOTES-1B.

ΔT [h]	exp [s]	mag	dmag	Filter
0.955	654	17.50	0.12	Clear
1.140	674	17.65	0.12	Clear
1.337	748	17.82	0.13	Clear
1.533	660	18.24	0.21	Clear
1.718	673	18.17	0.21	Clear
1.905	656	18.59	0.29	Clear

Table 14: GRB 121024A: observing log of BOOTES-1B.

ΔT [h]	exp [s]	mag	dmag	Filter
0.900	1200	18.2	0.5	Clear

All-sky camera at BOOTES-1 (CASSANDRA1) covered the event in real time and detected nothing down to $R \sim 7.5$ *(Zanioni et al. in prep.)*.

GRB 121001A. A bright and long *Swift*-detected GRB was originally designated as possibly galactic [66]. Afterglow was discovered by Andreev et al. [67].

BOOTES-2 observed this trigger starting 32 min after the trigger. An optical afterglow is detected in I-band with $I \sim 19.7$ (Vega) for a sum of images between 20:49 and 21:52 UT [68].

GRB 121024A. It is a bright *Swift*-detected GRB with a bright optical afterglow [69, 70]. It was detected also in radio [71]. Redshift is $z = 2.298$ by Tanvir et al. [72].

BOOTES-1B observed the optical afterglow of GRB 121024A. The observations started 40 minutes after the GRB trigger. The sum of 20 minutes of unfiltered images with a mean integration time 54 minutes after the GRB shows a weak detection of the optical afterglow with magnitude $R = 18.2 \pm 0.5$ [73]; see Table 14.

GRB 130418A. It is a bright and long burst with a well-detected optical afterglow somewhat peculiarly detected after a slew by *Swift* [74]. Observation by *Konus*-Wind showed that the burst started already 218 s before *Swift* triggered [75]. Redshift is $z = 1.218$ by de Ugarte Postigo et al. [76].

BOOTES-2 obtained a large set of unfiltered, r'-band and i'-band images starting 1.5 h after the trigger. The optical afterglow is well detected in the images. The light curve is steadily decaying with the power-law index of $\alpha = -0.93 \pm 0.06$, with the exception of the beginning, where there is a possible flaring with peak about 0.25 mag brighter than the steady power-law; see Table 15 and Figure 11.

GRB 130505A. A bright and intense GRB with a 14 mag optical afterglow was detected by *Swift* [77]. Redshift is $z = 2.27$ as reported by Tanvir et al. [78].

BOOTES-2 obtained the first image of this GRB 11.94 h after the trigger. A set of 60 s exposures was obtained. Combining the first hour of images taken, we clearly detect the optical afterglow, and using the calibration provided by Kann et al. [79], we measure $R_C = 19.26 \pm 0.06$; see Table 16.

Table 15: GRB 130418A: observing log of BOOTES-1B and BOOTES-2.

ΔT [h]	exp [s]	mag	dmag	Filter
1.514	3×15 s	17.09	0.08	Clear
1.529	3×15 s	16.95	0.07	Clear
1.544	3×15 s	16.90	0.06	Clear
1.558	3×15 s	16.62	0.07	Clear
1.573	3×15 s	17.03	0.07	Clear
1.590	4×15 s	16.92	0.06	Clear
1.610	4×15 s	17.04	0.07	Clear
1.749	7×15 s	17.22	0.05	Clear
1.865	60 s	16.92	0.18	r'
1.884	4×15 s	17.34	0.09	Clear
2.054	7×15 s	17.45	0.07	Clear
2.089	7×15 s	17.46	0.06	Clear
2.209	6×15 s	17.47	0.07	Clear
2.326	6×15 s	17.56	0.08	Clear
2.444	6×15 s	17.71	0.09	Clear
2.562	6×15 s	17.68	0.08	Clear
2.798	22×60 s	17.40	0.04	i'
3.061	15×60 s	17.90	0.09	r'
3.333	15×60 s	17.98	0.09	r'
3.604	15×60 s	17.90	0.09	r'
3.866	15×60 s	18.05	0.11	r'
4.130	15×60 s	18.53	0.19	r'
4.449	20×60 s	18.42	0.14	r'
4.808	20×60 s	18.61	0.23	r'

Table 16: GRB 130505A: observing log of BOOTES-2.

ΔT [h]	exp [s]	mag	dmag	Filter
12.488	51×60 s	19.26	0.06	Clear

GRB 130606A. A high-redshift GRB was detected by *Swift* [80], optical afterglow was discovered by BOOTES-2, and redshift is $z = 5.9$ by GTC [81].

BOOTES-2 reaction to this GRB alert was actually a failure; the system did not respond as well as it should and it had to be manually overridden to perform the observations. The first image has therefore been taken as late as 13 minutes after the trigger. These observations led to a discovery of a bright afterglow not seen by *Swift*-UVOT and prompted spectroscopic observations by 10.4 m GTC, which show redshift of this event to be $z = 5.9135$. Overall, 14 photometric points in i'-band and 7 in z'-band were obtained [81]; see Figure 12.

3. Summary

Eleven years of BOOTES-1B and BOOTES-2 GRB follow-up history are summarised in the textual and tabular form. Each GRB is given a short introductory paragraph as a reminder of the basic optical properties of the event. Although we do not discuss the properties in other wavelengths, we try to include a comprehensive reference of literature relevant to each burst. One by one, we show all the successful follow-ups that these telescopes have performed during the first ten years of the *Swift* era and the transition of the BOOTES network to the RTS-2 [14] observatory control system, first installed at BOOTES-2 in 2003 and made definitive during the summer of 2004.

The BOOTES telescopes, in spite of their moderate apertures ($\lesssim$60 cm), have proven to detect a significant number of afterglows—together over 20, contributing to the understanding of the early GRB phase.

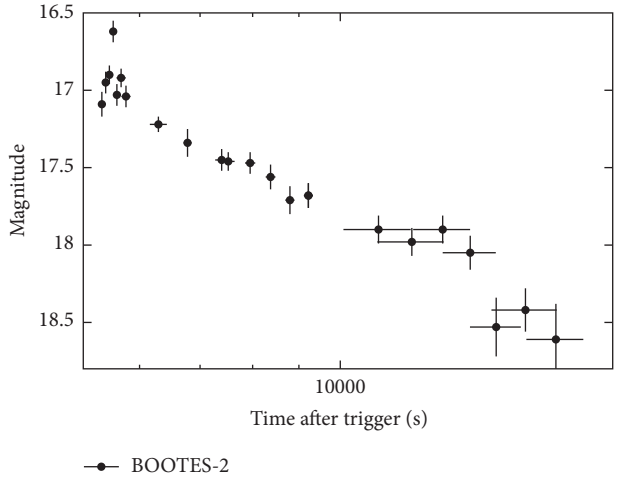

Figure 11: The optical light curve of GRB 130418A.

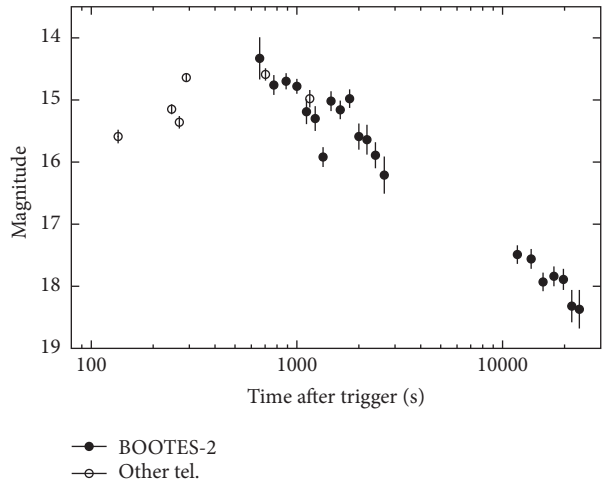

Figure 12: The optical light curve of GRB 130606A. i'-band points were shifted 2.4 mag up to match with the z'-band points.

Competing Interests

The authors declare that they have no competing interests.

Acknowledgments

The authors appreciate the auspices of INTA, IHSM-UMA/CSIC, and UMA as well as the financial support by

the Junta de Andaluca and the Spanish Ministry of Economy and Competitiveness through the Research Projects P07-TIC-03094, P12-TIC2839, AYA 2009-14000-C03-01, AYA 2010-39727-C03-01, and AYA-2015-71718-R. Martin Jelínek was supported by the postdoctoral fellowship of the Czech Academy of Sciences. This study was carried out in the framework of the Unidad Asociada IAA-CSIC at the Group of Planetary Science of ETSI-UPV/EHU. This work was supported by the Ikerbasque Foundation for Science. The Czech CVUT FEL team acknowledges the support by GA CR Grant 13-33324S.

References

[1] R. W. Klebesadel, I. B. Strong, and R. A. Olson, "Observations of gamma-ray bursts of cosmic origin," *The Astrophysical Journal*, vol. 182, pp. L85–L88, 1973.

[2] E. Costa, F. Frontera, J. Heise et al., "Discovery of an X-ray afterglow associated with the γ-ray burst of 28 February 1997," *Nature*, vol. 387, no. 6635, pp. 783–785, 1997.

[3] J. van Paradijs, P. J. Groot, T. Galama et al., "Transient optical emission from the error box of the γ-ray burst of 28 february 1997," *Nature*, vol. 386, no. 6626, pp. 686–689, 1997.

[4] J. L. Racusin, S. V. Karpov, M. Sokolowski et al., "Broadband observations of the naked-eye big γ-ray burst GRB 080319B," *Nature*, vol. 455, pp. 183–188, 2008.

[5] A. J. Castro-Tirado, M. Jelínek, T. J. Mateo Sanguino, and A. De Ugarte Postigo, "BOOTES: a stereoscopic robotic ground support facility," *Astronomische Nachrichten*, vol. 325, article 679, 2004.

[6] M. Jelínek, A. J. Castro-Tirado, A. D. U. Postigo et al., "Four years of real-time GRB followup by BOOTES-1B (2005–2008)," *Advances in Astronomy*, vol. 2010, Article ID 432172, 10 pages, 2010.

[7] O. Rabaza, M. Jelínek, A. J. Castro-Tirado et al., "Compact low resolution spectrograph, an imaging and long slit spectrograph for robotic telescopes," *Review of Scientific Instruments*, vol. 84, no. 11, Article ID 114501, 2013.

[8] L. Resmi, K. Misra, G. Jóhannesson et al., "Comprehensive multiwavelength modelling of the afterglow of GRB 050525A," *Monthly Notices of the Royal Astronomical Society*, vol. 427, no. 1, pp. 288–297, 2012.

[9] J. Sollerman, J. P. U. Fynbo, J. Gorosabel et al., "The nature of the X-ray flash of August 24 2005," *A&A*, vol. 466, no. 3, pp. 839–846, 2007.

[10] J. B. Haislip, M. C. Nysewander, D. E. Reichart et al., "A photometric redshift of $z = 6.39 \pm 0.12$ for GRB 050904," *Nature*, vol. 440, pp. 181–183, 2006.

[11] M. Jelínek, J. Gorosabel, A. J. Castro-Tirado et al., "BOOTES observation of GRB080603B," *Acta Polytechnica*, vol. 52, Article ID 010000, 2012.

[12] M. Jelínek, E. Gómez Gauna, and A. J. Castro-Tirado, "Photometric observations of GRB 080605 by Bootes-1b and Bootes-2," in *Gamma-Ray Bursts: 15 Years of GRB Afterglows*, A. J. Castro-Tirado, J. Gorosabel, and I. H. Park, Eds., vol. 61, pp. 475–477, EAS Publications Series, 2013.

[13] W. Zheng, R. F. Shen, T. Sakamoto et al., "Panchromatic observations of the textbook GRB 110205A: constraining physical mechanisms of prompt emission and afterglow," *The Astrophysical Journal*, vol. 751, no. 2, Article ID 90, 21 pages, 2012.

[14] P. Kubánek, M. Jelínek, M. Nekola et al., "RTS2—remote telescope system, 2nd version," in *Proceedings of the Gamma-Ray Bursts: 30 Years of Discovery*, vol. 727 of *AIP Conference Proceedings*, p. 753, Sante Fe, NM, USA, 2004.

[15] A. J. Blustin, D. Band, S. Barthelmy et al., "*Swift* panchromatic observations of the bright gamma-ray burst GRB 050525a," *The Astrophysical Journal*, vol. 637, no. 2, p. 901, 2006.

[16] M. Della Valle, D. Malesani, J. S. Bloom et al., "Hypernova signatures in the late rebrightening of GRB 050525A," *The Astrophysical Journal Letters*, vol. 642, no. 2, pp. L103–L106, 2006.

[17] A. de Ugarte Postigo, M. Jelínek, J. Gorosabel et al., "GRB 050525A: bootes simultaneous optical observations," GCN Circular 3480, 2005.

[18] J. Norris, L. Barbier, D. Burrows et al., "GRB 050822C: swift detection of a bright burst," GCN Circular 4013, 2005.

[19] H. Krimm, L. Barbier, S. Barthelmy et al., "GCN circular," Tech. Rep. 4020, 2005.

[20] G. Crew, G. Ricker, J.-L. Atteia et al., "HETE fregate observations of GRB 050922C," GCN Circular 4021, 2005.

[21] P. Jakobsson, J. P. U. Fynbo, D. Paraficz et al., "GRB 050922C: refined redshift," GCN Circular 4029, 2005.

[22] N. Mirabal, J. P. Halpern, S. Tonnesen et al., "GRB 051109A: a shallow optical afterglow decay," in *Proceedings of the American Astronomical Society Meeting*, vol. 207, American Astronomical Society, 2006, Abstract 210.02.

[23] E. Fenimore, L. Angelini, L. Barbier et al., "GRB 051109: Swift-BAT refined analysis," GCN Circular 4217, 2005.

[24] R. Quimby, D. Fox, P. Hoeich, B. Roman, and J. C. Wheeler, "GRB 051109: HET optical spectrum and absorption redshift," GCN Circular 4221, 2005.

[25] M. Jelínek, A. de Ugarte Postigo, A. J. Castro-Tirado et al., "GRB 051109a: bootes R & I-band detection of the early afterglow," GCN Circular 4227, 2005.

[26] N. Mirabal, J. Halpern, S. Tonnesen, J. Eastman, and J. Prieto, 2005, http://user.astro.columbia.edu/~jules/grb/051109a/.

[27] F. Yuan, E. S. Rykoff, B. E. Schaefer et al., *Prompt Optical Observations of GRB 080330 and GRB 080413A*, vol. 1065 of *American Institute of Physics Conference Series*, American Institute of Physics, 2008, Edited by Y.-F. Huang, Z.-G. Dai, & B. Zhang.

[28] J. Mao, C. Guidorzi, C. Markwardt et al., "Swift Observation of GRB 080330," GCN Report 132, 2008.

[29] F. E. Marshall, S. D. Barthelmy, D. N. Burrows et al., "Final swift observations of GRB 080413A," GCN Report 129, 2008.

[30] P. Kubánek, M. Jelínek, J. Gorosabel et al., "GCN circular," Tech. Rep. 7603, 2008.

[31] C. Guidorzi, M. Stamatikos, W. Landsman et al., "Swift Observations of GRB 080430," GCN Report 139, 2008.

[32] J. Aleksić, H. Anderhub, L. A. Antonelli et al., "MAGIC observation of the GRB 080430 afterglow," *Astronomy & Astrophysics*, vol. 517, article A5, 2010.

[33] M. Jelínek, P. Kubánek, J. Gorosabel et al., "A decade of GRB follow-up by BOOTES in Spain," 9 Circular 7648, 2008.

[34] A. Rau, A. V. Kienlin, K. Hurley, and G. G. Lichti, "The 1st INTEGRAL SPI-ACS gamma-ray burst catalogue," *Astronomy and Astrophysics*, vol. 438, no. 3, pp. 1175–1183, 2005.

[35] V. Mangano, A. Parsons, T. Sakamoto et al., "Swift observation of GRB 080603B," GCN Report 144, 2008.

[36] B. Sbarufatti, A. Parsons, T. Sakamoto et al., "Swift observation of GRB 080605," *GCN Report*, vol. 142, 2008.

[37] T. Kruhler, J. P. U. Fynbo, S. Geier et al., "The metal-enriched host of an energetic γ-ray burst at $z \approx 1.6$," *Astronomy & Astrophysics*, vol. 546, article A8, 2012.

[38] T. Zafar, D. Watson, Á. Elíasdóttir et al., "The properties of the 2175 å extinction feature discovered in GRB afterglows," *The Astrophysical Journal*, vol. 753, no. 1, p. 82, 2012.

[39] V. Rumyantsev and A. Pozanenko, "GRB 080605: optical observations," GRB Coordinates Network 7857, 2008.

[40] J. Mao, R. Margutti, T. Sakamoto et al., "Swift observations of GRB 090313," GCN Report 204, 2009.

[41] A. de Ugarte Postigo, P. Goldoni, C. C. Thone et al., "GRB 090313: X-shooter's first shot at a gamma-ray burst," *A&A*, vol. 513, article A42, 2010.

[42] A. Melandri, S. Kobayashi, C. G. Mundell et al., "GRB 090313 and the origin of optical peaks in γ-ray burst light curves: implications for lorentz factors and radio flares," *The Astrophysical Journal*, vol. 723, no. 2, p. 1331, 2010.

[43] J. R. Cummings, A. P. Beardmore, and P. Schady, "Swift observations of GRB 090813," GCN Report 240, 2009.

[44] J. Gorosabel, V. Terron, M. Fernandez et al., "GRB 090813: optical candidate from 1.23 m CAHA telescope," GCN Circular 9782, 2009.

[45] F. E. Marshall, L. A. Antonelli, D. N. Burrows et al., "The late peaking afterglow of GRB 100418A," *The Astrophysical Journal*, vol. 727, no. 2, p. 132, 2011.

[46] A. de Ugarte Postigo, C. C. Thone, P. Goldoni, and J. P. U. Fynbo, "Time resolved spectroscopy of GRB 100418A and its host galaxy with X-shooter," *Astronomische Nachrichten*, vol. 332, no. 3, pp. 297–298, 2011.

[47] A. Moin, P. Chandra, J. C. A. Miller-Jones et al., "Radio observations of GRB 100418a: test of an energy injection model explaining long-lasting grb afterglows," *The Astrophysical Journal*, vol. 779, no. 2, p. 105, 2013.

[48] S. Immler, T. Sakamoto, K. L. Page et al., "Swift observations of GRB 100901A," GCN Report 304, 2010.

[49] E. S. Gorbovskoy, G. V. Lipunova, V. M. Lipunov et al., "Prompt, early and afterglow optical observations of five γ-ray bursts: GRB 100901A, GRB 100902A, GRB 100905A, GRB 100906A and GRB 101020A," *MNRAS*, vol. 421, no. 3, pp. 1874–1890, 2012.

[50] O. E. Hartoog, K. Wiersema, P. M. Vreeswijk et al., "The host-galaxy response to the afterglow of GRB 100901A," *Monthly Notices of the Royal Astronomical Society*, vol. 430, no. 4, pp. 2739–2754, 2013.

[51] D. A. Kann, U. Laux, and B. Stecklum, "GRB 100901A: TLS observations, SDSS calibration, decay slope," GCN Circular 11236, 2010.

[52] V. Rumyantsev, D. Shakhovkoy, and A. Pozanenko, "GRB 100901A: CrAO optical observation," GCN Circular 11255, 2010.

[53] D. Gotz, S. Mereghetti, A. Paizis et al., "GRB 101112A: a long GRB detected by INTEGRAL," GCN Circular 11396, 2010.

[54] A. Goldstein, "GRB 101112A: Fermi GBM detection," GCN Circular 11403, 2010.

[55] S. Golenetskii, R. Aptekar, D. Frederiks et al., "Konus-wind observation of GRB 101112A," GCN Circular 11400, 2010.

[56] P. A. Evans and H. A. Krimm, "GRB 101112A—XRT source detection/analysis," GCN Circular 11399, 2010.

[57] C. Guidorzi, R. J. Smith, C. G. Mundell et al., "GRB101112A: Liverpool telescope afterglow candidate," GCN Circular 11397, 2010.

[58] P. Chandra, D. A. Frail, and S. B. Cenko, "Possible detection of INTEGRAL burst GRB 101112A by the EVLA," GCN Circular 11404, 2010.

[59] A. de Ugarte Postigo, P. Kubánek, J. C. Tello et al., "GRB 101112A: BOOTES-2/TELMA optical afterglow candidate," GCN Circular 11398, 2010.

[60] B. Gendre, J. L. Atteia, M. Boer et al., "GRB 110205A: anatomy of a long gamma-ray burst," *The Astrophysical Journal*, vol. 748, no. 1, Article ID 59, 2012.

[61] V. D'Elia, G. Stratta, N. P. M. Kuin et al., "Swift observation of GRB 110213A," GCN Report 323, 2011.

[62] A. Klotz, B. Gendre, M. Boer, and J. L. Atteia, "GRB 120326A: TAROT calern observatory afterglow optical detection," GCN Circular 13107, 2012.

[63] M. H. Siegel, N. P. M. Kuin, S. Holland et al., "Swift observations of GRB 120326A," GCN Report 409, 2013.

[64] B. Sbarufatti, S. D. Barthelmy, N. Gehrels et al., "GRB 120327A: swift detection of a burst with an optical counterpart," GCN Circular 13123, 2012.

[65] V. D'Elia, "VLT/X-shooter absorption spectroscopy of the GRB 120327a afterglow," in *EAS Publications Series*, A. J. Castro-Tirado, J. Gorosabel, and I. H. Park, Eds., vol. 61 of *EAS Publications Series*, pp. 247–249, 2013.

[66] V. D'Elia, J. R. Cummings, M. Stamatikos et al., "Swift observations of GRB 121001A," GCN Report 392, 2012.

[67] M. Andreev, A. Sergeev, and A. Pozanenko, "GRB 121001A: possible optical counterpart," GCN Circular 13833, 2012.

[68] J. C. Tello, R. Gimeno, J. Gorosabel et al., "Swift trigger 535026: optical decay confirmation with IAC80 and BOOTES-2/TELMA," GCN Circular 13835, 2012.

[69] C. Pagani, S. D. Barthelmy, W. H. Baumgartner et al., "GRB 121024A: swift detection of a burst with an optical counterpart," GCN Circular 13886, 2012.

[70] A. Klotz, B. Gendre, M. Boer, and J. L. Atteia, "GRB 121024A: TAROT calern observatory optical detection of a bright counterpart," GCN Circular 13887, 2012.

[71] T. Laskar, A. Zauderer, and E. Berger, "GRB 121024A: EVLA detection," GCN Circular 13903, 2012.

[72] N. R. Tanvir, J. P. U. Fynbo, A. Melandri et al., "GRB 121024A: VLT/X-shooter redshift," GCN Circular 13890, 2012.

[73] M. Jelínek, A. J. Castro-Tirado, and J. Gorosabel, "GRB 121024A: BOOTES-1B optical detection," GCN Circular 13888, 2012.

[74] M. de Pasquale, W. H. Baumgartner, A. P. Beardmore et al., "GRB 130418A: swift detection of a burst with an optical counterpart," GCN Circular 14377, 2013.

[75] S. Golenetskii, R. Aptekar, D. Frederiks et al., "Konus-wind observation of GRB 130418A," GCN Circular 14417, 2013.

[76] A. de Ugarte Postigo, C. C. Thoene, J. Gorosabel et al., "GRB 130418A: redshift from 10.4 m GTC," GCN Circular 14380, 2013.

[77] J. K. Cannizzo, S. D. Barthelmy, J. R. Cummings, A. Melandri, and M. de Pasquale, "Swift observations of GRB 130505A," GCN Report 429, 2013.

[78] N. R. Tanvir, A. J. Levan, T. Matulonis, and A. B. Smith, "GRB 130505A—Gemini-N/GMOS redshift determination," GCN Circular 14567, 2013.

[79] D. A. Kann, B. Stecklum, and F. Ludwig, "GRB 130505A: tautenburg afterglow observations," GCN Circular 14593, 2013.

[80] T. N. Ukwatta, M. Stamatikos, A. Maselli et al., "Swift observations of GRB 130606A," GCN Report 444, 2013.

[81] A. J. Castro-Tirado, R. Sánchez-Ramírez, S. L. Ellison et al., "GRB 130606A within a sub-DLA at redshift 5.91," http://arxiv.org/abs/1312.5631.

Hindawi Publishing Corporation
Advances in Astronomy
Volume 2016, Article ID 6341974, 12 pages
http://dx.doi.org/10.1155/2016/6341974

Review Article

Kilonova/Macronova Emission from Compact Binary Mergers

Masaomi Tanaka

National Astronomical Observatory of Japan, Mitaka, Tokyo 181-8588, Japan

Correspondence should be addressed to Masaomi Tanaka; masaomi.tanaka@nao.ac.jp

Received 11 March 2016; Accepted 16 May 2016

Academic Editor: WeiKang Zheng

We review current understanding of kilonova/macronova emission from compact binary mergers (mergers of two neutron stars or a neutron star and a black hole). Kilonova/macronova is emission powered by radioactive decays of r-process nuclei and it is one of the most promising electromagnetic counterparts of gravitational wave sources. Emission from the dynamical ejecta of $\sim 0.01 M_\odot$ is likely to have a luminosity of $\sim 10^{40}$–10^{41} erg s^{-1} with a characteristic timescale of about 1 week. The spectral peak is located in red optical or near-infrared wavelengths. A subsequent accretion disk wind may provide an additional luminosity or an earlier/bluer emission if it is not absorbed by the precedent dynamical ejecta. The detection of near-infrared excess in short GRB 130603B and possible optical excess in GRB 060614 supports the concept of the kilonova/macronova scenario. At 200 Mpc distance, a typical peak brightness of kilonova/macronova with $0.01 M_\odot$ ejecta is about 22 mag and the emission rapidly fades to >24 mag within ~10 days. Kilonova/macronova candidates can be distinguished from supernovae by (1) the faster time evolution, (2) fainter absolute magnitudes, and (3) redder colors. Since the high expansion velocity ($v \sim 0.1$–$0.2c$) is a robust outcome of compact binary mergers, the detection of smooth spectra will be the smoking gun to conclusively identify the gravitational wave source.

1. Introduction

Mergers of compact stars, that is, neutron star (NS) and black hole (BH), are promising candidates for direct detection of gravitational waves (GWs). On 2015 September 14, Advanced LIGO [1] has detected the first ever direct GW signals from a BH-BH merger (GW150914) [2]. This discovery marked the dawn of GW astronomy.

NS-NS mergers and BH-NS mergers are also important and leading candidates for the GW detection. They are also thought to be progenitors of short-hard gamma-ray bursts (GRBs [3–5]; see also [6, 7] for reviews). When the designed sensitivity is realized, Advanced LIGO [1], Advanced Virgo [8], and KAGRA [9] can detect the GWs from these events up to ~200 Mpc (for NS-NS mergers) and ~800 Mpc (for BH-NS mergers). Although the event rates are still uncertain, more than one GW event per year is expected [10].

Since localization only by the GW detectors is not accurate, for example, more than a few 10 deg^2 [11–14], identification of electromagnetic (EM) counterparts is essentially important to study the astrophysical nature of the GW sources. In the early observing runs of Advanced LIGO and Virgo, the localization accuracy can be >100 deg^2 [15–17]. In fact, the localization for GW150914 was about 600 deg^2 (90% probability) [18].

To identify the GW source from such a large localization area, intensive transient surveys should be performed (see, e.g., [19–24] for the case of GW150914). NS-NS mergers and BH-NS mergers are expected to emit EM emission in various forms. One of the most robust candidates is a short GRB. However, the GRB may elude our detection due to the strong relativistic beaming. Other possible EM signals include synchrotron radio emission by the interaction between the ejected material and interstellar gas [25–27] or X-ray emission from a central engine [28–31].

Among variety of emission mechanisms, optical and infrared (IR) emission powered by radioactive decay of r-process nuclei [32–37] is of great interest. This emission is called "kilonova" [34] or "macronova" [33] (we use the term of kilonova in this paper). Kilonova emission is thought to be promising: by advancement of numerical simulations, in particular numerical relativity [38–41], it has been proved that a part of the NS material is surely ejected from NS-NS and BH-NS mergers (e.g., [36, 42–49]). In the ejected

material, r-process nucleosynthesis undoubtedly takes place (e.g., [35, 36, 49–56]). Therefore the emission powered by r-process nuclei is a natural outcome from these merger events.

Observations of kilonova will also have important implications for the origin of r-process elements in the Universe. The event rate of NS-NS mergers and BH-NS mergers will be measured by the detection of GWs. In addition, as described in this paper, the brightness of kilonova reflects the amount of the ejected r-process elements. Therefore, by combination of GW observations and EM observations, that is, "multi-messenger" observations, we can measure the production rate of r-process elements by NS-NS and BH-NS mergers, which is essential to understand the origin of r-process elements. In fact, importance of compact binary mergers in chemical evolution has been extensively studied in recent years [72–82].

This paper reviews kilonova emission from compact binary mergers. The primal aim of this paper is providing a guide for optical and infrared follow-up observations for GW sources. For the physical processes of compact binary mergers and various EM emission mechanisms, see recent reviews by Rosswog [83] and Fernández and Metzger [84]. First, we give overview of kilonova emission and describe the expected properties of the emission in Section 2. Then, we compare kilonova models with currently available observations in Section 3. Based on the current theoretical and observational understanding, we discuss prospects for EM follow-up observations of GW sources in Section 4. Finally, we give summary in Section 5. In this paper, the magnitudes are given in the AB magnitude unless otherwise specified.

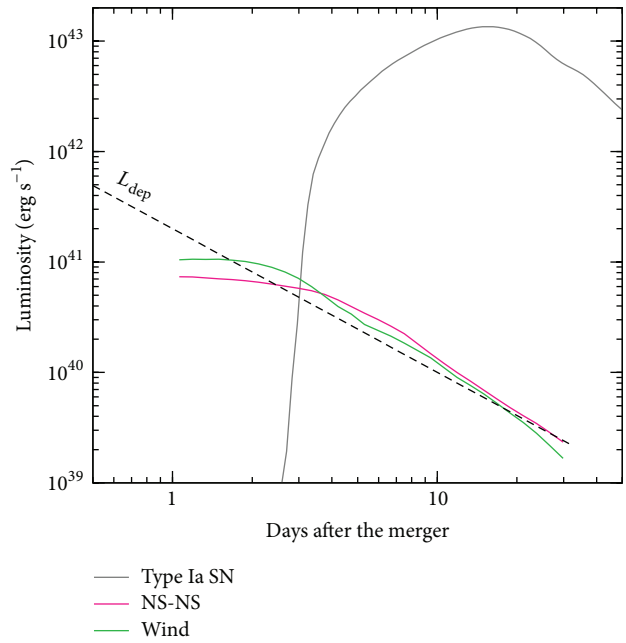

Figure 1: Bolometric light curves of a NS-NS merger model (red, $M_{ej} = 0.01M_\odot$ [57, 58]) and a wind model (green, $M_{ej} = 0.01M_\odot$) compared with a light curve of Type Ia SN model (gray, $M_{ej} = 1.4M_\odot$). The black dashed line shows the deposition luminosity by radioactive decay of r-process nuclei ($\epsilon_{dep} = 0.5$ and $M_{ej} = 0.01M_\odot$).

2. Kilonova Emission

2.1. Overview. The idea of kilonova emission was first introduced by Li and Paczyński [32]. The emission mechanism is similar to that of Type Ia supernova (SN). The main differences are the following: (1) a typical ejecta mass from compact binary mergers is only an order of $0.01M_\odot$ ($1.4M_\odot$ for Type Ia SN), (2) a typical expansion velocity is as high as $v \sim 0.1$–$0.2c = 30,000$–$60,000\,\mathrm{km\,s^{-1}}$ (~10,000 km s^{-1} for Type Ia SN), and (3) the heating source is decay energy of radioactive r-process nuclei (^{56}Ni for Type Ia SN).

Suppose spherical, homogeneous, and homologously expanding ejecta with a radioactive energy deposition. A typical optical depth in the ejecta is $\tau = \kappa\rho R$, where κ is the mass absorption coefficient or "opacity" (cm^2 g^{-1}), ρ is the density, and R is the radius of the ejecta. Then, the diffusion timescale in the ejecta is

$$t_{diff} = \frac{R}{c}\tau \simeq \frac{3\kappa M_{ej}}{4\pi c v t}, \tag{1}$$

by adopting $M_{ej} = (4\pi/3)\rho R^3$ (homogeneous ejecta) and $R = vt$ (homologous expansion).

When the dynamical timescale of the ejecta ($t_{dyn} = R/v = t$) becomes comparable to the diffusion timescale, photons can escape from the ejecta effectively [85]. From the condition of $t_{diff} = t_{dyn}$, the characteristic timescale of the emission can be written as follows:

$$\begin{aligned} t_{peak} &= \left(\frac{3\kappa M_{ej}}{4\pi c v}\right)^{1/2} \\ &\simeq 8.4\ \mathrm{days}\left(\frac{M_{ej}}{0.01M_\odot}\right)^{1/2} \\ &\quad \times \left(\frac{v}{0.1c}\right)^{-1/2}\left(\frac{\kappa}{10\ \mathrm{cm^2\ g^{-1}}}\right)^{1/2}. \end{aligned} \tag{2}$$

The radioactive decay energy of mixture of r-process nuclei is known to have a power-law dependence $\dot{q}(t) \simeq 2 \times 10^{10}\,\mathrm{erg\,s^{-1}\,g^{-1}}(t/1\ \mathrm{day})^{-1.3}$ [34, 35, 54, 86–88]. By introducing a fraction of energy deposition (ϵ_{dep}), the total energy deposition rate (or the deposition luminosity) is $L_{dep} = \epsilon_{dep} M_{ej}\dot{q}(t)$. A majority (~90%) of decay energy is released by β decay while the other 10% is released by fission [34]. For the β decay, about 25%, 25%, and 50% of the energy are carried by neutrinos, electrons, and γ-rays, respectively. Among these, almost all the energy carried by electrons is deposited, and a fraction of the γ-ray energy is also deposited to the ejecta. Thus, the fraction ϵ_{dep} is about 0.5 (see [89] for more details). The dashed line in Figure 1 shows the deposition luminosity L_{dep} for $\epsilon_{dep} = 0.5$ and $M_{ej} = 0.01M_\odot$.

Since the peak luminosity is approximated by the deposition luminosity at $t_{\rm peak}$ (so-called Arnett's law [85]), the peak luminosity of kilonova can be written as follows:

$$L_{\rm peak} = L_{\rm dep}\left(t_{\rm peak}\right) = \epsilon_{\rm dep} M_{\rm ej} \dot{q}\left(t_{\rm peak}\right) \simeq 1.3 \times 10^{40}\ {\rm erg\ s^{-1}} \times \left(\frac{\epsilon_{\rm dep}}{0.5}\right)^{1/2} \left(\frac{M_{\rm ej}}{0.01 M_\odot}\right)^{0.35} \times \left(\frac{v}{0.1c}\right)^{0.65} \left(\frac{\kappa}{10\ {\rm cm^2\ g^{-1}}}\right)^{-0.65}. \quad (3)$$

An important factor in this analysis is the opacity in the ejected material from compact binary mergers. Previously, the opacity had been assumed to be similar to that of Type Ia SN, that is, $\kappa \sim 0.1\ {\rm cm^2\ g^{-1}}$ (bound-bound opacity of iron-peak elements). However, recent studies [57, 90, 91] show that the opacity in the r-process element-rich ejecta is as high as $\kappa \sim 10\ {\rm cm^2\ g^{-1}}$ (bound-bound opacity of lanthanide elements). This finding largely revised our understanding of the emission properties of kilonova. As evident from (2) and (3), a higher opacity by a factor of 100 leads to a longer timescale by a factor of ~10 and a lower luminosity by a factor of ~20.

2.2. NS-NS Mergers. When two NSs merge with each other, a small part of the NSs is tidally disrupted and ejected to the interstellar medium (e.g., [36, 42]). This ejecta component is mainly distributed in the orbital plane of the NSs. In addition to this, the collision drives a strong shock, and shock-heated material is also ejected in a nearly spherical manner (e.g., [48, 92]). As a result, NS-NS mergers have quasi-spherical ejecta. The mass of the ejecta depends on the mass ratio and the eccentricity of the orbit of the binary, as well as the radius of the NS or equation of state (EOS, e.g., [48, 92–96]): a more uneven mass ratio and more eccentric orbit lead to a larger amount of tidally disrupted ejecta and a smaller NS radius leads to a larger amount of shock-driven ejecta.

The red line in Figure 1 shows the expected luminosity of a NS-NS merger model (APR4-1215 from Hotokezaka et al. [48]). This model adopts a "soft" EOS APR4 [97], which gives the radius of 11.1 km for a $1.35 M_\odot$ NS. The gravitational masses of two NSs are $1.2 M_\odot + 1.5 M_\odot$ and the ejecta mass is $0.01 M_\odot$. The light curve does not have a clear peak since the energy deposited in the outer layer can escape earlier. Since photons kept in the ejecta by the earlier stage effectively escape from the ejecta at the characteristic timescale (2), the luminosity exceeds the energy deposition rate at ~5–8 days after the merger.

Figure 2 shows multicolor light curves of the same NS-NS merger model (red line; see the right axis for the absolute magnitudes). As a result of the high opacity and the low temperature [90], the optical emission is greatly suppressed, resulting in an extremely "red" color of the emission. The red color is more clearly shown in Figure 3, where the spectral evolution of the NS-NS merger model is compared with the spectra of a Type Ia SN and a broad-line Type Ic SN. In fact, the peak of the spectrum is located at near-IR wavelengths [57, 90, 91].

Because of the extremely high expansion velocities, NS-NS mergers show feature-less spectra (Figure 3). This is a big contrast to the spectra of SNe (black and gray lines), where Doppler-shifted absorption lines of strong features can be identified. Even broad-line Type Ic SN 1998bw (associated with long-duration GRB 980425) showed some absorption features although many lines are blended. Since the high expansion velocity is a robust outcome of dynamical ejecta from compact binary mergers, the confirmation of the smooth spectrum will be a key to conclusively identify the GW sources.

The current wavelength-dependent radiative transfer simulations assume the uniform element abundances. However, recent numerical simulations with neutrino transport show that the element abundances in the ejecta becomes nonuniform [54, 92, 95, 96]. Because of the high temperature and neutrino absorption, the polar region can have higher electron fractions (Y_e or number of protons per nucleon), resulting in a wide distribution of Y_e in the ejecta. Interestingly the wide distribution of Y_e is preferable for reproducing the solar r-process abundance ratios [54, 56]. This effect can have a big impact on the kilonova emission: if the synthesis of lanthanide elements is suppressed in the polar direction, the opacity there can be smaller, and thus, the emission to the polar direction can be more luminous with an earlier peak.

2.3. BH-NS Mergers. Mergers of BH and NS are also important targets for GW detection (see [98] for a review). Although the event rate is rather uncertain [10], the number of events can be comparable to that of NS-NS mergers thanks to the stronger GW signals and thus larger horizon distances. BH-NS mergers in various conditions have been extensively studied by numerical simulations (e.g., [99–103]). In particular, for a low BH/NS mass ratio (or small BH mass) and a high BH spin, ejecta mass of BH-NS mergers can be larger than that of NS-NS mergers [59, 104–109]. Since the tidal disruption is the dominant mechanism of the mass ejection, a larger NS radius (or stiff EOS) gives a higher ejecta mass, which is opposite to the situation in NS-NS mergers, where shock-driven ejecta dominates.

Radiative transfer simulations in BH-NS merger ejecta show that kilonova emission from BH-NS mergers can be more luminous in optical wavelengths than that from NS-NS mergers [58]. The blue lines in Figure 2 show the light curve of a BH-NS merger model (APR4Q3a75 from Kyutoku et al. [59]), a merger of a $1.35 M_\odot$ NS and a $4.05 M_\odot$ BH with a spin parameter of $a = 0.75$. The mass of the ejecta is $M_{\rm ej} = 0.01 M_\odot$. Since BH-NS merger ejecta are highly anisotropic and confined to a small solid angle, the temperature of the ejecta can be higher for a given mass of the ejecta, and thus, the emission tends to be bluer than in NS-NS mergers. Therefore, even if the bolometric luminosity is similar, the optical luminosity of BH-NS mergers can be higher than that of NS-NS mergers.

It is emphasized that the mass ejection from BH-NS mergers has a much larger diversity compared with NS-NS mergers, depending on the mass ratio, the BH spin, and its orientation. As a result, the expected brightness also has a

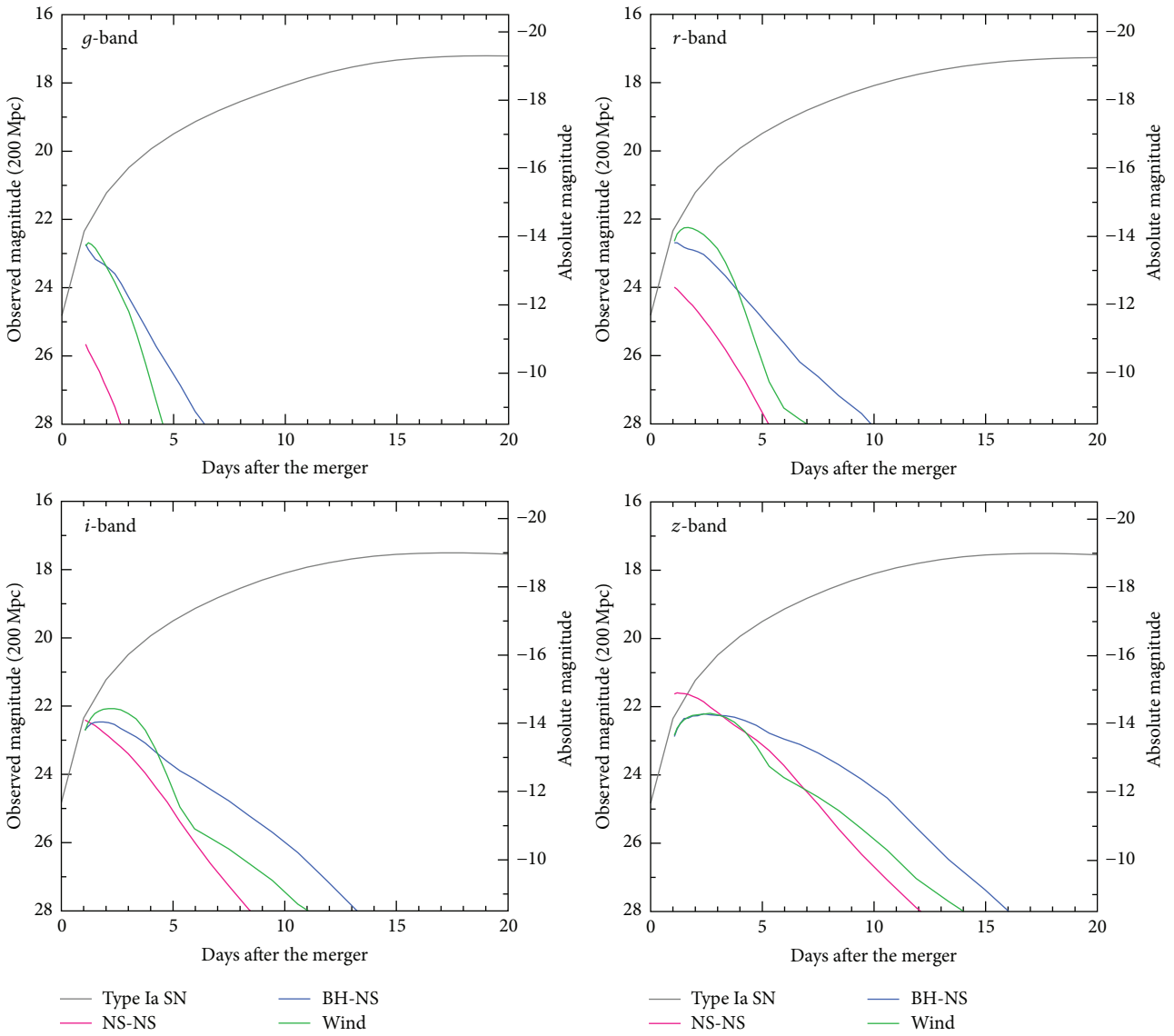

Figure 2: Expected observed magnitudes of kilonova models at 200 Mpc distance [57, 58]. The red, blue, and green lines show the models of NS-NS merger (APR4-1215, [48]), BH-NS merger (APR4Q3a75, [59]), and a wind model (this paper), respectively. The ejecta mass is $M_{\rm ej} = 0.01 M_\odot$ for these models. For comparison, light curve models of Type Ia SN are shown in gray. The corresponding absolute magnitudes are indicated in the right axis.

large diversity. See Kawaguchi et al. [110] for the expected kilonova brightness for a wide parameter space.

2.4. Wind Components. After the merger of two NSs, a hypermassive NS is formed at the center, and it subsequently collapses to a BH. During this process, accretion disk surrounding the central remnant is formed. A BH-accretion disk system is also formed in BH-NS mergers. From such accretion disk systems, an outflow or disk "wind" can be driven by neutrino heating, viscous heating, or nuclear recombination [56, 111–117]. A typical velocity of the wind is $v = 10,000$–$20,000$ km s^{-1}, slower than the precedent dynamical ejecta. Although the ejecta mass largely depends on the ejection mechanism, a typical mass is likely an order of $M_{\rm ej} = 0.01 M_\odot$ or even larger.

This wind component is another important source of kilonova emission [112, 113, 118–120]. The emission properties depend on the element composition in the ejecta. In particular, if a high electron fraction ($Y_e \gtrsim 0.25$) is realized by the neutrino emission from a long-lived hypermassive NS [118, 119] or shock heating in the outflow [115], synthesis of lanthanide elements can be suppressed in the wind. Then, the resulting emission can be bluer than the emission from the dynamical ejecta thanks to the lower opacity [57, 90]. This component can be called "blue kilonova" [84].

To demonstrate the effect of the low opacity, we show a simple wind model in Figures 1 and 2. In this model, we adopt a spherical ejecta of $M_{\rm ej} = 0.01 M_\odot$ with a density structure of $\rho \propto r^{-2}$ from $v = 0.01c$ to $0.1c$ (with the average velocity of $v \sim 20,000$ km s^{-1}). The elements in the ejecta are assumed

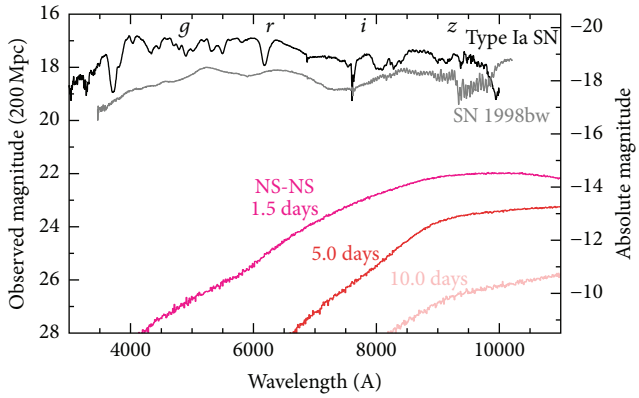

FIGURE 3: Expected observed spectra of the NS-NS merger model APR4-1215 ($M_{ej} = 0.01M_{\odot}$) compared with the spectra of normal Type Ia SN 2005cf [60–62] and broad-line Type Ic SN 1998bw [63, 64]. The spectra are shown in AB magnitudes (f_{ν}) at 200 Mpc distance. The corresponding absolute magnitudes are indicated in the right axis.

to be lanthanide-free: only the elements of $Z = 31$–54 are included with the solar abundance ratios. As shown by previous works [119], the emission from such a wind can peak earlier than that from the dynamical ejecta (Figure 1) and the emission is bluer (Figure 2).

Note that this simple model neglects the presence of the dynamical ejecta outside of the wind component. The effect of the dynamical ejecta is in fact important, because it works as a "lanthanide curtain" [119] absorbing the emission from the disk wind. Interestingly, as described in Section 2.2, the polar region of the dynamical ejecta can have a higher Y_e, and the "lanthanide curtain" may not be present in the direction. Also, in BH-NS mergers, the dynamical ejecta is distributed in the orbital plane, and disk wind can be directly observed from most of the lines of sight. If the wind component is dominant for kilonova emission and can be directly observed, the spectra are not as smooth as the spectra of dynamical ejecta because of the slower expansion [119]. More realistic simulations capturing all of these situations will be important to understand the emission from the disk wind.

3. Lessons from Observations

Since short GRBs are believed to be driven by NS-NS mergers or BH-NS mergers (see, e.g., [6, 7]), models of kilonova can be tested by the observations of short GRBs. As well known, SN component has been detected in the afterglow of long GRBs (see [121, 122] for reviews). If kilonova emission occurs, the emission can be in principle visible on top of the afterglow, but such an emission had eluded the detection for long time [123].

In 2013, a clear excess emission was detected in the near-IR afterglow of GRB 130603B [67, 68]. Interestingly, the excess was not visible in the optical data. Since this behavior nicely agrees with the expected properties of kilonova, the excess is interpreted to be the kilonova emission.

Figure 4(a) shows kilonova models compared with the observations of GRB 130603B. The observed brightness of the near-IR excess in GRB 130603B requires a relatively large ejecta mass of $M_{ej} \gtrsim 0.02M_{\odot}$ [67, 68, 73, 124]. As pointed out by Hotokezaka et al. [124], this favors a soft EOS for a NS-NS merger model (i.e., more shock-driven ejection) and a stiff EOS for a BH-NS merger model (i.e., more tidally driven ejection). Another possibility to explain the brightness may be an additional emission from the disk wind (green line in Figure 4; see [118, 119]).

Note that the excess was detected only at one epoch in one filter. Therefore, other interpretations are also possible, for example, emission by the external shock [125] or by a central magnetar [126, 127], or thermal emission from newly formed dust [128]. Importantly, a late-time excess is also visible in X-ray [129], and thus, the near-IR and X-ray excesses might be caused by the same mechanism, possibly the central engine [130, 131].

Another interesting case is GRB 060614. This GRB was formally classified as a long GRB because the duration is about 100 sec. However, since no bright SN was accompanied, the origin was not clear [132–135]. Recently the existence of a possible excess in the optical afterglow was reported [69, 70]. Figure 4(b) shows the comparison between GRB 060614 and the same sets of the models. If this excess is caused by kilonova, a large ejecta mass of $M_{ej} \sim 0.1M_{\odot}$ is required. This fact may favor a BH-NS merger scenario with a stiff EOS [69, 70]. It is however important to note that the emission from BH-NS merger has a large variation, and such an effective mass ejection requires a low BH/NS mass ratio and a high BH spin [110]. See also [136] for possible optical excess in GRB 050709, a genuine short GRB with a duration of 0.5 sec [137–140]. If the excess is attributed to kilonova, the required ejecta mass is $M_{ej} \sim 0.05M_{\odot}$.

Finally, an early brightening in optical data of GRB 080503 at $t \sim 1$–5 days can also be attributed to kilonova [141] although the redshift of this object is unfortunately unknown. Kasen et al. [119] give a possible interpretation with the disk wind model. Note that a long-lasting X-ray emission was also detected in GRB 080503 at $t \lesssim 2$ days, and it may favor a common mechanism for optical and X-ray emission [131, 142].

4. Prospects for EM Follow-Up Observations of GW Sources

Figure 2 shows the expected brightness of compact binary merger models at 200 Mpc (left axis). All the models assume a canonical ejecta mass of $M_{ej} = 0.01M_{\odot}$, and therefore, the emission can be brighter or fainter depending on the merger parameters and the EOS (see Section 2). Keeping this caveat in mind, typical models suggest that the expected kilonova brightness at 200 Mpc is about 22 mag in red optical wavelengths (i- or z-bands) at $t < 5$ days after the merger. The brightness quickly declines to >24 mag within $t \sim 10$ days after the merger. To detect this emission, we ultimately need 8 m class telescopes. Currently the wide-field capability for 8 m class telescopes is available only at the 8.2 m Subaru

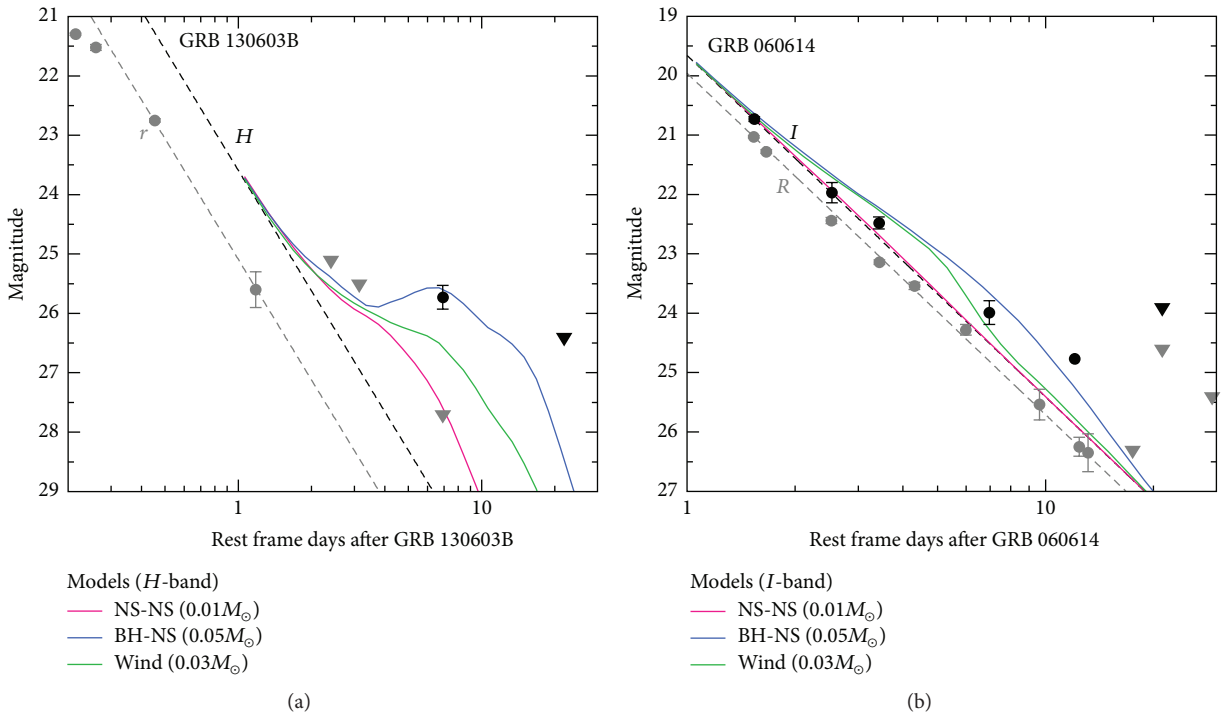

FIGURE 4: Comparison of kilonova models with GRB 130603B (a) and GRB 060614 (b). The models used in these plots are those with relatively high ejecta masses: APR4-1215 (NS-NS, $M_{ej} = 0.01M_\odot$ [48]), H4Q3a75 (BH-NS, $M_{ej} = 0.05M_\odot$ [59]), and a wind model with $M_{ej} = 0.03M_\odot$ (this paper). The H4Q3a75 model is a merger of a $1.35M_\odot$ NS and a $4.05M_\odot$ BH with a spin parameter of $a = 0.75$. This model adopts a "stiff" EOS H4 [65, 66] which gives a 13.6 km radius for $1.35M_\odot$ NS. For GRB 130603B, the afterglow component is assumed to be $f_\nu \propto t^{-2.7}$ [67, 68]. For GRB 060614, it is assumed to be $f_\nu \propto t^{-2.3}$ [69], which is a conservative choice (see [70] for a possibility of a steeper decline). The observed and model magnitudes for GRB 060614 are given in the Vega system as in the literature [70].

telescope: Subaru/Hyper Suprime-Cam (HSC) has the field of view (FOV) of 1.77 deg^2 [143, 144]. In future, the 8.4 m Large Synoptic Survey Telescope (LSST) with 9.6 deg^2 FOV will be online [145, 146]. Note that targeted galaxy surveys are also effective to search for the transients associated with galaxies [147, 148].

It is again emphasized that the expected brightness of kilonova can have a large variety. If the kilonova candidates seen in GRB 130603B ($M_{ej} \gtrsim 0.02M_\odot$) and GRB 060614 ($M_{ej} \sim 0.1M_\odot$) are typical cases (see Section 3), the emission can be brighter by ~1-2 mag. In addition, there are also possibilities of bright, precursor emission (e.g., [29, 130, 149]) which are not discussed in depth in this paper. And, of course, the emission is brighter for objects at closer distances. Therefore, surveys with small-aperture telescopes (typically with wider FOVs) are also important. See, for example, Nissanke et al. [13] and Kasliwal and Nissanke [16] for detailed survey simulations for various expected brightness of the EM counterpart.

A big challenge for identification of the GW source is contamination of SNe. NS-NS mergers and BH-NS mergers are rare events compared with SNe, and thus, much larger number of SNe are detected when optical surveys are performed over 10 deg^2 (see [21–23] for the case of GW150914). Therefore, it is extremely important to effectively select the candidates of kilonova from a larger number of SNe.

To help the classification, color-magnitude and color-color diagrams for the kilonova models and Type Ia SNe are shown in Figure 5. The numbers attached with the models are days after the merger while dots for SNe are given with 5-day interval. According to the current understanding, the light curves of kilonova can be characterized as follows.

(1) The timescale of variability should be shorter than that of SNe (Figure 2). This is robust since the ejecta mass from compact binary mergers is much smaller than SNe.

(2) The emission is fainter than SNe. This is also robust because of the smaller ejecta mass and thus the lower available radioactive energy (Figure 1).

(3) The emissions are expected to be redder than SNe. This is an outcome of a high opacity in the ejecta, but the exact color depends on the ejecta composition ([58, 90, 118, 119], Section 2).

Therefore, in order to effectively search for the EM counterpart of the GW source, multiple visits in a timescale of <10 days will be important so that the rapid time evolution can be captured. Surveys with multiple filters are also helpful to use color information. As shown in Figure 5, observed magnitudes of kilonovae at ~200 Mpc are similar to those of SNe at larger distances ($z \gtrsim 0.3$ for Type Ia SNe). Therefore,

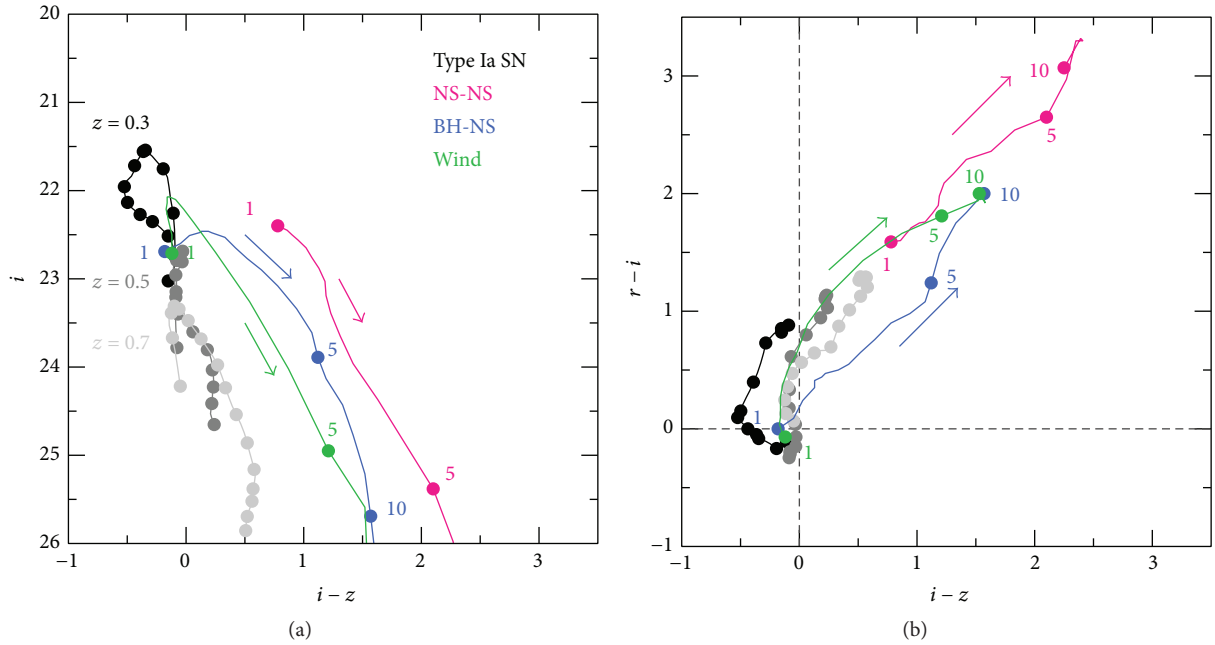

FIGURE 5: Color-magnitude diagram (a) and color-color diagram (b) for compact binary merger models ($M_{ej} = 0.01M_{\odot}$) at 200 Mpc compared with Type Ia SN with similar observed magnitudes ($z = 0.3$, 0.5, and 0.7). For Type Ia SN, we use spectral templates [71] with K-correction. The numbers for binary merger models show time from the merger in days while dots for Type Ia SN are given with 5-day interval.

if redshifts of the host galaxies are estimated, kilonova candidates can be further selected by the close distances and the intrinsic faintness.

5. Summary

The direct detection of GWs from GW150914 opened GW astronomy. To study the astrophysical nature of the GW sources, the identification of the EM counterparts is essentially important. In this paper, we reviewed the current understanding of kilonova emission from compact binary mergers.

Kilonova emission from the dynamical ejecta of $0.01M_{\odot}$ has a typical luminosity is an order of 10^{40}–10^{41} erg s^{-1} with the characteristic timescale of about 1 week. Because of the high opacity and the low temperature, the spectral peak is located at red optical or near-IR wavelengths. In addition to the emission from the dynamical ejecta, a subsequent disk wind can cause an additional emission which may peak earlier with a bluer color if the emission is not absorbed by the precedent ejecta.

The detection of excess in GRB 130603B (and possibly GRB 060614) supports the kilonova scenario. If the excesses found in these objects are attributed to the kilonova emission, the required ejecta masses are $M_{ej} \gtrsim 0.02M_{\odot}$ and $M_{ej} \sim 0.1M_{\odot}$, respectively. The comparison between such observations and numerical simulations gives important insight to study the progenitor of compact binary mergers and EOS of NS.

At 200 Mpc distance, a typical peak brightness of kilonova emission is about 22 mag in the red optical wavelengths (i- or z-bands). The emission quickly fades to >24 mag within ~10 days. To distinguish GW sources from SNe, observations with multiple visits in a timescale of <10 days are important to select the objects with rapid temporal evolution. The use of multiple filters is also helpful to select red objects. Since the extremely high expansion velocities ($v \sim 0.1$–$0.2c$) are unique features of dynamical mass ejection from compact binary mergers, detection of extremely smooth spectrum will be the smoking gun to conclusively identify the GW sources.

Competing Interests

The author declares that there is no conflict of interests regarding the publication of this paper.

Acknowledgments

The author thanks Kenta Hotokezaka, Yuichiro Sekiguchi, Masaru Shibata, Kenta Kiuchi, Shinya Wanajo, Koutarou Kyutoku, Kyohei Kawaguchi, Keiichi Maeda, Takaya Nozawa, and Yutaka Hirai for fruitful discussion on compact binary mergers, nucleosynthesis, and kilonova emission. The author also thanks Nozomu Tominaga, Tomoki Morokuma, Michitoshi Yoshida, Kouji Ohta, and the J-GEM collaboration for valuable discussion on EM follow-up observations. Numerical simulations presented in this paper were carried out with Cray XC30 at Center for Computational Astrophysics, National Astronomical Observatory of Japan. This research has been supported by the Grant-in-Aid for Scientific

Research of the Japan Society for the Promotion of Science (24740117, 15H02075) and Grant-in-Aid for Scientific Research on Innovative Areas of the Ministry of Education, Culture, Sports, Science and Technology (25103515, 15H00788).

References

[1] G. M. Harry and LIGO Scientific Collaboration, "Advanced LIGO: the next generation of gravitational wave detectors," *Classical and Quantum Gravity*, vol. 27, no. 8, Article ID 084006, 2010.

[2] B. P. Abbott, R. Abbott, T. D. Abbott et al. et al., "Observation of gravitational waves from a binary black hole merger," *Physical Review Letters*, vol. 116, no. 6, Article ID 061102, 2016.

[3] S. I. Blinnikov, I. D. Novikov, T. V. Perevodchikova, and A. G. Polnarev, "Exploding neutron stars in close binaries," *Soviet Astronomy Letters*, vol. 10, no. 3, pp. 177–179, 1984.

[4] D. Eichler, M. Livio, T. Piran, and D. N. Schramm, "Nucleosynthesis, neutrino bursts and γ-rays from coalescing neutron stars," *Nature*, vol. 340, no. 6229, pp. 126–128, 1989.

[5] B. Paczynski, "Gamma-ray bursters at cosmological distances," *The Astrophysical Journal*, vol. 308, pp. L43–L46, 1986.

[6] E. Berger, "Short-duration gamma-ray bursts," *Annual Review of Astronomy and Astrophysics*, vol. 52, pp. 43–105, 2014.

[7] E. Nakar, "Short-hard gamma-ray bursts," *Physics Reports*, vol. 442, no. 1–6, pp. 166–236, 2007.

[8] F. Acernese, M. Agathos, K. Agatsuma et al. et al., "Focus issue: advanced interferometric gravitational wave detectors," *Classical and Quantum Gravity*, vol. 32, no. 2, Article ID 024001, 2015.

[9] K. Somiya, "Detector configuration of KAGRA–the Japanese cryogenic gravitational-wave detector," *Classical and Quantum Gravity*, vol. 29, no. 12, Article ID 124007, 2012.

[10] J. Abadie, B. P. Abbott, R. Abbott et al., "Predictions for the rates of compact binary coalescences observable by ground-based gravitational-wave detectors," *Classical and Quantum Gravity*, vol. 27, Article ID 173001, 2010.

[11] B. P. Abbott, R. Abbott, T. D. Abbott et al., "Prospects for observing and localizing gravitational-wave transients with advanced LIGO and advanced virgo," *Living Reviews in Relativity*, vol. 19, article 1, 2016.

[12] L. Z. Kelley, I. Mandel, and E. Ramirez-Ruiz, "Electromagnetic transients as triggers in searches for gravitational waves from compact binary mergers," *Physical Review D*, vol. 87, no. 12, Article ID 123004, 16 pages, 2013.

[13] S. Nissanke, M. Kasliwal, and A. Georgieva, "Identifying elusive electromagnetic counterparts to gravitational wave mergers: an end-to-end simulation," *The Astrophysical Journal*, vol. 767, no. 2, article 124, 2013.

[14] S. Nissanke, J. Sievers, N. Dalal, and D. Holz, "Localizing compact binary inspirals on the sky using ground-based gravitational wave interferometers," *Astrophysical Journal*, vol. 739, no. 2, article 99, 2011.

[15] R. Essick, S. Vitale, E. Katsavounidis, G. Vedovato, and S. Klimenko, "Localization of short duration gravitational-wave transients with the early advanced ligo and virgo detectors," *Astrophysical Journal*, vol. 800, no. 2, article 81, 2015.

[16] M. M. Kasliwal and S. Nissanke, "On discovering electromagnetic emission from neutron star mergers: the early years of two gravitational wave detectors," *The Astrophysical Journal Letters*, vol. 789, no. 1, article L5, 2014.

[17] L. P. Singer, L. R. Price, B. Farr et al., "The first two years of electromagnetic follow-up with advanced ligo and virgo," *Astrophysical Journal*, vol. 795, no. 2, article 105, 2014.

[18] The LIGO Scientific Collaboration and the Virgo Collaboration, "Properties of the binary black hole merger GW150914," 2016, https://arxiv.org/abs/1602.03840.

[19] B. P. Abbott, R. Abbott, T. D. Abbott et al., "Localization and broadband follow-up of the gravitational-wave transient GW150914," 2016, https://arxiv.org/abs/1602.08492.

[20] P. A. Evans, J. A. Kennea, S. D. Barthelmy et al., "*Swift* follow-up of the gravitational wave source GW150914," *MNRAS Letters*, vol. 460, no. 1, pp. L40–L44, 2016.

[21] M. M. Kasliwal, S. B. Cenko, L. P. Singer et al., "iPTF search for anoptical counterpart to gravitational wave trigger GW150914," http://arxiv.org/abs/1602.08764.

[22] S. J. Smartt, K. C. Chambers, K. W. Smith et al., "Pan-STARRS and PESSTO search for the optical counterpart to the LIGO gravitational wave source GW150914," http://arxiv.org/abs/1602.04156.

[23] M. Soares-Santos, R. Kessler, E. Berger et al., "A dark energy camera search for anoptical counterpart to the first advanced LIGO gravitational wave event GW150914," http://arxiv.org/abs/1602.04198.

[24] T. Morokuma, M. Tanaka, Y. Asakura et al., "J-GEM follow-up observations to search for an optical counterpart of the first gravitational wave source GW150914," http://arxiv.org/abs/1605.03216.

[25] E. Nakar and T. Piran, "Detectable radio flares following gravitational waves from mergers of binary neutron stars," *Nature*, vol. 478, no. 7367, pp. 82–84, 2011.

[26] T. Piran, E. Nakar, and S. Rosswog, "The electromagnetic signals of compact binary mergers," *Monthly Notices of the Royal Astronomical Society*, vol. 430, no. 3, pp. 2121–2136, 2013.

[27] K. Hotokezaka and T. Piran, "Mass ejection from neutron star mergers: different components and expected radio signals," *Monthly Notices of the Royal Astronomical Society*, vol. 450, no. 2, pp. 1430–1440, 2015.

[28] T. Nakamura, K. Kashiyama, D. Nakauchi, Y. Suwa, T. Sakamoto, and N. Kawai, "Soft X-ray extended emissions of short gamma-ray bursts as electromagnetic counterparts of compact binary mergers: possible origin and detectability," *Astrophysical Journal*, vol. 796, no. 1, article 13, 2014.

[29] B. D. Metzger and A. L. Piro, "Optical and X-ray emission from stable millisecond magnetars formed from the merger of binary neutron stars," *Monthly Notices of the Royal Astronomical Society*, vol. 439, no. 4, pp. 3916–3930, 2014.

[30] S. Kisaka, K. Ioka, and T. Nakamura, "Isotropic detectable X-ray counterparts to gravitational waves from neutron star binary mergers," *The Astrophysical Journal Letters*, vol. 809, article L8, 2015.

[31] D. M. Siegel and R. Ciolfi, "Electromagnetic emission from long-lived binary neutron star merger remnants. II. light curves and spectra," *The Astrophysical Journal*, vol. 819, no. 1, p. 15, 2016.

[32] L.-X. Li and B. Paczyński, "Transient events from neutron star mergers," *The Astrophysical Journal*, vol. 507, no. 1, pp. L59–L62, 1998.

[33] S. R. Kulkarni, "Modeling supernova-like explosions associated with gamma-ray bursts with short durations," 2005, http://arxiv.org/abs/astro-ph/0510256.

[34] B. D. Metzger, G. Martínez-Pinedo, S. Darbha et al., "Electromagnetic counterparts of compact object mergers powered by the radioactive decay of r-process nuclei," *Monthly Notices of the Royal Astronomical Society*, vol. 406, no. 4, pp. 2650–2662, 2010.

[35] L. F. Roberts, D. Kasen, W. H. Lee, and E. Ramirez-Ruiz, "Electromagnetic transients powered by nuclear decay in the tidal tails of coalescing compact binaries," *The Astrophysical Journal Letters*, vol. 736, no. 1, article L21, 2011.

[36] S. Goriely, A. Bauswein, and H.-T. Janka, "R-process nucleosynthesis in dynamically ejected matter of neutron star mergers," *Astrophysical Journal Letters*, vol. 738, no. 2, article L32, 2011.

[37] B. D. Metzger and E. Berger, "What is the most promising electromagnetic counterpart of a neutron star binary merger?" *The Astrophysical Journal*, vol. 746, no. 1, p. 48, 2012.

[38] M. Shibata and K. Uryū, "Simulation of merging binary neutron stars in full general relativity: $\Gamma = 2$ case," *Physical Review D*, vol. 61, no. 6, Article ID 064001, 18 pages, 2000.

[39] M. Shibata, K. Taniguchi, and K. Uryū, "Merger of binary neutron stars with realistic equations of state in full general relativity," *Physical Review D*, vol. 71, no. 8, Article ID 084021, 2005.

[40] M. D. Duez, "Numerical relativity confronts compact neutron star binaries: a review and status report," *Classical and Quantum Gravity*, vol. 27, no. 11, Article ID 114002, 2010.

[41] J. A. Faber and F. A. Rasio, "Binary neutron star mergers," *Living Reviews in Relativity*, vol. 15, article 8, 2012.

[42] S. Rosswog, M. Liebendörfer, F.-K. Thielemann, M. B. Davies, W. Benz, and T. Piran, "Mass ejection in neutron star mergers," *Astronomy and Astrophysics*, vol. 341, no. 2, pp. 499–526, 1999.

[43] S. Rosswog, M. B. Davies, F.-K. Thielemann, and T. Piran, "Merging neutron stars: asymmetric systems," *Astronomy & Astrophysics*, vol. 360, pp. 171–184, 2000.

[44] M. Ruffert and H.-T. Janka, "Coalescing neutron stars—a step towards physical models III. Improved numerics and different neutron star masses and spins," *Astronomy and Astrophysics*, vol. 380, no. 2, pp. 544–577, 2001.

[45] S. Rosswog, "Mergers of neutron star-black hole binaries with small mass ratios: nucleosynthesis, gamma-ray bursts, and electromagnetic transients," *Astrophysical Journal*, vol. 634, no. 2, pp. 1202–1213, 2005.

[46] W. H. Lee and E. Ramirez-Ruiz, "The progenitors of short gamma-ray bursts," *New Journal of Physics*, vol. 9, article A17, 2007.

[47] S. Rosswog, "The dynamic ejecta of compact object mergers and eccentric collisions," *Royal Society of London Philosophical Transactions Series A*, vol. 371, no. 1992, Article ID 20272, 2013.

[48] K. Hotokezaka, K. Kiuchi, K. Kyutoku et al., "Mass ejection from the merger of binary neutron stars," *Physical Review D—Particles, Fields, Gravitation and Cosmology*, vol. 87, no. 2, Article ID 024001, 2013.

[49] A. Bauswein, S. Goriely, and H.-T. Janka, "Systematics of dynamical mass ejection, nucleosynthesis, and radioactively powered electromagnetic signals from neutron-star mergers," *Astrophysical Journal*, vol. 773, no. 1, article 78, 2013.

[50] J. M. Lattimer and D. N. Schramm, "Black-hole-neutron-star collisions," *Astrophysical Journal*, vol. 192, part 2, pp. L145–L147, 1974.

[51] J. M. Lattimer and D. N. Schramm, "The tidal disruption of neutron stars by black holes in close binaries," *The Astrophysical Journal*, vol. 210, pp. 549–567, 1976.

[52] C. Freiburghaus, S. Rosswog, and F.-K. Thielemann, "r-process in neutron star mergers," *The Astrophysical Journal*, vol. 525, no. 2, pp. L121–L124, 1999.

[53] O. Korobkin, S. Rosswog, A. Arcones, and C. Winteler, "On the astrophysical robustness of the neutron star merger r-process," *Monthly Notices of the Royal Astronomical Society*, vol. 426, no. 3, pp. 1940–1949, 2012.

[54] S. Wanajo, Y. Sekiguchi, N. Nishimura, K. Kiuchi, K. Kyutoku, and M. Shibata, "Production of all the r-process nuclides in the dynamical ejecta of neutron star mergers," *The Astrophysical Journal Letters*, vol. 789, no. 2, article L39, 2014.

[55] J. de Jesús Mendoza-Temis, M.-R. Wu, K. Langanke, G. Martínez-Pinedo, A. Bauswein, and H.-T. Janka, "Nuclear robustness of the r process in neutron-star mergers," *Physical Review C*, vol. 92, no. 5, Article ID 055805, 16 pages, 2015.

[56] O. Just, A. Bauswein, R. A. Pulpillo, S. Goriely, and H. T. Janka, "Comprehensive nucleosynthesis analysis for ejecta of compact binary mergers," *Monthly Notices of the Royal Astronomical Society*, vol. 448, no. 1, pp. 541–567, 2015.

[57] M. Tanaka and K. Hotokezaka, "Radiative transfer simulations of neutron star merger ejecta," *The Astrophysical Journal*, vol. 775, no. 2, article 113, 2013.

[58] M. Tanaka, K. Hotokezaka, K. Kyutoku et al., "Radioactively powered emission from black hole-neutron star mergers," *Astrophysical Journal*, vol. 780, no. 1, article 31, 2014.

[59] K. Kyutoku, K. Ioka, and M. Shibata, "Anisotropic mass ejection from black hole-neutron star binaries: diversity of electromagnetic counterparts," *Physical Review D*, vol. 88, no. 4, Article ID 041503, 2013.

[60] A. Pastorello, S. Taubenberger, N. Elias-Rosa et al., "ESC observations of SN 2005cf -I. Photometric evolution of a normal Type Ia supernova," *Monthly Notices of the Royal Astronomical Society*, vol. 376, no. 3, pp. 1301–1316, 2007.

[61] G. Garavini, S. Nobili, S. Taubenberger et al., "ESC observations of SN 2005cf. II. Optical spectroscopy and the high-velocity features," *Astronomy & Astrophysics*, vol. 471, no. 2, pp. 527–535, 2007.

[62] X. Wang, W. Li, A. V. Filippenko et al., "The golden standard type ia supernova 2005cf: observations from the ultraviolet to the near-infrared wavebands," *The Astrophysical Journal*, vol. 697, no. 1, pp. 380–408, 2009.

[63] K. Iwamoto, P. A. Mazzali, K. Nomoto et al., "A hypernova model for the supernova associated with the γ-ray burst of 25 April 1998," *Nature*, vol. 395, no. 6703, pp. 672–674, 1998.

[64] K. Iwamoto, P. A. Mazzali, K. Nomoto et al., "A hypernova model for the supernova associated with the γ-ray burst of 25 April 1998," *Nature*, vol. 395, no. 6703, pp. 672–674, 1998.

[65] N. K. Glendenning and S. A. Moszkowski, "Reconciliation of neutron-star masses and binding of the Λ in hypernuclei," *Physical Review Letters*, vol. 67, p. 2414, 1991.

[66] B. D. Lackey, M. Nayyar, and B. J. Owen, "Observational constraints on hyperons in neutron stars," *Physical Review D*, vol. 73, no. 2, Article ID 024021, 2006.

[67] N. R. Tanvir, A. J. Levan, A. S. Fruchter et al., "A 'kilonova' associated with the short-duration γ-ray burst GRB 130603B," *Nature*, vol. 500, no. 7464, pp. 547–549, 2013.

[68] E. Berger, W. Fong, and R. Chornock, "An r-process kilonova associated with the short-hard GRB 130603B," *The Astrophysical Journal Letters*, vol. 774, no. 2, article L23, 2013.

[69] B. Yang, Z.-P. Jin, X. Li et al., "A possible macronova in the late afterglow of the long-short burst GRB 060614," *Nature Communications*, vol. 6, article 7323, 2015.

[70] Z.-P. Jin, X. Li, Z. Cano, S. Covino, Y.-Z. Fan, and D.-M. Wei, "The light curve of the macronova associated with the long-short burst GRB 060614," *Astrophysical Journal Letters*, vol. 811, no. 2, article L22, 2015.

[71] P. Nugent, A. Kim, and S. Perlmutter, "K-corrections and extinction corrections for type Ia supernovae," *Publications of the Astronomical Society of the Pacific*, vol. 114, no. 798, pp. 803–819, 2002.

[72] D. Argast, M. Samland, F.-K. Thielemann, and Y.-Z. Qian, "Neutron star mergers versus core-collapse supernovae as dominant r-process sites in the early Galaxy," *Astronomy and Astrophysics*, vol. 416, no. 3, pp. 997–1011, 2004.

[73] T. Piran, O. Korobkin, and S. Rosswog, "Implications of GRB 130603B and itsmacronova for r-process nucleosynthesis," http://arxiv.org/abs/1401.2166.

[74] F. Matteucci, D. Romano, A. Arcones, O. Korobkin, and S. Rosswog, "Europium production: neutron star mergers versus core-collapse supernovae," *Monthly Notices of the Royal Astronomical Society*, vol. 438, no. 3, Article ID stt2350, pp. 2177–2185, 2014.

[75] T. Tsujimoto and T. Shigeyama, "Enrichment history of r-process elements shaped by a merger of neutron star pairs," *Astronomy and Astrophysics*, vol. 565, article L5, 2014.

[76] Y. Komiya, S. Yamada, T. Suda, and M. Y. Fujimoto, "The new model of chemical evolution of *r*-process elements based on the hierarchical galaxy formation. I. Ba and Eu," *The Astrophysical Journal*, vol. 783, no. 2, p. 132, 2014.

[77] G. Cescutti, D. Romano, F. Matteucci, C. Chiappini, and R. Hirschi, "The role of neutron star mergers in the chemical evolution of the Galactic halo," *Astronomy & Astrophysics*, vol. 577, article A139, 10 pages, 2015.

[78] B. Wehmeyer, M. Pignatari, and F.-K. Thielemann, "Galactic evolution of rapid neutron capture process abundances: the inhomogeneous approach," *Monthly Notices of the Royal Astronomical Society*, vol. 452, no. 2, pp. 1970–1981, 2015.

[79] Y. Ishimaru, S. Wanajo, and N. Prantzos, "Neutron star mergers as the origin of r-process elements in the galactic halo based on the sub-halo clustering scenario," *The Astrophysical Journal Letters*, vol. 804, no. 2, article L35, 2015.

[80] S. Shen, R. J. Cooke, E. Ramirez-Ruiz, P. Madau, L. Mayer, and J. Guedes, "The history of r-process enrichment in the milky way," *Astrophysical Journal*, vol. 807, no. 2, article 115, 2015.

[81] F. van de Voort, E. Quataert, P. F. Hopkins, D. Kereš, and C. Faucher-Giguere, "Galactic r-process enrichment by neutron star mergers in cosmological simulations of a Milky Way-mass galaxy," *Monthly Notices of the Royal Astronomical Society*, vol. 447, no. 1, pp. 140–148, 2015.

[82] Y. Hirai, Y. Ishimaru, T. R. Saitoh, M. S. Fujii, J. Hidaka, and T. Kajino, "Enrichment of r-process elements in dwarf spheroidal galaxies in chemo-dynamical evolution model," *The Astrophysical Journal*, vol. 814, no. 1, p. 41, 2015.

[83] S. Rosswog, "The multi-messenger picture of compact binary mergers," *International Journal of Modern Physics. D. Gravitation, Astrophysics, Cosmology*, vol. 24, no. 5, Article ID 1530012, 2015.

[84] R. Fernández and B. D. Metzger, "Electromagnetic signatures of neutron star mergers in the advanced LIGO era," 2015, http://arxiv.org/abs/1512.05435.

[85] W. D. Arnett, "Type I supernovae. I—analytic solutions for the early part of the light curve," *The Astrophysical Journal*, vol. 253, no. 2, pp. 785–797, 1982.

[86] S. Rosswog, O. Korobkin, A. Arcones, F.-K. Thielemann, and T. Piran, "The long-term evolution of neutron star merger remnants—I. The impact of r-process nucleosynthesis," *Monthly Notices of the Royal Astronomical Society*, vol. 439, no. 1, pp. 744–756, 2014.

[87] D. Grossman, O. Korobkin, S. Rosswog, and T. Piran, "The long-term evolution of neutron star merger remnants—II. Radioactively powered transients," *Monthly Notices of the Royal Astronomical Society*, vol. 439, no. 1, pp. 757–770, 2014.

[88] J. Lippuner and L. F. Roberts, "r-Process lanthanide production and heating rates in kilonovae," *The Astrophysical Journal*, vol. 815, no. 2, p. 82, 2015.

[89] K. Hotokezaka, S. Wanajo, M. Tanaka, A. Bamba, Y. Terada, and T. Piran, "Radioactive decay products in neutron star merger ejecta: heating efficiency and γ-ray emission," *Monthly Notices of the Royal Astronomical Society*, vol. 459, no. 1, pp. 35–43, 2016.

[90] D. Kasen, N. R. Badnell, and J. Barnes, "Opacities and spectra of the r-process ejecta from neutron star mergers," *Astrophysical Journal*, vol. 774, no. 1, article 25, 2013.

[91] J. Barnes and D. Kasen, "Effect of a high opacity on the light curves of radioactively powered transients from compact object mergers," *The Astrophysical Journal*, vol. 775, no. 1, p. 18, 2013.

[92] D. Radice, F. Galeazzi, J. Lippuner, L. F. Roberts, C. D. Ott, and L. Rezzolla, "Dynamical mass ejection from binary neutron star mergers," 2016, http://arxiv.org/abs/1601.02426.

[93] S. Rosswog, T. Piran, and E. Nakar, "The multimessenger picture of compact object encounters: binary mergers versus dynamical collisions," *Monthly Notices of the Royal Astronomical Society*, vol. 430, no. 4, pp. 2585–2604, 2013.

[94] C. Palenzuela, S. L. Liebling, D. Neilsen et al., "Effects of the microphysical equation of state in the mergers of magnetized neutron stars with neutrino cooling," *Physical Review D*, vol. 92, no. 4, Article ID 044045, 23 pages, 2015.

[95] Y. Sekiguchi, K. Kiuchi, K. Kyutoku, and M. Shibata, "Dynamical mass ejection from binary neutron star mergers: radiation-hydrodynamics study in general relativity," *Physical Review D*, vol. 91, no. 5, Article ID 064059, 2015.

[96] Y. Sekiguchi, K. Kiuchi, K. Kyutoku, M. Shibata, and K. Taniguchi, "Dynamical mass ejection from the merger of asymmetric binary neutron stars: radiation-hydrodynamics study in general relativity," http://arxiv.org/abs/1603.01918.

[97] A. Akmal, V. R. Pandharipande, and D. G. Ravenhall, "Equation of state of nucleon matter and neutron star structure," *Physical Review C—Nuclear Physics*, vol. 58, no. 3, pp. 1804–1828, 1998.

[98] M. Shibata and K. Taniguchi, "Coalescence of black hole-neutron star binaries," *Living Reviews in Relativity*, vol. 14, article 6, 2011.

[99] M. Shibata and K. Taniguchi, "Merger of binary neutron stars to a black hole: Disk mass, short gamma-ray bursts, and quasi-normal mode ringing," *Physical Review D*, vol. 73, Article ID 064027, 2006.

[100] Z. B. Etienne, J. A. Faber, Y. T. Liu, S. L. Shapiro, K. Taniguchi, and T. W. Baumgarte, "Fully general relativistic simulations of black hole-neutron star mergers," *Physical Review D*, vol. 77, no. 8, Article ID 084002, 2008.

[101] M. D. Duez, F. Foucart, L. E. Kidder, H. P. Pfeiffer, M. A. Scheel, and S. A. Teukolsky, "Evolving black hole-neutron star binaries in general relativity using pseudospectral and finite difference methods," *Physical Review D—Particles, Fields, Gravitation and Cosmology*, vol. 78, no. 10, Article ID 104015, 2008.

[102] K. Kyutoku, M. Shibata, and K. Taniguchi, "Gravitational waves from nonspinning black hole-neutron star binaries: dependence on equations of state," *Physical Review D*, vol. 82, Article ID 044049, 2010.

[103] K. Kyutoku, H. Okawa, M. Shibata, and K. Taniguchi, "Gravitational waves from spinning black hole-neutron star binaries: dependence on black hole spins and on neutron star equations of state," *Physical Review D*, vol. 84, no. 6, Article ID 064018, 2011.

[104] M. B. Deaton, M. D. Duez, F. Foucart et al., "Black hole-neutron star mergers with a hot nuclear equation of state: outflow and neutrino-cooled disk for a low-mass, high-spin case," *Astrophysical Journal*, vol. 776, no. 1, article 47, 2013.

[105] F. Foucart, M. B. Deaton, M. D. Duez et al., "Black-hole-neutron-star mergers at realistic mass ratios: equation of state and spin orientation effects," *Physical Review D—Particles, Fields, Gravitation and Cosmology*, vol. 87, no. 8, Article ID 084006, 2013.

[106] G. Lovelace, M. D. Duez, F. Foucart et al., "Massive disc formation in the tidal disruption of a neutron star by a nearly extremal black hole," *Classical and Quantum Gravity*, vol. 30, no. 13, Article ID 135004, 2013.

[107] F. Foucart, M. B. Deaton, M. D. Duez et al., "Neutron star-black hole mergers with a nuclear equation of state and neutrino cooling: dependence in the binary parameters," *Physical Review D*, vol. 90, no. 2, Article ID 024026, 2014.

[108] K. Kyutoku, K. Ioka, H. Okawa, M. Shibata, and K. Taniguchi, "Dynamical mass ejection from black hole-neutron star binaries," *Physical Review D—Particles, Fields, Gravitation and Cosmology*, vol. 92, no. 4, Article ID 044028, 2015.

[109] K. Kawaguchi, K. Kyutoku, H. Nakano, H. Okawa, M. Shibata, and K. Taniguchi, "Black hole-neutron star binary merger: dependence on black hole spin orientation and equation of state," *Physical Review D*, vol. 92, no. 2, Article ID 024014, 2015.

[110] K. Kawaguchi, K. Kyutoku, M. Shibata, and M. Tanaka, "Models of Kilonova/macronova emission from black hole-neutronstar mergers," http://arxiv.org/abs/1601.07711.

[111] L. Dessart, C. D. Ott, A. Burrows, S. Rosswog, and E. Livne, "Neutrino signatures and the neutrino-driven wind in binary neutron star mergers," *Astrophysical Journal*, vol. 690, no. 2, pp. 1681–1705, 2009.

[112] R. Fernández and B. D. Metzger, "Delayed outflows from black hole accretion tori following neutron star binary coalescence," *Monthly Notices of the Royal Astronomical Society*, vol. 435, no. 1, p. 502, 2013.

[113] A. Perego, S. Rosswog, R. M. Cabezón et al., "Neutrino-driven winds from neutron star merger remnants," *Monthly Notices of the Royal Astronomical Society*, vol. 443, no. 4, pp. 3134–3156, 2014.

[114] K. Kiuchi, K. Kyutoku, Y. Sekiguchi, M. Shibata, and T. Wada, "High resolution numerical relativity simulations for the merger of binary magnetized neutron stars," *Physical Review D—Particles, Fields, Gravitation and Cosmology*, vol. 90, no. 4, Article ID 041502, 2014.

[115] K. Kiuchi, Y. Sekiguchi, K. Kyutoku, M. Shibata, K. Taniguchi, and T. Wada, "High resolution magnetohydrodynamic simulation of black hole-neutron star merger: mass ejection and short gamma ray bursts," *Physical Review D*, vol. 92, no. 6, Article ID 064034, 8 pages, 2015.

[116] R. Fern, D. Kasen, B. D. Metzger, and E. Quataert, "Outflows from accretion discs formed in neutron star mergers: effect of black hole spin," *Monthly Notices of the Royal Astronomical Society*, vol. 446, no. 1, pp. 750–758, 2015.

[117] R. Fernández, E. Quataert, J. Schwab, D. Kasen, and S. Rosswog, "The interplay of disc wind and dynamical ejecta in the aftermath of neutron star-black hole mergers," *Monthly Notices of the Royal Astronomical Society*, vol. 449, no. 1, pp. 390–402, 2015.

[118] B. D. Metzger and R. Fernández, "Red or blue? A potential kilonova imprint of the delay until black hole formation following a neutron star merger," *Monthly Notices of the Royal Astronomical Society*, vol. 441, no. 4, pp. 3444–3453, 2014.

[119] D. Kasen, R. Fernández, and B. D. Metzger, "Kilonova light curves from the disc wind outflows of compact object mergers," *Monthly Notices of the Royal Astronomical Society*, vol. 450, no. 2, pp. 1777–1786, 2015.

[120] D. Martin, A. Perego, A. Arcones, F.-K. Thielemann, O. Korobkin, and S. Rosswog, "Neutrino-driven winds in the aftermath of a neutron star merger: nucleosynthesis and electromagnetic transients," *The Astrophysical Journal*, vol. 813, no. 1, p. 2, 2015.

[121] S. E. Woosley and J. S. Bloom, "The supernova-gamma-ray burst connection," *Annual Review of Astronomy and Astrophysics*, vol. 44, pp. 507–556, 2006.

[122] Z. Cano, S.-Q. Wang, Z.-G. Dai, and X.-F. Wu, "The observer's guide to the gamma-ray burst-supernovaconnection," https://arxiv.org/abs/1604.03549.

[123] D. A. Kann, S. Klose, B. Zhang et al., "The afterglows of *Swift*-era gamma-ray bursts. II. Type I GRB versus type II GRB optical afterglows," *The Astrophysical Journal*, vol. 734, no. 2, article 96, 2011.

[124] K. Hotokezaka, K. Kyutoku, M. Tanaka et al., "Progenitor models of the electromagnetic transient associated with the short gamma ray burst 130603B," *Astrophysical Journal Letters*, vol. 778, no. 1, article L16, 2013.

[125] Z.-P. Jin, D. Xu, Y.-Z. Fan, X.-F. Wu, and D.-M. Wei, "Is the late near-infrared bump in short-hard grb 130603B due to the Li-Paczynski kilonova?" *The Astrophysical Journal*, vol. 775, no. 1, p. L19, 2013.

[126] Y.-W. Yu, B. Zhang, and H. Gao, "Bright "Merger-nova" from the remnant of a neutron star binary merger: a signature of a newly born, massive, millisecond magnetar," *The Astrophysical Journal*, vol. 776, no. 2, p. L40, 2013.

[127] Y.-Z. Fan, Y.-W. Yu, D. Xu et al., "A supramassive magnetar central engine for GRB 130603B," *The Astrophysical Journal*, vol. 779, no. 2, p. L25, 2013.

[128] H. Takami, T. Nozawa, and K. Ioka, "Dust formation in macronovae," *The Astrophysical Journal Letters*, vol. 789, article L6, 2014.

[129] W. Fong, E. Berger, B. D. Metzger et al., "Short GRB 130603B: discovery of a jet break in the optical and radio afterglows, and a mysterious late-time X-ray excess," *Astrophysical Journal*, vol. 780, no. 2, article 118, 2014.

[130] S. Kisaka, K. Ioka, and H. Takami, "Energy sources and light curves of macronovae," *Astrophysical Journal*, vol. 802, no. 2, article 119, 2015.

[131] S. Kisaka, K. Ioka, and E. Nakar, "X-ray-powered macronovae," *The Astrophysical Journal*, vol. 818, no. 2, p. 104, 2016.

[132] N. Gehrels, J. P. Norris, S. D. Barthelmy et al., "A new γ-ray burst classification scheme from GRB 060614," *Nature*, vol. 444, no. 7122, pp. 1044–1046, 2006.

[133] J. P. U. Fynbo, D. Watson, C. C. Thöne et al., "No supernovae associated with two long-duration γ-ray bursts," *Nature*, vol. 444, no. 7122, pp. 1047–1049, 2006.

[134] M. D. Valle, G. Chincarini, N. Panagia et al., "An enigmatic long-lasting γ-ray burst not accompanied by a bright supernova," *Nature*, vol. 444, no. 7122, pp. 1050–1052, 2006.

[135] A. Gal-Yam, D. B. Fox, P. A. Price et al., "A novel explosive process is required for the γ-ray burst GRB 060614," *Nature*, vol. 444, no. 7122, pp. 1053–1055, 2006.

[136] Z.-P. Jin, K. Hotokezaka, X. Li et al., "The 050709 macronova and the GRB/macronovaconnection," https://arxiv.org/abs/1603.07869.

[137] J. S. Villasenor, D. Q. Lamb, G. R. Ricker et al., "Discovery of the short γ-ray burst GRB 050709," *Nature*, vol. 437, no. 7060, pp. 855–858, 2005.

[138] J. Hjorth, D. Watson, J. P. U. Fynbo et al., "The optical afterglow of the short γ-ray burst GRB 050709," *Nature*, vol. 437, no. 7060, pp. 859–861, 2005.

[139] D. B. Fox, D. A. Frail, P. A. Price et al., "The afterglow of GRB 050709 and the nature of the short-hard γ-ray bursts," *Nature*, vol. 437, no. 7060, pp. 845–850, 2005.

[140] S. Covino, D. Malesani, G. L. Israel et al., "Optical emission from GRB 050709: a short/hard GRB in a star-forming galaxy," *Astronomy & Astrophysics*, vol. 447, no. 2, pp. L5–L8, 2006.

[141] D. A. Perley, B. D. Metzger, J. Granot et al., "GRB 080503: implications of a naked short gamma-ray burst dominated by extended emission," *Astrophysical Journal*, vol. 696, no. 2, pp. 1871–1885, 2009.

[142] H. Gao, X. Ding, X.-F. Wu, Z.-G. Dai, and B. Zhang, "GRB 080503 late afterglow re-brightening: signature of a magnetar-powered merger-nova," *The Astrophysical Journal*, vol. 807, no. 2, p. 163, 2015.

[143] S. Miyazaki, Y. Komiyama, H. Nakaya et al., "HyperSuprime: project overview," in *Ground-based and Airborne Instrumentation for Astronomy*, vol. 6269 of *Proceedings of SPIE*, May 2006.

[144] S. Miyazaki, Y. Komiyama, H. Nakaya et al., "Hyper suprime-cam," in *Ground-based and Airborne Instrumentation for Astronomy IV*, vol. 8446 of *Society of Photo-Optical Instrumentation Engineers (SPIE) Conference Series*, 2012.

[145] Z. Ivezic, J. A. Tyson, E. Acosta et al., "LSST: from science drivers to reference design and anticipated data products," 2008, https://arxiv.org/abs/0805.2366.

[146] P. A. Abell, J. Allison, S. F. Anderson et al., "LSST science book,version 2.0," http://arxiv.org/abs/0912.0201.

[147] N. Gehrels, J. K. Cannizzo, J. Kanner, M. M. Kasliwal, S. Nissanke, and L. P. Singer, "Galaxy strategy for ligo-virgo gravitational wave counterpart searches," *The Astrophysical Journal*, vol. 820, no. 2, p. 136, 2016.

[148] L. P. Singer, H.-Y. Chen, D. E. Holz et al., "Going the distance: mapping host galaxies of LIGO and virgo sources in three dimensions using local cosmography and targeted follow-up," http://arxiv.org/abs/1603.07333.

[149] B. D. Metzger, A. Bauswein, S. Goriely, and D. Kasen, "Neutron-powered precursors of kilonovae," *Monthly Notices of the Royal Astronomical Society*, vol. 446, no. 1, pp. 1115–1120, 2014.

Hindawi Publishing Corporation
Advances in Astronomy
Volume 2016, Article ID 1592148, 10 pages
http://dx.doi.org/10.1155/2016/1592148

Review Article

Diverse Features of the Multiwavelength Afterglows of Gamma-Ray Bursts: Natural or Special?

J. J. Geng[1,2] and Y. F. Huang[1,2]

[1]*School of Astronomy and Space Science, Nanjing University, Nanjing 210046, China*
[2]*Key Laboratory of Modern Astronomy and Astrophysics (Nanjing University), Ministry of Education, Nanjing, China*

Correspondence should be addressed to Y. F. Huang; hyf@nju.edu.cn

Received 22 February 2016; Revised 7 April 2016; Accepted 10 April 2016

Academic Editor: WeiKang Zheng

The detection of optical rebrightenings and X-ray plateaus in the afterglows of gamma-ray bursts (GRBs) challenges the generic external shock model. Recently, we have developed a numerical method to calculate the dynamics of the system consisting of a forward shock and a reverse shock. Here, we briefly review the applications of this method in the afterglow theory. By relating these diverse features to the central engines of GRBs, we find that the steep optical rebrightenings would be caused by the fall-back accretion of black holes, while the shallow optical rebrightenings are the consequence of the injection of the electron-positron-pair wind from the central magnetar. These studies provide useful ways to probe the characteristics of GRB central engines.

1. Introduction

It is believed that gamma-ray bursts (GRBs) are generated from either the collapse of massive stars [1–4] or the merger of neutron stars (NSs) [5–7], during which collimated relativistic outflows can be launched. As the outflow propagates into the circum-burst medium, a relativistic blast wave will develop, whose dynamic evolution can be well described by the Blandford-McKee solution [8]. The blast wave would sweep up and accelerate the circum-burst electrons and generate afterglows at frequencies ranging from X-rays to radio waves [9–11]. This is the basic picture for GRB afterglows. In the pre-*Swift* era, many afterglow lightcurves showed a smooth power-law decay, which can be explained by the synchrotron radiation from electrons accelerated by the forward shock (FS). For a complete reference of the analytical synchrotron external shock afterglow models, one can see [12]. However, many unexpected features in the afterglows were later observed thanks to the *Swift* satellite [13–15] and other optical telescopes (e.g., GROND telescope; see [16]).

Early flares and shallow decay phase (or the so-called X-ray plateau) are common in the X-ray afterglow data [17]. This indicates that the central engines of GRBs are still active after the burst, giving us a useful clue to investigate the central engines. On the other hand, some optical afterglows show rebrightenings at late stages in the observer frame ($t_{\rm obs} \sim 10^4$–10^5 s). In some cases, bumps in X-rays are accompanied by optical rebrightenings (e.g., GRB 120326A [18, 19]), while, in other cases, no clear counterpart features are observed in optical bands (e.g., GRB 100814A [20]). Both the X-ray plateaus and the optical rebrightenings cannot be explained in the framework of a simple FS scenario. Thus researchers have proposed several refined models to interpret these unexpected features in recent years (see [21, 22] for a review). Stimulated by these refined models, it is urgent to answer whether X-ray plateaus and optical rebrightenings have a natural origin or they are special outcomes varying in different GRBs.

Normally, the energy released during the X-ray plateau is several percent of the prompt emission [23], which motivates researchers to favour the scenarios involving energy injection processes. According to the composition of the injected late outflow, there are generally three types of energy injection processes, that is, the pure Poynting-flux injections [24–27], the collision of kinetic energy dominated shells [28], and the injection of the electron-positron-pair winds (e^+e^- winds [29, 30]). If one further considers the optical rebrightenings,

some other scenarios are called for, including the circum-burst density jumps [31–33], two-component jets [34, 35], and varying microphysical parameters [36]. All these models have succeeded to some extent in explaining one or several afterglows according to previous studies. On the other hand, most researchers believe that the central engines of GRBs are either black holes (BHs) or magnetars. Therefore, it may be reasonable to deduce that some specific groups of afterglows should have common features, and these features are associated with the physics of the central engines.

According to previous researches, late activities of BHs may be sustained by the accretion of fall-back material that fails to escape from the progenitor star [37–39]. The energy injection is expected to be delayed by the fall-back time $t_{\rm fb}$. If the FS is affected by such a delayed energy injection, the shock dynamics should rapidly evolve from a noninjection phase to an injection-dominated phase [40]. As a result, afterglows with steep optical rebrightenings (with the time scale of the rebrightening $\delta t_{\rm obs} < t_{\rm obs}$) are generated. We thus proposed that steep optical rebrightenings are caused by the fall-back processes of central accreting BHs. By contrast, the energy flow from a magnetar may be in the form of a continuous e^+e^- wind. The e^+e^- wind model was initially proposed to explain the X-ray plateau [41]. The end time of the plateau phase is roughly the typical spin-down timescale ($T_{\rm sd}$) of the newly born magnetar. For the broad and shallow optical rebrightening, its peak time also coincides with $T_{\rm sd}$, which motivates us to believe that the e^+e^- wind model should work for afterglows with both a shallow optical rebrightening and an accompanied X-ray feature.

We have developed a semianalytic method to solve the dynamic of a system including a FS and a reverse shock (RS). It can be applied in different situations such as when a density jump medium or the e^+e^- wind is involved. In this review, we briefly describe our related studies in recent years and show how the investigations help to shed light on the nature of GRBs. In Section 2, we revisit the circum-burst density jump scenario and compare our results with previous hydrodynamic simulations [42, 43]. The delayed energy injection model is discussed in Section 3. In Section 4, we show that the e^+e^- wind model would naturally produce the optical rebrightenings and some characteristics of the central magnetar may be derived by comparing the theoretical results with observations. Finally, our conclusions are summarized in Section 5.

2. Density Jump Scenario

After the prompt emission of GRB, a FS will form and propagate into the circum-burst medium. The dynamic of the FS can be described by a set of differential equations proposed by [44–46]. Assuming the number density profile of the circum-burst medium is a step function of radius R, $n = n_0$ ($R < R_0$) and $n = n_1$ ($R \geq R_0$), where R_0 is the transition radius and $n_1 > n_0$. Before the FS reaching R_0, the evolution of the Lorentz factor of the FS (Γ_2) is given by [47]

$$\frac{d\Gamma_2}{dm_2} = -\frac{4\left(\Gamma_2^2 - 1\right)}{8\left(1-\varepsilon_2\right)\Gamma_2 m_2 + 3\varepsilon_2 m_2 + 3M_{\rm ej}}, \tag{1}$$

where $M_{\rm ej}$ is the initial mass of the outflow, m_2 is the mass of the ambient medium swept up by the FS, and ε_2 is the radiation efficiency of the shocked material. The subscript "2" is used to mark quantities in the shocked region.

When the FS encounters the density jump at R_0, a RS will form and propagate back into the hot shell [48, 49]. These two shocks (FS and RS) and the contact discontinuity will separate the system into four regions: (1) unshocked high-density medium, (2) forward-shocked high-density medium, (3) reverse-shocked hot shell, and (4) unshocked hot shell. In this paper, quantities in Region "i" are denoted by subscripts "i." We extend the derivation of [44] to include the role of the reverse shock. Firstly, it is assumed that the Lorentz factors of Region 2 (Γ_2) and Region 3 (Γ_3) are equal; that is, $\Gamma_2 = \Gamma_3 = \Gamma$. Secondly, we can calculate the energy of each region E_i and the total energy $E_{\rm tot} = \sum_{i=2}^{4} E_i$. For the mass increment of Region 3, dm_3, the radiative energy of the FS-RS system is $dE_{\rm rad}$. By equating $dE_{\rm tot}$ with $dE_{\rm rad}$ and using some additional equations, we can obtain

$$\frac{d\Gamma_2}{dm_2} = -\frac{(4/3)\left(\Gamma_2^2 - 1\right) + f_1\left(dm_3/dm_2\right) + \left(1-\varepsilon_3\right) f_2 \Gamma_2 \Gamma_{42}\left(1 - \beta_{42}/\beta_4\right) m_3 \left(d\psi_4/dm_2\right)}{(8/3)\left(1-\varepsilon_2\right)\Gamma_2 m_2 + \varepsilon_2 m_2 + \left(1-\varepsilon_3\right) f_3 m_3 + \varepsilon_3 m_3}, \tag{2}$$

where Γ_{42} (β_{42}) is the relative Lorentz factor (velocity) of Region 4 as measured in the rest of the frame of Region 2, β_4 is the velocity of Region 4, and f_1, f_2, f_3, and ψ_4 are functions of other variables (see Appendix A of [47]). Γ_2 ($R > R_0$) could be finally derived with some other equations involving m_2, m_3, Γ_4, and R.

Here, we briefly describe how the flux densities are calculated after solving (1) and (2). Customarily, the energy distribution function, $dN_e'/d\gamma_e'$, of the shocked electrons is taken as the two-segment power-law form [50], with the indices of $-p$ and $-p-1$. Hereinafter, we use prime ($'$) on variables to denote quantities in the shock comoving frame and characters without a prime to denote quantities in the observer frame. Synchrotron and inverse Compton (IC) radiation are then considered to calculate the emission from electrons. Basic formulation can be found in [45, 51–53]. Finally, the observed flux densities are obtained by integrating emission from electrons on the equal arrival time surface [54, 55].

According to some previous studies [31–33], the optical rebrightening is attributed to the radiation from Region 3. However, results from our refined calculations are different. In our work, we find that the magnitude of the emission from Region 3 is mainly determined by two factors. One is the

thermal Lorentz factor of baryons in Region 3; that is, Γ_{43} ($\Gamma_{43} = \Gamma_{42}$). The other factor is the number density of electrons in Region 3, n_3'. We set the initial values of the outflow parameters as the isotropic kinetic energy $E_{K,\mathrm{iso}} = 10^{53}$ erg, the initial Lorentz factor $\Gamma_{2,0} = 300$, $n_0 = 1\,\mathrm{cm}^{-3}$, $R_0 = 3.4 \times 10^{17}$ cm, and the redshift $z = 1$. In Figure 1, we calculate two cases with different density jump ratios (n_1/n_0), of 10 and 100 times, respectively. Results from our semianalytic method show that Γ_{43} given by the analytical solution is overestimated (see Figure 1). Moreover, we use the comoving volume of Region 3 to calculate the volume-averaged n_3', which is significantly lower than that predicted by the shock jump conditions (see Figure 2 of [47]). As a result, the radiation from Region 3 is actually lower than that given by previous analytical studies. Figure 2 shows the corresponding lightcurves in two cases. No notable bumps emerge after the density jump in these cases. This is consistent with the results from several hydrodynamic simulations [42, 43]. In our calculations, typical values are adopted for parameters of the plasma in all regions [56]; that is, the equipartition parameter for electron energy $\epsilon_e = 0.1$, the equipartition parameter for magnetic field energy $\epsilon_B = 0.01$, the electron distribution index $p = 2.3$, and the half-opening angle $\theta_j = 0.1$.

3. Delayed Energy Injection Model

We now focus on the afterglows with steep optical rebrightenings. We show that the steep optical rebrightening can be naturally generated in the delayed energy injection scenario. In this model, the central engine after burst is assumed to be a BH. Considering the vicinity along the spin axis of the BH at late times should be clean, we can assume the energy flow is in type of Poynting-flux. The delayed Poynting-flux would be absorbed by the hot plasma behind the FS and modify the dynamics of the FS. If the luminosity of the Poynting-flux is L, then the dynamic of the FS can be described by [40]

$$\frac{d\Gamma}{dm} = -\frac{\left(\Gamma^2 - 1\right) - \left(\left(1-\beta\right)/\beta c^3\right)\Omega_j L\left(t_b - R/c\right)\left(dR/dm\right)}{M_{\mathrm{ej}} + 2\left(1-\varepsilon\right)\Gamma m + \varepsilon m}, \tag{3}$$

where $\Gamma = 1/\sqrt{1-\beta^2}$ is the bulk Lorentz factor of the FS, $\Omega_j = (1 - \cos\theta_j)/2$ is the beaming factor of the GRB outflow, m is the swept-up mass by the shock, ε is the radiative efficiency, R is the radius of the FS, and t_b is the time from the event measured in the burster frame. Such a delayed energy injection would lead to a rapid change in the evolution of Γ according to (3); consequently the flux would show a steep rise.

The energy injection power (with a luminosity of L) during the fall-back accretion may come from some magnetic processes [58–60]; however, its exact temporal profile is still uncertain. Here, we use two possible modes in our calculations. One is the top-hat mode in which the injected power L is a constant from a start time $t^{\mathrm{s}}_{\mathrm{obs}}$ to an end time $t^{\mathrm{e}}_{\mathrm{obs}}$ [38]. The other is the broken-power-law mode, in which the luminosity profile is similar to the profile of the mass accretion rate during the fall-back [3, 39, 61, 62]; that is,

$$L = L_{\mathrm{p}}\left[\frac{1}{2}\left(\frac{t_{\mathrm{obs}} - t^{\mathrm{s}}_{\mathrm{obs}}}{t^{\mathrm{p}}_{\mathrm{obs}} - t^{\mathrm{s}}_{\mathrm{obs}}}\right)^{-\alpha_r s} + \frac{1}{2}\left(\frac{t_{\mathrm{obs}} - t^{\mathrm{s}}_{\mathrm{obs}}}{t^{\mathrm{p}}_{\mathrm{obs}} - t^{\mathrm{s}}_{\mathrm{obs}}}\right)^{-\alpha_d s}\right]^{-1/s}, \tag{4}$$

where L_{p} is the peak luminosity at the peak time $t^{\mathrm{p}}_{\mathrm{obs}}$, α_r, α_d are the rising and decreasing index respectively, and s is the sharpness of the peak. In Figure 3, we show lightcurves calculated in the two modes, from which we find that the steep optical rebrightening would be generated. The initial conditions of the outflow and the key parameters involved in the radiation process are the same as those in Section 2.

This model has been used to interpret the steep rebrightenings in the lightcurves of GRB 081029 [40, 63, 64] and GRB 100621A [40, 65]. We notice that $t^{\mathrm{s}}_{\mathrm{obs}}/(1+z)$ is just equal to t_{fb}, which gives

$$\frac{t^{\mathrm{s}}_{\mathrm{obs}}}{1+z} \simeq \left(\frac{\pi^2 r_{\mathrm{fb}}^3}{8GM_{\mathrm{BH}}}\right)^{1/2}, \tag{5}$$

where r_{fb} is the fall-back radius, G is the gravitational constant, and M_{BH} is the mass of central BH. Moreover, the injected energy should come from the potential energy of the fall-back material; that is,

$$\frac{\Omega_j}{1+z}\int_{t^{\mathrm{s}}_{\mathrm{obs}}}^{t^{\mathrm{e}}_{\mathrm{obs}}} L\,dt_{\mathrm{obs}} \simeq \eta\frac{GM_{\mathrm{BH}}M_{\mathrm{fb}}}{r_{\mathrm{fb}}}, \tag{6}$$

where M_{fb} is the total fall-back mass and η is the efficiency of the energy conversion. In the top-hat mode, (5) and (6) will give

$$M_{\mathrm{fb}} = \frac{2}{1+z}\eta^{-1}\left(\frac{t^{\mathrm{s}}_{\mathrm{obs}}}{1+z}\right)^{2/3}\left(\pi GM_{\mathrm{BH}}\right)^{-2/3} \cdot \Omega_j L\left(t^{\mathrm{e}}_{\mathrm{obs}} - t^{\mathrm{s}}_{\mathrm{obs}}\right). \tag{7}$$

Therefore, in principle, M_{fb} can be inferred from the fitting to the optical rebrightenings in the scenario.

4. e^+e^- Wind Model

In the prior section, we interpret the steep optical rebrightenings by using the delayed energy injection model. Now, we discuss another group of afterglows, of which the optical rebrightenings are shallower.

After a GRB, the remaining object of the progenitor may be a magnetar, which will lose its rotational energy by ejecting a continuous Poynting-flux. In the e^+e^- wind model, the Poynting-flux may convert into an e^+e^- wind, as hinted from phenomena associated with pulsar wind nebulae [66–68]. As the e^+e^- wind catches up with the FS, a long-lasting RS will form and propagate back into the e^+e^- wind. The RS-shocked

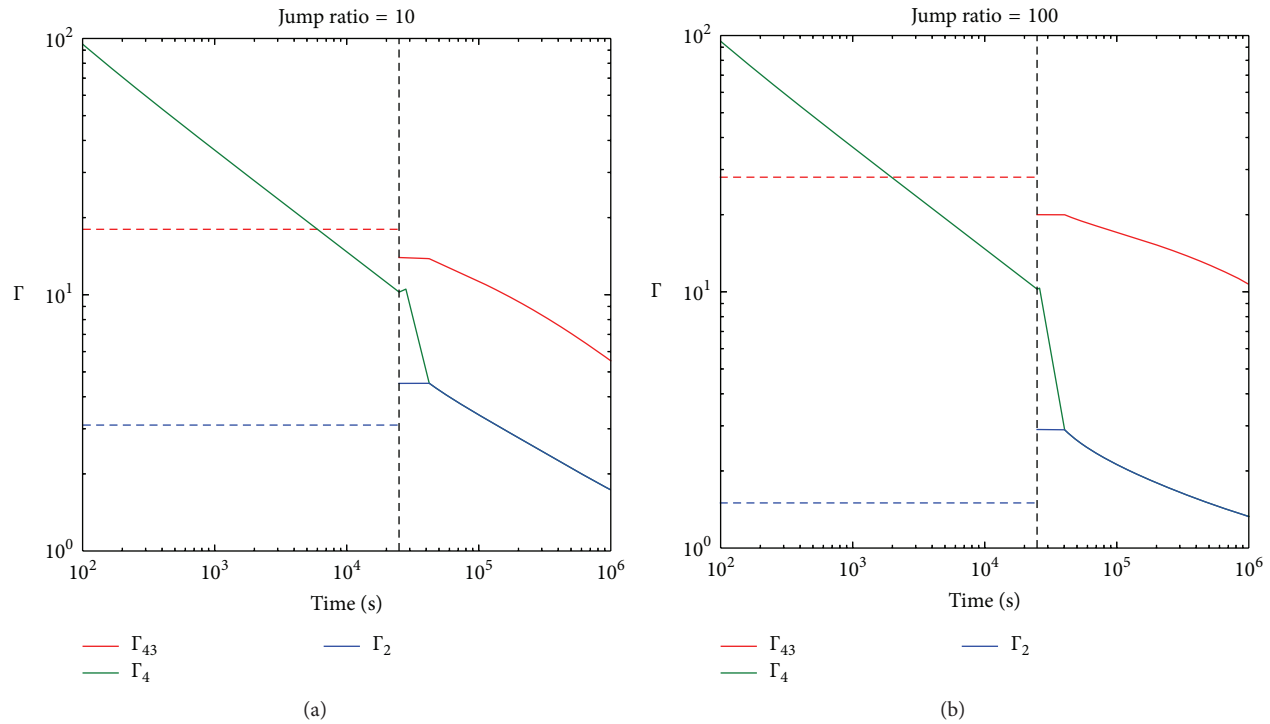

FIGURE 1: Evolution of the Lorentz factors of different regions when there is a density jump [47]. Two cases are calculated: one corresponds to the density jump ratio of 10 (a), and the other corresponds to the jump ratio 100 (b). The vertical dashed line marks the time of encountering the density jump. The green solid lines represent Γ_2 before encountering the density jump and Γ_4 during the encountering, both denoted by Γ_4. The blue solid lines and red solid lines represent Γ_2 (or Γ_3, $\Gamma_2 = \Gamma_3$) and the thermal Lorentz factor of the baryons in Region 3 (Γ_{43}) after the encountering, respectively. The horizontal dashed lines mark the values of corresponding Lorentz factors (which remain constant during the reverse shock crossing time) given by [57]. Note that Γ_4 (see the green solid lines) during the encounter is almost constant (slowly increasing due to adiabatic expansion), which is shown as a "plateau" that is significantly shorter than that of Γ_2. The shortness of the "plateau" of Γ_4 is due to the different transformation formula between the burst frame time and the apparent time in the observer frame.

e^+e^- will act as another emitting source besides the electrons shocked by the FS. Consequently, the afterglow lightcurves are the combination of two components. This model has been proposed to interpret the X-ray plateau previously. However, we find this model may account for the common origin for shallow optical rebrightenings around 10^4 s.

For a newly born magnetar, its Poynting-flux luminosity $L_w(t_{\rm obs})$ is [69]

$$L_w \simeq 4.0 \times 10^{47} B_{\rm NS,14}^2 R_{\rm NS,6}^6 P_{\rm NS,-3}^{-4} \left(1 + \frac{t_{\rm obs}}{T_{\rm sd}}\right)^{-2} \ {\rm erg\,s^{-1}}, \quad (8)$$

and its spin-down timescale is

$$T_{\rm sd} \simeq 5.0 \times 10^4 \, (1+z) \, B_{\rm NS,14}^{-2} I_{45} R_{\rm NS,6}^{-6} P_{\rm NS,-3}^2 \ {\rm s}, \quad (9)$$

where $B_{\rm NS}$, $R_{\rm NS}$, $P_{\rm NS}$, and I are the surface magnetic field strength, radius, spin period, and moment of inertia of the magnetar, respectively. The convention $Q_x = Q/10^x$ in cgs units is adopted hereafter. We assume the Poynting-flux is converted into e^+e^- pairs; then the particle density in the comoving frame of the unshocked wind is $n_4' = L_w/(4\pi R^2 \Gamma_4^2 m_e c^3)$, where Γ_4 is the bulk Lorentz factor of the unshocked wind (referred to as Region 4 below). Unlike the rapid evolution of Γ_2 in the delayed energy injection scenario, the evolution of Γ_2 is shallow due to the smoothly evolving L_w here.

The dynamics of the FS-RS system here can be solved by applying the method mentioned in Section 2. Meanwhile, another method, called the mechanical method [70, 71], was also proposed to solve the dynamics of such FS-RS system. Here, we first compare these two methods. Let us consider an outflow with an isotropic kinetic energy of $E_{K,\rm iso} = 8.0 \times 10^{52}$ erg and an initial Lorentz factor of $\Gamma_{2,0} = 150$, and we set $n_0 = 0.1\,{\rm cm^{-3}}$, $\Gamma_4 = 10^4$, and $B_{\rm NS} = 2 \times 10^{14}$ G. The evolution of Γ_2 can thus be obtained by using the two methods, respectively. In Figure 4, we see that the results from our method and the mechanical method are consistent with each other. Below, we adopt the mechanical method to solve the dynamics of the FS-RS system.

After taking the parameters $\epsilon_{e,2} = 0.05$, $\epsilon_{B,2} = 0.01$, $\epsilon_{B,3} = 0.2$, $\epsilon_{e,3} = 1 - \epsilon_{B,3} = 0.8$, $p_2 = 2.1$, and $p_3 = 2.4$, the corresponding lightcurves can be calculated (see Figure 5). In this case, it is clearly shown that the flux from the RS begins to exceed that from the FS at $\sim 5 \times 10^4$ s,

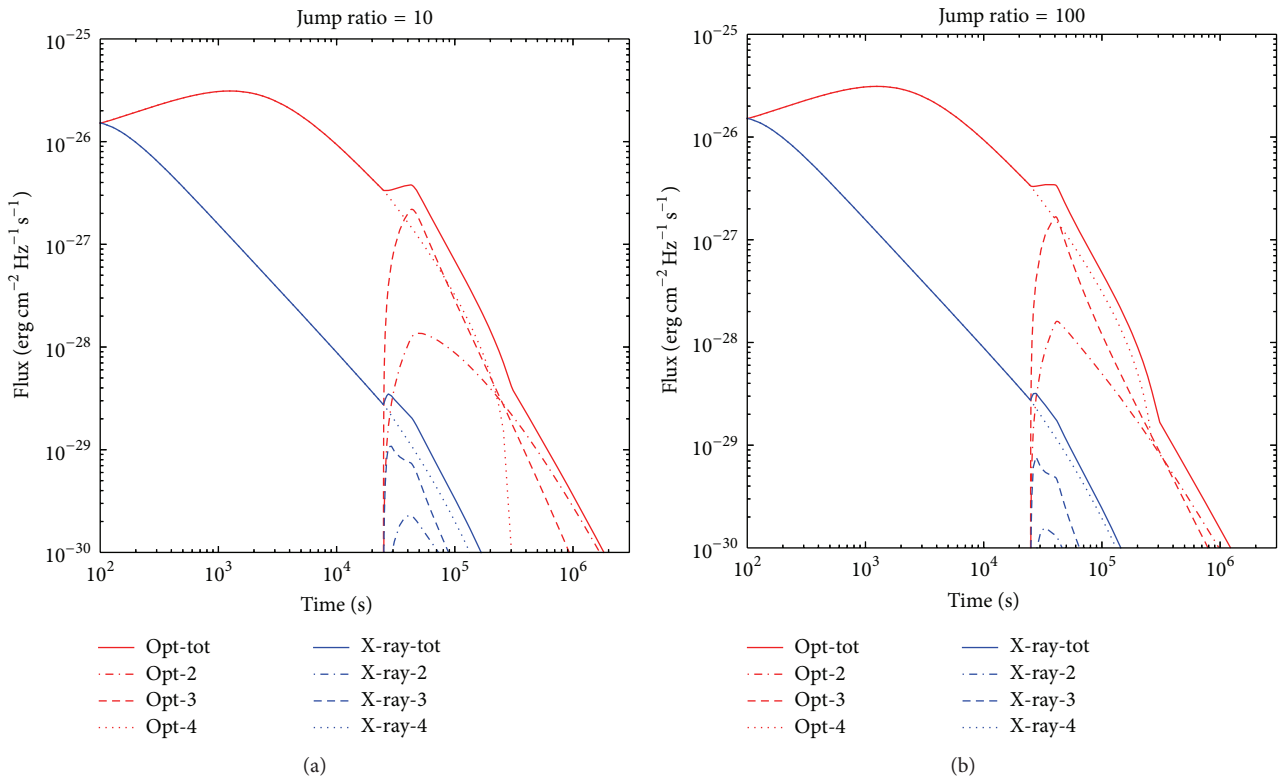

FIGURE 2: Corresponding afterglow lightcurves for the two cases in Figure 1. The red, blue lines are lightcurves in the optical band (4×10^{14} Hz) and the X-ray band (0.3 keV), respectively. The dotted lines (Opt-4 or X-ray-4) represent the flux density of Region 2 before the density jump and the flux density of Region 4 after the jump. The dashed lines (Opt-3 or X-ray-3) are the contribution from Region 3 after the density jump. The dash-dotted lines (Opt-2 or X-ray-2) mark the flux density of Region 2 after the jump. Total flux densities of all the components are presented by the solid lines (Opt-tot or X-ray-tot). For a similar plot, see [47].

leading to the emergence of the optical rebrightening and the X-ray plateau simultaneously. Due to the effect of the equal arrival time surface [54, 55, 72], the peak time of the optical rebrightening would be delayed, that is, larger than $T_{\rm sd}$. However, this kind of delay in X-rays can be ignored. As a result, optical rebrightenings are relatively easier to emerge than "X-ray rebrightenings." In other words, it is often the case that only a X-ray plateau or no equivalent feature in X-rays accompanies the optical rebrightening. This property in our model is interestingly consistent with many observations. In Figure 6, optical afterglows are calculated using different values of $B_{\rm NS}$. From these results, it is found that the flux from the long-lasting RS would account for the shallow optical rebrightening. The e^+e^- wind model has been applied (paper submitted) to explain the afterglows of GRB 080413B [73], GRB 090426 [74], GRB 091029 [75], and GRB 100814A [20].

Since the flux from the RS is sensitive to L_w and $T_{\rm sd}$, the e^+e^- wind scenario provides a useful way to probe the characteristics of newly born magnetars. Considering the fact that L_w and $T_{\rm sd}$ are uniquely determined by the parameter $B_{\rm NS}$, we suggest that $B_{\rm NS}$ may be constrained from the fitting to the observed rebrightenings.

5. Discussion

In this review, we show that the density jump scenario could not account for many of the observed optical rebrightenings in GRB afterglows. Furthermore, we classify the observed afterglows with optical rebrightenings into two groups and investigate their intrinsic origin. The afterglows with steep optical rebrightenings are interpreted by the delayed energy injection model, which is associated with a central accreting BH. Meanwhile, the afterglows with shallow optical rebrightenings are explained by the e^+e^- wind model, of which the central engine is a magnetar.

Although the above two groups of afterglows have similar origins for rebrightenings, some other factors will make the situation different. The observational data of some afterglows clearly show that their spectral indices are evolving [75]. It is hard to satisfactorily model them only by using the simple models discussed here and/or other customary models. For the simple e^+e^- wind model or the two-component jet model, the spectral evolution would occur only when the characteristic frequencies are crossing the observational band, or when later component begins to dominate, but it cannot work well for some special GRBs. In such cases, including

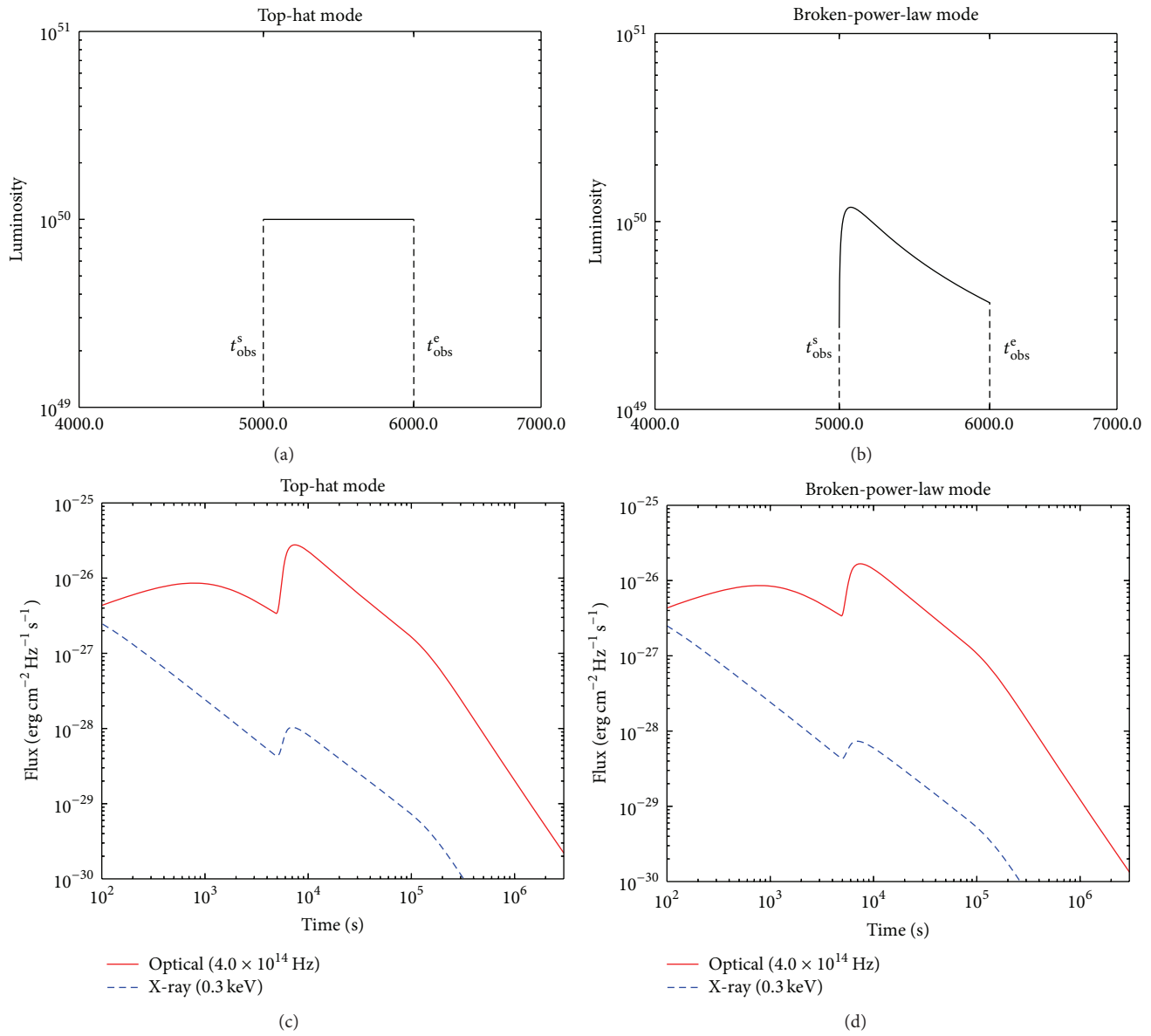

FIGURE 3: (a) Schematic illustration of the top-hat injection mode, in which $L_0 = 10^{50}$ erg s^{-1} (isotropic), $t^{s}_{obs} = 5000$ s, and $t^{e}_{obs} = 6000$ s. (b) Schematic illustration of the broken-power-law (see (4)) injection mode, in which $L_p = 10^{50}$ erg s^{-1} (isotropic), $t^{s}_{obs} = 5000$ s, $t^{p}_{obs} = 5200$ s, $t^{e}_{obs} = 6000$ s, $\alpha_r = 0.5$, $\alpha_d = -1.5$, and s $= 0.5$. (c) and (d) show the corresponding afterglows of the two modes correspondingly. In the calculations, a redshift of $z = 1$ is assumed. Similar plots can be found at [40].

some microphysical processes may be necessary to match the observations. For example, in the varying microphysical parameters scenarios [36], the varying electron distribution index p would help to explain some unexpected spectral evolutions [75]. Varying microphysical parameters may be related to the acceleration performance of relativistic shocks [76]. Since the acceleration performance of shocks may depend on the magnetization (or other factors) of the plasma and the magnetization is highly variable [77], some special afterglows are foreseeable.

It has been suggested that the two-component jets could also account for some shallow rebrightenings. The collapsar model of long-duration GRBs offers a natural mechanism to generate two-component jets; that is, a high speed jet emerging from a star is accompanied by a relatively slow cocoon [78, 79]. The rebrightening lightcurve itself will not help to definitely discriminate the e^+e^- wind model from the two-component jet model, since the role of the wide jet is somehow similar to the role of the RS. However, there is another way that can help us in the future. A two-component jet should be associated with a collapsar. If the rebrightening is observed to be associated with the double NS merger (by detections of the gravitational waves [80]) but not a collapsar, then the e^+e^- wind model would be preferred.

The intrinsic origins of optical rebrightenings would help to probe the characteristics of central engines. In the delayed

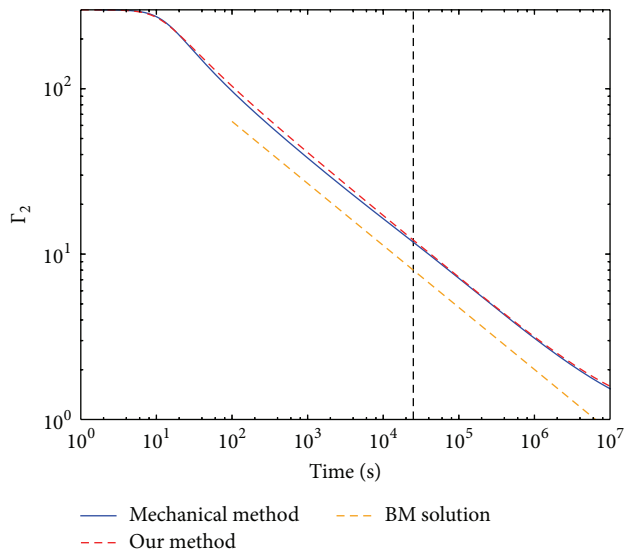

Figure 4: Comparison of the two methods used in solving the temporal evolution of Γ_2 in the e^+e^- wind model. The initial parameter values are $E_{K,\mathrm{iso}} = 8.0\times10^{52}$ erg, $\Gamma_{2,0} = 150$, $n_0 = 0.1\,\mathrm{cm}^{-3}$, $\Gamma_4 = 10^4$, and $B_{\mathrm{NS}} = 2\times10^{14}$ G. The thick dashed orange line represents the BM solution (schematic); that is, $\Gamma \propto t_{\mathrm{obs}}^{3/8}$ and the vertical dashed line denote the position of T_{sd}.

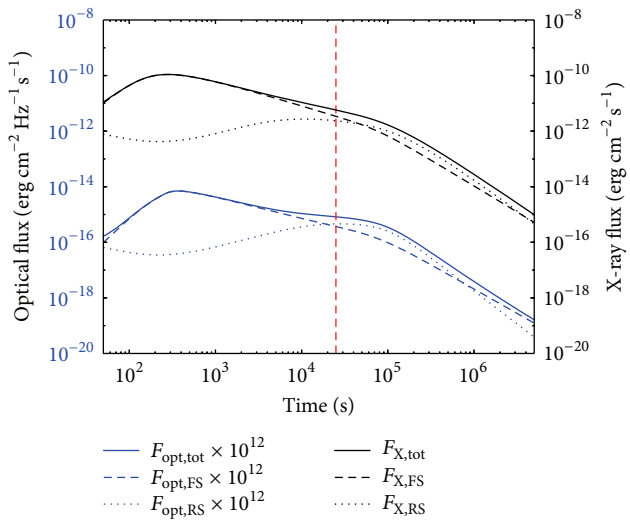

Figure 5: Corresponding afterglow lightcurves of Figure 4. The dashed lines represent the flux from Region 3, while the dotted lines are emissions from Region 2. The total flux is shown as the solid lines. In the calculations, the optical band is taken as 4.0×10^{14} Hz and the X-ray band is taken as 0.3–10 keV. The red dashed vertical line marks the position of T_{sd}.

energy injection model, t_{fb} can be derived from the start time of the rebrightening, and r_{fb} can thus be obtained. If the observational data is good enough, L can be constrained in the fitting process, and we can estimate the total mass of the fall-back material. Furthermore, the fall-back accretion theory requires that the steep optical rebrightening should be

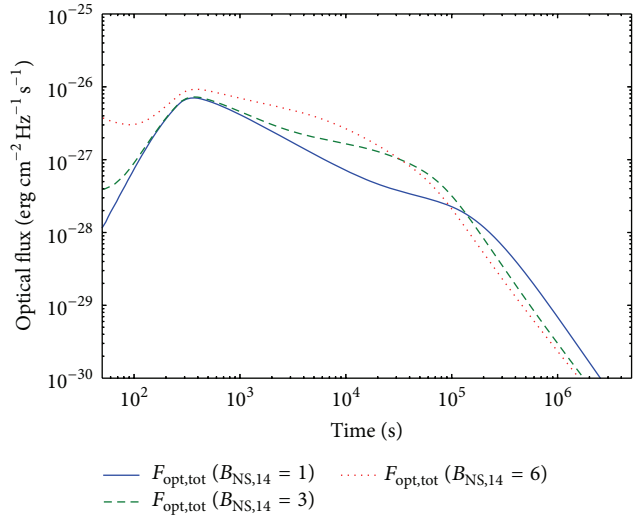

Figure 6: Optical lightcurves in the electron-positron wind model with different B_{NS}. All the parameters are the same as those in Figure 5, except for $B_{\mathrm{NS,14}} = 1$ (solid line), $B_{\mathrm{NS,14}} = 3$ (dashed line), and $B_{\mathrm{NS,14}} = 6$ (dotted line).

accompanied by a low energy supernova, in which the fall-back material can survive during the explosion. This model thus can be tested by future observations of GRB-supernova association. In the e^+e^- wind model, T_{sd} can be roughly inferred from the peak time of the optical rebrightening. In general, an earlier rebrightening means that B_{NS} is larger or P_{NS} is smaller. So B_{NS} and P_{NS} can be constrained from observations. Thus the e^+e^- model provides a potential way to probe the characteristics of the central magnetar.

Competing Interests

The authors declare that there are no competing interests related to this paper.

Acknowledgments

The authors thank Liang Li for helpful discussion. This work was supported by the National Basic Research Program of China with Grant no. 2014CB845800 and by the National Natural Science Foundation of China with Grant no. 11473012.

References

[1] S. E. Woosley, "Gamma-ray bursts from stellar mass accretion disks around black holes," *The Astrophysical Journal*, vol. 405, no. 1, pp. 273–277, 1993.

[2] R. Popham, S. E. Woosley, and C. Fryer, "Hyperaccreting black holes and gamma-ray bursts," *The Astrophysical Journal*, vol. 518, no. 1, pp. 356–374, 1999.

[3] A. I. Macfadyen, S. E. Woosley, and A. Heger, "Supernovae, jets, and collapsars," *The Astrophysical Journal*, vol. 550, no. 1, pp. 410–425, 2001.

[4] R. Narayan, T. Piran, and P. Kumar, "Accretion models of gamma-ray bursts," *The Astrophysical Journal*, vol. 557, no. 2, pp. 949–957, 2001.

[5] D. Eichler, M. Livio, T. Piran, and D. N. Schramm, "Nucleosynthesis, neutrino bursts and γ-rays from coalescing neutron stars," *Nature*, vol. 340, no. 6229, pp. 126–128, 1989.

[6] B. Paczynski, "Cosmological gamma-ray bursts," *Acta Astronomica*, vol. 41, no. 4, pp. 257–267, 1991.

[7] J. Grindlay, S. Portegies Zwart, and S. McMillan, "Short gamma-ray bursts from binary neutron star mergers in globular clusters," *Nature Physics*, vol. 2, no. 2, pp. 116–119, 2006.

[8] R. D. Blandford and C. F. McKee, "Fluid dynamics of relativistic blast waves," *Physics of Fluids*, vol. 19, no. 8, pp. 1130–1138, 1976.

[9] T. Piran, A. Shemi, and R. Narayan, "Hydrodynamics of relativistic fireballs," *Monthly Notices of the Royal Astronomical Society*, vol. 263, no. 4, pp. 861–867, 1993.

[10] P. Mészáros and M. J. Rees, "Optical and long-wavelength afterglow from gamma-ray bursts," *The Astrophysical Journal*, vol. 476, no. 1, pp. 232–237, 1997.

[11] R. Sari and T. Piran, "Predictions for the very early afterglow and the optical flash," *The Astrophysical Journal*, vol. 520, no. 2, pp. 641–649, 1999.

[12] H. Gao, W.-H. Lei, Y.-C. Zou, X.-F. Wu, and B. Zhang, "A complete reference of the analytical synchrotron external shock models of gamma-ray bursts," *New Astronomy Reviews*, vol. 57, no. 6, pp. 141–190, 2013.

[13] N. Gehrels, G. Chincarini, P. Giommi et al., "The swift gamma-ray burst mission," *The Astrophysical Journal*, vol. 611, no. 2, pp. 1005–1020, 2004.

[14] D. N. Burrows, J. E. Hill, J. A. Nousek et al., "The swift X-ray telescope," *Space Science Reviews*, vol. 120, no. 3-4, pp. 165–195, 2005.

[15] N. Gehrels, E. Ramirez-Ruiz, and D. B. Fox, "Gamma-ray bursts in the *Swift* era," *Annual Review of Astronomy and Astrophysics*, vol. 47, no. 1, pp. 567–617, 2009.

[16] J. Greiner, W. Bornemann, C. Clemens et al., "GROND—a 7-channel imager," *Publications of the Astronomical Society of the Pacific*, vol. 120, no. 866, pp. 405–424, 2008.

[17] B. Zhang, Y. Z. Fan, J. Dyks et al., "Physical processes shaping gamma-ray burst X-ray afterglow light curves: theoretical implications from the swift X-ray telescope observations," *The Astrophysical Journal*, vol. 642, no. 1, pp. 354–370, 2006.

[18] A. Melandri, F. J. Virgili, C. Guidorzi et al., "The nature of the late achromatic bump in GRB 120326A," *Astronomy and Astrophysics*, vol. 572, p. A55, 2014.

[19] S. J. Hou, J. J. Geng, K. Wang et al., "The origin of the plateau and late rebrightening in the afterglow of GRB 120326A," *The Astrophysical Journal*, vol. 785, no. 2, p. 113, 2014.

[20] M. De Pasquale, N. P. M. Kuin, S. Oates et al., "The optical rebrightening of GRB100814A: an interplay of forward and reverse shocks?" *Monthly Notices of the Royal Astronomical Society*, vol. 449, no. 1, pp. 1024–1042, 2015.

[21] H. Gao and P. Mészáros, "Reverse shock emission in gamma-ray bursts revisited," *Advances in Astronomy*, vol. 2015, Article ID 192383, 16 pages, 2015.

[22] P. Kumar and B. Zhang, "The physics of gamma-ray bursts & relativistic jets," *Physics Reports*, vol. 561, pp. 1–109, 2015.

[23] L. Li, X.-F. Wu, Y.-F. Huang et al., "A correlated study of optical and X-ray afterglows of GRBs," *The Astrophysical Journal*, vol. 805, no. 1, article 13, 2015.

[24] Z. G. Dai and T. Lu, "Gamma-ray burst afterglows and evolution of postburst fireballs with energy injection from strongly magnetic millisecond pulsars," *Astronomy and Astrophysics*, vol. 333, no. 3, pp. L87–L90, 1998.

[25] B. Zhang and P. Mészáros, "Gamma-ray burst afterglow with continuous energy injection: signature of a highly magnetized millisecond pulsar," *Astrophysical Journal Letters*, vol. 552, no. 1, pp. L35–L38, 2001.

[26] Y.-Z. Fan and D. Xu, "The X-ray afterglow flat segment in short GRB 051221A: energy injection from a millisecond magnetar?" *Monthly Notices of the Royal Astronomical Society*, vol. 372, no. 1, pp. L19–L22, 2006.

[27] S. Kong and Y. Huang, "Afterglow from GRB 070610/Swift J195509.6+261406: an explanation using the fireball model," *Science China Physics, Mechanics, and Astronomy*, vol. 53, supplement 1, pp. 94–97, 2010.

[28] B. Zhang and P. Mészáros, "Gamma-ray bursts with continuous energy injection and their afterglow signature," *The Astrophysical Journal*, vol. 566, no. 2, pp. 712–722, 2002.

[29] Z. G. Dai, "Relativistic wind bubbles and afterglow signatures," *The Astrophysical Journal*, vol. 606, no. 2, pp. 1000–1005, 2004.

[30] Y. W. Yu, X. W. Liu, and Z. G. Dai, "Observational signatures of high-energy emission during the shallow decay phase of gamma-ray burst X-ray afterglows," *The Astrophysical Journal*, vol. 671, no. 1, pp. 637–644, 2007.

[31] D. Lazzati, E. Rossi, S. Covino, G. Ghisellini, and D. Malesani, "The afterglow of GRB 021004: surfing on density waves," *Astronomy & Astrophysics*, vol. 396, no. 2, pp. L5–L9, 2002.

[32] Z. G. Dai and X. F. Wu, "GRB 030226 in a density-jump medium," *Astrophysical Journal Letters*, vol. 591, no. 1, pp. L21–L24, 2003.

[33] E. Nakar and T. Piran, "Modeling fluctuations in gamma-ray burst afterglow light curves," *The Astrophysical Journal*, vol. 598, no. 1, pp. 400–410, 2003.

[34] E. Berger, S. R. Kulkarni, G. Pooley et al., "A common origin for cosmic explosions inferred from calorimetry of GRB 030329," *Nature*, vol. 426, no. 6963, pp. 154–157, 2003.

[35] Y. F. Huang, X. F. Wu, Z. G. Dai, H. T. Ma, and T. Lu, "Rebrightening of XRF 030723: further evidence for a two-component jet in a gamma-ray burst," *The Astrophysical Journal*, vol. 605, no. 1, pp. 300–306, 2004.

[36] S. W. Kong, A. Y. L. Wong, Y. F. Huang, and K. S. Cheng, "Variation of microphysics in wind bubbles: an alternative mechanism for explaining the rebrightenings in gamma-ray burst afterglows," *Monthly Notices of the Royal Astronomical Society*, vol. 402, no. 1, pp. 409–416, 2010.

[37] R. Perna, P. J. Armitage, and B. Zhang, "Flares in long and short gamma-ray bursts: a common origin in a hyperaccreting accretion disk," *Astrophysical Journal Letters*, vol. 636, no. 1, pp. L29–L32, 2006.

[38] P. Kumar, R. Narayan, and J. L. Johnson, "Mass fall-back and accretion in the central engine of gamma-ray bursts," *Monthly Notices of the Royal Astronomical Society*, vol. 388, no. 4, pp. 1729–1742, 2008.

[39] X.-F. Wu, S.-J. Hou, and W.-H. Lei, "Giant X-ray bump in GRB 121027A: evidence for fall-back disk accretion," *Astrophysical Journal Letters*, vol. 767, no. 2, article L36, 2013.

[40] J. J. Geng, X. F. Wu, Y. F. Huang, and Y. B. Yu, "Delayed energy injection model for gamma-ray burst afterglows," *The Astrophysical Journal*, vol. 779, no. 1, article 28, 2013.

[41] Y. W. Yu and Z. G. Dai, "Shallow decay phase of GRB X-ray afterglows from relativistic wind bubbles," *Astronomy and Astrophysics*, vol. 470, no. 1, pp. 119–122, 2007.

[42] H. J. van Eerten, Z. Meliani, R. A. M. J. Wijers, and R. Keppens, "No visible optical variability from a relativistic blast wave encountering a wind termination shock," *Monthly Notices of the Royal Astronomical Society*, vol. 398, no. 1, pp. L63–L67, 2009.

[43] I. Gat, H. van Eerten, and A. MacFadyen, "No flares from gamma-ray burst afterglow blast waves encountering sudden circumburst density change," *The Astrophysical Journal*, vol. 773, no. 1, article 2, 2013.

[44] Y. F. Huang, Z. G. Dai, and T. Lu, "A generic dynamical model of gamma-ray burst remnants," *Monthly Notices of the Royal Astronomical Society*, vol. 309, no. 2, pp. 513–516, 1999.

[45] Y. F. Huang, L. J. Gou, Z. G. Dai, and T. Lu, "Overall evolution of jetted gamma-ray burst ejecta," *The Astrophysical Journal*, vol. 543, no. 1, pp. 90–96, 2000.

[46] A. Pe'er, "Dynamical model of an expanding shell," *Astrophysical Journal Letters*, vol. 752, no. 1, article L8, 2012.

[47] J. J. Geng, X. F. Wu, L. Li, Y. F. Huang, and Z. G. Dai, "Revisiting the emission from relativistic blast waves in a density-jump medium," *The Astrophysical Journal*, vol. 792, no. 1, article 31, 2014.

[48] R. Sari and T. Piran, "Hydrodynamic timescales and temporal structure of gamma-ray bursts," *Astrophysical Journal Letters*, vol. 455, p. L143, 1995.

[49] S. Kobayashi, T. Piran, and R. Sari, "Hydrodynamics of a relativistic fireball: the complete evolution," *The Astrophysical Journal*, vol. 513, no. 2, pp. 669–678, 1999.

[50] R. Sari, T. Piran, and R. Narayan, "Spectra and light curves of gamma-ray burst afterglows," *The Astrophysical Journal Letters*, vol. 497, no. 1, pp. L17–L20, 1998.

[51] G. B. Rybicki and A. P. Lightman, *Radiative Processes in Astrophysics*, Wiley-Interscience, New York, NY, USA, 1979.

[52] Y. Fan and T. Piran, "Gamma-ray burst efficiency and possible physical processes shaping the early afterglow," *Monthly Notices of the Royal Astronomical Society*, vol. 369, no. 1, pp. 197–206, 2006.

[53] X.-Y. Wang, H.-N. He, Z. Li, X.-F. Wu, and Z.-G. Dai, "Klein-nishina effects on the high-energy afterglow emission of gamma-ray bursts," *The Astrophysical Journal*, vol. 712, no. 2, pp. 1232–1240, 2010.

[54] E. Waxman, "Angular size and emission timescales of relativistic fireballs," *The Astrophysical Journal Letters*, vol. 491, no. 1, pp. L19–L22, 1997.

[55] J. Granot, T. Piran, and R. Sari, "Images and spectra from the interior of a relativistic fireball," *The Astrophysical Journal*, vol. 513, no. 2, pp. 679–689, 1999.

[56] Y. F. Huang, Z. G. Dai, and T. Lu, "On the optical light curves of afterglows from jetted gamma-ray burst ejecta: effects of parameters," *Monthly Notices of the Royal Astronomical Society*, vol. 316, no. 4, pp. 943–949, 2000.

[57] Z. G. Dai and T. Lu, "Hydrodynamics of relativistic blast waves in a density-jump medium and their emission signature," *The Astrophysical Journal Letters*, vol. 565, no. 2, pp. L87–L90, 2002.

[58] R. D. Blandford and R. L. Znajek, "Electromagnetic extraction of energy from Kerr black holes," *Monthly Notices of the Royal Astronomical Society*, vol. 179, no. 3, pp. 433–456, 1977.

[59] H. K. Lee, R. A. M. J. Wijers, and G. E. Brown, "The Blandford-Znajek process as a central engine for a gamma-ray burst," *Physics Reports*, vol. 325, no. 3, pp. 83–114, 2000.

[60] F. Yuan and B. Zhang, "Episodic jets as the central engine of gamma-ray bursts," *The Astrophysical Journal*, vol. 757, no. 1, article 56, 2012.

[61] W. Zhang, S. E. Woosley, and A. Heger, "Fallback and black hole production in massive stars," *The Astrophysical Journal*, vol. 679, no. 1, pp. 639–654, 2008.

[62] Z. G. Dai and R.-Y. Liu, "Spin evolution of millisecond magnetars with hyperaccreting fallback disks: implications for early afterglows of gamma-ray bursts," *The Astrophysical Journal*, vol. 759, no. 1, article 58, 2012.

[63] M. Nardini, J. Greiner, T. Krühler et al., "On the nature of the extremely fast optical rebrightening of the afterglow of GRB 081029," *Astronomy and Astrophysics*, vol. 531, p. A39, 2011.

[64] S. T. Holland, M. De Pasquale, J. Mao et al., "GRB 081029: a gamma-ray burst with a multi-component afterglow," *The Astrophysical Journal*, vol. 745, no. 1, article 41, 2012.

[65] J. Greiner, T. Krühler, M. Nardini et al., "The unusual afterglow of the gamma-ray burst 100621A," *Astronomy and Astrophysics*, vol. 560, article A70, 2013.

[66] M. J. Rees and J. E. Gunn, "The origin of the magnetic field and relativistic particles in the Crab Nebula," *Monthly Notices of the Royal Astronomical Society*, vol. 167, no. 1, pp. 1–12, 1974.

[67] Y. Lyubarsky and J. G. Kirk, "Reconnection in a striped pulsar wind," *The Astrophysical Journal*, vol. 547, no. 1, pp. 437–448, 2001.

[68] B. D. Metzger and A. L. Piro, "Optical and X-ray emission from stable millisecond magnetars formed from the merger of binary neutron stars," *Monthly Notices of the Royal Astronomical Society*, vol. 439, no. 4, pp. 3916–3930, 2014.

[69] S. L. Shapiro and S. A. Teukolsky, *Black Holes, White Dwarfs and Neutron Stars: The Physics of Compact Objects*, National Science Foundation, Arlington, Va, USA; Wiley-Interscience, New York, NY, USA, 1983.

[70] A. M. Beloborodov and Z. L. Uhm, "Mechanical model for relativistic blast waves," *Astro-Physical Journal Letters*, vol. 651, no. 2, pp. L1–L4, 2006.

[71] Z. L. Uhm, "A semi-analytic formulation for relativistic blast waves with a long-lived reverse shock," *The Astrophysical Journal*, vol. 733, no. 2, article 86, 2011.

[72] Y.-F. Huang, Y. Lu, A. Y. L. Wong, and K. S. Cheng, "A detailed study on the equal arrival time surface effect in gamma-ray burst afterglows," *Chinese Journal of Astronomy and Astrophysics*, vol. 7, no. 3, pp. 397–404, 2007.

[73] R. Filgas, T. Krühler, J. Greiner et al., "The two-component jet of GRB 080413B," *Astronomy and Astrophysics*, vol. 526, article A113, 2011.

[74] A. Nicuesa Guelbenzu, S. Klose, A. Rossi et al., "GRB 090426: discovery of a jet break in a short burst afterglow," *Astronomy and Astrophysics*, vol. 531, article L6, 2011.

[75] R. Filgas, J. Greiner, P. Schady et al., "GRB 091029: at the limit of the fireball scenario," *Astronomy and Astrophysics*, vol. 546, article A101, 2012.

[76] L. Sironi, A. Spitkovsky, and J. Arons, "The maximum energy of accelerated particles in relativistic collisionless shocks," *The Astrophysical Journal*, vol. 771, no. 1, article 54, 2013.

[77] B. Zhang and S. Kobayashi, "Gamma-ray burst early afterglows: reverse shock emission from an arbitrarily magnetized ejecta," *The Astrophysical Journal*, vol. 628, no. 1, pp. 315–334, 2005.

[78] E. Ramirez-Ruiz, A. Celotti, and M. J. Rees, "Events in the life of a cocoon surrounding a light, collapsar jet," *Monthly Notices of the Royal Astronomical Society*, vol. 337, no. 4, pp. 1349–1356, 2002.

[79] D. Lazzati, B. J. Morsony, and D. López-Cámara, "Numerical simulations of gamma-ray burst explosions," *Journal of High Energy Astrophysics*, vol. 7, pp. 17–22, 2015.

[80] B. P. Abbott, R. Abbott, T. D. Abbott et al., "Observation of gravitational waves from a binary black hole merger," *Physical Review Letters*, vol. 116, no. 6, Article ID 061102, 2016.